Novel Cantilever Sensor for Antibody-based and *hly*A gene-based Sensitive Detection of Foodborne Pathogen: *Listeria monocytogenes*

A Thesis

Submitted to the Faculty

Of

Drexel University

by

Harsh Pradipkumar Sharma

in partial fulfillment of the

requirements for the degree

of

Doctor of Philosophy

November 2012

© Copyright 2012

Harsh P. Sharma. All Rights Reserved.

Dedications

To my parents and brother

for all their love, support and encouragement

Acknowledgements

I would like to thank my advisor, Dr. Raj Mutharasan, for his guidance, support and patience throughout the course of this project. His ability to think out of the box, his dedication to research have provided inspiration whenever needed.

I would also like to thank my committee members, Dr. Richard Cairncross, Dr. Shivanthi Anandan, Dr. Jennifer Quinlan and Dr. Cameron Abrams for their valuable insights, input and guidance. Additional thanks to Dr. Margaret Wheatley for her guidance.

Special thanks are in order for the lab members and who have helped with learning and understanding several techniques and equipments and for their camaraderie; these are: Dr. Gossett Campbell, Dr. David Maraldo, Dr. Kishan Rijal, Dr. Angela Leung, David deLesdernier, Dr. Sen Xu, Pranam Shetty, Dr. Ramji Lakshmanan, Dr. Yanjun Ding, Blake Johnson and Ruben Rosario. Special thanks to Dan ve Luu for all his help.

My friends at graduate school have made the journey enjoyable and have given me some of my best memories till date. I thank Dr. Ranjita Bose, Vishesh Singh, Dr. Kevin McPeak, Dr. Michael Walters, Harsha Kotthapalli, Dr. Eleanor Small, Dr. Vamshi Gangupomu, Dr. Chetana Sunkari, Siamak Nejati, and Megan Hums.

Finally, I would like to thank my parents, Mr. Pradipkumar Sharma and Mrs. Minaxi Sharma, and my brother Dr. Parth Sharma for their constant love, support and strength that made this possible.

Table of Contents

List of Tables

List of Figures

Abstract

Novel Cantilever Sensor for Antibody-based and *hly*A gene-based Sensitive Detection of Foodborne Pathogen: *Listeria monocytogenes*

Harsh P. Sharma

Raj Mutharasan, Ph. D., Advisor

The objectives of this research can be broadly categorized as: 1) Cantilever sensor design and characteristics, 2) Improved surface chemistry for immobilization of recognition molecules and 3) Sensing of contaminants in food and cell-culture matrix.

A novel asymmetrically anchored piezoelectric millimeter-sized cantilever (aPEMC) design was developed. The new cantilever design is simpler and has lesser fabrication variables that improved the reproducibility of these devices. The sensor design was corroborated and characterized using finite element modeling and these were shown to be highly sensitive (~1 fg/Hz) via molecular chemisorption studies. The importance of the binding strength between the sensor and the added mass was shown to govern the type of resonance frequency change exhibited by the cantilever sensors and the high-order resonance oscillation modes were characterized by comparing responses to that quartz crystal microbalance (QCM) and finite element modeling.

A novel and dry method for grafting reactive amine groups on polyurethane surfaces using pulsed-plasma generation of ammonia gas was demonstrated. Grafting of amine groups was corroborated by FTIR studies and SEM micrographs in addition to the

cantilever sensor responses to protein immobilization. A method using tris(2-carboxyethyl)phosphine (TCEP) to reduce the disulfide bridges in antibody molecules, without affecting the antigen binding activity, to expose their native thiol groups for immobilization of gold surfaces was developed. The half antibody fragments were shown to improve the detection sensitivity of QCM biosensors without loss of selectivity.

Piezoelectric millimeter-sized cantilever (PEMC) sensors were used to demonstrate detection of cell-culture mycoplasmas in buffer and cell-culture matrix at 10^3 CFU/mL. The detection responses were confirmed by using a second antibody binding step, much like ELISA sandwich format. aPEMC sensors were used to show detection of foodborne pathogen, *Listeria monocytogenes* (LM), in buffer and milk at concentration of 10^3/mL. The detection sensitivity was limited by commercially available low-avidity antibody. The single copy, virulence *hly*A gene of LM was used to design a DNA probe that was used to detect genomic DNA extracted from LM in the presence of ~10^4 times higher non-target genomic DNA. Detection of genomic DNA equivalent to 7×10^2 LM was achieved within ~90 min.

Chapter 1 . Introduction

1.1. Background

Infectious diseases cause about 40% of the approximate 50 million deaths annually worldwide.[1] Foodborne infections in the United States alone have been estimated to cause ~76 million illnesses, more than 300,000 hospitalizations and 5000 deaths each year.[2, 3] Culture and plating techniques are still considered as the gold standard for detection of food-borne pathogens. These techniques are sensitive, selective and can also be used for quantification purposes but need trained personnel and can take upto 7 days to yield results. The commercial biosensors as well as myriad of newly developed detection and sensing methods such as Enzyme linked immunosorption assay (ELISA), Multi-photon Detection (MPD) coupled with immuno-sensing (IA-MPD), polymerase chain reaction (PCR) and Surface Plasmon Resonance (SPR) have been developed to improve upon the time to results (TTR) .

The methods such as ELISA[4]and IA-MPD[5] are very sensitive but require skilled technicians to properly implement the multi-step technique, SPR[6], [7] faces problems of low detection sensitivity and compromised selectivity and the PCR based techniques involve the high cost of operation to amplify the signal and also the need of trained personnel to operate the machine.

To be practical, a biosensor has to be an easy to use device that is sensitive, robust and must possess a high level of specificity. In addition to this, the time to results (TTR) must be on the order of minutes to improve upon the conventional plating techniques and the more recently developed novel detection techniques.

Developing robust biosensors for food-borne pathogens with low detection sensitivities and rapid TTR will enable early detection of contaminated foods before they reach the market and infect the masses.

1.2. Research Aims

The work presented in this thesis is presented as results of the investigations towards three broad research aims. These research aims along with the specific investigations are as follows:

1.2.1. Sensor design and response characteristics

The piezoelectric excited millimeter-sized cantilever (PEMC) sensors developed and investigated so far are composites, where a piezoelectric layer is bonded with a non-piezoelectric layer to induce out-of-plane oscillations when externally excited. The fabrication of these sensors involves multiple steps and variables. The need to develop a sensor with lesser fabrication steps and variables while maintaining the mass-change sensitivity was addressed.

The effect of interaction between the cantilever sensor surface and the deposited mass on the sensor response has not been thoroughly investigated. The effect of the adhesion strength between the deposited mass and the sensor on the frequency response it exhibits was studied.

The specific objectives are:

1. Investigate and develop new sensor designs with simpler fabrication steps that can help make the device reproducible as well as sensitive.
2. Characterize the piezoelectric cantilever response with respect to the strength of adhesion between the sensor and the added mass.
3. Can we understand the type of oscillation exhibited by the higher-order modes of the composite design PEMC sensor?

1.2.2. Improved surface chemistry methods

Most immobilization protocols involve wet-chemistry methods to develop surface functional groups. a pulsed-plasma based, simple, rapid and dry method for grafting amine groups on sensor surfaces for immobilization of recognition molecules was developed.

Oriented immobilization of antibodies increases the available binding sites exposed to the target. Proteins with affinity for certain antibody classes are commonly used to achieve this goal on gold-coated sensors. The amount of antibody immobilization thus depends on the amount of such proteins present on the sensor and it is an additional step that should be avoided, if possible, to simply the method. A rapid and simple method for reduction of disulfide bridges in the antibody molecules was developed. The antibody fragments thus formed were used for detection experiments and improvement in sensor response was demonstrated.

The specific objectives are:

1. Can we develop a simple and dry pulsed-plasma based method fo grafting reactive amine groups on polyurethane surfaces using ammonia gas for immobilization of the recognition molecules?
2. Can we use the native thiol groups present in the antibodies for direct immobilization with proper orientation of the antigen binding regions? Does this method improve device sensitivity?

1.2.3. Sensing applications for the cantilever sensors

Outbreaks of listeriolysis caused by the presence of LM in milk and milk products have caused great concern to the dairy industries due to ~30% mortality rate.[8, 9] Immuno-compromised individuals, such as pregnant women, new-borns and elderly people are more susceptible to listeriolysis. A small infectious dose and ability to survive and grow make this especially dangerous pathogen. A commercial low-avidity antibody limited the detection of *Listeria monocytogenes* to ~100 cells/mL using novel cantilever biosensors whereas *hly*A gene-based detection of the genomic DNA of the pathogen at concentration equivalent to 7×10^3 cells were demonstrated within ~ 90 min.

Most laboratories and industrial bioreactors are often infected by mycoplasmas and detection at low concentrations is not possible using the conventional techniques. Detection of low concentration mycoplasmas in cell-culture medium was demonstrated using cantilever sensors with a 4 orders of magnitude improvement in detection limit over commercial ELISA kit.

The specific objectives are:

1. Rapid detection of mycoplasmas in buffer and cell-culture matrix at low concentrations and comparison with commercial ELISA kit.
2. Detection of foodborne pathogen *Listeria monocytogenes* in buffer and milk, as a food matrix, at 100 cells/mL within 60 min using a low avidity antibody
3. Detection of genomic DNA of *Listeria* using DNA probes designed to hybridize to the single copy of the virulence *hly*A gene.

1.3. Contributions

The main contributions of this research are:

1. It was shown for the first time that self-exciting and self-sensing piezoelectric cantilevers consisting only of lead zirconate titanate (PZT) measure resonance only if they are asymmetrically anchored. Symmetric-anchoring did not give rise to electrically measurable bending resonant modes in the 0-100 kHz range. Sensitivity of first and second bending mode resonances was characterized in a flow apparatus using small density changes in liquid (0.003 to 0.01 g/cm^3) and by dodecanethiol chemisorption at 30 pM. Density change results were consistent with existing models of submerged cantilevers, and yielded mass-change sensitivity of ~33 ng/Hz and 217 pg/Hz for the first two modes. In chemisorption experiments, where binding was localized to 1 mm^2 distal tip of the PZT

cantilever, sensitivity improved by an order of magnitude to 2 pg/Hz and 414 fg/Hz for the same two resonant modes.

This is a collaborative work and my contributions are specified in the beginning of Chapter 3. This work has been published: **H. Sharma**, R.S. Lakshmanan, B.N. Johnson, R. Mutharasan, Piezoelectric cantilever sensors with asymmetric anchor exhibit picogram sensitivity in liquids, Sensors and Actuators B: Chemical, 153(2011) 64-70.

We also fabricated novel cantilever designs that express torsional and lateral modes that exhibited excellent mass-change sensitivity to molecular self-assembly on gold (75 – 135 fg/Hz) which was superior to that of widely investigated bending modes. Lead zirconate titanate (PZT) millimeter-sized cantilevers were designed with two types of anchor asymmetry that induced expression of either torsional or lateral modes in the 0 – 80 kHz frequency range. Experiments, analytical models, and finite element simulations show that anchor asymmetry enables resonant mode impedance-coupling. The sensitive torsional and lateral modes enabled measurement of self-assembled monolayer formation rate. The anchor design principle was extended to micro-cantilevers via finite element simulations, which caused 97 % sensitivity improvement relative to conventional designs and created new non-classical resonant mode shapes.

This is a collaborative work and my contributions are specified in the beginning of Chapter 4. This work has been submitted for publication: B. N. Johnson, **H. Sharma**, R. Mutharasan, Torsional and Lateral Resonant Modes of

Cantilevers as Biosensors: Alternatives to Bending Modes, Analytical Chemistry (under review)

2. The response of resonant-mode cantilever sensors depends on the binding strength of analyte mass to the sensor surface. Comparison of cantilever response to attachment of three macro-sized pieces: quartz (300 µg and 600 µg, water contact angle (Φ)=10°), silanized quartz (300 µg, Φ=99°) and polytetrafluoroethylene (PTFE; 1.5 mg, Φ=85°), with water and ethanol films indicated that the resonance frequency decrease was larger for higher liquid surface tension and lower contact angle. For example, quartz piece (1×1×0.160 mm^3, L×W×H) weighing 300 µg caused a 1987±214 Hz(n=22) decrease in the resonance frequency with a water film while the hydrophobic silanized quartz caused a significantly lower frequency shift of 1218±187Hz(n=22).

   The results of this study are presented in Chapter 5 and were published: **H. Sharma**, R. Mutharasan, Adhesion determines resonance response of piezoelectric cantilever sensors, Applied Physics Letters, 98(2011) 114101-3.

3. Characterization of the type of oscillation exhibited by the higher-order resonance mode of the composite PEMC design as having a shear component, similar to a quartz crystal microbalance (QCM) was demonstrated. For various binding strengths and various masses, the fundamental modes decreased in resonance frequency. For the same mass addition experiments on the high-order modes of

PEMC sensors, anomalous increase in resonance frequency was observed and is the subject of this report. For cantilever sensors manifesting a high-order resonance mode with a shear-type oscillation, the expectation of decrease in resonance frequency for increase in mass is experimentally shown not to be true.

The results of this work are presented in Chapter 6 and are to be submitted for publication: **H. Sharma**, R. Mutharasan, Anomalous behavior of high-order resonance mode in cantilever sensors, Applied Physics Letters (to be submitted)

4. Reliable surface chemistry is necessary for immobilization of biological recognition molecules on sensor surfaces. A dry and rapid method of pulsed-plasma assisted grafting of amine surface functional groups, using ammonia gas on polyurethane surfaces is successfully demonstrated by using pulse cycle times of 1s-180s (on-off). One cycle of plasma treatment was found to generate higher amine groups as they tend to degrade upon longer exposure to the high-energy radicals. Successful amination of the polyurethane surfaces was demonstrated by Fourier transform infrared spectroscopy (FTIR). To establish the availability of the surface amine groups for reaction, 1 μm carboxylated polybeads were reacted to polyurethane-coated piezo-electric excited millimeter-sized cantilever (PEMC) sensors before and after plasma treatment. Scanning electron microscope micrographs of PEMC sensors exposed to the same concentration of beads show more than four-fold increase in the presence of beads post pulsed-plasma

treatment. Application of this method for protein immobilization was established by BSA chemisorption on plasma treated PEMC sensors.

The results of this work are presented in Chapter 7 and were published: **H. Sharma**, R. Mutharasan, A novel pulsed-plasma approach for protein immobilization by grafting reactive amine groups on polyurethane-coated biosensors, Sensors and Actuators B: Chemical, 173(2012) 569-74.

5. It was shown for the first time that half antibody fragments containing the *E.coli* O157:H7 antigen binding region give a larger response with shear-mode resonating mass sensors. Tris(2-carboxyethyl)phosphine (TCEP) was used to reduce the disulfide bridges in antibodies to cleave them into two half antibody fragments, while preserving the antigen- binding region. Cleavage exposes the native thiol group in the antibody that readily chemisorb on gold surfaces with proper orientation for immobilized antibody to bind to its antigen. Comparing responses obtained on a quartz crystal microbalance for the detection of pathogenic *E.coli* O157:H7 using TCEP-reduced antibody fragments with conventional antibody immobilization protocols showed that the proposed method enhances device sensitivity. Examining the half antibody fragments for detection of target cells in the presence of non-target *E.coli* JM 101 showed that the fragments retain their specific antigen binding capability without loss of selectivity upon reduction by TCEP.

   The results of this study are presented in Chapter 8 will be submitted for publication: **H. Sharma**, R. Mutharasan, Half antibody fragments improve

biosensor sensitivity without loss of selectivity, Analytical Chemistry (to be submitted)

6. We reported a new biosensor-based method that is more sensitive and rapid than the current approach for detecting mycoplasma in cell culture samples. Piezoelectric-excited millimeter-sized cantilever (PEMC) sensors respond to mass change via resonant frequency change. They are sensitive at femtogram level, and can be used directly in liquid for label-free detection. Common cell culture contaminant, *Acholeplasma laidlawii* was detected in both buffer and cell culture medium. Two different sources (positive control from a commercial kit and ATCC 23206) were analyzed using antibody-immobilized PEMC sensor. Resonant frequency decrease caused by binding of *A. laidlawii* was monitored in real-time using an impedance analyzer. Positive detection was confirmed by a second antibody binding. The limit of detection (LOD) was lower than 10^3 CFU/mL in cell culture medium using PEMC sensor while parallel ELISA assays showed LOD as 10^7 CFU/mL. This study shows PEMC sensor can be used for sensitive and rapid mycoplasma detection in cell culture samples.

   This is a collaborative work and my contributions are mentioned in the beginning of Chapter 9 and were published: S. Xu, **H. Sharma**, R. Mutharasan, Sensitive and selective detection of mycoplasma in cell culture samples using cantilever sensors, Biotechnology and Bioengineering, 105(2010) 1069-77.

7. *Listeria monocytogenes* (LM), an important food-borne pathogen that has a high mortality rate (~30%), was successfully detected within an hour at the infectious dose limit of 10^3 /mL, both in buffer and milk. LM detection was demonstrated using a highly sensitive (~28 Hz/pg), novel asymmetrically anchored cantilever sensor and a commercially available antibody. Sensor responses were confirmed using a secondary antibody binding step, similar to the sandwich ELISA assays, as a means of signal amplification that also reduced the occurrence of false negatives. Detection of LM at a concentrations of 10^2/mL was achieved, by incorporating a third antibody binding step, which is an order of magnitude smaller than the infectious dose (< 1000 cells) for LM. The commercially available antibody for LM used in this work is shown to have low avidity which partially explains the relatively low sensitivity reported for LM as compared to other pathogens.

   The results of this work are presented in Chapter 10 and are under review for publication: **H. Sharma**, R. Mutharasan, Rapid and sensitive immunodetection of *Listeria monocytogenes* in milk using a novel piezoelectric cantilever sensor, Biosensors and Bioelectronics (under revision)

8. Piezoelectric cantilever sensors are shown to exhibit sensitive and selective detection of based on a specific identifying gene from genomic extract at 10^2-10^3 cells of foodborne pathogen, *Listeria monocytogenes* (LM). A probe designed for the virulence hemolysin gene, *hly*A, was immobilized on the gold-coated sensor and hybridization detection of a synthetic target (based on

the *hly*A sequence) is shown that spans over 6 orders of magnitude in concentration. Hybridization response was confirmed using two methods: 1) the use of a fluorescent indicator for the presence of double-stranded DNA (ds-DNA) and 2) hybridization response of a secondary single-strand DNA (ss-DNA) to the target much like in the ELISA sandwich format. Hybridization of the secondary ss-DNA tagged to gold nanoparticles amplified as well as confirmed the target hybridization to the *hly*A probe on the sensor. Genomic DNA from LM was extracted, sheared and melted and was exposed to the *hly*A probe on the sensor in proteinous background with and without the presence of up to 10^4 times excess non-target genomic DNA extracted from *E.coli* JM 101 (EC), for the gene-specific detection of LM. Discernable detection limit of 7×10^2 LM cells (equivalent genomic DNA) was achieved in proteinous background. The detection limit deteriorated to 7×10^3 LM in the presence of genomic DNA from EC. Hybridization response times were within ~90 min, thus significantly improving over the conventional detection techniques in terms of detection time with comparable detection limit.

The results of this work are presented in Chapter 11 and will be submitted for publication: **H. Sharma**, R. Mutharasan, *hly*A gene-based sensitive detection of *Listeria monocytogenes* using a novel cantilever sensor, Analytical Chemistry (to be submitted)

1.4. References

[1] D. Ivnitski, I. Abdel-Hamid, P. Atanasov, E. Wilkins, Biosensors for detection of pathogenic bacteria, Biosens Bioelectron, 14(1999) 599-624.

[2] P.S. Mead, L. Slutsker, V. Dietz, L.F. McCaig, J.S.Bresee, C. Shapiro, et al., **Food-Related Illness and Death in the United States**, Emerging Infectious Diseases, 5(1999) 607-25.

[3] S.P. Oliver, D.A. Patel, T.R. Callaway, M.E. Torrence, ASAS Centennial Paper: Developments and future outlook for preharvest food safety, J Anim Sci, 87(2009) 419-37.

[4] N.L. Rosi, C.A. Mirkin, Nanostructures in Biodiagnostics, Chem Rev, 105(2005) 1547-62.

[5] A.K. Drukier, N. Ossetrova, E. Schors, L.R. Brown, J. Tomaszewski, R. Sainsbury, et al., Ultra-Sensitive Immunoassays Using Multi-Photon-Detection in Diagnostic Proteomics of Blood, J Proteome Res, 4(2005) 2375-8.

[6] B. Liedberg, I. Lundstrom, E. Stenberg, Principles of biosensing with an extended coupling matrix and surface plasmon resonance, Sensors and Actuators B: Chemical, 11(1993) 63-72.

[7] J. Melendez, R. Carr, D.U. Bartholomew, K. Kukanskis, J. Elkind, S. Yee, et al., A commercial solution for surface plasmon sensing, Sensors and Actuators B: Chemical, 35(1996) 212-6.

[8] M.W. Griffiths, Listeria monocytogenes: Its importance in the dairy industry, J Sci Food Agric, 47(1989) 133-58.

[9] C.W. Donnelly, Detection and Isolation of *Listeria monocytogenes* from Food Samples: Implications of Sublethal Injury, J AOAC Intl, 85(2002) 495-500

Chapter 2 . Review of Biosensors for Foodborne Pathogens

2.1. Introduction

Infectious diseases cause about 40% of the approximate 50 million deaths annually worldwide. [1] Foodborne infections in the United States alone have been estimated to cause ~76 million illnesses, more than 300,000 hospitalizations and 5000 deaths each year.[2, 3] Recent *Salmonella* outbreak in 2007 affected consumers in 44 states, and is considered one of the larger case of foodborne disease in recent history. Over 1400 cases of serious illness were reported as of August 2007.[4] According to the investigation carried out by the U.S. Food and Drug Administration (FDA) for human *Salmonella* serotype Saintpaul infections, it is believed that Jalapeno pepper and tomatoes were the carriers of the pathogen. This recent incident highlights the need for rapid, selective and easy-to-use testing of food substances for pathogens and toxins of bacterial and fungal origin that can be used in a practical environment. This review examines current conventional methods and the emerging biosensor methods for detecting bacterial pathogens and toxins, with a focus on food.

2.2. Common Foodborne Pathogens

The most common foodborne infections are those caused by the bacteria *E. coli* O157:H7, *Salmonellae*, *Listeria monocytogenes* and *Campylobacter jejuni* and by the calicivirus, also called Norwalk viruses. In this review we will focus on the biosensor

detection methods reported for these species. A more comprehensive list of pathogens may be found at FDA website.[5]

E. coli O157:H7 is a bacterial pathogen that is commonly found in the intestinal tracts in cattle and is carried over to the consumers via ground beef. Ingestion of the bacteria causes severe and bloody diarrhea and painful abdominal cramps. In a small number of cases, a complication called hemolytic uremic syndrome (HUS) can occur which can cause profuse bleeding, and kidney failure. The current policy of the United States Department of Agriculture—Food Safety and Inspection Service (USDA-FSIS) towards *E. coli* O157:H7 is zero tolerance, which means absence of the pathogen is to be demonstrated using a well-defined sampling plan and measurement method articulated by USDA-FSIS.[6] The current limit of detection by the approved USDA-FSIS method is 1 CFU per 65 g sample of meat. Emphasis is not on enumeration, but rather on the presence and identification of the pathogen.

Campylobacter jejuni is a gram-negative, spiral, microaerophilic bacteria. It has now been identified as one of the main causes of bacterial foodborne diseases in the USA.[7] Along with *Campylobacter jejuni*, *Campylobacter coli* cause fever, diarrhea, and abdominal cramps and gastroenteritis in humans. *C. jejuni* can lead to the development of Guillian-Barre Syndrome (GBS), a disorder of the peripheral nervous system often leading to partial paralysis.[8] The food matrixes that act as carriers for *C. jejuni* are poultry, meat and milk. *Campylobacter* is thermo-tolerant and can survive and grow at 40^{o}C. These bacteria live in the intestines of chicken, and are often carried over with raw poultry. Eating undercooked chicken is the most frequent source of infection.

Salmonella is a bacterium that is often found in the intestines of chickens. It also affects the ovaries of healthy-looking hens which lead to presence of this microbe in raw eggs. The illness caused is salmonellosis and manifests as fever, diarrhea and abdominal cramps. Salmonellosis can spread from the intestines to the blood stream and then to other parts of the body resulting in life-threatening infections in patients who are in poor health or weakened immune systems, and has been known to be fatal. Among the over 2000 serovars that have been identified and characterized, S. Enteritidis and S. Typhimurium are the epidemiologically the most important ones because they are the causative agent in 80% of all human infections reported word wide.

Calicivirus which includes Norovirus is an RNA virus that causes nausea, vomiting, diarrhea, and abdominal pain with headache and low-grade fever. Its infection is usually self limiting and resolves in a few days. Unlike many foodborne bacterial pathogens described that are of animal origin, calicivirus is spread primarily from infected persons. Infected food handlers can contaminate food which becomes the carrier.

Toxins produced by the pathogens are also contaminants that are to be monitored for assuring food safety. Some are produced by the pathogens identified above while others are produced by common organisms. The conditions under which the toxins are expressed is not well understood. Common bacterium, *Staphylococcus aureus*, grows on food substances and produces enterotoxins such as Staphylococcal enterotoxin A and B that have super-antigenic activities and cause a form of food poisoning. *E. coli* O157:H7 produces shiga-like toxin 1 and 2 that cause dysentery, hemorrhagic colitis, and hemolytic uremic syndrome. *Listeria monocytogenes* produces an exotoxin called

lysteriolysin O that has hemolysin functionality. Many of these toxins are heat stable and survive common food heating methods and persist in their active form.

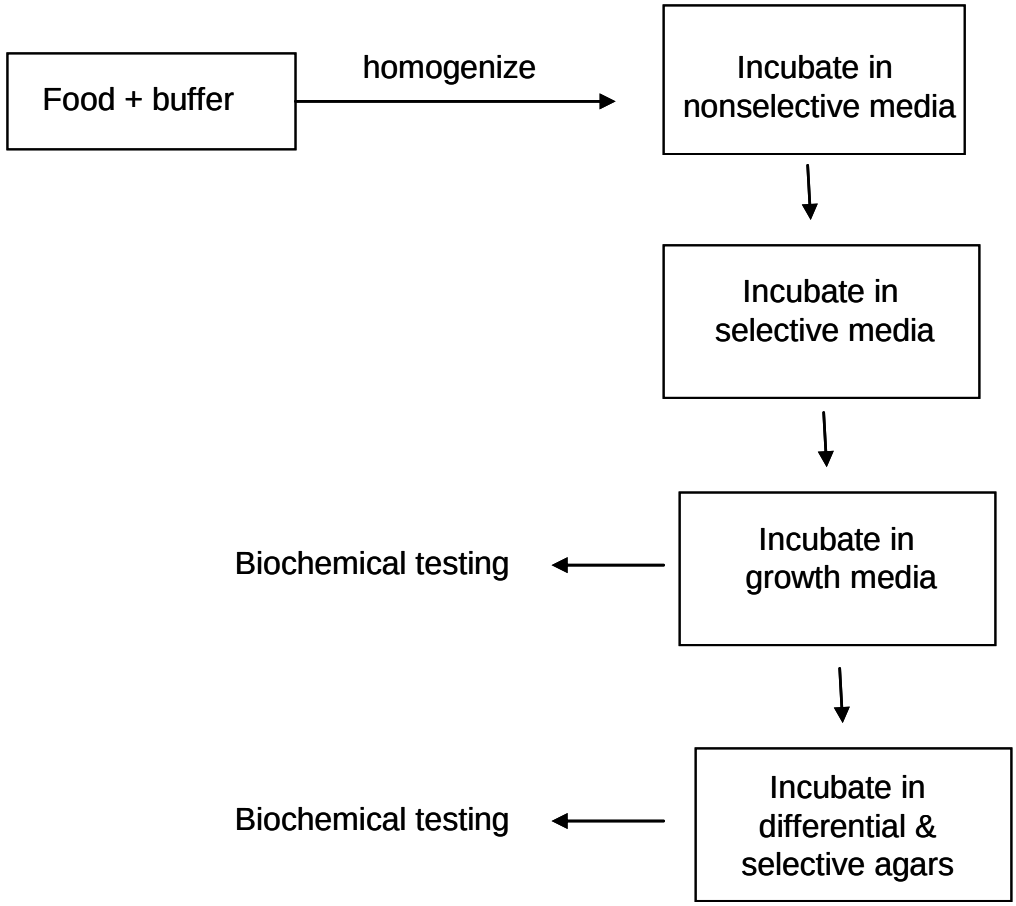

Figure 2-1 Schematic of the culture and plating methods. The contaminated matrix is homogenized to be cultured in non-selective medium for growth if the starting concentration of the pathogens is not high. It is then grown on a selective medium for separation of the target antigen followed by various biochemical tests to ensure the presence of the target.

2.3. Conventional Microbiological Methods

Conventional methods are briefly noted here for c ompleteness and are not critically reviewed. A fairly comprehensive review is available from reference[9]. Conventional methods involve culture enrichment by growth on a nutrient rich medium which supports growth of all viable organisms, and is followed by growth on single or multiple sequential selective media that supports preferably the growth of target pathogen. In Figure 1, a generic approach used in microbial testing is illustrated. The culture and plating techniques are sensitive, inexpensive (~$8 - $12 per assay) and can be designed to be quantitative. However, they are laborious and time-wise lengthy. For example, the method for *Listeria monocytogenes* outlined by the international reference method NF EN ISO 11290-1 and 11290-2 requires 3- 7 days for obtaining results, and is not considered to be highly sensitive[10]. Additionally some microbes may enter a state of viable dormancy but not culturable (VBNC) which can subsequently lead to underestimation of the pathogen and yield false negatives.[11] Identification is carried out by an antibody-based approach or polymerase chain reaction (PCR) of unique and identifying genes. [9, 11] Although antibody-based detection methods can provide fairly accurate and reliable results, there is an increasing trend of adopting DNA-based tests. DNA-based methods provide a more highly stringent means of identifying the pathogen; for a detailed discussion see reference[12]. Most current DNA-based methods rely on PCR which uses a thermo-stable polymerase enzyme to amplify identifying target DNA or RNA for detection using labeled probes.

Table 2-1 Typical detection sensitivities reported in food and related matrixes using conventional plating techniques.

Detection Technique	Pathogen	Sample Matrix	Analysis Time	Detection Limit (cfu/ml)	Reference
ELISA	*E.coli* O157:H7	ground beef	~24 h	10^3	[14]
PCR-ELISA		milk	5 h	10^3	[122]
RT-PCR		culture medium	~6h	<500 cells/ml	[123]
		ground beef	~4 h	10^3 cells/g	
RT-PCR coupled to fluorescence		drinking water	~6 h	10^2	[124]
IMS-ELISA	*Salmonella*	raw chicken	24 h	10	[125]
Electrochemical sandwich ELISA		meat	~20 h	10 cells/25 g	[65]
PCR-ELISA		milk	24 h	10^3	[126]
PCR	*Listeria monocytogenes*	beef	24 h	10^3 cfu/g	[127]
RT- PCR		salad	~20 h	10^3	[60]
ELISA	*Campylobacter jejuni*	bovine vaginal mucus	5 days	10^5	[128]
RT-PCR-IMS		chicken feces	4 h	10^2	[129]

PCR is not free of disadvantages such as cost, lack of portability and the requirement of labeled reagents. More importantly, significant loss of sensitivity in detection occurs when the sample is in complex background, as in food matrixes. Nucleic acid-based detection is more specific and sensitive than the antibody-based detection schemes. However, the latter can be more rapid, less expensive and have the ability to detect not only the pathogen but also the food toxins.[13] Common reaction volume for PCR reactions is 50µl. The sensitivity of PCR is determined as number of copies of target DNA strand per reaction volume. If the sensitivity is reported as 10 copies per reaction volume, it converts to an effective concentration of 200 cells/ml in sample when a single gene is used for detection. Such a concentration often exceeds infective dosage. Therefore, for effective PCR application analyte would have to be concentrated from a sample volume of several hundred milliliters prior to analysis.

In Table 1 we summarize the time to carry out analysis and detection sensitivity reported by conventional methods for detection of common foodborne pathogens. In all examples listed, an incubation step allowing growth of the target bacteria is followed by a detection step. For example in reference[14] in attempting to detect E. coli O157:H7, the authors inoculated *E. coli* O157-negative ground beef, and then incubated the beef sample at 42°C for 24 h. in a growth medium, and the ELISA assay was carried out with the 24-h sample. It is a common practice in the field to report measurement sensitivity as the cell concentration in sample prior to incubation, and not the concentration at the time ELISA assay is carried out. On the other hand most, if not all, biosensor results in the literature is reported based on the sample concentration exposed to the sensor. The

reader should be aware of this important difference in the way sensitivity is reported by the group of researchers.

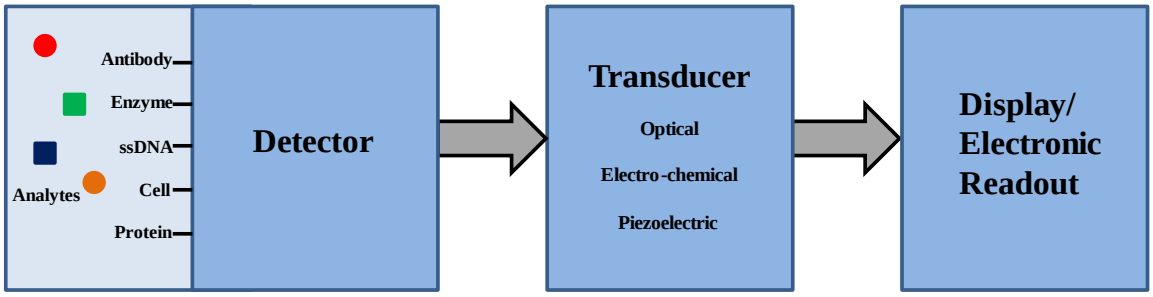

Figure 2-2 Schematic of a biosensor. The three main parts of the biosensor are: 1) detector that has the recognition molecules and interacts with the target antigen to produce a signal, 2) transducer that converts the signal received from the detector to a useful electronic output and 3) the display or readout system to record the response.

2.4. Definition of a biosensor

Biosensors are defined as an analytical device that integrates a biologically derived molecular recognition molecule such as antibodies, phages, aptamers or single-stranded DNA, with a suitable physicochemical transducing mechanism. Common transducing elements are optical, electrochemical, thermometric, piezoelectric, magnetic and others.[15] Biosensors produce an electronic or optical signal proportional to the

specific interaction between the analyte and the recognition molecule present on the biosensor.[16] Biosensors transform biological interactions into electronic signals that can be conveniently measured and recorded. Biosensors can detect a wide range of targets from small protein molecules to large pathogens. Compared to the conventional methods, a biosensor is a device for the detection of pathogenic antigens and does not require highly trained personnel for using it. Further, if a biosensor is highly sensitive and selective it can provide results more rapidly than culture-based methods making them ideal for practical and field applications. A schematic of biosensors is shown in Figure 2.

Desired characteristics of biosensors, summarized in Table 2, include accuracy, near real-time assay, sensitivity, specificity, reproducibility, robustness and ease of use. The number of false-positive and false-negative results of a biosensor should be very low, ideally zero, for it to be an acceptable practical device. Assay times less than 1 h are desirable since that is the essential characteristic that differentiates biosensors from conventional methods. Sensitive sensors are a must for the food industry since any false-negative result can lead to an expensive recall and the loss of public confidence. Similarly false positives will increase cost to the manufacturer, and ultimately to the consumer. Quantitative and reproducible sensor responses are highly desirable. These sensors should be mechanically and biochemically stable and robust. Lastly they should be easy to use so that high level of training and skilled personnel would not be required.

Table 2-2 Requirements of a microbial biosensor

Property	Desired Characteristics
Accuracy	No or low false-positive and false-negative results
Assay time	Near real-time response desired (< 1h desirable)
Sensitivity	False-negatives can be catastrophic
Specificity	Discriminate between the target organism or toxin and other organisms (often 1 in 10^6 required)
Reproduciblity	Measured reproducibility within 10% and should be easy to calibrate
Robustness	Both mechanical and chemical stability are required
Ease of use	Should be automated and require minimal operator skills
Compatible interface	Should be compatible with the transduction principle and resist non-specific binding
Validation	Should be evaluated against current standard techniques and a LOD obtained.

2.5. Types of Biosensors

In this paper, we divide the reported biosensors on the basis of transduction mechanism used. All biosensors use a recognition molecule such as an antibody for detecting specific targets. Among the many transduction methods investigated, three mechanisms dominate the research literature. These are optical, electrochemical and piezoelectric devices. Therefore we limit the scope of the review to these three mechanisms in this paper. After describing the transduction mechanisms application

examples of foodborne pathogen detection is presented. Although these biosensors can potentially be used for other biological applications, the examples discussed have been limited to foodborne agents.

2.5.1 Optical biosensors

Majority of the biosensors used for detection of foodborne pathogens and toxins in research laboratories and industry use optical transduction. The sensor signals are versatile because they can be used directly or amplified for detection in conjunction with other techniques. Of the various optical techniques investigated, we focus on two common methods, namely surface plasmon resonance (SPR) and evanescent field optical fiber biosensors. Several commercials instruments using SPR are available from companies such as BIAcore [17] and Biosensing Intruments Inc.[18] Research International has commercialized an evanescent field fiber optic biosensor, RAPTOR^{TM}.

Surface Plasmon Resonance

SPR is an optical phenomenon where a p-polarized light beam satisfies the resonance condition by exciting electrons and generating an electron density wave known as surface plasmon wave (SPW). The geometry for a SPR sensor is a noble metal, usually gold, coated onto a dielectric material, such as quartz. Figure 3A depicts the geometry, optical path and signal transduction mechanism in SPR sensors. An evanescent electromagnetic field is generated at the metal-dielectric interface and propagates into the ambient medium. Since the evanescent field diminishes exponentially from the surface, SPR detects only surface-confined interactions.[19, 20] When SPR occurs, the intensity

of reflected light is greatly reduced. The wavelength or angle at which resonance occurs depends on the refractive index of the layer adjacent to the metal layer. Shifts in resonance can be monitored by changes in reflected angle, wavelength, or reflection intensity changes. From the resonance angle or wavelength one can obtain the refractive index(RI) of the interface.[21] The most popular and commercially available configuration for SPR is the Krestchmann configuration (see Figure 3A), which consists of a metallic layer deposited on the base of a quartz prism. More recently, tapered fiber geometry has been used for SPR-based sensing.[22] Low cost, small size and potential multichannel and remote sensing are some of the advantages of the fiber-based SPR sensors.

Commercial SPR instruments have a detection limit of 10^5 cells/ml for *Listeria monocytogenes*.[23] Using the amplification step of exposing the antigen bound on the sensor to a second polyclonal antibody specific to the pathogen, Taylor et al[24] established a limit of detection of ~10^5 cfu/ml in PBS for each of the four pathogens, *E. coli* O157:H7, *Listeria monocytogenes*, *Campylobacter jejuni*, and *Salmonella* Typhimurium. The limit of detection did not deteriorate for these four pathogens when they were present simultaneously in apple juice matrix. Following the same sandwich assay on an SPR sensor, the specificity of the assay for *Staphylococcus aureus* showed a detection limit of 10^5 cell/ml in a background containing non-target *E. coli* O157:H7. However the sensitivity of the sensor decreased when non-target concentration was greater than 10^2 cfu/ml.[25]

Table 2-3 SPR sensors for detection of foodborne pathogens and toxins

Target	Sample Matrix	Analysis Time	Detection Limit[a] (cfu/ml)	Reference
E.coli O157:H7	Skim milk	< 45 min	25	[130, 131]
Salmonella Enteritidis	Skim milk	<45 min	23	[131]
Salmonella Typhimurium	PBS with background of five non-target pathogens	NA	10^2	[132]
	Chicken carcass wash	~ 3 min	10^6	[133]
Listeria monocytogenes	HEPES buffer	~2 h	10^5	[134]
SEB	Phosphate buffer	10 min	10 ng/ml	[27]

In Table 3 we summarize the various pathogens that have been measured using SPR sensors in various matrixes. SPR biosensors showed sensitivities that were comparable to enzyme-linked immunosorption assay (ELISA).[26] Detection of Staphylococcus enterotoxin B (SEB) using a fiber-optic SPR biosensor at concentration of 10 ng/ml in 10 min has been demonstrated [27]; see Figure 3A2. Lower detection limit of 0.5 ng/ml was achieved in milk matrix.[28] The commercially available low-cost SPREETA^{TM} SPR biosensor was compared to a bulk acoustic wave sensor (discussed in **4.3**) for detecting an *E. coli* O157:H7 enterotoxin, *STX1* and a detection limit of ~300 pmol was reported.[29]

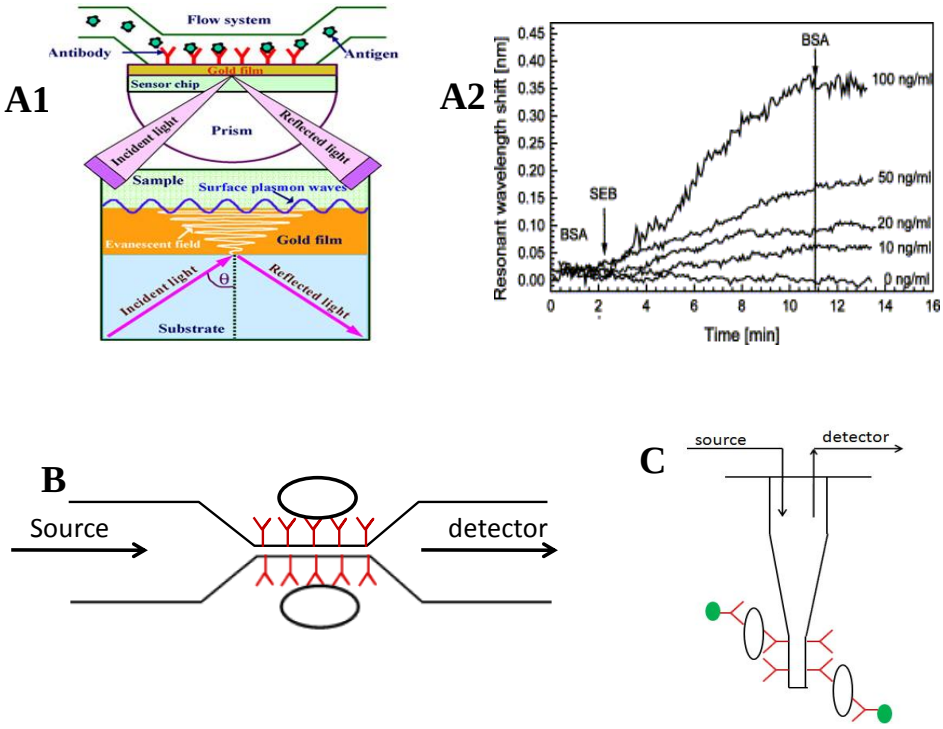

Figure 2-3 Schematic view of Optical Sensors. The geometries of different optical sensors is shown. **Panel A1.** Geometry and signal transduction mechanism of SPR sensors (reproduced from ref[19]). **Panel A2.** Response of a fiber-optic SPR biosensor to various concentrations of SEB in 5 µg/ml BSA in PBS at 50 µl/min flow rate. The arrows show the point of change of the flowing solution. Reproduced with permission from Reference [27]) **Panel B.** Geometry of a tapered fiber optic biosensor. Antibody is immobilized in the waist region where the evanescent field is largest due to smaller diameter compared to upstream fiber. Sensor response is obtained by measuring total light energy transmitted to the detector. **Panel C.** Geometry of tapered tip optical fiber biosensors. The distal end of the fiber may be flat and coated with a reflective material as shown in the diagram or the end is fabricated into a tip. The evanescent field is designed to excite the fluorescent-labeled antibody and the source and the emitted light couples back into the fiber and collect from the divergent section and transmitted to the detector.

Evanescent Field Fiber Optic Sensors

Fiber optic sensors respond to changes in the evanescent field arising from the alterations in refractive index that occur due to analyte binding. When the sensing surface of the fiber is prepared with specific recognition molecules, target analytes bind specifically to the modified surface. This causes modulation of refractive index at the surface leading to changes in the evanescent field resulting in changes in optical throughput. Geometric depiction of optical fiber sensors is shown in Figure 3B and C. Optical fibers exhibit minimal loss of light as the transmitted light undergoes total internal reflection in the core of the fiber. The propagating light has two components; namely, the guided field in the core and the exponentially decreasing evanescent field in the cladding. For evanescent field sensing, interaction of this evanescent field with the surroundings is important. This can be achieved by either removing or thinning down the cladding. Since the evanescent field dimensions are a few hundred nanometers, extremely small refractive index perturbations at the surface due to analyte binding can cause significant changes in the optical transmission. In a manner of speaking, evanescent field sensing samples the surface of the sensor, and not the entire sample volume.

Light propagation through an optical fiber can be described by the wave theory. The properties of light in the fiber core are determined by the number of modes *N*. In a multimode fiber, there is a one-to-one relationship between modes and angles of incidence. The number of modes is directly related to a dimensionless parameter known as the V-number, given as[30]:

$$V_{core} = (2\pi/\lambda)\rho\,[n^2_{core} - n^2_{clad}]^{1/2} \qquad (1)$$

where ρ is the radius of the core, λ is the wavelength of the light, n_{core} and n_{clad} are refractive index of the core and cladding, respectively. In a uniform diameter single mode fiber, the light propagates in single mode. However, if V changes along the fiber due to geometry or local RI changes, the single mode fiber may behave as a multimode fiber. The coupling of modes take place so that transmission occurs in multiple modes thereby increasing the evanescent portion of transmission. The increase in evanescent field increases the amount of light that interacts with surface immobilized molecules and forms the basis for detection.

Although various methods are available for increasing the evanescent field of Fiber-Optic Biosensors (FOBS), the most versatile method is the use of tapered geometry. There are two types of tapered fiber optical biosensor (TFOBS) geometries currently used in biosensing: tapered tips and continuous tapered fibers. These are further discussed below.

Tapered Tips

A schematic of a tapered tip fiber optic biosensor is shown in Figure 3C. A tapered tip consists of an optical fiber which gradually decreases in diameter until it becomes a micron-sized tip. The tip is used as the sensing element. The geometry of the tip makes it conducive to both launching of source light and collection of the response light for measurement. Tapered tips of various geometries such as step-etched, conical, and combination tapers have been investigated extensively for biochemical and clinical applications.[31-34]

The step-etched geometry is fabricated by immersing into hydrofluoric acid and it results in a chemically etched fiber tip with an abrupt decrease in diameter. This geometry has been reported to exhibit low sensitivity due to poor V-number match that leads to large power loss.[35, 36] The diameter of a conical tapered tip decreases continuously until it becomes a nanometer-radius tip and offers an improved optical design. The diameter of a combination tapered tip decreases in a nonlinear fashion, such that the V-number is matched continuously and results in very low signal loss.[35] The recognition molecule is immobilized on the taper surface in the smallest diameter region where the evanescent field is strongest.

Continuous Biconical Tapered Fibers

A continuous biconical taper, illustrated in Figure 3B, consists of three regions: a convergent region of decreasing diameter, a region of almost constant diameter called the waist, and a divergent region of increasing diameter.[37] The waist region is used for sensing because the evanescent field is at its maximum in the region of the smaller diameter. Changes in absorption, scattering, fluorescence, and resonance can occur in the waist region. The emission resulting from fluorescence, the transmitted and the scattered light are collected in the divergent region for detection purpose.[38]

The two major optical sensing mechanisms present in TFOBS are related to the intensity and absorption of light. The changes in the evanescent field caused by the binding analyte leads to changes in refractive index (RI). Intensity-based sensors were the earliest investigated and one of the most widely used to date.[39]

Table 2-4 TFOBS for foodborne pathogen and toxin detection

Target Analyte	LOD	Matrix	Taper Geometry	Fiber Type	Detection Principle	References
Staphylococcus aureus Protein A	1 ng/mL	Not described	Not described	Multimode	Fluorescent sandwich	[135]
Escherichia coli O157:H7	10-800*	buffer	Biconical taper	Multimode	Absorption	[49]
	70 cells/ mL	Buffer	Biconical taper	Single mode	Intensity	[37]
	1 cfu/ml	ground beef	Uniform	Multimode	Fluorescent sandwich	[51, 136]
Salmonella	50 cfu/g	irrigation water	Tapered tip	Multimode	Fluorescent sandwich assay	[53]
	10^4 cfu/ml	Hotdog	Tapered tip	Multimode	Fluorescent sandwich	[137]
	10^4 cfu/mL	Nutrient broth	Tapered tip	Multimode	Fluorescent sandwich	[54]
Staphylococcal Enterotoxin B (SEB)	0.5 ng/ml	Buffer, serum, urine, ham	Tapered tip	ND	Fluorescent sandwich	[138]
E. coli lipopolysaccharide endotoxin	10 ng/ml	Buffer and plasma	Combination tapered tip	ND	Fluorescent sandwich	[139]
Listeria monocytogenes	10^5 cfu/ml	Frankfurter	Tapered tip	Multimode	Fluorescent sandwich	[57]

Listeria monocytogenes	10^7 cfu/ml	Hotdog	Tapered tip	Multimode	Fluorescent sandwich	[56]
	10^3 cfu/ml	Buffer	Uniform	Multimode	Fluorescent sandwich	[55]

* = at inoculation

When light is transmitted through a tapered fiber the resulting evanescent field interacts with the analytes on the tapered surface causing the transmission to decrease if the analytes absorb at the transmission wavelength. The magnitude of the transmission decrease is in proportion to the analyte concentration. To use these tapers, the light source wavelength should be selected based on the analyte absorption spectra. Changes in the magnitude of the evanescent field are detected by measuring the changes in output power in a de-cladded uniform fiber or TFOBS. Geometric parameters dominate the performance of intensity-based sensors. Factors such as bending, radius, length, and taper ratio influence the sensitivity of an intensity-based TFOBS.[40] Bending of a tapered fiber increases the fraction of evanescent field in the sensing region, and therefore increases sensitivity.[39, 41-45] Similarly, the smaller radii are associated with higher sensitivity[43]. Longer fibers can be used to overcome a small penetration depth at short wavelength.[46] The tapered region in the distal end converts lower order modes to higher order modes that couple efficiently into the cladding. A ray model that relates

penetration depth to refractive indices, numerical aperture, taper ratio, length, launch angle, and position along the taper axis was reported in reference [47]. An optimum taper ratio (taper diameter/ fiber diameter) is necessary for sensitive response. When the taper ratio is large the evanescent wave is negligible, resulting in a poor sensor. On the other hand, if the it is too small the mode is so highly spread out that it tends towards a free-space wave which also results in low signals to the detector and thus a poor sensor.[48] Consequently, an optimum taper ratio is implicated and depends on the optical properties of sample medium surrounding the tapered region and the wavelength used.

Detection in buffer can easily be achieved with fiber optic biosensors. If non-target molecules are present in the target matrix they interfere with the recognition process by non-specifically binding to the recognition molecules. Several investigations are summarized in Table 4 that lists various types of optical fiber sensors investigated for detection of foodborne pathogens and toxins.

Detection applications of fiber-optic biosensors

An intensity-based evanescent sensor for the detection of *Escherichia coli O157:H7* growth[49] was fabricated by chemically etching a multimode fiber. Sensing was based on the attenuation of evanescent-field coupling due to the presence of bacteria. The power loss was proportional to the intrinsic bulk absorption and scattering, which depends on the concentration of the bacteria. Similarly, TFOBS were successfully used to detect the growth of a non pathogen *Escherichia coli JM 101*.[50] Tapered surface was coated with poly-L-lysine and *E.coli JM 101* were immobilized. Growth was monitored

by light transmission through the tapered fiber. The transmission decreased exponentially with cell growth. In a follow up study pathogenic *E. coli O157:H7* was detected using an antibody-immobilized TFOBS at concentrations as low as 70 cells/mL by measuring changes in intensity.[37] Using tip geometry, *Escherichia coli O157:H7* in seeded ground beef samples was detected by a sandwich immunoassay using a dye-labeled polyclonal anti-*E. Coli O157:H7*. Responses were obtained in 20 minutes, and concentrations at 3 to 30 cfu/ml were detected. Sensor was selective and showed no response to *Listeria monocytogenes, Salmonella* Typhimurium, and non-pathogenic *E. coli*. A similar study with a sandwich fluorescent antibody-based FOBS provided detection of *Escherichia coli O157:H7* in ground beef. The sensor detected 10^3 cfu/ml of *E. coli O157: H7* grown in culture broth. Detection of artificially inoculated *E. coli O157: H7* at concentration of 1 cfu/ml in ground beef required 4 hours of enrichment.[51]

Fluorescence resonance energy transfer (FRET) involves the non-radiative energy transfer from a fluorescent donor molecule to an acceptor molecule due to dipole-dipole interactions when the two are in close proximity. FRET principle was used with an optical fiber tip sensor for detecting *Salmonella* Typhimurium.[52] The antibody to *Salmonella* labeled with a FRET donor fluorophore (Alexa Fluor 546) and Protein G (PG) labeled with FRET acceptor fluorophore (Alexa Fluor 594) were used as it binds specifically to the Fc portion of the antibody. When binding of *S.* Typhimurium to the antibody occured, the conformation of the antibody changed, which decreased the distance between the donor and acceptor, and resultd in increase in fluorescence. The limit of detection was determined as 10^3 cells/ml by measuring the lowest concentration that generated a significant change in signal over the baseline. The fiber probes were

shown to work in food samples as well by detecting *S.* Typhimurium at 10^5 cfu/g in homogenized pork samples[52]. Fluorescence sandwich method[53] was used for detection of *Salmonella* Typhimurium in rinse-water from artificially contaminated sprouted alfalfa seeds. The sprout rinse-water was assayed with the RAPTOR™, which uses a fluorescent sandwich assay with a polystyrene tapered tip. Using this method, *Salmonella* Typhimurium was identified for seeds that were contaminated at a concentration of 50 cfu/g. Tapered fiber tips with different shapes and treatments were investigated and optimized, and *Salmonella* was detected at 10^4 cfu/ml.[54]

An antibody-based sandwich fluorescence FOBS for detection of *Listeria monocytogenes* with a LOD of $4.3x10^3$ cfu/ml in culture medium was reported.[55] This sensor was specific for *L. monocytogenes* as shown by the significantly lower signals caused by other *Listeria* species or microorganisms. After 24 h enrichment step, a FOBS could detect *L. monocytogenes* in hot dog or bologna spiked with 10-1,000 cfu/g. Recently, *L. monocytogenes* was also detected using the previously described fiber optic tip sensor, RAPTOR™.[56] Detection of *L. monocytogenes* in hotdog sample showed a LOD of 5.4×10^7 cfu/ml in buffer and the use of sample flow significantly decreased the LOD to 1×10^3 cfu/ml.[57] The flow through mode, when applied to food samples exhibited an increased LOD of 5×10^5 cfu/ml for *Listeria monocytogenes*. The same fiber optic tip biosensor was also successfully used for detecting a biothreat agent, *Bacillus anthracis* at a concentration of 3.2×10^5 spores/mg in spiked powders in less than 1 hour.[58]

2.5.2. Electrochemical biosensors

Use in a turbid media, good sensitivity and miniaturization potential are some of the advantages of electrochemical biosensors over others.[59] Electrochemical sensors measure current or potential changes due to interactions that occur at the sensor electrode and sample matrix interface. Figure BA shows a schematic of an electrochemical biosensor. Based on the measured parameter the techniques are classified as amperometric (current), potentiometric (potential) and impedimetric (impedance).[60] Several technologies such as Thick-film technology can be used for highly reproducible mass production of electrochemical sensors. Design of high throughput electrode sensors can be achieved by screen printing electrodes using inks of different conductivities.[11, 59, 60]

Amperometric Biosensors

Amperometric detection of microbes involves measurement of current generated by enzyme catalyzed redox reactions or by their involvement in a bioaffinity reaction at the working electrode surface. Working electrode is maintained at a constant potential with respect to a reference electrode, usually Ag/AgCl. Typical electrode materials are platinum(Pt), gold(Au), graphite, modified forms of carbon or conducting polymers.[1]

Table 2-5 Electrochemical sensors for detection of foodborne pathogens

Target	Sample Matrix	Analysis Time	Detection Limit[a] (cfu/ml)	Reference
E.coli O157:H7	Culture medium	30 min	10^2	[68]
	Culture medium	10 min	10^4	[84]
	Water	10 min	10^7	
	Vegetable wash water	6 min	10^2	[140]
	PBS	~ 30 min	10^2	[141]
	Milk		10^3	
	Mixed culture containing five different microbes	10 min	10^2	[142]
	River and tap water	~1 h	10	[143]
Salmonella Typhimurium	Phosphate buffer	~10 min	20	[144]
	Culture and water	1-2 h	10^4	[62]
	Chicken carcass wash	~15 min	10^2 cfu	[145]
Listeria monocytogenes	Phosphate buffer and milk	3-4 h	10^2	[146]
Campylobacter jejuni	Culture and chicken carcass wash water	2 -3 h	10^3	[70]

[a] unless noted otherwise

Antibodies to specific targets are immobilized on the working electrode surface. Binding of the target to the antibodies can generate a current signal to show detection response. Signal amplification can also be done by using a second enzyme-antibody complex that would bind to the target on the electrode. The enzyme would then catalyze a

redox reaction to generate an electroactive product leading to an enhanced current signal. Electrochemical sensors have been investigated for detection of various proteins and chemical but only a limited investigation is done on foodborne pathogen detection. Table 5 lists representative examples of the applications of electrochemical sensors for detection of various foodborne pathogens.

An amperometric sensor for detection of *E. coli* O157:H7 was reported with a detection limit of 5000 cells/ml in 25 min.[61] The cells were labeled by incubating them with an alkaline phosphatase-antibody conjugate and concentrated using a filter. The cells bound to the enzyme-antibody complex when brought in contact with the electrode generated a signal by converting the substrate (para-aminophenyl phosphate) to an electroactive product (para-aminophenol). Immobilization of antibodies directly on the surface of the electrode for rapid detection of *Salmonella* and *Staphylococcus* has also been demonstrated.[62, 63] Figure BB shows the increase in current for various concentrations of *E.coli* O157:H7, *Listeria monocytogenes* and *Campylobacter jejuni* in chicken extract matrix for an amperometric sensor with a detection limit of 50, 10 and 50 cell/ml respectively.[64] A sandwich immunosensor assay for detection of *Salmonellae* in pork, chicken, and beef artificially contaminated with different concentrations of the pathogens has also been demonstrated.[65] For this assay, activity of the enzyme label, horseradish peroxidase, was measured electrochemically using 3,3',5,5'-termethyl benzidine as substrate. Detection of *Listeria monocytogenes* and *Bacillus cereus* was reported to demonstrate one-step quantitative detection of food pathogens based on diffusion of a redox probe using screen printed Au electrodes and thiol-based self-assembled monolayer for antibody immobilization.[66] Use of immobilized

bacteriophages on the electrodes as recognition elements with a detection limit of 10 cells/ml has also been reported for detection of *Mycobacterium smegmatis* and *Bacillus cereus*.[67] A flow-injection amperometric immunofiltration assay for detecting *E.coli* was developed.[68] The sensor assemble had an antibody-modified filter resting on a hollow carbon rod acting as the working electrode. This was a sandwich immunoassay where the amperometric signal was produced by reduction of iodine at the working electrode and was proportional to the sandwich complex. The limit of detection (LOD) for this assay was 100 cells/ml with a working range of 100-600 cells/ml in an overall assay time of 30 min. This sensor was further developed to be used for other pathogens and LOD of 50 cells/ml was achieved for both *E.coli* O157:H7 and *Salmonella* Typhimurium.[69] An amperometric biosensor integrated with an ELISA assay for detection of *Campylobacter jejuni* was developed and a detection range of 10^3-10^7 cfu/ml in chicken-wash matrix was reported.[70] Electrochemical immunosensors for detection of algal toxins that sometimes end up in the food chain such as microcystin-LR and domoic acid were also reported. [71-73]

Potentiometric Biosensors

Potentiometric sensors using ion-selective field effect transistors (ISFETs) and light-addressable potentiometric sensors (LAPS) are two major potentiometric sensor schemes that have been investigated.

The basic principle behind potentiometric measurements is the development of electrochemical potential in proportion to the analyte activity, a_1, in the sample through Nernst relationship:

$$E = E_0 \pm \left(\frac{RT}{nF}\right) \ln a_1 \quad (2)$$

where E_0 is the standard potential for a_1=1 mol L^{-1}, R is the gas constant, F is the Faraday constant, T is the temperature in K, n is the total number charges of ion i, and the sign (+ or –) are for cations and anions, respectively.

Potentiometric biosensors consist of a perm-selective outer layer and a bioactive element, usually an enzyme. Enzyme-catalyzed reactions either consume or generate a chemical species which is measured using conventional electrochemical cell measurement techniques. Since potentiometry yields a logarithmic concentration response the technique has a wide dynamic range and is especially sensitive at low concentrations.

ISFETs use an electric field to create regions of excess charge in a semiconductor substrate in order to enhance or attenuate local electrical conductivity.[74] The gate insulator is covered by an ion-selective membrane that is selective to ions such as K^+, Ca^{2+}, F^-. ISFETs have not made progress as other techniques because of the incompatibility immobilization protocols with the ISFET fabrication technology. Reported results indicate poor detection limit and poor device stability.[59, 60]

The recent development of LAPS based on field effect transistors (FET) was shown to be suitable for pathogen detection.[1] LAPS is based on coupling a transient photo-

current to an insulated n-doped or p-doped silicon thin layer that is in contact with an electrolyte where the desired immunoreaction occurs. Changes in the potential at the silicon interface are detected by the difference in charge distribution between the surface of insulator and FET. LAPS measures an alternating photocurrent generated by a light source, such as a light emitting diode (LED), so the changes in potential can be transduced into voltage per time differentials.

Detection of *Salmonella* in spiked chicken caracass wash at various concentrations of the antigen was reported with a detection limit of 100 cfu/ml in an assay time of about 15 min.[75] The antigen was sandwiched between a biotin-labeled antibody and another fluoroscein-labeled antibody and this sandwich complex was captured on a streptavidin immobilized filter. The membrane was then washed with urease-labeled antibody and then pressed against the silicon layer of LAPS in the presence of urea. Urease activity changed the pH of the electrolyte as it produced ammonia and carbon dioxide. The local value of the surface potential depends on the pH of the electrolyte. The signal was then read with an AC photocurrent that was generated when an intensity-modulated light-source was shone on the bulk silicon. Detection of *E.coli O157:H7* with a detection limit of 10^2 heat-killed cells/ml and 10^4 live cells/ml was also reported.[76] This technique was also used for antibody-based detection of *E.coli* in vegetables. Commercial vegetable samples of lettuce, carrots and rucola were washed with peptone water and blended to detach the bacterial cells and recover them in the liquid medium. This liquid was then analyzed by a LAPS system and it detected concentrations of 10 cells/ml in 1.5 hrs.[77] LAPS was also used for detection of Y*erisinia pestis* and *Bacillus globigii* spores with a LOD of 10 cells or spores/ml.[75]

Impedimetric Biosensors

Impedimetric biosensors are based on the commonly used technique called Electrochemical Impedance Spectroscopy (EIS). The impedance method is accepted by the Association of Official Analytical Chemists (AOAC) as a method for detection of *Salmonella* in food.[59] In this technique, a low voltage sinusoidal electrical signal is applied at various frequencies to an electrochemical cell and the resulting current is used to determine the impedance as a function of the probed frequencies.[78] On one of the electrodes of the electrochemical cell antibodies are immobilized that capture the target and cause changes in the electrical impedance. Impedance measurement is one of the earliest physicochemical methods for detection of bacteria in foods. Microbial metabolism usually leads to an increase both in conductance and capacitance of the medium thereby decreasing its impedance.[79]

The imposed signal may involve a range of frequencies and amplitudes, and the results may be interpreted by two routes. The most rigorous approach involves solving the system for partial differential equations governing the system. The second route, which is often preferred, because of simplicity is the interpretation of data in terms of equivalent circuits.[80-82] EIS has remarkable selectivity but poor detection limits are its main disadvantage.[83] The label-free nature of EIS is its major advantage over amperometric and potentiometric sensors.

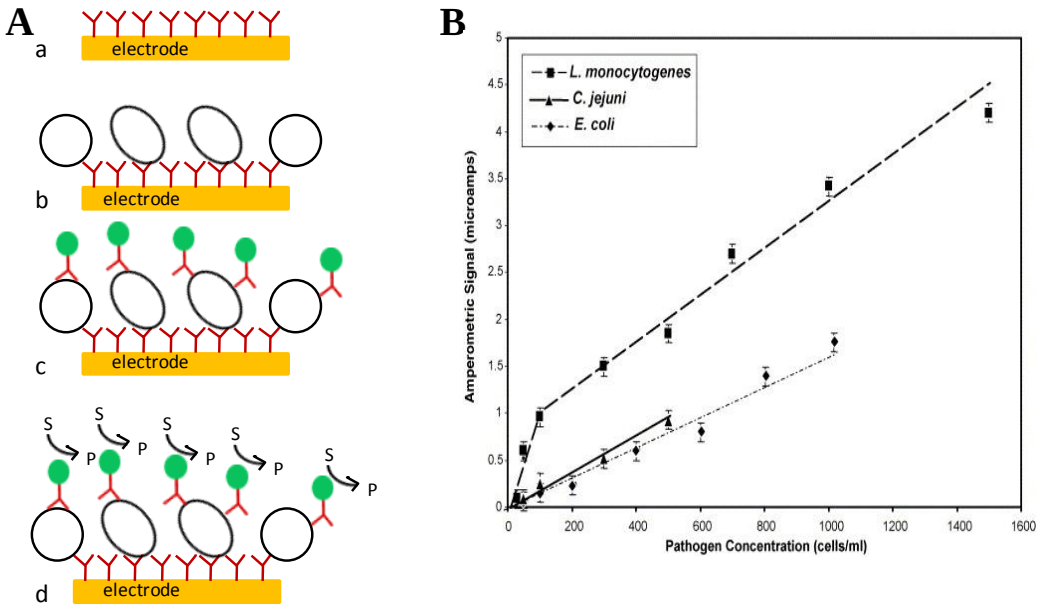

Figure 2-4 Electrochemical sensors. **Panel A.** The transduction mechanism used in a typical ectrochemical sensor is depicted. a) electrode is immobilized with the recognition molecule, b) antigen is bound to the recognition molecule on the electrode, c) labeled second antibody binds to the antigen and d) the labeling molecule catalyzes a redox reaction in solution phase that alters an electrical signal (current, voltage, impedance). **Panel B.** Calibration curves for the determination of total *E. coli* O157:H7, *L. monocytogenes*, and *C. jejuni* in chicken extract using an amperometric sensor. Reproduced with permission from Reference [64]. Chicken-wash samples were passed through a 50µm filter to remove large solids and then this samples was diluted 10-times before spiking with the targets. Horse-radish peroxidase –labeled second antibody was used to catalyze a redox reaction and electric current was monitored at electrode working potential of 105mV.

A high density electrode biosensor was used to improve the sensitivity of impedance sensors and used them for detecting *E.coli O157:H7*.[84] The impedance change caused was measured over a frequency range of 100 Hz to10 MHz in both pure culture and inoculated food samples with detection range of 10^4-10^7 cfu/ml.

2.5.3 Acoustic wave biosensors

Acoustic wave biosensors are mass-sensitive detectors that operate on the basis of an oscillating crystal that resonates at a fundamental frequency that depends on its geometry. These sensors are based on quartz-crystal resonators which became of when it was demonstrated that there is a quantitative relationship between mass adsorbed on the surface and the resonant frequency of the crystal in air or vacuum.[85] Their application to biological samples became possible when suitable oscillator circuits for operation in liquids were developed by Nomura et al.[86]

Exposing the specific biological recognition molecule-immobilized crystal causes a quantifiable change in the resonant frequency of the crystal which correlates with the mass-change on the crystal surface. A vast majority of acoustic wave biosensors use piezoelectric transducers since piezoelectric materials have the ability to generate and transmit acoustic waves in a frequency-dependent manner.[87] Most commonly used materials are quartz (SiO_2) and lithium niobate ($LiTaO_3$). Label-free online analysis of the recognition event, possibility of various immunoassay formats for increased

specificity and sensitivity, low cost and ease of use are the major advantages of these sensors over others.

Acoustic wave sensors can be classified as Bulk acoustic wave resonators (BAW), Flexural-plate-wave resonators (FPW), Surface acoustic wave resonators (SAW) and Shear-horizontal-acoustic-plate-mode resonators (SH-APM). Of these largely only BAW resonators have been investigated for liquid samples.[88]

Bulk acoustic wave resonators

These are also known as piezoelectric quartz crystals (PQC), thickness shear mode (TSM) resonators and quartz crystal microbalance (QCM). These devices transmit as acoustic wave from one face of the crystal to the other. An electric field applied to two parallel circular electrodes on each side of a thin cut crystal leads to a potential difference across the two faces of the crystal causing a shear deformation. This produces mechanical oscillation of a standing wave at a characteristic vibrational frequency across the bulk of the cut crystal. This frequency depends on the physical properties of the crystal such as its size and density and the properties of the phase in contact with the crystal surface. The TSM mode of vibration, commonly used by AT and BT cut crystals, results in displacement parallel to the cut surface and is sensitive to changes in mass. Most BAW devices use AT cut crystals since they are more stable and less temperature dependant than BT cut crystals.[89]

Table 2-6 QCM sensors for detection of foodborne pathogens

Target	Sample Matrix	Analysis Time	Detection Limit[a] (cfu/ml)	Reference
E.coli O157:H7	Culture/water	~ 3 hr	10^3	[128]
	Phosphate buffered saline (PBS)	30-50 min	10^3	[95]
Salmonella	PBS with background of non-target *E.coli* at 10^8 cells/ml	60 min	10^4	[96]
Salmonella Typhimurium	Buffer	~3 hr	10^3	[93]
	PBS	~1.5 hr	10^6	[147]
		< 3 min	10^2	[148]
	Chicken wash	~ 1h	10^2	[149]
Listeria monocytogenes	Culture	30-60 min	10^7	[92]

[a] unless noted otherwise

QCM sensors have been extensively investigated for detection of proteins and DNA but limited work has been done on pathogen detection. QCM sensors can be immobilized with appropriate recognition molecules specific to microbial cells, surface antigens and microbial toxins.[90] These biosensors are usually used a part of a flow setup with flow rate of about 100µl/min and the contact volume of about 100µl. A summary of various applications of foodborne pathogen detection using QCM sensors is

shown in Table 6. A QCM biosensor for detection of *Salmonella* Enteritidis with a detection limit of 10^5cells/ml in an assay time of 35 min has been reported.[91]

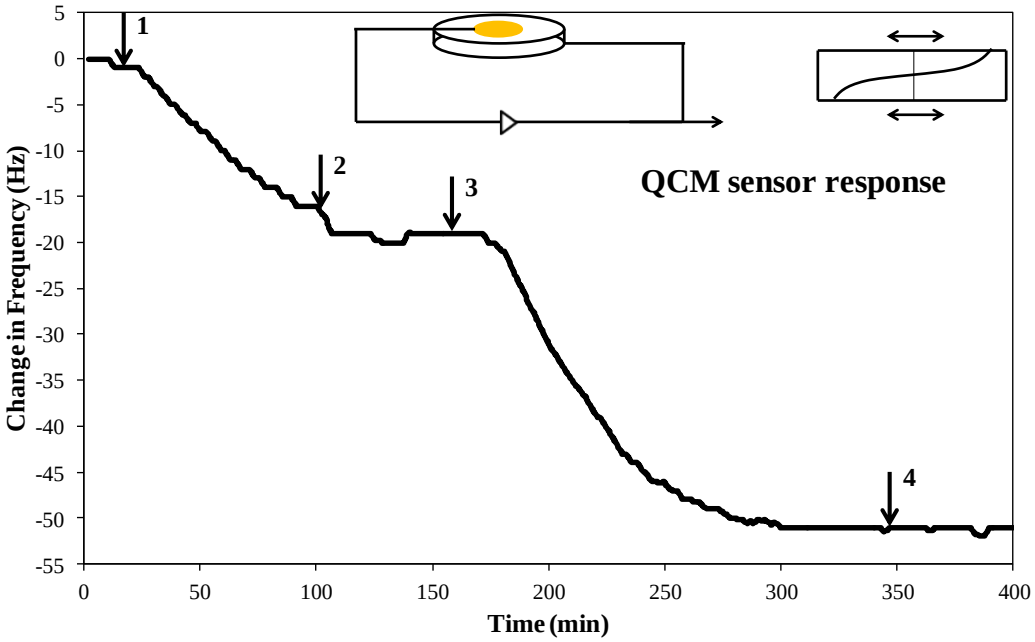

Figure 2-5 Quartz crystal microbalance. The chart shows detection response to the immobilization of antibody against *E,coli* O157:H7 (Label 1) which caused a ~20 Hz decrease in the resonance frequency of the QCM. When exposed to the target cells at 107/mL concentration, the resonance frequency decreased further by ~32 Hz due to the cells binding to the immobilized antibody and QCM surface. The inset shows a QCM crystal and the propagation of the thickness shear oscillation.

Similar detection sensitivities were reported for different foodborne pathogens such as *Listeria monocytogenes*[92] and *E.coli* O157:H7.[93-95] A test that distinguished

between *Salmonella spp.* from other relevant pathogenic serogroups (*S.* Paratyphi, *S.* Typhimurium, *S.* Enteritidis) with a detection limit of 10^4cells/ml in the presence of 10^8 cells/ml of other non-pathogenic strains of *Salmonella* and *E.coli* was also reported.[96] A signal amplification step using enzyme conjugated antibody that causes an increase the adsorbed mass on the sensor via a precipitation reaction was demonstrated.[97] A flow injection QCM sensor for *Staphylococcus* enterotoxin B was reported with a detection sensitivity of 0.1 µg/ml.[98] A schematic of a QCM sensor and detection response to *E,coli* O157:H7 is shown in Figure 5.

QCM sensors have detection sensitivity and time-scale of sensing that are comparable to SPR and electrochemical biosensors. Sensitivity of QCM sensors can be improved by using crystals with higher fundamental resonant frequency, or by exciting the crystal at higher modes[90].

2.5.4. Cantilever Sensors

In this paper we limit the discussion on two of the many cantilever sensing modalities; namely surface-stress sensing and mass sensing. Surface-stress measuring cantilever sensors are also known as bending-mode cantilever sensors since the change in surface-stress causes the cantilever to bend. These are micron-sized and are good for detection of small protein molecules but not very useful for pathogen detection. Mass sensing cantilevers are also called resonant-mode cantilever sensors. The change in mass of these cantilever sensors cause change in resonant frequency which is measured during a sensing experiment.

Bending-mode Cantilever Sensors

The bending-mode is the most common operating mode of cantilever sensors used for biosensing. The change in surface-stress caused by changes occurring in medium around the cantilever or on its surface leads to either the expansion or contraction of the cantilever surface. By selectively making only one side of the cantilever bind to the target asymmetric stress is introduced in the structure causing the cantilever to bend. For isotropic materials, the surface stress, σ relates to the reversible work, dw of elastically deforming a surface and the change in the surface area, dA by[99]:

$$dw = \sigma \times dA \qquad (4.4.1)$$

The schematic of bending-mode cantilever sensors is shown in Figure 6. It is important to notice that the surface stresses detected by the bending-mode cantilevers are changes in the surface stress and not the absolute stress.[100] From a molecular point of view, binding on the sensor surface may lead to electrostatic repulsion, attraction, steric effects, intermolecular interactions or a combination of these that alter the stress on the surface.[101] For a bending-mode cantilever with the deflection, Δz can be related to the length, L, thickness, t, and change in surface stress, $\Delta\sigma$, by the equation[102]:

$$\Delta z \sim \left(\frac{L^2}{t^2}\right)\Delta\sigma \qquad (4.4.2)$$

The above equation suggests that for a given surface stress a cantilever deflects more and is more sensitive if it is thinner and longer. On the other hand longer and thinner cantilevers will be more flexible and responsive to thermal and environmental noise.

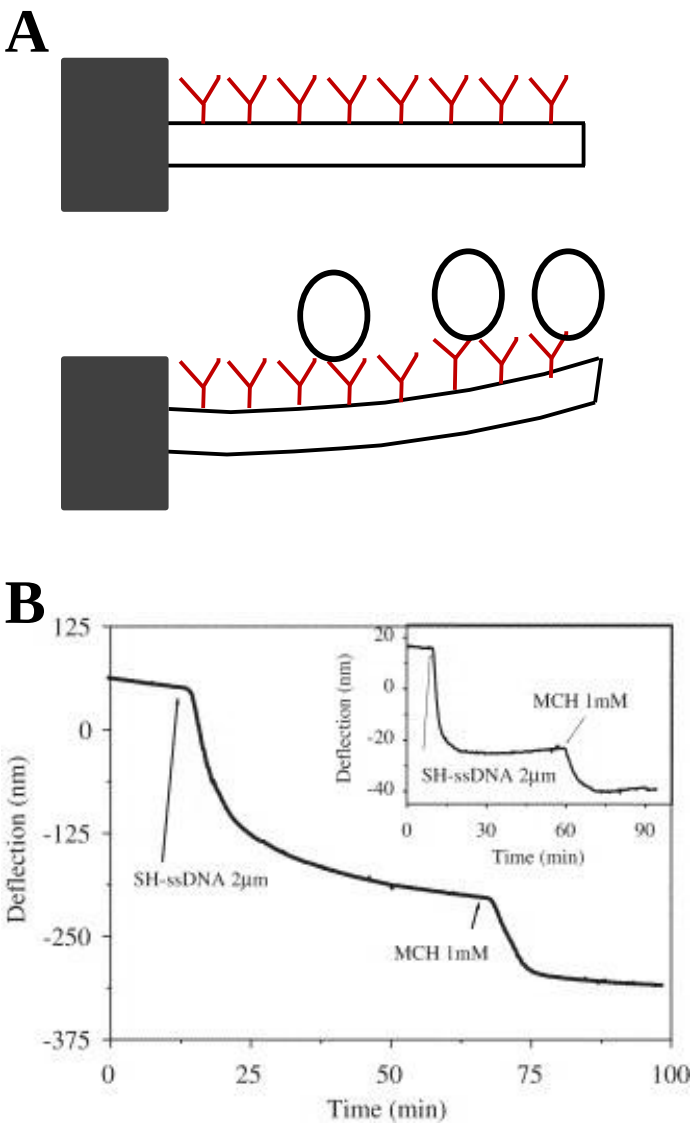

Figure 2-6 Panel A. Schematic representation of bending-mode cantilevers. Binding of antigen to the antibody immobilized on the cantilever surface induces a change in the surface stress causing the sensor surface to bend. **Panel B.** Adsorption of 2 µM thiolated, 12 nucleotide long ss-DNA on a gold-coated SU-8 cantilever. The cantilever was 1.3 µm thick and 200 µm long. Introduction of 1 mM MCH was also gave a further bending response. The compressive surface stress on the gold-coated side produced the bending of the cantilever. The inset shows the same experiment but performed with a commercial silicon nitride cantilever 0.8 µm thick and 200 µm long. The deflection signal is six times larger for the measurement performed with the SU-8 cantilever. Convincing experimental data on pathogen detection is yet to be reported. However, fairly extensive experimental studies on molecular binding have been investigated. Reproduced from reference. [156]

Table 2-7 Cantilever sensors for detection of foodborne pathogens and toxins

Target Pathogen	Transduction Mechanism	Limit of Detection (cells/ml)[a]	Matrix	Reference
E coli 0157:H7	Resonant cantilever	50	Ground beef wash	[115]
		10	Ground beef wash	[150]
		10	Buffer in presence of wild E coli strain	[114]
		1 cell	Buffer	[151, 152]
		1	Buffer	[153]
		10^6	Buffer	[113]
		10	Spinach, spring lettuce washes	[117]
Group A *Streptococcus pyogenes*		700	Buffer	[118]
Salmonella Typhimurium		500	Buffer	[154]
SEB		2.5 fg/ml	Milk	[116]
		25fg/ml	Apple juice	
Salmonella Enterica	Bending mode	25 cells	Buffer	[155]

[a] unless noted otherwise

Resonant-mode piezoelectric cantilever sensors

A material that is piezoelectric develops a voltage across it when mechanically stressed, which is referred to as the direct piezoelectric effect. Conversely, the application of a potential across the piezoelectric material generates a strain, which is the converse piezoelectric effect. The piezoelectric effect is caused by charge distribution within the material molecular structure due to applied stress. Therefore, the piezoelectric effect converts mechanical into electrical energy and vice versa.

The piezoelectric ceramic used in the construction of piezoelectrically excited millimeter-sized cantilever (PEMC) sensors is made from oxides of lead, zirconium, and titanium and is referred to as lead zirconate titanate (PZT). The PZT gives a sensitive response to weak stresses due to the direct piezoelectric effect and generate high strain via the converse piezoelectric phenomenon. PEMC sensors are fabricated to provide predominantly the bending mode vibration.

A schematic of the PEMC sensors is shown in Figure 7A. An electric voltage applied across the thickness of the PZT film will lengthen or shorten the film depending on the polarity of the electric field. Such a change in dimension causes the cantilever to bend, twist or buckle. If the applied field is alternated periodically, the composite cantilever would vibrate, and exhibit resonance when the electric excitation frequency coincides with the mechanical or natural resonance frequency of the structure. The natural frequency of the cantilever depends on the flexural modulus and the mass density of the composite cantilever. At resonance the cantilever undergoes a significantly higher level of vibration and larger stresses. As a consequence, the PZT layer exhibits a sharp

change in impedance, and is conveniently followed by measuring phase angle.[103] The position of the resonant frequency of the cantilever sensors is inversely proportional to their respective masses. Therefore increase in mass of the sensor due to immobilization of the bio-recognition molecule and subsequently due to the capture of the target pathogen by the bio-recognition molecule will cause the resonant frequency of the cantilever to decrease in value. This measurement corresponding to the mass change gives the cantilever sensor its biosensing capability. Transient response of resonant frequency change for the detection sequence of E. coli O157:H7 at 10, 100, 1000, and 10 000 cells/mL in 30 mL of PBS is shown in Figure 6B. The frequency change during the release of the bound *E. coli* equals approximately the change because of attachment, and no loss in antibody activity was observed for at least two regeneration cycles.

Pathogen assays

While optical, electrochemical and QCM sensors [24, 26, 37, 104-112] have been investigated for detecting pathogens, only a few research groups have examined this case on cantilever sensors. Detection of *E. coli* 0157:H7 has been investigated by a number of research groups in various matrices using both bending and resonating cantilever sensors. Most investigators have used buffer as the medium of choice that does not contain any interfering organisms or molecules leading to good sensor response. Detection in real matrix (ground beef washes, vegetable washes) and detection in presence of other contaminating species are very few; see Table 7. It is also of interest to note that the limit of detection reported varies over a very large range and modality used

is also quite varied from continuous measurement under sample flow conditions to dipping into sample followed by drying prior to making resonant frequency measurements. In many cases the objective appears to be demonstrating the sensors' sensitivity rather than selectivity.

A silicon-based microcantilever immobilized with antibody to *E. coli* O157:H7 (EC) was used in bending mode for *in-situ* detection.[113] The sensor deflection was measured optically and it showed a detection limit of 10^6 cfu/ml. When the EC sample was replaced with a buffer, the cantilever's deflection did not change. Furthermore, the reference sensor showed little or no deflection in the EC sample.

PEMC sensors have been used to detect *E.coli O157:H7* in complex matrixes such as broth, broth + raw ground beef and broth + sterile ground beef inoculated with target cells. Successful detections at concentrations of 50 cells/ml were reported in these complex matrixes and 10 cells/ml in buffer.[114] Attempt was made to determine concentration of target cells in the complex matrix using the most probable number method (MPN) and comparison to the six-drop modified method used by the US-FDA were made.[115] Table 7 lists different types of cantilever sensors used for the detection of foodborne pathogens and toxins. The limit of detection for SEB using PEMC sensors was reported as 2.5 fg/ml and 25 fg/ml in milk and apple juice matrix respectively in 20 min.[116] These samples were prepared by spiking the respective matrixes with known concentrations of SEB and were used in the flow system without any concentration or enrichment. Confirmation of detection was shown using two methods: by releasing the bound antigen using a low pH buffer and by selectively adding more mass to the sensor

surface using polyclonal second antibodies to bind to the SEB molecules on the sensor surface.

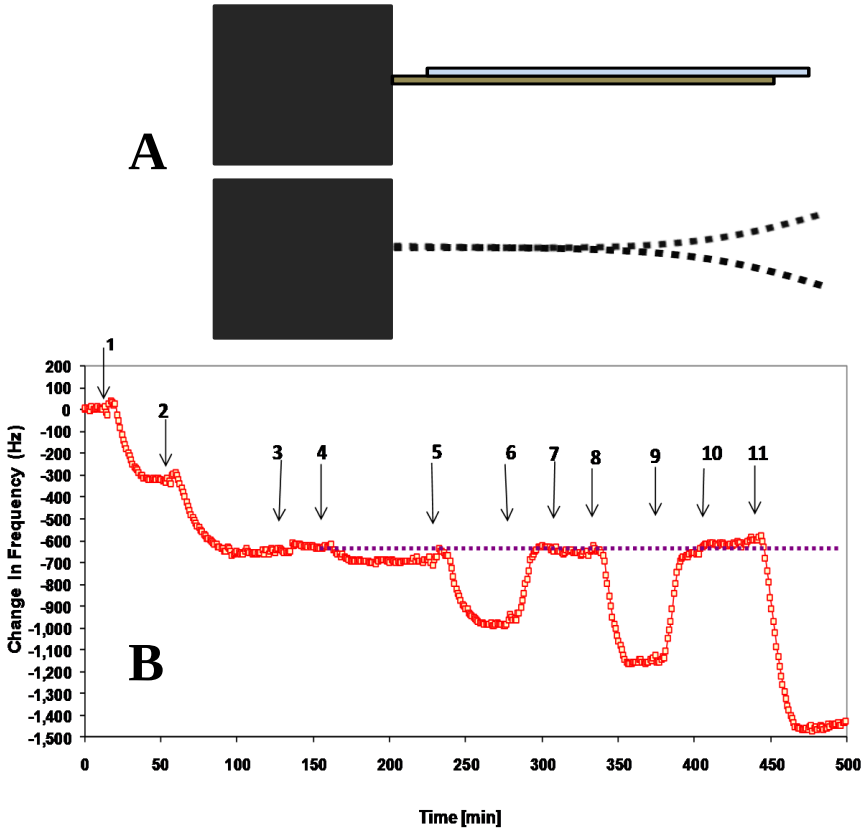

Figure 2-7 Panel A. Schematic representation of a PEMC sensor. Typical width is 1 mm and length is 2 to 4 mm. Glass and PZT are bonded and PZT is anchored in epoxy. **Panel B.** Response of a PEMC sensor to successively increasing target concentrations. A PEMC sensor, as shown in the schematic, was gold coated and installed in a flowcell and allowed to reach a constant frequency. 1) Protein G, when introduced to the flow system chemisorbs onto the gold surface inducing a decrease in the resonant frequency, 2) subsequent introduction of antibody (Ab) to *E.coli* O157:H7 (EC) lead to further decrease in resonant frequency, 3) the flow system was rinsed with PBS, 4) introduction of target EC at 10 cells/ml concentration lead to mass addition on the sensor due to EC binding shown by reduction in resonant frequency, 5) introducing 100 cells/ml concentration

leads to a larger decrease in resonant frequency as more EC bind to Ab on the sensor surface, 6) the cells bound to the sensor surface were released by rinsing with a low pH release buffer, exhibited by increase in frequency, 7) the flow system was rinsed with PBS, 8) EC at 1000 cells/ml was introduced and it induced a larger decrease in the resonant frequency, 9) attached EC cells were then released using the low pH buffer, the resonant frequency increased and stabilized at the same value as before; the dotted horizontal line indicates the resonant frequency of the sensor with Protein G and Ab immobilized, 10) the sensor was again rinsed with PBS and 11) samples containing 10,000 cells/ml EC were introduced to the flow system that caused a large decrease in resonant frequency.

PEMC sensors have also been used for detection of *E.coli* O157:H7 in 1ml unspiked samples of 25 g each of commercially available spinach, spring mix and ground beef washed in 10ml of phosphate-buffered saline.[117] Following these samples the addition of each of the above mentioned matrixes spiked with 10^3cells/ml of target exhibited a change in the resonant frequency as expected. Later detection of 10^2 cells/ml target spiked in a mixture of spinach, spring-mix and ground beef washes was shown to emphasize on the selectivity of the PEMC sensors.

PEMC sensors have also been used for detection of other pathogens of clinical interest such as Group A Streptococcus(GAS) with detection limit of 700 cells/ml in an assay time of 25 min was also reported.[118] Scanning electron microscope (SEM) pictures of the sensors were also taken to confirm detection of the target. Detection of biothreat agent *Bacillus anthracis* in the presence of high concentrations of non-target *Bacillus thuringiensis* and *Bacillus cereus* to establish target specificity was also shown.[119] Use of microcantilevers as resonance mass sensors for detection of *Bacillus anthracis* (BA) was shown both in air and liquid.[120] The authors concluded that as few

as 50 spores on the cantilever can be detected in water. They estimated that measurement sensitivity was 0.1 fg/Hz in air and 10 fg/Hz in liquid.

Cantilever sensors for detection of other foodborne pathogens such *Listeria monocytogenes*, *Campylobacter jejuni* and *Salmonella* have still not been investigated extensively. These pathogens and the toxins they produce are suitable targets for cantilever sensing in food matrixes.

2.6. Summary

Culture based detection of foodborne pathogens is highly sensitive and selective with the drawbacks of tedious procedure, need for trained personnel and long time to yield results.25g of the sample food is pre-enriched in selective medium for separation of *Listeria spp.* followed by a battery of tests and comparison to standards for identification of *Listeria monocytogenes*.[121] It takes about 7 days for this procedure to complete and yield results. Similarly for *Salmonellae*, *E.coli* and *Campylobacter* the length of the tedious procedure and need for trained personnel underlined the need for improvement in these techniques. Development of antibody-based ELISA and DNA-based PCR techniques helped in improving the time required to yield results. The selectivity and sensitivity of ELISA depends on the binding strength of the antibody to its antigen and they work well for samples without interfering molecules such as other non-target cells, proteins and DNA. PCR on the other hand has high selectivity and good sensitivity and takes a shorter time than culture based techniques but need of trained personnel and

expensive equipments limits it use in practical environment. Using these techniques for detection of pathogens present in food matrixes requires an enrichment step for concentrating the pathogens from the complex media and dispensing them in buffer for the actual detection. One popular technique used for enrichment is the use of magnetic beads. Specific antibodies are immobilized on the magnetic beads and these are then mixed with the contaminated food matrix. The antigens bind to the antibodies on the magnetic beads which can then be separated from the matrix using a magnet. These beads are then be immersed in buffer and the antigens are released in it. This enriched and cleaner sample of pathogens can be easily used for ELISA and PCR assays.

Biosensors are devices that are easy to use without training, yield results in nearly real-time with sensitivity and selectivity comparable to the culture-based methods. These devices can work with fairly complex target samples without the need for sample enrichment and without a major compromise on either sensitivity or selectivity. However they are still found to be irregular and in need of improvement.

Detection in food matrixes is critical for the use of biosensors for on-site monitoring in food-processing plants. Sample enrichment and separation is the route taken by most of the research community to overcome the complexity of using a real food matrix but this additional step is time-consuming. Most of the pathogen detection to-date is dependent on the binding affinity of the antibodies to their specific antigens which either deteriorate or change with time. DNA on the other hand is very stable molecule. Targeting the unique DNA signature in any particular pathogen will be a much more reliable test for detection and quantification of pathogens in food matrixes.

2.7. References

[1] D. Ivnitski, I. Abdel-Hamid, P. Atanasov, E. Wilkins, Biosensors for detection of pathogenic bacteria, Biosens Bioelectron, 14(1999) 599-624.

[2] P.S. Mead, L. Slutsker, V. Dietz, L.F. McCaig, J.S.Bresee, C. Shapiro, et al., **Food-Related Illness and Deathin the United States**, Emerging Infectious Diseases, 5(1999) 607-25.

[3] S.P. Oliver, D.A. Patel, T.R. Callaway, M.E. Torrence, ASAS Centennial Paper: Developments and future outlook for preharvest food safety, J Anim Sci, 87(2009) 419-37.

[4] Centre for Disease Control and Prevention, Salmonella outbreak, , 2008.

[5] F.J. Elmer, M. Dreier, Eigenfrequencies of a rectangular atomic force microscope cantilever in a medium, Journal of Applied Physics, 81(1997) 7709-14.

[6] G.A. Campbell, R. Mutharasan, Sensing of liquid level at micron resolution using self-excited millimeter-sized PZT-cantilever, Sensors and Actuators a-Physical, 122(2005) 326-34.

[7] H. Rosenquist, A. Bengtsson, T.B. Hansen, A collaborative study on a Nordic standard protocol for detection and enumeration of thermotolerant Campylobacter in food (NMKL 119, 3. Ed., 2007), International Journal of Food Microbiology, 118(2007) 201-13.

[8] R. Nayak, T.M. Stewart, M.S. Nawaz, PCR identification of Campylobacter coli and Campylobacter jejuni by partial sequencing of virulence genes, Molecular and Cellular Probes, 19(2005) 187-93.

[9] E. de Boer, R.R. Beumer, Methodology for detection and typing of foodborne microorganisms, International Journal of Food Microbiology, 50(1999) 119-30.

[10] G. Midelet-Bourdin, G. Leleu, P. Malle, Evaluation of the International Reference Methods NF EN ISO 11290-1 and 11290-2 and an In-House Method for the Isolation of Listeria monocytogenes from Retail Seafood Products in France, Journal of Food Protection, 70(2007) 891-900.

[11] P. Leonard, S. Hearty, J. Brennan, L. Dunne, J. Quinn, T. Chakraborty, et al., Advances in biosensors for detection of pathogens in food and water, Enzyme Microb Technol, 32(2003) 3-13.

[12] A.K. Deisingh, M. Thompson, Strategies for the detection of *Escherichia coli* O157 : H7 in foods, Journal of Applied Microbiology, 96(2004) 419-29.

[13] S.S. Iqbal, M.W. Mayo, J.G. Bruno, B.V. Bronk, C.A. Batt, J.P. Chambers, A review of molecular recognition technologies for detection of biological threat agents, Biosens Bioelectron, 15(2000) 549-78.

[14] B.W. Blais, J. Leggate, J. Bosley, A. Martinez-Perez, Comparison of fluorogenic and chromogenic assay systems in the detection of Escherichia coli O157 by a novel polymyxin-based ELISA, Letters in Applied Microbiology, 39(2004) 516-22.

[15] C.K. Lee, T. Itoh, T. Ohashi, R. Maeda, T. Suga, Development of a piezoelectric self-excitation and self-detection mechanism in PZT microcantilevers for dynamic scanning force microscopy in liquid, J Vac Sci Technol, B, 15(1997) 1559-63.

[16] A.P.F. Turner, BIOCHEMISTRY: Biosensors-Sense and Sensitivity, Science, 290(2000) 1315-7.

[17] Y.H. Su, M.J. Wang, D.E. Brenner, A. Ng, H. Melkonyan, S. Umansky, et al., Human urine contains small, 150 to 250 nucleotide-sized, soluble DNA derived from the circulation and may be useful in the detection of colorectal cancer, Journal of Molecular Diagnostics, 6(2004) 101-7.

[18] D.V. Lim, J.M. Simpson, E.A. Kearns, M.F. Kramer, Current and developing technologies for monitoring agents of bioterrorism and biowarfare, Clinical Microbiology Reviews, 18(2005) 583-+.

[19] D.R. Shankaran, K.V. Gobi, N. Miura, Recent advancements in surface plasmon resonance immunosensors for detection of small molecules of biomedical, food and environmental interest, Sensors and Actuators B: Chemical, 121(2007) 158-77.

[20] J.E. Dover, G.M. Hwang, E.H. Mullen, B.C. Prorok, S.-J. Suh, Recent advances in peptide probe-based biosensors for detection of infectious agents, Journal of Microbiological Methods, 78(2009) 10-9.

[21] A.J.C. Tubb, Single-mode optical fibre surface plasma wave chemical sensor, Sensors and Actuators B-Chemical, 41(1997) 71-9.

[22] A.K. Sharma, B.D. Gupta, On the sensitivity and signal to noise ratio of a step-index fiber optic surface plasmon resonsnace sensor with bimetallic layers, Optics Communications, (2004).

[23] P. Leonard, S. Hearty, J. Quinn, R. O'Kennedy, A generic approach for the detection of whole Listeria monocytogenes cells in contaminated samples using surface plasmon resonance, Biosens Bioelectron, 19(2004) 1331-5.

[24] A.D. Taylor, J. Ladd, Q. Yu, S. Chen, J. Homola, S. Jiang, Quantitative and simultaneous detection of four foodborne bacterial pathogens with a multi-channel SPR sensor, Biosens Bioelectron, 22(2006) 752-8.

[25] A. Subramanian, J. Irudayaraj, T. Ryan, Mono and dithiol surfaces on surface plasmon resonance biosensors for detection of Staphylococcus aureus, Sensors and Actuators B-Chemical, 114(2006) 192-8.

[26] V. Koubova, E. Brynda, L. Karasova, J. Skvor, J. Homola, J. Dostalek, et al., Detection of foodborne pathogens using surface plasmon resonance biosensors, Sensors and Actuators B: Chemical, 74(2001) 100-5.

[27] R. Slavík, J. Homola, E. Brynda, A miniature fiber optic surface plasmon resonance sensor for fast detection of staphylococcal enterotoxin B, Biosens Bioelectron, 17(2002) 591-5.

[28] J. Homola, J. Dostálek, S. Chen, A. Rasooly, S. Jiang, S.S. Yee, Spectral surface plasmon resonance biosensor for detection of staphylococcal enterotoxin B in milk, International Journal of Food Microbiology, 75(2002) 61-9.

[29] B.D. Spangler, E.A. Wilkinson, J.T. Murphy, B.J. Tyler, Comparison of the Spreeta® surface plasmon resonance sensor and a quartz crystal microbalance for detection of Escherichia coli heat-labile enterotoxin, Analytica Chimica Acta, 444(2001) 149-61.

[30] J.A. Buck, Fundamentals of Optic Fibers: John Wiley & Sons, Inc.; 1995.

[31] L. Tang, Y.J. Ren, B. Hong, K.A. Kang, Fluorophore-mediated, fiber-optic, multi-analyte, immunosensing system for rapid diagnosis and prognosis of cardiovascular diseases, Journal of Biomedical Optics, 11(2006) 21011-1 to -10.

[32] L. Wen-Xu, C. Jian, Continuous monitoring of adriamycin in vivo using fiber optic-based fluorescence chemical sensor, Anal Chem, 75(2003) 1458-62.

[33] N. Nath, S.R. Jain, S. Anand, Evanescent wave fibre optic sensor for detection of L-donovani specific antibodies in sera of kala azar patients, Biosens Bioelectron, 12(1997) 491-8.

[34] B.M. Cullum, G.D. Griffin, G.H. Miller, T. Vo-Dinh, Intracellular measurements in mammary carcinoma cells using fiber-optic nanosensors, Analytical Biochemistry, 277(2000) 25-32.

[35] G.P. Anderson, J.P. Golden, F.S. Ligler, A Fiber Optic Biosensor - Combination Tapered Fibers Designed for Improved Signal Acquisition, Biosens Bioelectron, 8(1993) 249-56.

[36] H.J. Kharat, K.P. Kakde, D.J. Shirale, V.K. Gade, P.D. Gaikwad, P.A. Savale, et al., Designing of optical fiber sensing probe, Fiber and Integrated Optics, 25(2006) 411-22.

[37] K. Rijal, A. Leung, P.M. Shankar, R. Mutharasan, Detection of pathogen *Escherichia coli O157:H7* at 70 cells/mL using antibody-immobilized biconical tapered fiber sensors, Biosens Bioelectron, 21(2005) 871-80.

[38] P.J. Wiejata, P.M. Shankar, R. Mutharasan, Fluorescent sensing using biconical tapers, Sensors and Actuators B-Chemical, 96(2003) 315-20.

[39] M. Sheeba, M. Rajesh, C.P.G. Vallabhan, V.P.N. Nampoori, P. Radhakrishnan, Fibre optic sensor for the detection of adulterant traces in coconut oil, Measurement Science & Technology, 16(2005) 2247-50.

[40] A. Leung, P.M. Shankar, R. Mutharasan, A review of fiber-optic biosensors, Sensors and Actuators B-Chemical, 125(2007) 688-703.

[41] A.G. Mignani, R. Falciai, L. Ciaccheri, Evanescent wave absorption spectroscopy by means of bi-tapered multimode optical fibers, Applied Spectroscopy, 52(1998) 546-51.

[42] J. Villatoro, D. Luna-Moreno, D. Monzon-Hernandez, Optical fiber hydrogen sensor for concentrations below the lower explosive limit, Sensors and Actuators B-Chemical, 110(2005) 23-7.

[43] N. Diaz-Herrera, M.C. Navarrete, O. Esteban, A. Gonzalez-Cano, A fibre-optic temperature sensor based on the deposition of a thermochromic material on an adiabatic taper, Measurement Science & Technology, 15(2004) 353-8.

[44] H.S. Mackenzie, F.P. Payne, Evanescent Field Amplification in a Tapered Single-Mode Optical Fiber, Electronics Letters, 26(1990) 130-2.

[45] S.P. Guo, S. Albin, Transmission property and evanescent wave absorption of cladded multimode fiber tapers, Optics Express, 11(2003) 215-23.

[46] G. Chen, Profile optimization of tapered waveguide sensors by fluorescence imaging in: M.A. Marcus, B. Culshaw, J. Dakin (Eds.), Proceedings of SPIE on Fiber Optic Sensor Technology and Applications III, SPIE, Philadelphia,PA, 2004, pp. 70-7.

[47] M. Ahmad, L.L. Hench, Effect of taper geometries and launch angle on evanescent wave penetration depth in optical fibers, Biosens Bioelectron, 20(2005) 1312-9.

[48] J. Bures, R. Ghosh, Power density of the evanescent field in the vicinity of a tapered fiber, Journal of the Optical Society of America a-Optics Image Science and Vision, 16(1999) 1992-6.

[49] A.P. Ferreira, M.M. Werneck, R.M. Ribeiro, Development of an evanescent-field fibre optic sensor for Escherichia coli O157 : H7, Biosens Bioelectron, 16(2001) 399-408.

[50] D. Maraldo, P.M. Shankar, R. Mutharasan, Measuring bacterial growth by tapered fiber and changes in evanescent field, Biosens Bioelectron, 21(2006) 1339-44.

[51] T. Geng, J. Uknalis, S.I. Tu, A.K. Bhunia, Fiber-optic biosensor employing Alexa-Fluor conjugated antibody for detection of Escherichia coli O157 : H7 from ground beef in four hours, Sensors, 6(2006) 796-807.

[52] S.H. Ko, S.A. Grant, A novel FRET-based optical fiber biosensor for rapid detection of Salmonella typhimurium, Biosens Bioelectron, 21(2006) 1283-90.

[53] M.F. Kramer, D.V. Lim, A rapid and automated fiber optic-based biosensor assay for the detection of salmonella in spent irrigation water used in the sprouting of sprout seeds, J Food Prot, 67(2004) 46-52.

[54] C.H. Zhou, P. Pivarnik, S. Auger, A. Rand, S. Letcher, A compact fiber-optic immunosensor for Salmonella based on evanescent wave excitation, Sensors and Actuators B-Chemical, 42(1997) 169-75.

[55] T. Geng, M.T. Morgan, A.K. Bhunia, Detection of low levels of Listeria monocytogenes cells by using a fiber-optic immunosensor, Applied and Environmental Microbiology, 70(2004) 6138-46.

[56] G. Kim, M.T. Morgan, D. Ess, B.K. Hahm, A. Kothapalli, A. Valadez, et al., Detection of Listeria monocytogenes using an automated fiber-optic biosensor: RAPTOR, Advanced Nondestructuve Evaluation I, Pts 1 and 2, Proceedings, 321-323(2006) 1168-71.

[57] V. Nanduri, G. Kim, M.T. Morgan, D. Ess, B.K. Hahm, A. Kothapalli, et al., Antibody immobilization on waveguides using a flow-through system shows improved Listeria monocytogenes detection in an automated fiber optic biosensor: RAPTOR (TM), Sensors, 6(2006) 808-22.

[58] T.B. Tims, D.V. Lim, Rapid detection of Bacillus anthracis spores directly from powders with an evanescent wave fiber-optic biosensor, Journal of Microbiological Methods, 59(2004) 127-30.

[59] I. Palchetti, M. Mascini, Electroanalytical biosensors and their potential for food pathogen and toxin detection, Anal Bioanal Chem, 391(2008) 455-71.

[60] O. Lazcka, F.J.D. Campo, F.X. Munoz, Pathogen detection: A perspective of traditional methods and biosensors, Biosensors and Bioelectronics, 22(2007) 1205-17.

[61] J.D. Brewster, R.S. Mazenko, Filtration capture and immunoelectrochemical detection for rapid assay of Escherichia coli O157:H7, Journal of Immunological Methods, 211(1998) 1-8.

[62] J.D. Brewster, A.G. Gehring, R.S. Mazenko, L.J. Van Houten, C.J. Crawford, Immunoelectrochemical Assays for Bacteria: Use of Epifluorescence Microscopy and Rapid-Scan Electrochemical Techniques in Development of an Assay for Salmonella, Anal Chem, 68(1996) 4153-9.

[63] B. Mirhabibollahi, J.L. Brooks, R.G. Kroll, A semi-homogeneous amperometric immunosensor for protein A-bearing Staphylococcus aureus in foods, Applied Microbiology and Biotechnology, 34(1990) 242-7.

[64] S. Chemburu, E. Wilkins, I. Abdel-Hamid, Detection of pathogenic bacteria in food samples using highly-dispersed carbon particles, Biosens Bioelectron, 21(2005) 491-9.

[65] L. Croci, E. Delibato, G. Volpe, G. Palleschi, A rapid electrochemical ELISA for the detection of salmonella in meat samples, Anal Lett, 34(2001) 2597-607.

[66] S. Susmel, G.G. Guilbault, C.K. O'Sullivan, Demonstration of labeless detection of food pathogens using electrochemical redox probe and screen printed gold electrodes, Biosens Bioelectron, 18(2003) 881-9.

[67] M. Yemini, Y. Levi, E. Yagil, J. Rishpon, Specific electrochemical phage sensing for Bacillus cereus and Mycobacterium smegmatis, Bioelectrochemistry, 70(2007) 180-4.

[68] I. Abdel-Hamid, D. Ivnitski, P. Atanasov, E. Wilkins, Flow-through immunofiltration assay system for rapid detection of E. coli O157:H7, Biosens Bioelectron, 14(1999) 309-16.

[69] I. Abdel-Hamid, D. Ivnitski, P. Atanasov, E. Wilkins, Highly sensitive flow-injection immunoassay system for rapid detection of bacteria, Analytica Chimica Acta, 399(1999) 99-108.

[70] Y. Che, Y. Li, M. Slavik, Detection of Campylobacter jejuni in poultry samples using an enzyme-linked immunoassay coupled with an enzyme electrode, Biosens Bioelectron, 16(2001) 791-7.

[71] M. Campàs, J.-L. Marty, Highly sensitive amperometric immunosensors for microcystin detection in algae, Biosens Bioelectron, 22(2007) 1034-40.

[72] L. Micheli, A. Radoi, R. Guarrina, R. Massaud, C. Bala, D. Moscone, et al., Disposable immunosensor for the determination of domoic acid in shellfish, Biosens Bioelectron, 20(2004) 190-6.

[73] M. Kania, M. Kreuzer, E. Moore, M. Pravda, B. Hock, G. Guillbault, Development of polyclonal antibodies against domoic acid for their use in electrochemical biosensors, Anal Lett, 36(2003) 1851-63.

[74] P. Bergveld, Thirty years of ISFETOLOGY: What happened in the past 30 years and what may happen in the next 30 years, Sensors and Actuators B: Chemical, 88(2003) 1-20.

[75] K. Dill, J.H. Song, J.A. Blomdahl, J. D. Olson, Rapid, sensitive and specific detection of whole cells and spores using the light-addressable potentiometric sensor, Journal of Biochemical and Biophysical Methods, 34(1997) 161-6.

[76] A.G. Gehring, D.L. Patterson, S.-I. Tu, Use of a Light-Addressable Potentiometric Sensor for the Detection ofEscherichia coliO157:H7, Analytical Biochemistry, 258(1998) 293-8.

[77] C. Ercole, M. Del Gallo, L. Mosiello, S. Baccella, A. Lepidi, Escherichia coli detection in vegetable food by a potentiometric biosensor, Sensors and Actuators B: Chemical, 91(2003) 163-8.

[78] E. Barsoukov, J.R. Macdonald, Impedance Spectroscopy: Theory, Experiment, and Applications, 2nd Edition, John Wiley & Sons Ltd., Hoboken,NJ2005.

[79] D. Ivnitski, I. Abdel-Hamid, P. Atanasov, E. Wilkins, S. Stricker, Application of electrochemical biosensors for detection of food pathogenic bacteria, Electroanalysis, 12(2000) 317-25.

[80] L. Yang, Y. Li, G.F. Erf, Interdigitated Array Microelectrode-Based Electrochemical Impedance Immunosensor for Detection of Escherichia coli O157:H7, Anal Chem, 76(2004) 1107-13.

[81] E. Katz, I. Willner, Probing biomolecular interactions at conductive and semiconductive surfaces by impedance spectroscopy: Routes to impedimetric immunosensors, DNA-Sensors, and enzyme biosensors, Electroanalysis, 15(2003) 913-47.

[82] C. Gabrielli, Identification of Electrochemical Processes by Frequency Response Analysis, Solartron Analytical1990.

[83] E.C. Alocilja, S.M. Radke, Market analysis of biosensors for food safety, Biosens Bioelectron, 18(2003) 841-6.

[84] S.M. Radke, E.C. Alocilja, A high density microelectrode array biosensor for detection of E. coli O157:H7, Biosens Bioelectron, 20(2005) 1662-7.

[85] G. Sauerbrey, ZPhys, 155(1959) 206-22.

[86] T. Nomura, M. Okuhara, Frequency shifts of piezoelectric quartz crystals immersed in organic liquids, Analytica Chimica Acta, 142(1982) 281-4.

[87] D. Griffiths, G. Hall, Biosensors -- what real progress is being made?, Trends in Biotechnology, 11(1993) 122-30.

[88] H.-J.G. Andreas Janshoff, Claudia Steinem,, Piezoelectric Mass-Sensing Devices as Biosensors - An Alternative to Optical Biosensors?, Angewandte Chemie, 39(2000) 4004-32.

[89] R.L. Bunde, E.J. Jarvi, J.J. Rosentreter, Piezoelectric quartz crystal biosensors, Talanta, 46(1998) 1223-36.

[90] M. Cooper, V. Singleton, a survey of the 2001 to 2005 quartz crystal microbalance biosensor literature: applications of acoustic physics to the analysis of iomolecular interactions, Journal of Molecular Recognition, 20(2007) 154-84.

[91] S.-H. Si, X. Li, Y.-S. Fung, D.-R. Zhu, Rapid detection of *Salmonella enteritidis* by piezoelectric immunosensor Microchemical Journal, 68(2001) 21-7.

[92] R.D. Vaughan, C.K. O'Sullivan, G.G. Guilbault, Development of a quartz crystal microbalance (QCM) immunosensor for the detection of Listeria monocytogenes, Enzyme and Microbial Technology, 29(2001) 635-8.

[93] G.-H. Kim, A.G. Rand, S.V. Letcher, Impedance characterization of a piezoelectric immunosensor part II: Salmonella typhimurium detection using magnetic enhancement, Biosens Bioelectron, 18(2003) 91-9.

[94] N. Kim, I.-S. Park, Application of a flow-type antibody sensor to the detection of Escherichia coli in various foods, Biosens Bioelectron, 18(2003) 1101-7.

[95] X.-L. Su, Y. Li, A self-assembled monolayer-based piezoelectric immunosensor for rapid detection of Escherichia coli O157:H7, Biosens Bioelectron, 19(2004) 563-74.

[96] Y.Y. Wong, S.P. Ng, M.H. Ng, S.H. Si, S.Z. Yao, Y.S. Fung, Immunosensor for the differentiation and detection of Salmonella species based on a quartz crystal microbalance, Biosens Bioelectron, 17(2002) 676-84.

[97] X. Su, S.F.Y. Li, Serological determination of Helicobacter pylori infection using sandwiched and enzymatically amplified piezoelectric biosensor, Analytica Chimica Acta, 429(2001) 27-36.

[98] J.L.N. Harteveld, M.S. Nieuwenhuizen, E.R.J. Wils, Detection of Staphylococcal Enterotoxin B employing a piezoelectric crystal immunosensor, Biosens Bioelectron, 12(1997) 661-7.

[99] P. Muller, R. Kern, ABOUT THE MEASUREMENT OF ABSOLUTE ISOTROPIC SURFACE STRESS OF CRYSTALS, Surf Sci, 301(1994) 386-98.

[100] J. Fritz, Cantilever Biosensors, The Analyst, 133(2008) 855-63.

[101] H.-F. Ji, H. Gao, K.R. Buchapudi, X. Yang, X. Xu, M. Schulte, Microcantilever biosensors based onconformational change of proteins, The Analyst, 133(2008) 434-43.

[102] T. Miyatani, M. Fujihira, Calibration of surface stress measurements with atomic force microscopy, Journal of Applied Physics, 81(1997) 7099-115.

[103] G.A. Campbell, R. Mutharasan, Detection and quantification of proteins using self-excited PZT-glass millimeter-sized cantilever, Biosens Bioelectron, 21(2005) 597-607.

[104] J. Waswa, J. Irudayaraj, C. DebRoy, Direct detection of *E. Coli O157:H7* in selected food systems by a surface plasmon resonance biosensor, LWT - Food Science and Technology, 40(2007) 187-92.

[105] S. Balasubramanian, I.B. Sorokulova, V.J. Vodyanoy, A.L. Simonian, Lytic phage as a specific and selective probe for detection of Staphylococcus aureus--A surface plasmon resonance spectroscopic study, Biosens Bioelectron, 22(2007) 948-55.

[106] F. Zezza, M. Pascale, G. Mule, A. Visconti, Detection of Fusarium culmorum in wheat by a surface plasmon resonance-based DNA sensor, Journal of Microbiological Methods, 66(2006) 529-37.

[107] M.W. Oli, W.P. McArthur, L.J. Brady, A whole cell BIAcore assay to evaluate P1-mediated adherence of Streptococcus mutans to human salivary agglutinin and inhibition by specific antibodies, Journal of Microbiological Methods, 65(2006) 503-11.

[108] K. Arora, S. Chand, B.D. Malhotra, Recent developments in bio-molecular electronics techniques for food pathogens, Analytica Chimica Acta, 568(2006) 259-74.

[109] R.E.W. Hancock, J.B. McPhee, Salmonella's Sensor for Host Defense Molecules, Cell, 122(2005) 320-2.

[110] A.D. Taylor, Q. Yu, S. Chen, J. Homola, S. Jiang, Comparison of *E. coli O157:H7* preparation methods used for detection with surface plasmon resonance sensor, Sensors and Actuators B: Chemical, 107(2005) 202-8.

[111] X.L. Su, Y. Li, Surface plasmon resonance and quartz crystal microbalance immunosensors for detection of Escherichia coli O157 : H7, Transactions of the Asae, 48(2005) 405-13.

[112] R.D. Vaughan, R.M. Carter, C.K. O'Sullivan, G.G. Guilbault, A quartz crystal microbalance (QCM) sensor for the detection of Bacillus cereus, Anal Lett, 36(2003) 731-47.

[113] J. Zhang, H.F. Ji, An anti *E-coli O157 : H7* antibody-immobilized microcantilever for the detection of Escherichia coli (E-coli), Analytical Sciences, 20(2004) 585-7.

[114] D. Maraldo, K. Rijal, G. Campbell, R. Mutharasan, Method for Label-Free Detection of Femtogram Quantities of Biologics in Flowing Liquid Samples, Anal Chem, 79(2007) 2762-70.

[115] G.A. Campbell, J. Uknalis, S.-I. Tu, R. Mutharasan, Detection of *Escherichia coli* O157:H7 in ground beef samples using piezoelectric excited millimeter-sized cantilever (PEMC) sensors, Biosens Bioelectron, 22(2007) 1296-302.

[116] D. Maraldo, R. Mutharasan, Detection and confirmation of staphylococcal enterotoxin B in apple juice and milk using piezoelectric-excited millimeter-sized cantilever sensors at 2.5 fg/mL, Anal Chem, 79(2007) 7636-43.

[117] D. Maraldo, R. Mutharasan, Preparation-free method for detecting Escherichia coli O157 : H7 in the presence of spinach, spring lettuce mix, and ground beef particulates, J Food Prot, 70(2007) 2651-5.

[118] G.A. Campbell, R. Mutharasan, PEMC sensor's mass change sensitivity is 20 pg/Hz under liquid immersion, Biosens Bioelectron, 22(2006) 35-41.

[119] G.A. Campbell, R. Mutharasan, Method of measuring *Bacillus anthracis* spores in the presence of copious amounts of *Bacillus thuringiensis* and *Bacillus cereus*, Anal Chem, 79(2007) 1145-52.

[120] A.P. Davila, J. Jang, A.K. Gupta, T. Walter, A. Aronson, R. Bashir, Microresonator mass sensors for detection of Bacillus anthracis Sterne spores in air and water, Biosens Bioelectron, 22(2007) 3028-35.

[121] A.D. Hitchins, K. Jinneman, Detection and Enumeration of *Listeria monocytogenes* in Foods, Bacteriological Analytical Manual 8th ed., AOAC International1998.

[122] P. Daly, T. Collier, S. Doyle, PCR-ELISA detection of Escherichia coli in milk, Letters in Applied Microbiology, 34(2002) 222-6.

[123] Z. Fu, S. Rogelj, T.L. Kieft, Rapid detection of Escherichia coli O157:H7 by immunomagnetic separation and real-time PCR, International Journal of Food Microbiology, 99(2005) 47-57.

[124] J.A. Higgins, S. Nasarabadi, J.S. Karns, D.R. Shelton, M. Cooper, A. Gbakima, et al., A handheld real time thermal cycler for bacterial pathogen detection, Biosens Bioelectron, 18(2003) 1115-23.

[125] L.P. Mansfield, S.J. Forsythe, The detection of Salmonella serovars from animal feed and raw chicken using a combined immunomagnetic separation and ELISA method, Food Microbiol, 18(2001) 361-6.

[126] S. Perelle, F. Dilasser, B. Malorny, J. Grout, J. Hoorfar, P. Fach, Comparison of PCR-ELISA and LightCycler real-time PCR assays for detecting Salmonella spp. in milk and meat samples, Molecular and Cellular Probes, 18(2004) 409-20.

[127] H.S. Liu, Y. Li, X.X. Huang, Y. Kawamura, T. Ezaki, Use of the dnaJ gene for the detection and identification of all Legionella pneumophila serogroups and description of the primers used to detect 16S rDNA gene sequences of major members of the genus Legionella, Microbiology and Immunology, 47(2003) 859-69.

[128] B.W. Brooks, J. Devenish, C.L. Lutze-Wallace, D. Milnes, R.H. Robertson, G. Berlie-Surujballi, Evaluation of a monoclonal antibody-based enzyme-linked immunosorbent assay for detection of Campylobacter fetus in bovine preputial washing and vaginal mucus samples, Veterinary Microbiology, 103(2004) 77-84.

[129] M. Lund, S. Nordentoft, K. Pedersen, M. Madsen, Detection of Campylobacter spp. in Chicken Fecal Samples by Real-Time PCR, J Clin Microbiol, 42(2004) 5125-32.

[130] B.-K. Oh, W. Lee, B.S. Chun, Y.M. Bae, W.H. Lee, J.-W. Choi, Surface plasmon resonance immunosensor for the detection of Yersinia enterocolitica, Colloids and Surfaces A: Physicochemical and Engineering Aspects, 257-258(2005) 369-74.

[131] J.W. Waswa, C. Debroy, J. Irudayaraj, RAPID DETECTION OF *SALMONELLA ENTERITIDIS* AND *ESCHERICHIA COLI* USING SURFACE PLASMON RESONANCE BIOSENSOR, Journal of Food Process Engineering, 29(2006) 373-85.

[132] B.-K. Oh, Y.-K. Kim, K.W. Park, W.H. Lee, J.-W. Choi, Surface plasmon resonance immunosensor for the detection of Salmonella typhimurium, Biosens Bioelectron, 19(2004) 1497-504.

[133] Y.-b. Lan, S.-z. Wang, Y.-g. Yin, W.C. Hoffmann, X.-z. Zheng, Using a Surface Plasmon Resonance Biosensor for Rapid Detection of Salmonella Typhimurium in Chicken Carcass, Journal of Bionic Engineering, 5(2008) 239-46.

[134] P. Leonard, S. Hearty, G. Wyatt, J. Quinn, R. O'Kennedy, Development of a Surface Plasmon Resonance-Based Immunoassay for Listeria monocytogenes, J Food Prot, 68(2005) 728-35.

[135] Y.H. Chang, T.C. Chang, E.F. Kao, C. Chou, Detection of protein a produced by Staphylococcus aureus with a fiber-optic-based biosensor, Bioscience Biotechnology and Biochemistry, 60(1996) 1571-4.

[136] D.R. DeMarco, E.W. Saaski, D.A. McCrae, D.V. Lim, Rapid detection of Escherichia coli O157 : H7 in ground beef using a fiber-optic biosensor, Journal of Food Protection, 62(1999) 711-6.

[137] M.T. Morgan, G. Kim, D. Ess, A. Kothapalli, B.K. Hahm, A. Bhunia, Binding inhibition assay using fiber-optic based biosensor for the detection of foodborne pathogens, Advanced Nondestructuve Evaluation I, Pts 1 and 2, Proceedings, 321-323(2006) 1145-50.

[138] L.A. Tempelman, K.D. King, G.P. Anderson, F.S. Ligler, Quantitating staphylococcal enterotoxin B in diverse media using a portable fiber-optic biosensor, Analytical Biochemistry, 233(1996) 50-7.

[139] E.A. James, K. Schmeltzer, F.S. Ligler, Detection of endotoxin using an evanescent wave fiber-optic biosensor, Applied Biochemistry and Biotechnology, 60(1996) 189-202.

[140] Z. Muhammad-Tahir, E.C. Alocilja, A disposable biosensor for pathogen detection in fresh produce samples, Biosyst Eng, 88(2004) 145-51.

[141] Y.-H. Lin, S.-H. Chen, Y.-C. Chuang, Y.-C. Lu, T.Y. Shen, C.A. Chang, et al., Disposable amperometric immunosensing strips fabricated by Au nanoparticles-modified screen-printed carbon electrodes for the detection of foodborne pathogen Escherichia coli O157:H7, Biosens Bioelectron, 23(2008) 1832-7.

[142] Z. Muhammad-Tahir, E.C. Alocilja, A conductometric biosensor for biosecurity, Biosens Bioelectron, 18(2003) 813-9.

[143] V. Escamilla-Gómez, S. Campuzano, M. Pedrero, J.M. Pingarrón, Gold screen-printed-based impedimetric immunobiosensors for direct and sensitive Escherichia coli quantisation, Biosens Bioelectron, 24(2009) 3365-71.

[144] F. Salam, I.E. Tothill, Detection of Salmonella typhimurium using an electrochemical immunosensor, Biosens Bioelectron, 24(2009) 2630-6.

[145] K. Dill, L.H. Stanker, C.R. Young, Detection of salmonella in poultry using a silicon chip-based biosensor, Journal of Biochemical and Biophysical Methods, 41(1999) 61-7.

[146] E.L. Crowley, C.K. O'Sullivan, G.G. Guilbault, Increasing the sensitivity of Listeria monocytogenes assays: evaluation using ELISA and amperometric detection, Analyst, 124(1999) 295-9.

[147] I.-S. Park, N. Kim, Thiolated Salmonella antibody immobilization onto the gold surface of piezoelectric quartz crystal, Biosens Bioelectron, 13(1998) 1091-7.

[148] E.V. Olsen, I.B. Sorokulova, V.A. Petrenko, I.H. Chen, J.M. Barbaree, V.J. Vodyanoy, Affinity-selected filamentous bacteriophage as a probe for acoustic wave biodetectors of Salmonella typhimurium, Biosens Bioelectron, 21(2006) 1434-42.

[149] X.-L. Su, Y. Li, A QCM immunosensor for Salmonella detection with simultaneous measurements of resonant frequency and motional resistance, Biosens Bioelectron, 21(2005) 840-8.

[150] D. Maraldo, R. Mutharasan, 10-minute assay for detecting *Escherichia coli* O157 : H7 in ground beef samples using piezoelectric-excited millimeter-size cantilever sensors, J Food Prot, 70(2007) 1670-7.

[151] B. Ilic, D. Czaplewski, H.G. Craighead, P. Neuzil, C. Campagnolo, C. Batt, Mechanical resonant immunospecific biological detector, Applied Physics Letters, 77(2000) 450-2.

[152] B. Ilic, D. Czaplewski, M. Zalalutdinov, H.G. Craighead, P. Neuzil, C. Campagnolo, et al., Single cell detection with micromechanical oscillators, J Vac Sci Technol, B, 19(2001) 2825-8.

[153] G.A. Campbell, R. Mutharasan, A method of measuring Escherichia coli O157 : H7 at 1 cell/mL in 1 liter sample using antibody functionalized piezoelectric-excited millimeter-sized cantilever sensor, Environ Sci Technol, 41(2007) 1668-74.

[154] Q. Zhu, W.Y. Shih, W.-H. Shih, In situ, in-liquid, all-electrical detection of Salmonella typhimurium using lead titanate zirconate/gold-coated glass cantilevers at any dipping depth, Biosens Bioelectron, 22(2007) 3132-8.

[155] B.L. Weeks, J. Camarero, A. Noy, A.E. Miller, L. Stanker, J.J. De Yoreo, A microcantilever-based pathogen detector, Scanning, 25(2003) 297-9.

[156] M. Calleja, M. Nordstrom, M. Alvarez, J. Tamayo, L.M. Lechuga, A. Boisen, Highly sensitive polymer-based cantilever-sensors for DNA detection, Ultramicroscopy, 105(2005) 215-22.

Chapter 3 . Piezoelectric cantilever sensors with asymmetric anchor exhibit picogram sensitivity in liquids

This chapter presents a collaborative work on a novel cantilever sensor design, detailed description of which can be found in Appendix A. This new design was my idea that simplified sensor fabrication and made the process more reproducible. My contributions, in addition to fabrication, characterization and writing a part of the manuscript, are reported in Figures 3.2, 3.4 and 3.6 of this chapter. Finite element modeling presented in this chapter was done by a fellow graduate student; Blake Johnson and chemisorption experiments were performed by myself (50%) and a fellow lab member; Ramji Lakshmanan. My contribution to writing this manuscript was 30%.

It was shown for the first time that self-exciting and self-sensing piezoelectric cantilevers consisting only of lead zirconate titanate (PZT) measure resonance only if they are asymmetrically anchored. Symmetric-anchoring did not give rise to electrically measurable bending resonant modes in the 0-100 kHz range. Sensitivity of first and second bending mode resonances was characterized in a flow apparatus using small density changes in liquid (0.003 to 0.01 g/cm^3) and by dodecanethiol chemisorption at 30 pM. Density change results were consistent with existing models of submerged cantilevers, and yielded mass-change sensitivity of ~33 ng/Hz and 217 pg/Hz for the first two modes. In chemisorption experiments, where binding was localized to 1 mm^2 distal tip of the PZT cantilever, sensitivity improved by an order of magnitude to 2 pg/Hz and 414 fg/Hz for the same two resonant modes.

Chapter 4 . Torsional and Lateral Resonant Modes of Cantilevers as Biosensors: Alternatives to Bending Modes

This chapter presents a collaborative study to explore new designs of asymmetrically anchored PEMC sensors for manifestation of torsional and lateral modes of resonance, their characterization and possible applications for biosensing. Details are presented in Appendix B. I was instrumental in fabrication and characterization of these new designs and provided 50% of the results to show that the chemisorption sensitivity of both torsional and lateral resonance modes is similar to those observed for bending resonance modes as shown in Figures 4.3 and 4.5. All modeling work was performed by a fellow graduate student; Blake Johnson. My contribution to writing this manuscript was 20%.

Fabrication of novel cantilever designs that express torsional and lateral modes that exhibited excellent mass-change sensitivity to molecular self-assembly on gold (75 – 135 fg/Hz), which was superior to that of widely investigated bending modes, was shown. Lead zirconate titanate (PZT) millimeter-sized cantilevers were designed with two types of anchor asymmetry that induced expression of either torsional or lateral modes in the 0 – 80 kHz frequency range. Experiments, analytical models, and finite element simulations show that anchor asymmetry enables resonant mode impedance-coupling. The sensitive torsional and lateral modes enabled measurement of self-assembled monolayer formation rate. The anchor design principle was extended to micro-cantilevers via finite element simulations, which caused 97 % sensitivity improvement relative to conventional designs and created new non-classical resonant mode shapes.

Chapter 5 . Adhesion determines resonance response of piezoelectric cantilever sensors

5.1 Introduction

The resonance frequency of a cantilever sensor decreases in response to increase in its mass. Cantilever sensors such as the piezoelectric-excited millimeter-sized cantilever (PEMC) sensors and others require the target analytes to bind to the sensor for causing a resonance frequency decrease. High-order resonance modes (~1MHz) in PEMC sensors are sensitive at femtogram to picogram levels, and have been reported for *in-liquid* detection of analytes such as pathogens, protein biomarkers and nucleic acids using recognition chemistry[1-4]. The molecular binding between antigen-antibody can be of varied strengths[5-7]. To examine the broader question of the role of binding strength (not molecular binding) on the cantilever resonance frequency response, we examined the sensor responses to macro-sized flat pieces of various hydrophobicity attached to the sensor by liquid films of various surface tension. In this study, we show that the PEMC sensors do not respond to an added mass if it is not bound to the sensor surface even though it is in direct physical contact and lying on the sensor surface. Flat pieces of two dimensions and surface hydrophobicity were placed on the macro-sized cantilever sensors such that the masses were bound to the sensor via surface tension of liquid films (water, ethanol).

We hypothesize that the induced response magnitude depends on the strength of adhesion to the sensor surface. This can be tested by systematically altering the adhesion

strength between the two surfaces using liquid films of different surface tension as binding agents and by altering the surface hydrophobicity of the interacting surfaces.

5.2 Results and Discussion

PEMC sensors were fabricated from a 2×1×0.160 mm^3 (L×W×H) quartz piece and a 5×1×0.127 mm^3 (L×W×H) piezoelectric lead-zirconate-titanate (PZT) layer and the composite was anchored in epoxy as described previously.[8] The sensors were coated with a 10 µm thick parylene-C film (PDS-2010 Labcoter® 2). Resonance frequency was measured from frequency sweeps (Agilent-4294A; 100 mV) followed by determining the frequency at which a sharp change in phase angle occurred between the excitation voltage and the resulting current.[9] A typical PEMC sensor exhibited a sharp resonant mode at 72.89 kHz (Q = 52). Finite element calculations (COMSOL Multiphysics) using the dimensions of the sensor indicate that this mode is a second order bending mode. Although several high-order (~1MHz) modes were present, the current study was focused on the second-order mode. Depending on the sensor dimensions, the second order mode was found in the range of 57-78 kHz.

To test the sensor response to mass addition, we first placed a 300 µg dry quartz piece (quartz-A; 1×1×0.160 mm^3, L×W×H) on a dry sensor surface at its free end and to our surprise no appreciable response was seen; see Figure 5-1(a), Label 1. Gentle removal from the sensor surface caused no resonance frequency shift (Label 2). Several such repeat experiments gave the same result. Addition of a 0.4 µL water droplet, 400 µg (Figure 5-1(a), Label 3) on the sensor surface caused a mass-change response of 1495 Hz

decrease. A picture of the PEMC sensor with the water droplet dispensed on its surface is shown in Figure 5-2(a). Even though quartz-A piece weighs almost the same as the 0.4 µL water droplet, the absence of response on the dry surface suggests that the sensor oscillations ignore the dry quartz slab.

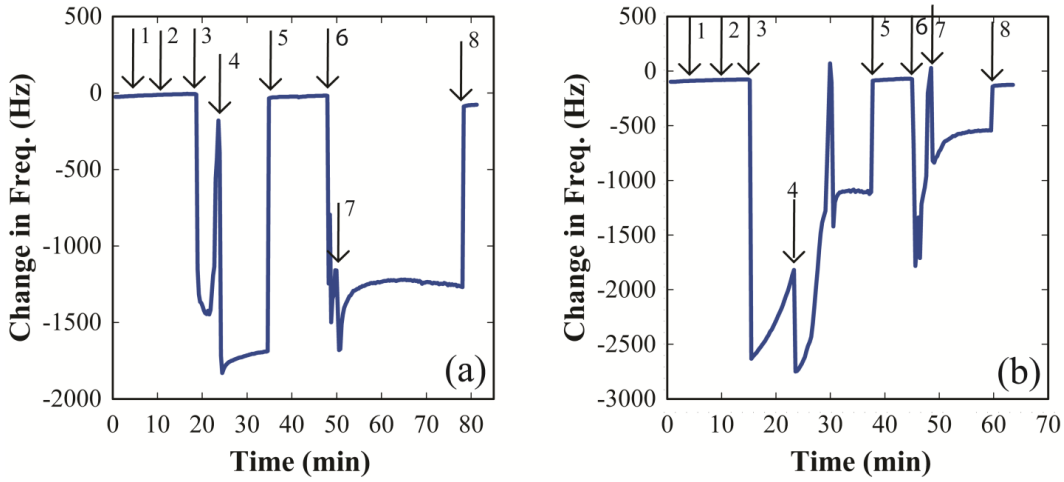

Figure 5-1 Panel (a). Resonant frequency change caused by dry quartz-A piece placed on a dry PEMC sensor surface (1, 2), bound with a thin water film (4-5) and by a thin film of ethanol (7-8). Quartz-A was removed at 8. **Panel (b).** Resonance frequency response to HMDS-quartz-A. Label numbers in the two panels refer to the same experimental step.

On the other hand, the deionized (DI) water droplet binds to the sensor surface (Φ of DI water on parylene C is 101°) and the sensor responds to the increase in mass causing the observed resonance frequency decrease. As the droplet reduced in mass due

to evaporation, the sensor resonance frequency increased. The quartz-A piece was gently placed on the sensor (Figure5-1(a), Label 4) containing residual water film. The added mass caused an immediate decrease of 1527 Hz in the resonance frequency; Φ of DI water-quartz is 10°. Contrast this with the same placement on a dry sensor (Figure 5-1(a), Label 1). Figure 5-2(b) shows the picture of a PEMC sensor with quartz-A placed on the evaporating water droplet. As the exposed water evaporated the resonance frequency rose and appeared to reach a stable value of 1770 Hz, which was below the initial bare sensor value. At this stage, the water film is very thin and is entrapped between the two layers (Figure 5-2(c)). The quartz-A slab remained attached to the sensor surface even when the sensor was changed to vertical position subsequent to attaining steady stated. The entrapped water film remained intact for at least a period of 36 hrs at 25^{o}C, 60% relative humidity (RH). Longer time experiments were not conducted. It should be pointed out that in the absence of a liquid film the quartz-A plate did not attach to the sensor. It is, therefore, reasonable to conclude that the surface tension of the entrapped water film provided the binding energy and induced the observed decrease in resonance frequency since it stabilized at a lower than the initial baseline resonance frequency. Removal of the quartz plate (Figure 5-1(a), Label 5) caused the resonance frequency to rapidly recover to the initial baseline value indicating that the frequency response observed was indeed due to the adhesion of the quartz mass and the entrapped water film was extremely thin. Subsequently a 0.4 μL ethanol droplet was added (Figure 5-1(a), Label 6) on the sensor surface (Φ of ethanol-parylene-C is 10°) which caused a resonance frequency decrease of 1249 Hz. The lower frequency response for the same droplet volume of ethanol compared to water indicates a lower mass loading which is

consistent with the difference in the density of these liquids. Further the low contact angle of ethanol on parylene-C suggests the droplet wets the sensor surface, and was observable as ethanol rapidly spread over the entire sensor area. In contrast, water droplet remained "beaded" as shown in Figure 5-1(a). Interestingly, the ratio of the frequency response for 0.4 µL droplets of ethanol to that of water was 0.81, and is close to the ratio of the droplet masses (0.79). As the ethanol was evaporating, a clean quartz-A piece was gently placed on it (Figure 5-1(a), Label 7) and the sensor frequency decreased by 497 Hz.

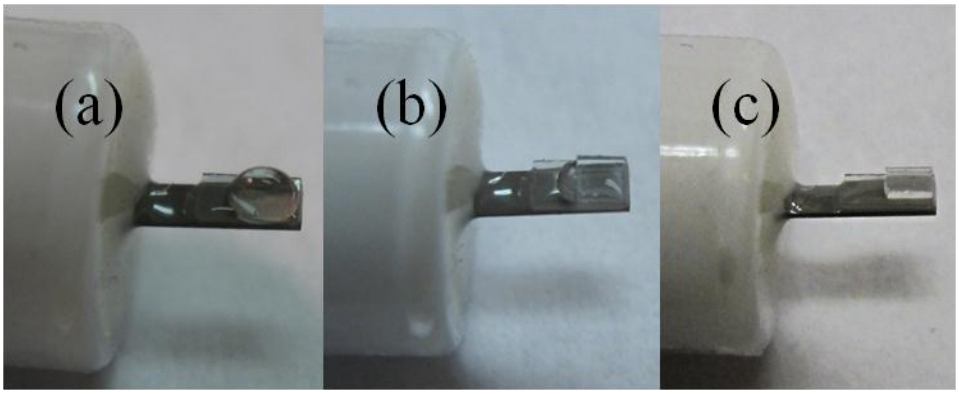

Figure 5-2 A PEMC sensor loaded with a DI water droplet (a), after placing quartz-A on the evaporating water droplet (b) and finally after all the exposed water had evaporated and quartz-A is attached to sensor surface by the entrapped thin water film (c).

Ethanol completely wets quartz and the measured contact angle was ~ 0°. As the exposed ethanol evaporated the resonance frequency increased ultimately reaching a steady state value 557 Hz below the baseline value. The ethanol film entrapped between quartz-A and the sensor provided the physical binding energy between the two. As with the water film, the sensor resonance frequency recovered to the initial value upon removal of quartz-A (Figure 5-1(a), Label 8). In the experiment illustrated in Figure 5-1(a), the mass of the quartz-A piece was the same, yet the responses obtained with the ethanol film were lower than those with a water film. It is noteworthy that the surface tension of water is 72.7 dynes/cm while that of ethanol is 22.1 dynes/cm at 25^{o}C, suggesting the role of the liquid film surface tension in determining the sensor response magnitude. The steady state resonance frequency with ethanol film was 1211 Hz lower than with water film. Several repeat experiments (n=22) gave an average response of 1987 ± 214 Hz with water as the entrapped liquid and 1157 ± 447 Hz with ethanol. Binary mixtures of ethanol in water with increasing ethanol concentration have decreasing surface tension values that range between water and ethanol[10]. Liquid film experiments conducted with 10% aqueous solution of ethanol (surface tension 36.6 dynes/cm) and quartz-A piece gave an average response of 1533 ± 593 Hz (n=18), which is between that of water and ethanol. This suggests that the adhesion is one of the properties that determinines the cantilever response magnitude.

In order to further test the adhesion hypothesis, we altered the hydrophobicity of the quartz-A plate by treating it with 1,1,1,3,3,3-hexamethyldisilazane[11, 12] (HMDS) which altered the contact angle for a water droplet on native quartz from 10° to 99° after treatment. Contact angles were measured by an Optical Contact Angle and Surface

Tension Meter (CAM 200, KSV Instruments). The effect of altered contact angle between water and HMDS treated quartz-A (HMDS-quartz-A) is shown in Figure 5-1(b). Labels 1 through 8 follow the same experimental steps for HMDS-quartz-A as was described for native quartz-A in Figure 5-1(a). Comparison of the two responses shows significant reduction in response from 1987 ± 214 Hz (n=22) for native quartz-A to 1218 ± 187 Hz (n=18) for HMDS-quartz-A attached to the sensor by water film. Note that the mass of the quartz slab was the same since the two experiments were conducted with the same quartz piece. With the ethanol film, which has a lower surface tension than water, the resonance frequency decreased from 1157 ± 447 (n=22) Hz to 504 ± 418 Hz (n=18), prior to and post HMDS treatment.

Yet another approach to test the adhesion hypothesis is to alter the contact area between the quartz slab and the sensor surface. The results, summarized in Table 5-1, show that 600 µg quartz piece (quartz-B; 2×1×0.160 mm^3, L×W×H), and a 1.5 mg polytetrafuoroethylene slab (PTFE; 2×1×0.450 mm^3, L×W×H) when placed on water or ethanol film gave results consistent with the adhesion hypothesis. The PTFE slab (water contact angle 85°) gave a smaller resonant frequency change than quartz-B and is consistent for the surface-tension values of water and ethanol.

The resonant frequency depends on both, the mass and the spring constant of the oscillating sensor as described by a lumped-mass model[13]. The differences in the resonant frequency change reported in this work for the same masses with different adhesion to the sensor surface can be attributed to the possible changes in the spring constant of the overall oscillating structure as has been shown for microcantilever sensors[14-17].

Table 5-1 Responses to thin slabs of various hydrophobicity and sizes bound to the sensor by liquid films of various surface tensions. ± Standard Deviation (n=18 to 22)

	Mass (μg)	**Water**	**Ethanol**
Quartz-A ($1\times1\times0.160$ mm^3)	300	-1987 ± 214	-1157 ± 447
HMDS-Quartz-A ($1\times1\times0.160$ mm^3)	300	-1218 ± 187	-504 ± 418
Quartz-B ($2\times1\times0.160$ mm^3)	600	-4130 ± 332	-2076 ±563
PTFE ($2\times1\times0.450$ mm^3)	1500	-1394 ± 253	-567 ± 467

5.3. Conclusion

Rresonant frequency response of cantilever sensors to macro-sized pieces of quartz and PTFE depends on the strength of adhesion. Stronger adhesion causes a larger frequency decrease for the same mass.

5.4. References

[1] G.A. Campbell, M.B. Medina, R. Mutharasan, Detection of Staphylococcus enterotoxin B at picogram levels using piezoelectric-excited millimeter-sized cantilever sensors, Sensors and Actuators, B: Chemical, 126(2007) 354-60.

[2] D. Maraldo, F.U. Garcia, R. Mutharasan, Method for quantification of a prostate cancer biomarker in urine without sample preparation, Analytical Chemistry, 79(2007) 7683-90.

[3] K. Rijal, R. Mutharasan, PEMC-based Method of Measuring DNA Hybridization at Femtomolar Concentration Directly in Human Serum and in the Presence of Copious Noncomplementary Strands, Analytical Chemistry, 79(2007) 7392-400.

[4] G.A. Campbell, J. Uknalis, S.I. Tu, R. Mutharasan, Detect of *Escherichia coli* O157 : H7 in ground beef samples using piezoelectric excited millimeter-sized cantilever (PEMC) sensors, Biosens Bioelectron, 22(2007) 1296-302.

[5] R.C. Birkmeyer, T.K. Dewey, A.L. Tan-Wilson, Determination of relative antigen-antibody affinities by reverse quantitative immunoelectrophoresis, Journal of Immunological Methods, 49(1982) 141-50.

[6] M. Werthén, H. Nygren, Effect of antibody affinity on the isotherm of antibody binding to surface-immobilized antigen, Journal of Immunological Methods, 115(1988) 71-8.

[7] U. Bruderer, M. Deusinger, U. Schürch, A.B. Lang, Analyses of affinity distributions within polyclonal populations of antigen-specific antibodies : Evaluation of their accuracy in population detection using monoclonal antibodies, Journal of Immunological Methods, 151(1992) 157-64.

[8] D. Maraldo, R. Mutharasan, Preparation-free method for detecting Escherichia coli O157 : H7 in the presence of spinach, spring lettuce mix, and ground beef particulates, Journal of Food Protection, 70(2007) 2651-5.

[9] H. Sharma, R.S. Lakshmanan, B.N. Johnson, R. Mutharasan, Piezoelectric cantilever sensors with asymmetric anchor exhibit picogram sensitivity in liquids, Sensors and Actuators B: Chemical, 153(2011) 64-70.

[10] C. Wohlfarth, Surface tension of ethanol, in: M.D. Lechner (Ed.) Data extract from Landolt-Börnstein IV/24: Surface Tension of Pure Liquids and Binary Liquid Mixtures, Springer-Verlag Berlin Heidelberg2008.

[11] H. Yokogawa, M. Yokoyama, Hydrophobic silica aerogels, Journal of Non-Crystalline Solids, 186(1995) 23-9.

[12] S. Yoda, Y. Takebayashi, T. Sugeta, K. Otake, Platinum-silica aerogels via supercritical drying and impregnation, Journal of Non-Crystalline Solids, 350(2004) 320-5.

[13] N. Lavrik, M. Sepaniak, P. Datskos, Cantilever transducers as a platform for chemical and biological sensors, Review of Scientific Instruments, 75(2004) 2229.

[14] G.Y. Chen, T. Thundat, E.A. Wachter, R.J. Warmack, Adsorption-induced surface stress and its effects on resonance frequency of microcantilevers, Journal of Applied Physics, 77(1995) 3618-22.

[15] T. Thundat, E.A. Wachter, S.L. Sharp, R.J. Warmack, Detection of mercury vapor using resonating microcantilevers, Applied Physics Letters, 66(1995) 1695-7.

[16] S. Cherian, T. Thundat, Determination of adsorption-induced variation in the spring constant of a microcantilever, Applied Physics Letters, 80(2002) 2219-21.

[17] A.W. McFarland, M.A. Poggi, M.J. Doyle, L.A. Bottomley, J.S. Colton, Influence of surface stress on the resonance behavior of microcantilevers, Applied Physics Letters, 87(2005) 053505-3.

Chapter 6 . Anomalous behavior of high-order resonance mode in cantilever sensors

6.1. Introduction

Increase in mass of a cantilever sensor causes a decrease in its resonance frequency. In earlier work[1], for the fundamental mode of a piezoelectric millimeter-sized cantilever (PEMC) the response was dependent on the binding strength of macro-sized quartz pieces to the sensor surface. For various binding strengths and various masses, the fundamental modes decreased in resonance frequency. For the same mass addition experiments on the high-order modes of PEMC sensors, anomalous increase in resonance frequency was observed and is the subject of this report. For cantilever sensors manifesting a high-order resonance mode with a shear-type oscillation, the expectation of decrease in resonance frequency for increase in mass is experimentally shown not to be true.

The high-order (~1MHz) mode of PEMC sensors has shown sensitivities in the low fg/Hz range[2] for sensing of analytes such as biomarkers[3], DNA[4], toxins[5] and pathogens[6-8] in a variety of complex matrixes by measuring the decrease in its frequency. Their characterization will enhance our understanding of the anomalous increase in response to the macro-sized masses. The first step in this direction is to gain a better understanding of the type of oscillations that these modes exhibit. The aim of this paper is to experimentally show the presence of thickness-shear oscillations as a part of the combination of oscillations that is expressed in the high-order PEMC modes and is corroborated by finite element modeling (FEM).

We hypothesize that by comparing the responses of the high-order mode of PEMC sensors, subjected to the addition of macro-sized flat masses, to those observed on resonant sensors with known type of oscillation, we will be able to characterize the complex high-order PEMC modes. Since a quartz crystal microbalance (QCM) exhibits only a thickness-shear oscillation, we compared the high-order mode response to the QCM.

6.2 Results and Discussion

PEMC sensors were fabricated by bonding a 2×1×0.160 mm^3 (L×W×H) quartz piece to one end of 5×1×0.127 mm^3 (L×W×H) PZT slab using polyurethane as reported previously[9]. The sensors were coated with a 10 μm thick parylene-C film (PDS-2010 Labcoter® 2). QCM apparatus (QCM200) was used for experiments with a 5MHz, AT cut, 1" diameter quartz crystal with circular gold electrodes.

The PEMC sensor was connected to an impedance analyzer and resonance frequency was measured from frequency sweeps (Agilent-4294A; 100 mV) followed by determining the frequency at which a sharp change in phase angle occurred between the excitation voltage and the resulting current[1]. After sensor frequency established a stable baseline a droplet of a liquid of known surface tension was dispensed on the quartz side of the PEMC sensor towards its free end. Five minutes into the evaporation of the droplet an additional mass was placed on the liquid droplet on the PEMC sensor and the changes in the resonance frequency were recorded. As the liquid evaporated, a thin film of the liquid was entrapped between the two layers.

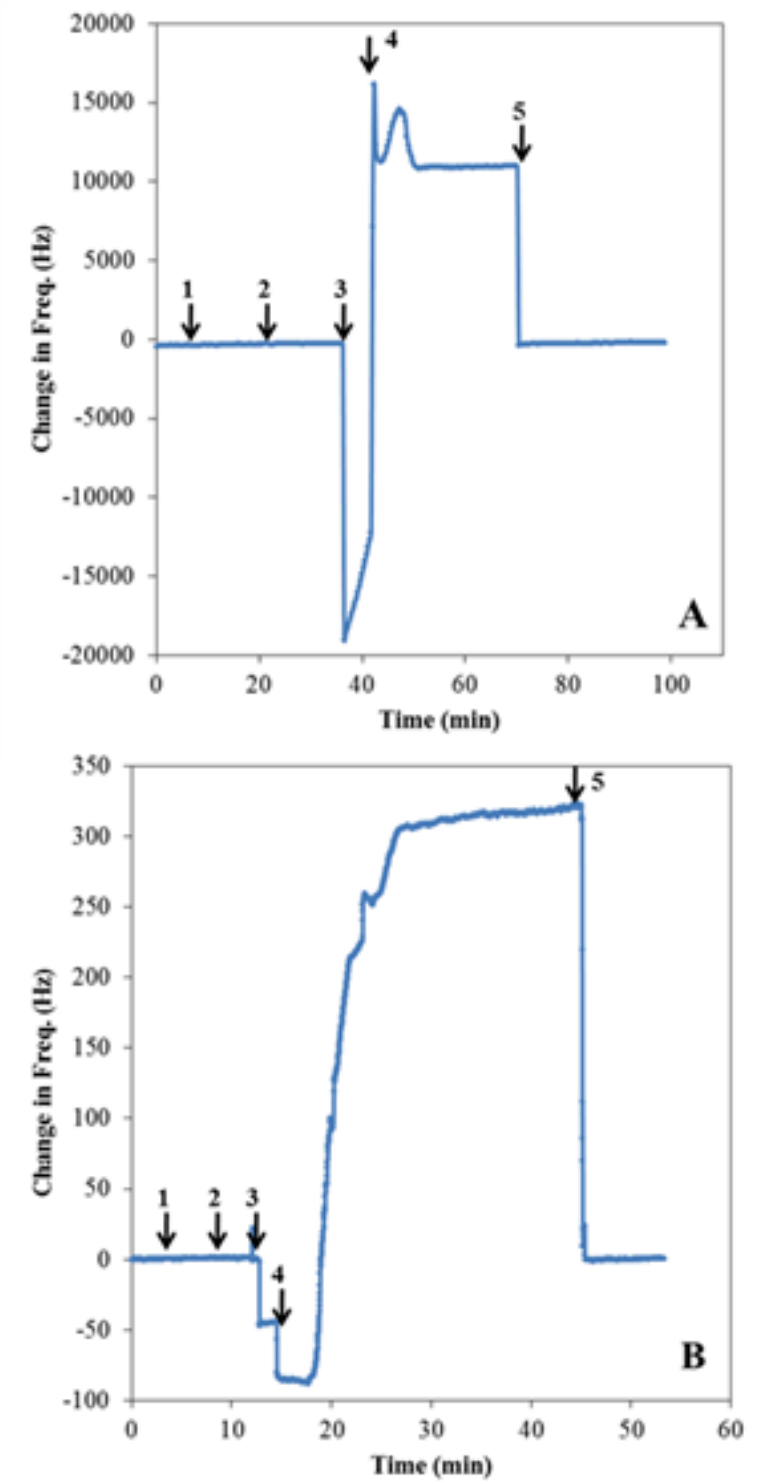

Figure 6-1 shows a typical responses of the high-mode of PEMC sensors (Panel A) and QCM (Panel B) to the addition of dry Quartz-A (Label 1) which did not cause any change

in the resonance frequency followed by its removal from the sensor surface (Label 2). 0.4 µL water droplet (Label 3) followed by the placement of Quartz-A on the evaporating droplet (Label 4) which causes the resonance frequency to increase beyond the initial stable value and on removal of Quartz-A from the sensor surface (Label 5) the resonance frequency recovers back to the initial value.

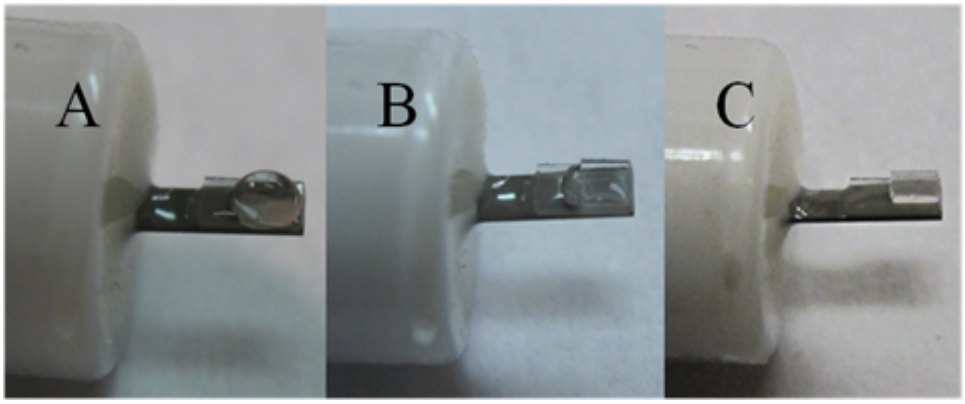

Figure 6-2 A PEMC sensor loaded with a DI water droplet (A), after placing quartz-A on the evaporating water droplet (B) and finally after all the exposed water had evaporated and quartz-A is attached to sensor surface by the entrapped thin water film (C).

The surface tension of this entrapped liquid provided the binding necessary for inducing sensor response. Similar steps were followed to record the change in the resonance frequency due to addition of quartz slabs of various dimensions; Quartz-A: 1x1x0.160 mm^3 (L×W×H), Quartz-B: 2×1×0.160 mm^3 (L×W×H), and a PTFE slab,

$2\times1\times0.450$ mm^3 (L×W×H), on the evaporating liquid droplet. These experiments were repeated using liquids of various surface tensions.

Typical response of a high-order mode of PEMC sensor to the addition of a 0.4 µL droplet of DI water and subsequent addition of Quartz-A on the evaporating droplet is shown in Figure 1A. Prior to the addition of the water droplet, dry Quartz-A piece was gently placed at the free end of the sensor after it had reached a stable frequency value. As expected [1], no change in the resonance frequency was observed even though mass was added on the cantilever. The addition of a water droplet to the glass side of the sensor towards its free end (Figure 2A) decreased the resonance frequency by 19.39 ± 1.52 kHz (n = 10) and then gradually increased as the droplet evaporated. The droplet was allowed to evaporate for 5 min and then Quartz-A was placed on the remaining droplet as shown in Figure 2B. Contrary to expectations, the addition of Quartz-A on the sensor surface caused an increase in the resonance frequency. As the exposed droplet continued to evaporate a thin film of water was entrapped between Quartz-A and the resonating sensor. The sensor frequency adjusted and finally stabilized 10.9 ± 1.21 kHz (n = 10) above the initial value. As shown in Figure 2C, Quartz-A was adhered to the resonating sensor by the water film surface tension. The resonance frequency recovered completely back to the initial value when Quartz-A was physically removed from the sensor surface.

In order to confirm the unexpected increase in the resonance frequency in response to the addition of Quartz-A on the PEMC sensor, the experiment shown in Figure 1A was repeated with ethanol, a lower surface tension liquid (22.14 dynes/cm at 25°C), to reduce the binding strength of Quartz-A to the resonating structure.

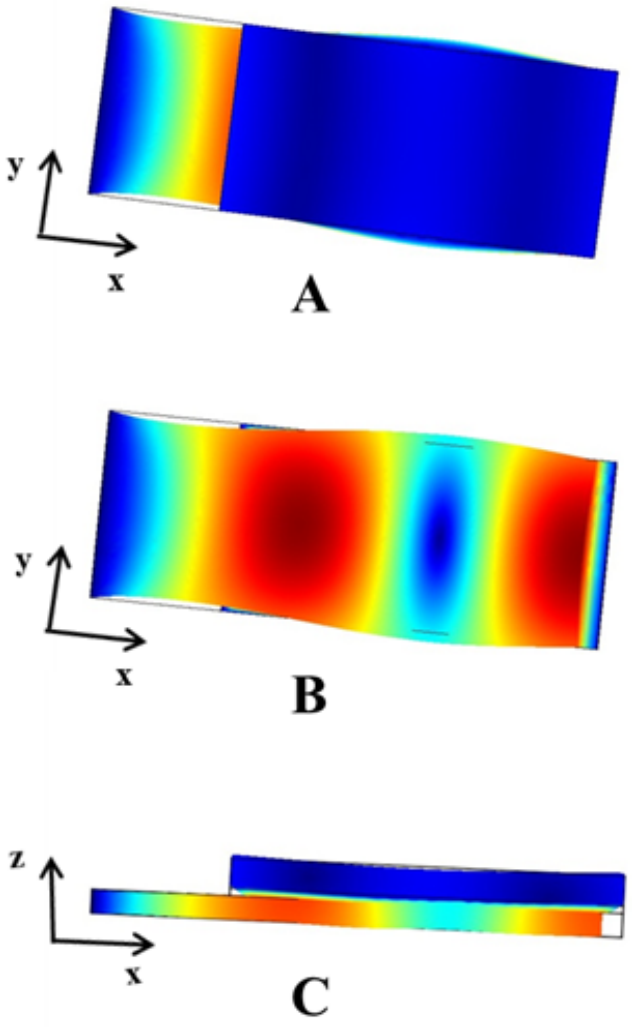

Figure 6-3 Typical mode shape generated for total displacement is shown for the high-order mode of PEMC. Panel A shows the top down view looking at the glass side, Panel B shows the top down view looking at the PZT side and Panel C shows the side view of the PEMC.

Even with ethanol as the entrapped liquid film, the resonance frequency of the high-mode of PEMC sensors increased by 5.53 ± 2.98 kHz (n = 10) beyond the initial stable value. The observed magnitude of increase for ethanol was lower than that with water which has a higher surface tension (72.7 dynes/cm at 25°C). To further alter the binding energy between Quartz-A and the sensor, 10% solution of ethanol in water was used as the entrapped liquid film. Increasing ethanol in aqueous ethanolic solution reduces its surface tension value and 10% solution of ethanol in water has a surface tension of 36.6 dynes/cm at 25°C. This solution has an intermediate surface tension value between water and ethanol. The frequency increase induced when it was used as the binding liquid was 7.11 ± 2.67 kHz (n = 5) which is also between the responses for water and ethanol as the binding liquid films.

Another strategy to alter the binding strength between the sensor and added mass is to change the contact area between the two. Quartz-B, which is twice the area of Quartz-A was used for this experiment. Frequency of PEMC high-order mode increased by 14.89 ± 1.21 kHz (n = 5) when Quartz-B was bound with water and it increased only by 9.67 ± 2.65 kHz (n = 5) when Quartz-B was bound with ethanol. Thus, we found that the sensor response magnitude increased with increase in contact area and with surface tension of entrapped liquid film.

Yet another method of manipulating the binding energy is to alter the surface hydrophobicity. We adopted two strategies: (1) use a hydrophobic material and (2) alter the hydrophobicity of quartz. First, hydrophobic (Φ = 85°) polytetrafluoroethylene (PTFE) piece, PTFE, was used to determine responses on PEMC sensors with both water

and ethanol. PTFE induced an increase in the resonance frequency of 0.56 ± 0.13 kHz (n = 5) and 0.24 ± 0.09 kHz (n = 5) on high-order mode of PEMC.

The second approach to increase hydrophobicity of quartz pieces was achieved via silanization using 1,1,1,3,3,3-hexamethyldisilazane (HMDS) which replaced the hydrophilic hydroxyl surface functional groups to hydrophobic methyl groups. The water contact angle (Φ) on HMDS treated Quartz-A (HMDS-Quartz-A) increased to 99° from 10° which is the water contact angle on native Quartz-A surface. The experiment described earlier was repeated on the high-mode of PEMC sensors with HMDS-Quartz-A with both water and ethanol as the entrapped liquid film. HMDS-Quartz-A bound to the PEMC sensor with water caused the resonance frequency to increase by 6.88 ± 1.04 kHz (n = 10) while the frequency increased only by 2.54 ± 1.8 kHz (n = 10) when ethanol was used as the entrapped liquid.

Characterization of the high-order PEMC mode in order to understand the anomalous behavior was done using finite element modeling. The structural mechanics and piezoelectric module with plane-stress approximation (COMSOL Multiphysics® 3.4) enabled finite element modeling of the resonance frequency. The shape of the investigated PEMC high-order mode is shown in Figure 3. The dark red colored areas are those with high deformation while the dark blue colored regions show the lowest deformation.

Table 6-1 Comparing responses (Δf) shown by PEMC high-mode and QCM to the different masses bound by liquids of different surface tension values.

	Mass (μg)	**Solvent**	**High-mode PEMC, Δf (kHz)**	**QCM, Δf (Hz)**
Quartz-A (1×1×0.160 mm^3)	300	Water	10.93 ± 1.21	316 ± 89
		10% Ethanol in Water	7.11 ± 2.67	98 ± 37
		Ethanol	5.53 ± 2.98	67 ± 34
HMDS-Quartz-A (1×1×0.160 mm^3)	300	Water	6.88 ± 1.94	146 ± 38
		Ethanol	2.54 ± 1.8	27 ± 13
Quartz-B (2×1×0.160 mm^3)	600	Water	14.89 ± 1.21	432 ± 78
		Ethanol	9.67 ± 2.65	139 ± 29
PTFE (2×1×0.450 mm^3)	1500	Water	0.56 ± 0.13	45 ± 9
		Ethanol	0.24 ± 0.09	13 ± 5

To determine the type of oscillations we need to compare the displacements of various edges of PEMC. The PZT layer showed y-displacement in the order of microns, along the cantilever length, whereas it was in the order of nanometers for the glass layer. A box-diagram of a PEMC sensor is shown in supplementary materials (Figure S1, Panel A) along with the highlighted edges whose displacements are compared here.

A typical spectrum of the PEMC sensors used for this study is shown in Figure S1, Panel B. The resonance mode investigated is marked by an asterisk (*). These high-order resonance modes manifest at ~ 870-1000 kHz and have a Q-value of ~ 35-50 in air. A comparison of the y-displacements for the left edge of PEMC, along the cantilever length, from the bottom layer of PZT; (c), to the top layer of glass; (a), is shown in Figure S2. Larger y-displacement in the bottom layer;(c), as compared to the top layer;(a), gives this mode a shear-type oscillation similar to the one present in a quartz crystal microbalance (QCM). Figure S3, in the supplementary materials, compares the y-displacement and z-displacement, along the length of the cantilever, for the top right edge of the glass layer; (d). The z-displacements for both the bottom edges of PZT layer; (c) and (e), are in the order of microns as shown in Figure S4 but they are not in phase. Larger displacement on one side of PZT than the other shows the presence of a transverse oscillation along with a torsional character to the mode.

FEM, thus, showed that the high-order mode of PEMC is complex and manifests multiple types of oscillations. The larger, out of phase y-displacement of the bottom PZT layer; (c), as compared to the top glass layer; (a), strongly suggests the presence of the a thickness shear-type oscillation.

Since the high-order PEMC mode showed a frequency increase and has a thickness-shear type oscillation, we repeated the above described experiments on a QCM to determine if the resonant mode type contributed to the observed response. The QCM apparatus (5 MHz) was subjected to the additions of droplets of liquids of various surface tension values various masses (Quartz-A, HMDS-Quartz-A, Quartz-B and PTFE) in the same way as described for the high-mode of PEMC sensors.

After allowing the crystal resonance frequency to reach a stable value, dry Quartz-A was placed on the sensor and no change in the resonance frequency was observed; see Figure 1B. Addition of 0.4 µL DI water droplet caused the resonance frequency to decrease by 45.8 Hz. The droplet was allowed to evaporate for 2 min before placing Quartz-A on the water droplet. As soon as the quartz mass was added to the oscillating sensor there was a further decrease in the resonance frequency of 39 Hz. With the evaporation of the exposed water droplet, the resonance frequency increased and finally stabilized 316 ± 89 Hz higher than the initial value. As the droplet evaporated a thin film of water was entrapped between Quartz-A and the crystal and provided the binding necessary for inducing a sensor response. Upon gentle removal of the Quartz-A piece from the crystal surface the resonance frequency recovered and stabilized back at the initial value.

Ethanol and 10% aqueous ethanolic solutions were used to change the binding strength and the net increase in resonance frequency caused by Quartz-A bound to the crystal using these liquids was 67 ± 34 Hz (n = 5) and 98 ± 37 Hz (n =5), respectively. Experiments on the QCM sensor with Quartz-B, to study the effect of contact area, gave an increase of 432 ± 78 Hz (n = 5) and 139 ± 29 Hz (n = 5) with water and ethanol,

respectively. The trends of the responses observed on the QCM are the same as those on the high-order mode of PEMC but the response magnitudes are larger for PEMC sensors.

For PTFE, the net increase values were 45 ± 9 Hz (n = 5) and 13 ± 5 Hz (n = 5) using water and ethanol, respectively while for the experiments with HMDS-Quartz-A bound by water and ethanol the increases were considerably higher, 146 ± 38 Hz (n = 5) and 27 ± 13 Hz (n = 5), respectively. A summary of the responses of both the high-order mode of PEMC sensors and the QCM using the various liquids and different macroscopic masses is given in Table 6-1.

Increase in the resonance frequency of QCM has been reported in response to borosilicate glass spheres physically placed on the crystal surface as well as when the particles were held by liquid surface tension [10]. For the dry beads the increase for the 5MHz mode was ~1.5 kHz which was considerably lower than that in the presence of moisture, ~12 kHz. The responses were interpreted as providing a measure of the binding force between the oscillating crystal and the spherical particles. The crystal-particle system was modeled as a coupled multi-body resonance and used to explain that the QCM senses the elastic stiffness of the particle-crystal contact.[11, 12] The increase in frequency of the crystal implies that for such interactions the increase in stiffness of the sphere-crystal composite dominates over any decrease in frequency due to mass increase.

The resonance frequency of PEMC sensors depends on the mass of the cantilever as well as its stiffness. The effect of change in stiffness on the frequency response of the high-order PEMC mode has been studied previously[13] where the anomalous increase in frequency was experimentally observed during viscoelastic liquid film formation. For the high-order mode, increasing mass of the sensor manifests as a decrease in resonance

frequency whereas an increase in the spring constant leads to a frequency increase. For any addition on a resonating PEMC the frequency response is determined by the net change caused by these two opposing effects.

In this study, the entrapped viscoelastic liquid films caused an increase in the stiffness of the cantilever, thus, contributing to the anomalous increase in its resonance frequency. However, the different surface tensions affect the stiffness such that the differences in interaction are measurable in the form of different sensor responses.

6.3 Conclusion

The high-mode of PEMC sensors exhibits a shear-type oscillation as shown by FEM calculations and its resonance frequency increases in response to macro-sized pieces of quartz and PTFE based on the binding strength. The addition of macro-sized pieces causes a greater increase in its stiffness than the oscillating mass contributing to the anomalous increase in resonance frequency.

6.4. Supplementary Materials

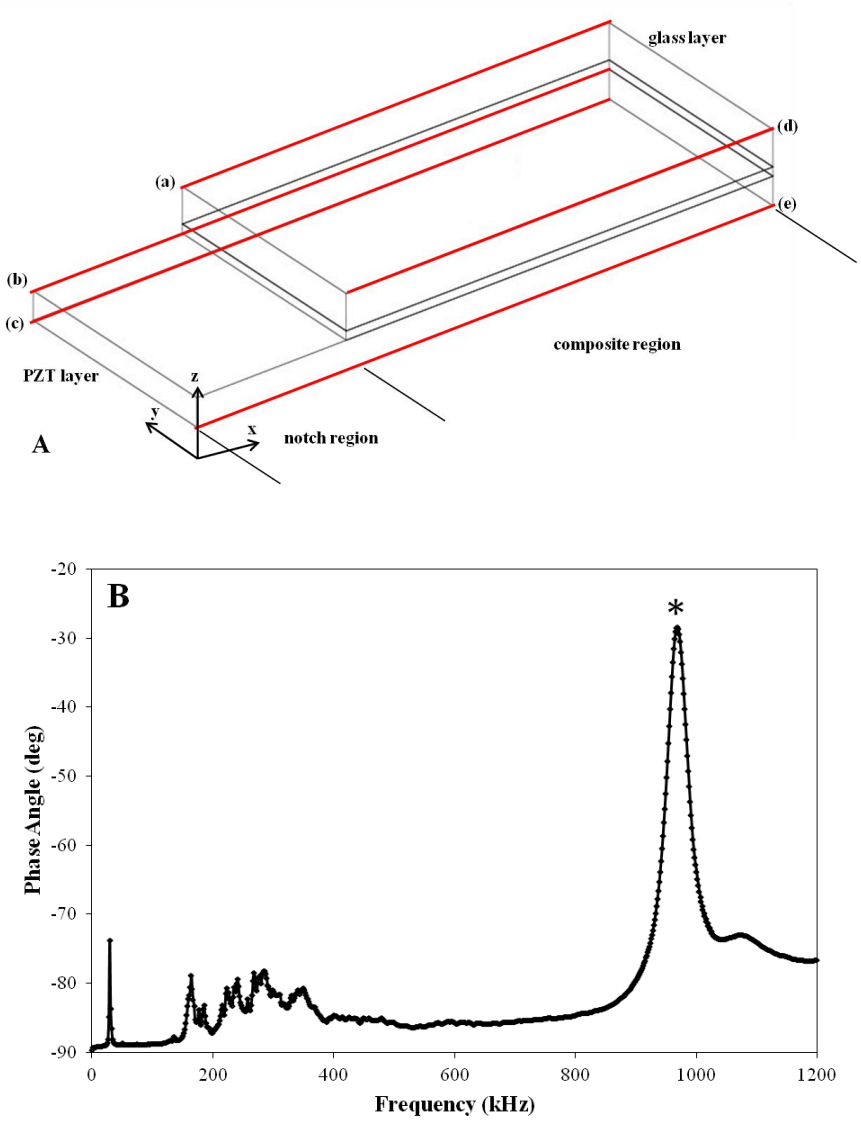

Figure S1. Panel A shows a schematic design of the composite PEMC sensors used in this study. The displacements of the edges that are named and marked in red were compared to show that the high-order resonance mode of these sensors has a shear-type oscillation character. **Panel B** shows a typical spectrum of the PEMC sensors. The resonance mode marked by an asterisk (*) is the mode investigated in this study and has been used previously for biosensing.

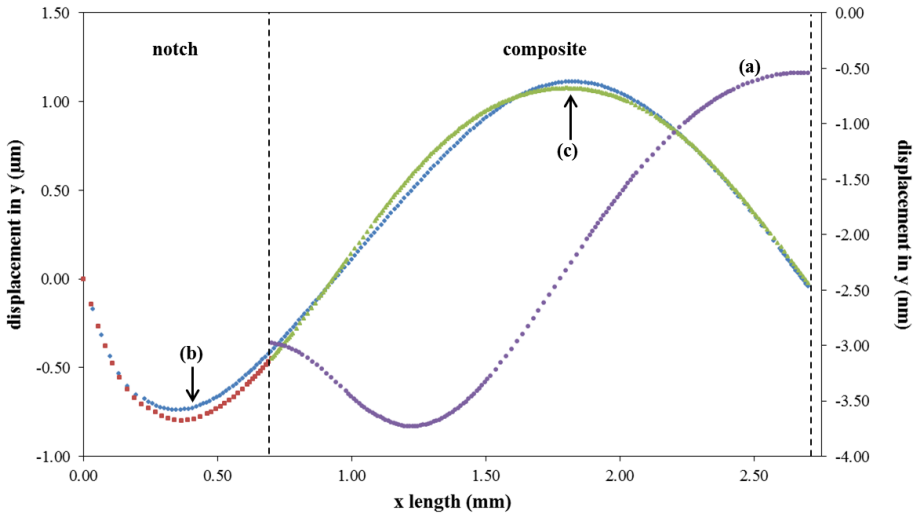

Figure S2. Comparison of the y-direction displacement of the different edges of a PEMC sensor is shown. The edges (c) and (b) are the bottom and top edges of the PZT as shown in Figure S1, Panel A. The displacement in these edges seems to be in phase with each other unlike edge (a) representing the top edge of the glass which seems to follow the displacement in the PZT with a lag. This behavior suggests the presence of a shear-type oscillation for this mode.

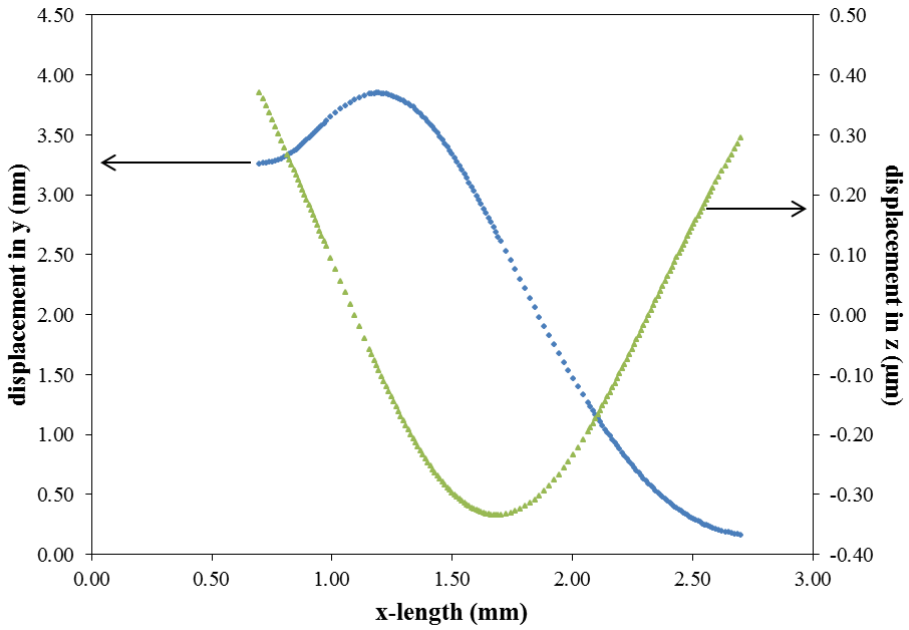

Figure S3. The y-direction and z-direction displacement of edge (d), the top free edge of glass is shown. This shows that as the edge (d) shows shear-type oscillation in the y-direction, it also has a flexural oscillation character in the z-direction.

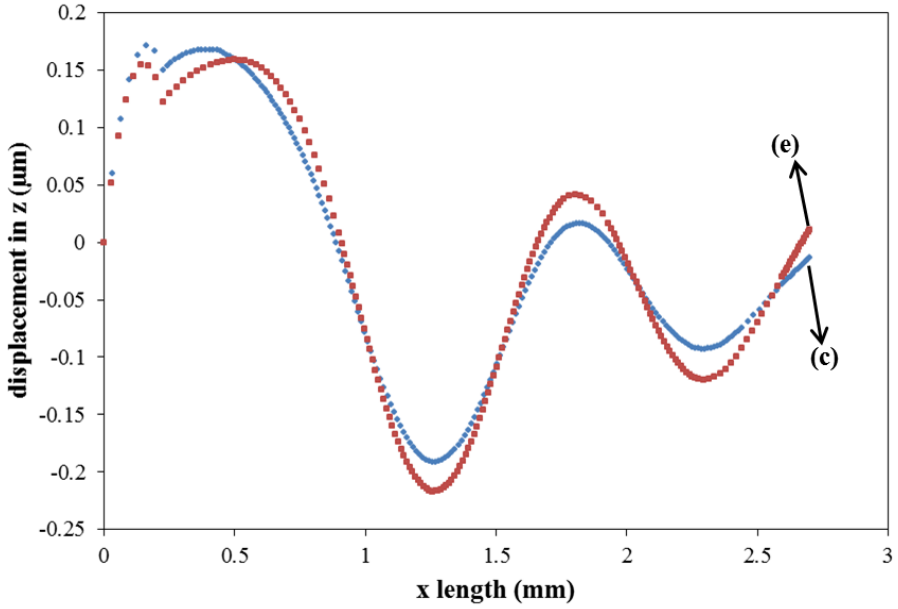

Figure S4. The z-direction displacement of the bottom long edges of the PZT, (c) and (e), are compared here. This comparison shows that this high-order mode of PEMC sensors has a flexural character to it but since the z-displacements for the two edges are out of phase there is a slight torsional character to this mode as well.

6.5. References

[1] H. Sharma, R. Mutharasan, Adhesion determines resonance response of piezoelectric cantilever sensors, Applied Physics Letters, 98(2011) 114101-3.

[2] D. Maraldo, R. Mutharasan, Mass-change sensitivity of high-order mode of piezoelectric-excited millimeter-sized cantilever (PEMC) sensors: Theory and experiments, Sensors and Actuators B-Chemical, 143(2010) 731-9.

[3] D. Maraldo, F.U. Garcia, R. Mutharasan, Method for quantification of a prostate cancer biomarker in urine without sample preparation, Analytical Chemistry, 79(2007) 7683-90.

[4] K. Rijal, R. Mutharasan, PEMC-based Method of Measuring DNA Hybridization at Femtomolar Concentration Directly in Human Serum and in the Presence of Copious Noncomplementary Strands, Analytical Chemistry, 79(2007) 7392-400.

[5] D. Maraldo, R. Mutharasan, Detection and confirmation of staphylococcal enterotoxin B in apple juice and milk using piezoelectric-excited millimeter-sized cantilever sensors at 2.5 fg/mL, Analytical Chemistry, 79(2007) 7636-43.

[6] G.A. Campbell, J. Uknalis, S.-I. Tu, R. Mutharasan, Detection of *Escherichia coli* O157:H7 in ground beef samples using piezoelectric excited millimeter-sized cantilever (PEMC) sensors, Biosensors and Bioelectronics, 22(2007) 1296-302.

[7] D. Maraldo, R. Mutharasan, 10-minute assay for detecting *Escherichia coli* O157 : H7 in ground beef samples using piezoelectric-excited millimeter-size cantilever sensors, J Food Prot, 70(2007) 1670-7.

[8] D. Maraldo, R. Mutharasan, Preparation-free method for detecting Escherichia coli O157 : H7 in the presence of spinach, spring lettuce mix, and ground beef particulates, J Food Prot, 70(2007) 2651-5.

[9] H. Sharma, R.S. Lakshmanan, B.N. Johnson, R. Mutharasan, Piezoelectric cantilever sensors with asymmetric anchor exhibit picogram sensitivity in liquids, Sensors and Actuators B: Chemical, 153(2011) 64-70.

[10] J.N. D'Amour, J.J.R. Stalgren, K.K. Kanazawa, C.W. Frank, M. Rodahl, D. Johannsmann, Capillary Aging of the Contacts between Glass Spheres and a Quartz Resonator Surface, Physical Review Letters, 96(2006) 058301.

[11] G.L. Dybwad, A sensitive new method for the determination of adhesive bonding between a particle and a substrate, Journal of Applied Physics, 58(1985) 2789-90.

[12] A. Laschitsch, D. Johannsmann, High frequency tribological investigations on quartz resonator surfaces, Journal of Applied Physics, 85(1999) 3759-65.

[13] R.S. Lakshmanan, R. Mutharasan, A method for characterizing mechanical properties of sugar films using a piezoelectric-excited millimeter sized cantilever (PEMC) sensor, Sensors and Actuators B: Chemical, 160(2011) 1304-8.

Chapter 7 . A novel pulsed-plasma approach for protein immobilization by grafting reactive amine groups on polyurethane-coated biosensors

7.1. Introduction

Immobilization of recognition molecules on a sensor is a critical step for successful biosensing and establishing limit of detection [1, 2]. Antibodies, DNA, enzymes, phages and aptamers are some of the recognition molecules used in biosensing. They are rich in surface functional groups that can covalently react to complementary surface functional groups on the sensor surface. Although many methods have been explored for surface immobilization [3], three major techniques are used extensively. Sensor surfaces are often silica due to the availability of many established fabrication techniques used in semiconductor processing. Silica surfaces are functionalized with amine groups via salinization reactions [4]. Second method for generating reactive functional groups is to coat the sensor surface with a reactive polymer such as agarose gel or polyacrylamide. [5]. Deposition of gold on the sensor surface provides Au<111> sites for chemisorption of thiolated biological molecules [3]. These three techniques are effective, but involve multiple steps and often require wet-chemistry preparations. It is desirable to develop a single-step method that does not involve wet-chemistry to simplify functionalization, and is the subject of this work.

A promising dry approach is the use of plasma for grafting functional groups. Plasma, a quasi-neutral gas, is a collection of electrons, ions, radicals and atomic and molecular species generated by electromagnetic fields. Advantages of plasma-assisted

functionalization are that it is a relatively easy to perform, single-step method that does not involve wet-chemistry or any post-functionalization treatment. Although plasma-assisted functionalization has been examined [6-8], its application for immobilization of recognition molecules has been investigated only to a limited extent [9-11]. Investigations for applications on biosensors are even fewer.

Sensors often have an electrically-active layer such as piezoelectric or piezo-resistive elements that are to be electrically insulated by a hydrophobic coating such as polyurethane (PU) [12] or SU-8 [13]. Since the antibodies are immobilized via their exposed amine or carboxylic acid groups, in the current work, we investigated grafting amine groups on polyurethane-coated sensors. For surfaces that have some exposed functional groups plasma-grafting is employed whereas for surfaces that do not have any functional groups *in situ* plasma-polymerization can be used. For plasma-polymerization, however, good adhesion of the polymer film with the sensor surface is paramount for mass-sensitive devices.

For amine functionalization, one can use gaseous ammonia (NH_3) [14] or amine containing volatile reagents such as ethylene diamine [9]. To date the former was used to functionalize polytetrafluoroehtylene in a prostheses study while the latter was investigated by *in situ* polymerization on gold electrode of a quartz crystal microbalance (QCM). The quality of surface functionalization in the latter was subsequently characterized with sensing experiments and was shown to be superior to polyethylenimine and (γ-aminopropyl) triethoxysilane. [9]

In the above reported studies continuous plasma treatment was employed for both grafting and polymerization. On the other hand pulsed plasma has the potential to yield higher retention of the desired functional groups compared to continuous plasma due to the shorter exposure to the plasma that is generated which contains highly reactive radicals. Consequently, to increase the likelihood of retaining the desired amine functional group on the PU surface a pulsed-plasma approach was investigated.

Ammonia, unlike ethylene diamine is a gaseous reagent and therefore is more compatible with gas-phase plasma systems and requires a simpler experimental arrangement. Further, there is no need to control polymerization as was the case with ethylene diamine [8]. To the authors' knowledge, the current study is the first one that examined ammonia gas for grafting amine functional groups on PU surface for the purpose of immobilizing recognition molecules for biosensing.

Piezoelectric excited millimeter-sized cantilever (PEMC) sensors are mass-sensitive sensors which contain the electro-active element, lead zirconate-titanate (PZT) that is insulated by PU coating [15]. In the current work we characterize amination of PU surfaces by spectroscopic analysis and the effectiveness of amination was determined by sensor responses to immobilization of carboxylated polystyrene beads as substitutes for proteins that can be visualized under a scanning electron microscope (SEM) as confirming visual evidence of the effectiveness of the investigated approach. Bovine serum albumin (BSA) chemisorption, for direct evidence of protein immobilization is also shown.

7.2. Materials and Methods

7.2.1. Sensor fabrication

PEMC sensors were fabricated by attaching a 2×1×0.160 mm^3 (L×W×H) quartz piece to a 5×1×0.127 mm^3 (L×W×H) PZT layer and the composite was anchored in epoxy as described previously [16]. Electrical insulation was provided by coating the finished sensors with electronic-grade polyurethane (Wasser High-Tech Coatings). PEMC sensors were brush-coated with PU and allowed to cure at room temperature for 7 days prior to use.

7.2.2. Ammonia plasma treatment

A plasma reactor (PDC-001, Harrick Plasma) was used for generation of ammonia plasma. A schematic of the plasma apparatus is shown in Figure 7-1A. Anhydrous ammonia gas (99%) from Airgas, Inc was connected to the inlet of the plasma reactor via a mass flow controller (Aalborg Instruments and Controls, Inc.). The substrates were placed near the exit of the reaction chamber and along the axis of the exit tube to ensure good contact with the generated radicals.

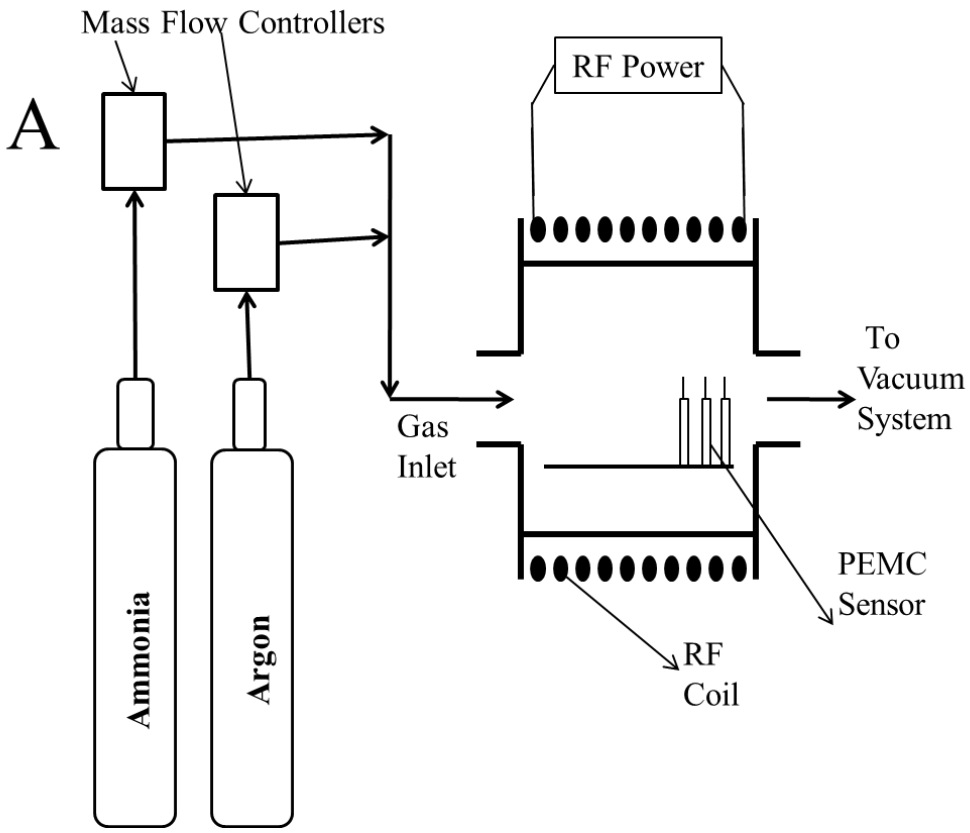
A
Mass Flow Controllers
RF Power
To
Vacuum
System
Gas
Inlet
PEMC
Sensor
RF
Coil
Ammonia
Argon

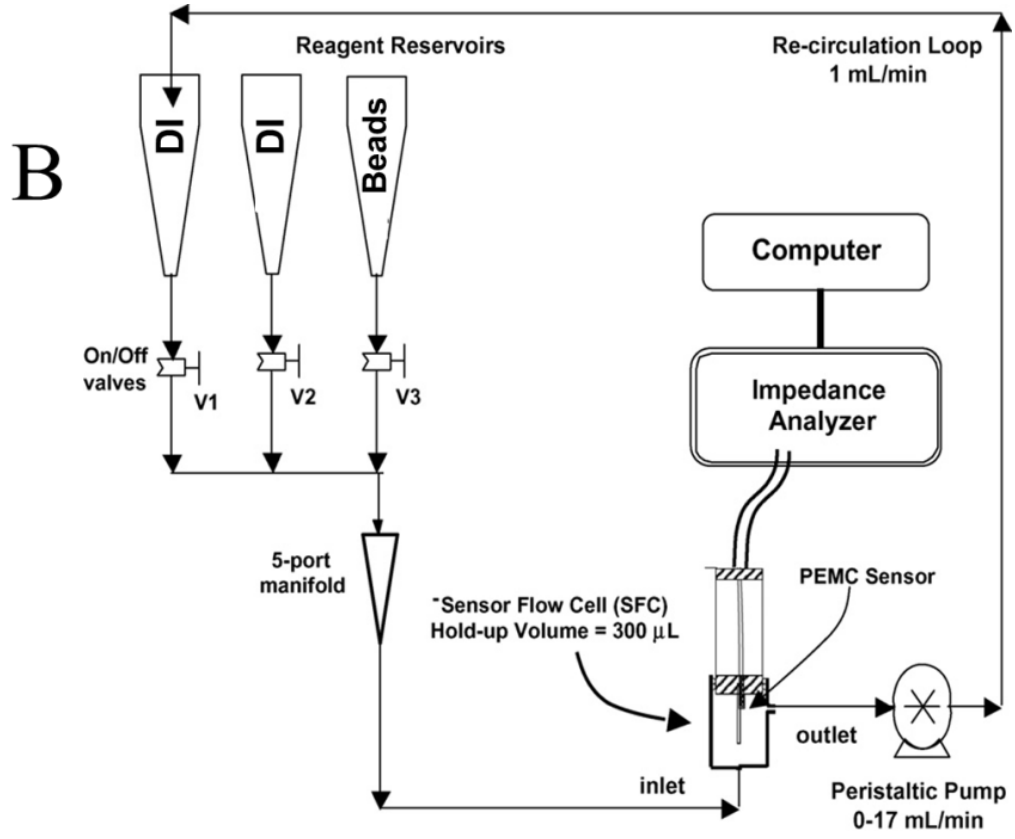
B
Reagent Reservoirs
Re-circulation Loop
1 mL/min
DI
DI
Beads
Computer
Impedance
Analyzer
On/Off
valves
V1
V2
V3
5-port
manifold
Sensor Flow Cell (SFC)
Hold-up Volume = 300 µL
PEMC Sensor
outlet
inlet
Peristaltic Pump
0-17 mL/min

Figure 7-1 Panel A shows the schematic of the plasma reactor and the experimental arrangement. **Panel B** shows the schematic of the flow apparatus for the binding experiments with PEMC sensors and the carboxylated beads.

The pressure in the reaction chamber was pumped down to 100 mTorr and anhydrous ammonia was then introduced into the reaction chamber at 7 sccm. The chamber pressure rose and was allowed to stabilize at 200 mTorr. The RF generator, set at 7W, was turned on for 1 second followed by a period of 180 seconds during which the RF generator was turned off and ammonia flow was continued at the same flow rate. When the RF generator was turned on a white colored glow discharge was visible through the view port. The on-time of 1 sec was used because that was the minimum achievable on the apparatus. To determine the influence of plasma treatment on the amination achieved, the substrates were pulsed-plasma treated for 1, 2 and 10 cycles. Pulsed-plasma treatment was used in this work with on-off times of 1s-180s, respectively, in order to reduce further breakdown of generated ammonia radicals.

7.2.3. FTIR characterization and sensor response

Infra-red (IR) spectra of plasma treated and untreated PU surfaces were obtained in the attenuated total reflectance (ATR) mode using the golden gate accessory (diamond crystal) on Nicolet 6700 FT-IR spectrometer. To avoid the spurious spectral properties of glass, single-side polished, 500 μm thick Si<100> wafers (WRS Materials, San Jose, CA)

spin coated with PU (1000 RPM, 15 seconds) were used as substrates for the spectral characterization. Same samples were subjected to increasing number of cycles of plasma treatment for determining extent of amination.

Carboxylated polybeads (1 μm diameter, Polysciences, Inc.) were used to test the reactivity of surface amine groups on plasma-treated surfaces. Since the PEMC sensor is a resonance mode mass-change sensor, resonance frequency was measured from frequency sweeps (Agilent-4294A; 100 mV) followed by determining the frequency at which a sharp change in phase angle occurred between the excitation voltage and the resulting current [16]. In these experiments 2 mm^2 area at the distal end of the sensor was plasma-treated by masking the rest of the sensor to prevent amination. Figure 7-1B shows a schematic of the flow system used for these experiments.

The PEMC sensor was housed in a custom-built flow cell which has a hold-up volume of 300 μL. Reservoirs containing deionized (DI) water and a suspension of carboxylated beads in DI water were connected to the flow cell via on-off valves and a 5-port manifold. A peristaltic pump was used to control the flow rate at 1 mL/min. After the sensor reached a stable resonance frequency, 1 mL of a suspension of 1 μm diameter carboxylated beads in DI water (10^4 and 10^7 beads/mL) was introduced into the flow loop. The reaction between carboxyl groups on the beads and the amine groups on the sensor caused the mass of the oscillating sensor to increase which was monitored by resonance frequency sweeps. For visual confirmation, SEM micrographs (XL-30 ESEM FEG, FEI) of the PEMC sensors after reaction with 1 μm diameter polybeads were obtained.

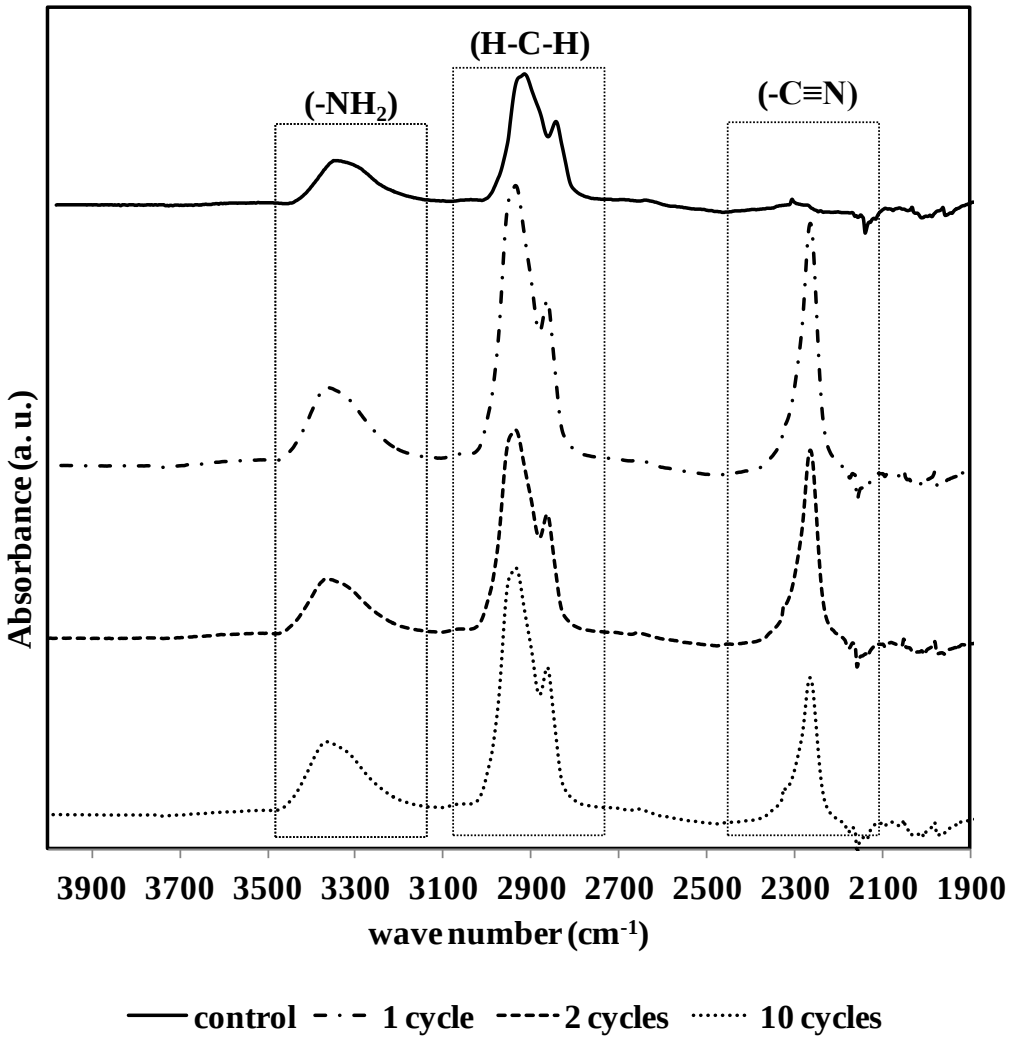

Figure 7-2 ATR-FTIR spectra of the PU samples pulse-plasma treated with ammonia for 1, 2 and 10 cycles are compared to a control, untreated native PU sample. The changes in the nitrile (-C≡N) group peak centered at 2260 cm^{-1} and amine group twin-peak set centered at3353 cm^{-1} indicates an increase in the presence of the nitrogen on the plasma-treated samples. Increasing plasma cycles caused a monotonic decrease in the nitrile peak. The amine peak on the other hand showed an increase after 1 plasma cycle followed by a decrease between 1 and 2 cycles of plasma treatment and then an increase between 2 and 10 cycles.

The PEMC sensor was housed in a custom-built flow cell which has a hold-up volume of 300 µL. Reservoirs containing deionized (DI) water and a suspension of carboxylated beads in DI water were connected to the flow cell via on-off valves and a 5-port manifold. A peristaltic pump was used to control the flow rate at 1 mL/min. After the sensor reached a stable resonance frequency, 1 mL of a suspension of 1 µm diameter carboxylated beads in DI water (10^4 and 10^7 beads/mL) was introduced into the flow loop. The reaction between carboxyl groups on the beads and the amine groups on the sensor caused the mass of the oscillating sensor to increase which was monitored by resonance frequency sweeps. For visual confirmation, SEM micrographs (XL-30 ESEM FEG, FEI) of the PEMC sensors after reaction with 1 µm diameter polybeads were obtained.

Bovine serum albumin (BSA) and phosphate buffered saline (PBS) were purchased from Sigma Aldrich. Ammonia plasma treated PEMC sensor was installed in the flow cell as described above and allowed to reach a stable frequency value in PBS at 1 mL/min flow rate. BSA at 500 pg/mL concentration was introduced to the flow loop and its chemisorption on the sensors was observed in the form of resonance frequency decrease.

7.3. Results and Discussion

7.3.1. ATR-FTIR Analysis

Several combination of on-off times for plasma treatment were investigated for the generation of amine functional groups on the PU-coated PEMC sensors and the combination of 1s-180s for on-off cycle gave the desired results and was used subsequently. Figure 7-2 shows a typical comparison of the background-subtracted ATR-FTIR scans (64-scan average; 2 cm^{-1} resolution) of the PU substrates after plasma treatment for various numbers of cycles. The peak centered at 2260 cm^{-1} represents the nitrile (–C≡N) bond [17]. From Figure 7-2 it is clear that the untreated control PU substrate did not show the nitrile associated peaks. After one cycle of plasma, the spectrum begins to show the presence of nitrogen on the surface in the form of nitrile group. With increasing plasma cycles the nitrile peak decreased in magnitude. After 2 cycles the area under the 2260 cm^{-1} peak reduced by 20% and further treatment for 10 cycles reduced the area further by 35%. The decrease in nitrile group with increasing plasma cycles can be attributed to degradation caused by prolonged exposure to high-energy radicals. Similarly, the twin-peak set centered at 3353 cm^{-1} shows the presence of nitrogen on the substrate in the form of nitrogen-hydrogen (-NH) bonds. The unresolved twin-peak suggests the presence of primary amines ($-NH_2$) on the PU surface [17]. From Figure 7-2, it is clear that native PU has amine surface functional groups and that the intensity of the peak representing the (-N-H) bond increased after one plasma cycle. When compared to the area under the peak after one cycle, the area decreased by 45% and 25% after two and ten cycles respectively. The non-monotonic response of amine group is in contrast to the observed monotonic decrease in surface nitrile groups with increasing cycles of plasma treatment. The changes in the presence of amine groups

between one and two cycles of plasma treatment can be attributed to the longer exposure to high-energy radicals and it suggests that the rate of formation of amine groups was higher than the rate of degradation. The results in Figure 7-2 indicate that surface –NH and $–NH_2$ groups are formed with a one second ammonia plasma treatment and that longer exposure of the surface bound amine groups leads to their partial degradation and simultaneously new amine groups are generated on the surface by these radicals.

7.3.2. Validation of reactivity with carboxyl groups

ATR-FTIR analysis showed the presence of amine groups on the PU surface but their reactivity to carboxyl groups was tested for surface immobilization of biological molecules. Since FTIR samples the evanescent region, the measurement includes functional groups that are near the surface but not necessarily those that react with the carboxyl groups present on another entity. Concentration of surface-reactive amine groups is best established by examining reactivity with commercially available 1 μm carboxylated polybeads. Since each bead weighs 500 fg, their reaction with a PEMC sensor should cause the resonance frequency to decrease and can be continuously measured by an impedance analyzer.[16] Use of carboxylated polybeads also gave us the ability to visually confirm the presence of the beads that bound to the sensors. Ammonia-plasma treated PEMC sensors were installed in a flow cell with DI water as the running buffer in the flow apparatus shown in Figure 7-1B. After sensor stabilization, 1 mL of 1 μm carboxylated beads was introduced into the flow circuit. In Figure 7-3 we compare the response obtained on a PEMC sensor coated with PU that was not ammonia-plasma

treated (Figure 7-3(a)) with that observed on sensors that had undergone 1 plasma cycle (Figure 7-3(b, c)).

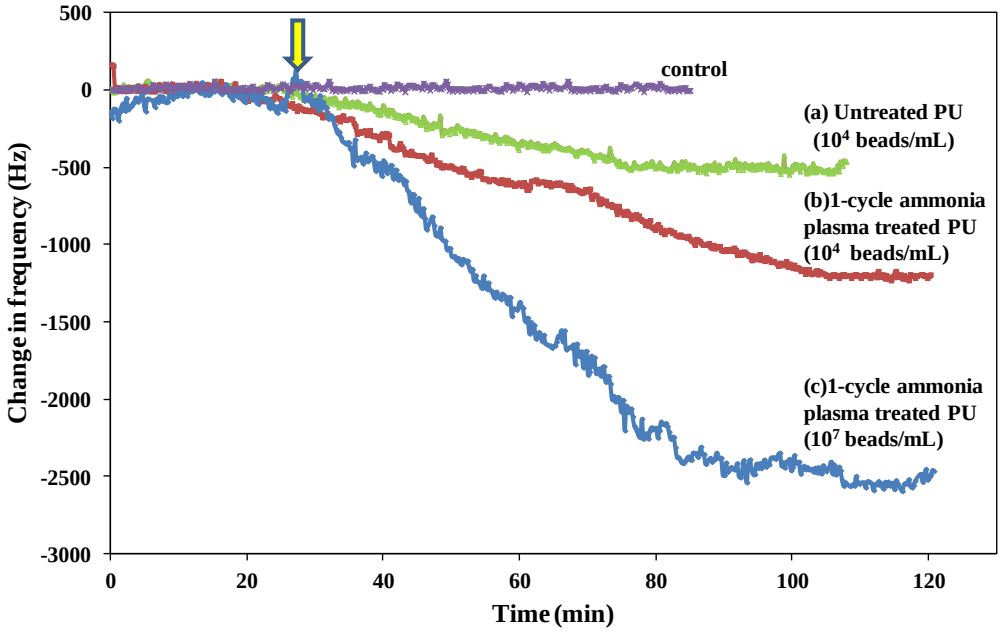

Figure 7-3 Comparison of PEMC sensor response to carboxylated beads. Sensor that was not plasma treated (a) when exposed to 10^4 beads/mL gave a response of -522 Hz. One cycle plasma-treated PEMC sensors, when exposed to concentrations of 10^4 beads/mL, same as the control sensor (b) and 10^7 beads/mL (c) gave responses of -1217 Hz and -2511 Hz respectively.

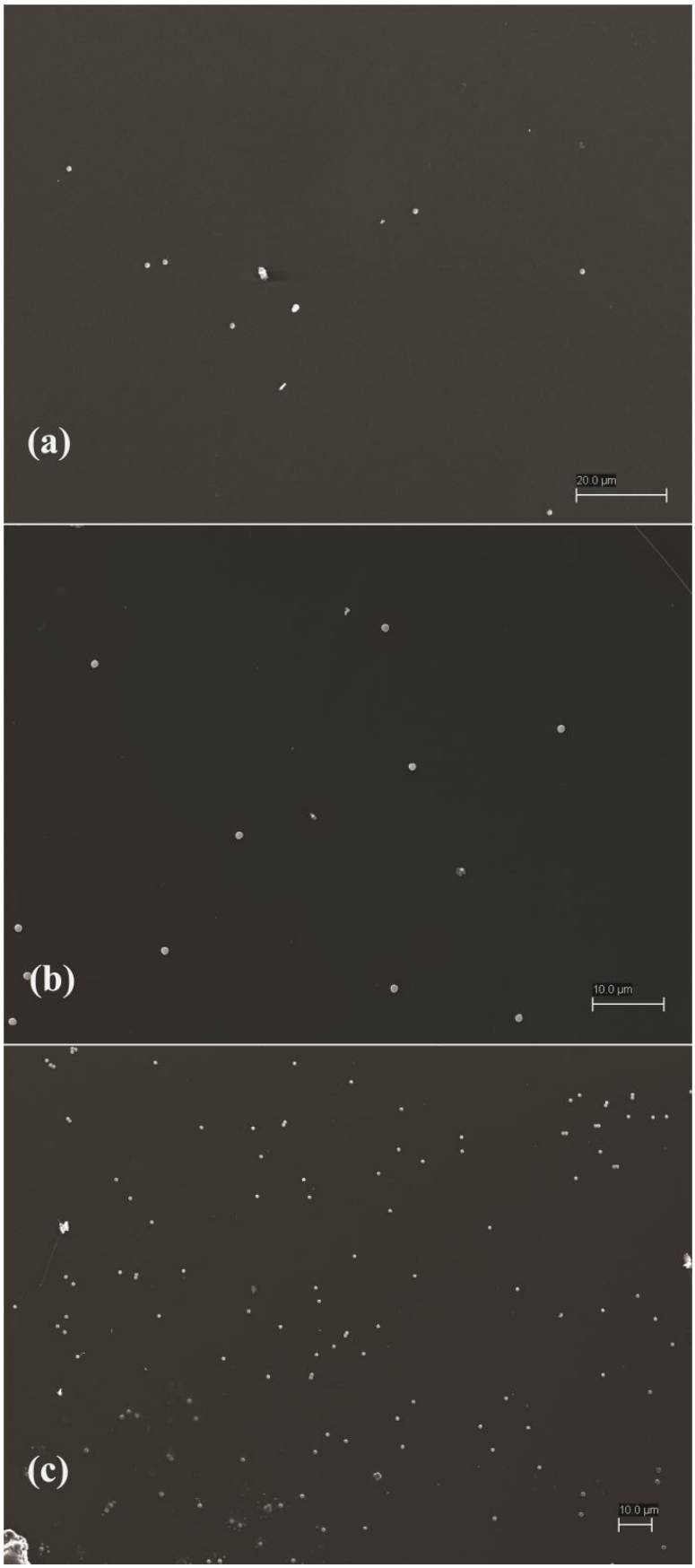
(a)
20.0 µm
(b)
10.0 µm
(c)
10.0 µm

Figure 7-4 SEM micrographs of untreated (a) and 1 cycle ammonia plasma-treated (b, c) sensors are shown. Sensors (a) and (b) were exposed to the same concentration of beads (10^4 beads/mL). Sensor (c) was exposed to a higher concentration of 10^7 beads/mL.

Two sets of experiments were done. In the first 1 mL of 10^4 beads/mL samples was used and in the second, 10^7 beads/mL was used to investigate the effect of increasing the sample concentration. The control sensor was not plasma treated and when it was exposed to 10^4 carboxylated beads/mL, the resonance frequency decreased by 522 ± 52 Hz (n=3) suggesting that the native PU surface has reactive amine groups. The FTIR spectrum (Figure 7-2) confirmed the presence of the surface amine functional groups. The increase in mass on the sensor due to the reaction between the carboxyl groups on the beads and the surface amine groups in native PU caused the observed resonance frequency decrease. We can further validate the reaction by examining the SEM micrographs of the sensor exposed to the beads (Figure 7-4(a)). The bead count on the control sensor, as estimated from the micrographs, was 186 ± 32 per mm^2 and corresponds to a mass-loading of ~186 ± 16 pg. By this count the sensitivity of the PEMC sensor can be calculated as 356 fg/Hz at a mass loading of 186 pg and is comparable to previous designs[18]. In comparison, a larger number of the beads were attached to one-cycle ammonia plasma treated sensor when exposed to the same bead concentration. The resulting response was over two-fold larger at 1217 ± 37 Hz (n=4). The bead count on the SEM micrograph (Figure 7-4(b)) was considerably higher than the untreated sensor at 837±18 per mm^2 and corresponded to a mass addition of 877 ± 9 pg.

Further, to investigate the effect of higher concentration of beads the sensor was exposed to 1 mL of 10^7/mL carboxylated beads which caused the resonance frequency to decrease by 2511 ± 24 Hz (n=3). In Figure 7-4(c) SEM micrograph of this sensor showed the bead count to be nearly four-fold higher at 3437±23 per mm^2 that caused the mass loading to be ~3.6 ± 12 ng. Plasma-treated sensors, when exposed to higher concentration of carboxylated beads exhibited a larger frequency response because a larger number of beads became bound to them.

The kinetics for the reaction between the carboxyl groups on the beads and amine surface functional group are exponential in nature as shown in Figure 7-3. Although the beads are 1 μm particles and are much larger than molecules such as thiols, the exponential character of the kinetics is similar to thiol chemisorption on gold surfaces. Thus, it is reasonable to consider Langmuir model for characterizing kinetics [19, 20].

If we assumed that all the surface amine groups have the same reactivity and the reaction is reversible, the rate of reaction can be expressed as

$$\frac{dn}{dt} = k_a C_B^o (N - n) - k_d n \qquad (1)$$

where n is the number of carboxylated beads on the plasma-aminated PU surface at time t, N is the maximum number of beads that can bind to the PU surface, therefore, (N-n) is the number of reactive amine groups present on the PU surface at time t. k_a and k_b are the

intrinsic forward and backward rate constants, respectively. C_B^o is the bulk concentration of the carboxylated beads. Integrating the above and rearranging gives

$$\frac{n}{N} = \frac{k_a C_B^o}{k_a C_B^o + k_d}\left(1 - e^{-(k_a C_B^o + k_d)t}\right) \quad (2)$$

At equilibrium the net rate of reaction is zero and thus the above can be rearranged to

$$\frac{n_{eq}}{N} = \frac{k_a C_B^o}{k_a C_B^o + k_d} \quad (3)$$

The change in the resonance frequency (-Δf) of the PEMC sensors is proportional to the change in its mass. The change in resonance frequency at any time *t*, is given by$(-\Delta f) = m_B n/\sigma$, where m_B is the mass of one bead and σ is the mass-change sensitivity of the sensor. At steady state when all of the surface amine groups have reacted, the change in resonance frequency is designated as $\left(-\Delta f_{eq}\right) = m_B N/\sigma$. Therefore the change in frequency can be expressed in terms of the bulk bead concentration and the intrinsic rate constants as

$$\ln\left(\frac{(-\Delta f_{eq}) - (-\Delta f(t))}{-\Delta f_{eq}}\right) = -k_{obs} t \quad (4)$$

where $k_{obs} = k_a C_B^o + k_b$ and is therefore the observed reaction rate constant. The slope of the straight line plot of left-hand side (LHS) of the above equation versus time would yield the value of the observed rate constant.

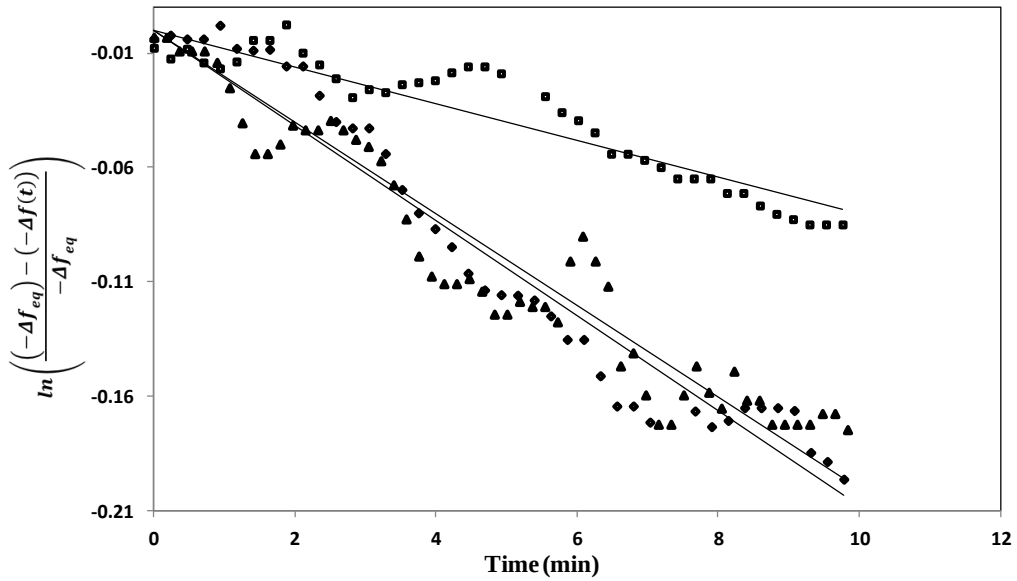

Figure 7-5 Initial rate analysis based on Lagmuir kinetic model of the carboxylated beads binding to the control and plasma-aminated sensors at different concentrations are shown. An increase in the value of the rate constant of the reaction was observed with increasing concentration of beads. [▲] control sensor exposed to 10^4 beads/mL; [♦] one cycle plasma treated sensor exposed to 10^4 beads/mL; [■] one cycle plasma treated sensor exposed to 10^7 beads/mL.

For the carboxylated bead experiments the concentration of the available reactive amine surface groups decreases with reaction time and to compensate for this decrease initial rate kinetic analysis limited to the first ten minutes was carried out. The data in Figure 7-3 when modeled using the Langmuir kinetic model gave the following values of the observed binding rate constant (min^{-1}): 0.02, 0.008 and 0.021 for a control sensor exposed to 10^4 beads/mL, 1-cycle plasma-treated sensor exposed to 10^4 beads/mL and 1-cycle plasma-treated sensors exposed to 10^7 beads/mL respectively. The correlation

coefficients for linear fits to this data as shown in Figure 7-5 were 0.92, 0.88 and 0.95 respectively. Investigation of similar reactions of humic acid adsorption on amine functionalized surfaces indicated a comparable value of 0.037 min^{-1} for the rate constant. [21] For 1-cycle plasma-treated sensors the binding rate constant showed an increase with increasing concentration of the carboxylated beads.

7.3.3. BSA chemisorption

Carboxylated polybeads worked as good substitutes for proteins to show that grafting amine functional groups using ammonia plasma can be used for immobilization via PEMC sensor response as well as SEM micrographs. Direct evidence of protein immobilization one cycle ammonia plasma treated PEMC sensors was also achieved using BSA as a model protein. After the PEMC sensor had stabilized in the flow cell in PBS, introduction of 1 mL of BSA at 500 pg/mL concentration into the flow loop caused the resonance frequency to decrease by 843 ± 42 Hz (n=2) as shown in Figure 7-6. Positive control experiments were run where a control sensor was exposed to the same concentration of BSA and no frequency response was observed. Despite the presence of some surface amine groups on the control polyurethane surface, the mass addition due to BSA chemisorption was not sufficient to cause a decrease in resonance frequency.

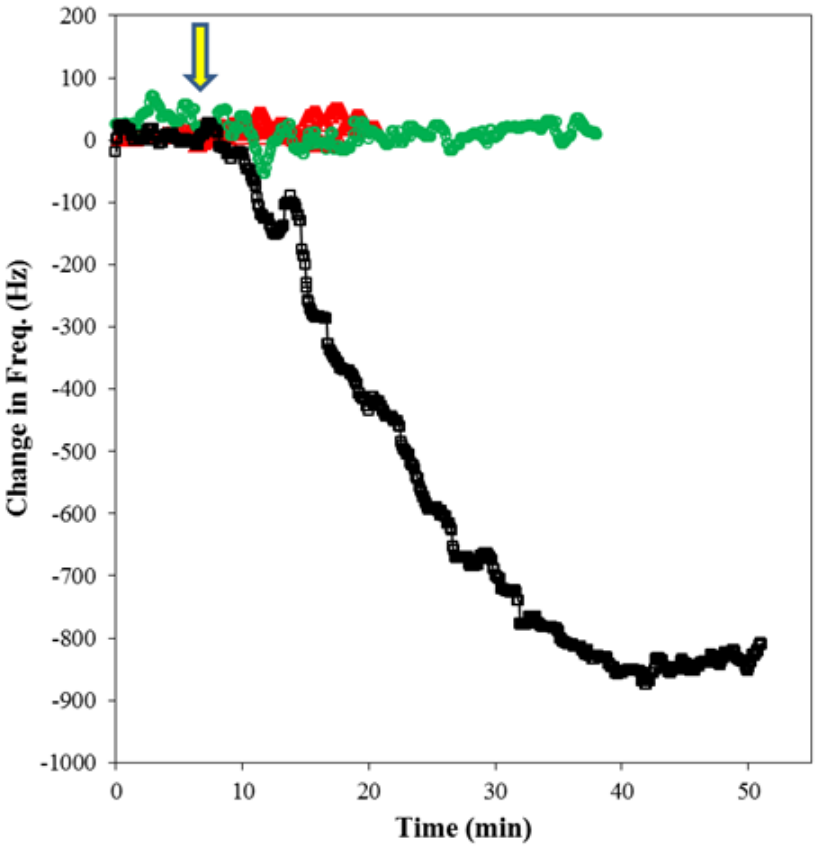

Figure 7-6 Typical response for chemisorption of BSA at 500 pg/mL concentration on one cycle ammonia plasma treated PEMC sensors is shown in black. BSA chemisorption caused the resonance frequency to decrease by 843 Hz. The curve in green represents the positive control; when a PEMC sensor without any ammonia plasma treatment was exposed to 500 pg/mL of BSA and did not exhibit a frequency shift. The curve in red is the negative control for one cycle ammonia plasma treated PEMC sensor in PBS.

7.4. Conclusion

Pulsed plasma treatment of PU surface with ammonia gas was shown to be a successful dry and rapid method for amination. With increasing number of cycles of plasma treatment the exposed functional groups on PU surface degrade due to exposure to the high-energy radicals. The reactive surface amine groups generated by the method can be used for immobilization of biological molecules for biosensing experiments as was successfully demonstrated by the reaction of carboxylated beads and BSA on PEMC sensors.

7.5. References

[1] J.P. Alarie, M.J. Sepaniak, T. Vo-Dinh, Evaluation of antibody immobilization technqiues for fiber optic-based fluoroimmunosensing, Anal. Chim. Acta, 229 (1990) 169-176.

[2] H. Berney, P. Roseingrave, J. Alderman, W. Lane, J.K. Collins, Biosensor surface characterisation: confirming multilayer immobilisation, determining coverage of the biospecies and establishing detection limits, Sens. Actuators, B, 44 (1997) 341-349.

[3] G.T. Hermanson, Bioconjugate Techniques, Second ed., Academic Press, 2008.

[4] P.B. Daniels, J.K. Deacon, M.J. Eddowes, D.G. Pedley, Surface plasmon resonance applied to immunosensing, Sens. Actuators, 15 (1988) 11-18.

[5] J. Rubio Retama, M. Sánchez-Paniagua López, J.P. Hervás Pérez, G. Frutos Cabanillas, E. López-Cabarcos, B. López-Ruiz, Biosensors based on acrylic microgels: A comparative study of immobilized glucose oxidase and tyrosinase, Biosens. Bioelectron., 20 (2005) 2268-2275.

[6] A. Hiratsuka, I. Karube, Plasma polymerized films for sensor devices, Electroanalysis, 12 (2000) 695-702.

[7] B. Gupta, N. Anjum, Plasma and Radiation-Induced Graft Modification of Polymers for Biomedical Applications, in: Radiation Effects on Polymers for Biological Use, Springer-Verlag Berlin, Berlin, 2003, pp. 35-61.

[8] F.F. Shi, Recent advances in polymer thin films prepared by plasma polymerization Synthesis, structural characterization, properties and applications, Surf. Coat. Technol., 82 (1996) 1-15.

[9] K. Nakanishi, H. Muguruma, I. Karube, A Novel Method of Immobilizing Antibodies on a Quartz Crystal Microbalance Using Plasma-Polymerized Films for Immunosensors, Anal. Chem., 68 (1996) 1695-1700.

[10] K. Kojima, A. Hiratsuka, H. Suzuki, K. Yano, K. Ikebukuro, I. Karube, Electrochemical Protein Chip with Arrayed Immunosensors with Antibodies Immobilized in a Plasma-Polymerized Film, Anal. Chem., 75 (2003) 1116-1122.

[11] Z. Zhang, W. Knoll, R. Förch, Amino-functionalized plasma polymer films for DNA immobilization and hybridization, Surf. Coat. Technol., 200 (2005) 993-995.

[12] D. Maraldo, R. Mutharasan, 10-minute assay for detecting *Escherichia coli* O157 : H7 in ground beef samples using piezoelectric-excited millimeter-size cantilever sensors, J. Food Prot., 70 (2007) 1670-1677.

[13] K. Rijal, R. Mutharasan, Method for measuring the self-assembly of alkanethiols on gold at femtomolar concentrations, Langmuir, 23 (2007) 6856-6863.

[14] M. Crombez, P. Chevallier, R.C. Gaudreault, E. Petitclerc, D. Mantovani, G. Laroche, Improving arterial prosthesis neo-endothelialization: Application of a proactive VEGF construct onto PTFE surfaces, Biomaterials, 26 (2005) 7402-7409.

[15] G.A. Campbell, R. Mutharasan, Method of measuring *Bacillus anthracis* spores in the presence of copious amounts of *Bacillus thuringiensis* and *Bacillus cereus*, Anal. Chem., 79 (2007) 1145-1152.

[16] D. Maraldo, K. Rijal, G.A. Campbell, R. Mutharasan, Method for Label-Free Detection of Femtogram Quantities of Biologics in Flowing Liquid Samples, Anal. Chem., 79 (2007) 2762-2770.

[17] D. Lin-Vien, N.B. Colthup, W.G. Fateley, J.G. Grasselli, The Handbook of Infrared and Raman Characteristic Frequencies of Organic Molecules, Academic Press, Inc, Boston, 1991.

[18] D. Maraldo, R. Mutharasan, Detection and confirmation of staphylococcal enterotoxin B in apple juice and milk using piezoelectric-excited millimeter-sized cantilever sensors at 2.5 fg/mL, Anal. Chem., 79 (2007) 7636-7643.

[19] D.S. Karpovich, G.J. Blanchard, Direct Measurement of the Adsorption Kinetics of Alkanethiolate Self-Assembled Monolayers on a Microcrystalline Gold Surface, Langmuir, 10 (1994) 3315-3322.

[20] D. Yan, J.A. Saunders, G.K. Jennings, Kinetics of formation for n-alkanethiolate self-assembled monolayers onto gold in aqueous micellar solutions of $C_{12}E_6$ and $C_{12}E_7$, Langmuir, 18 (2002) 10202-10212.

[21] T.S. Anirudhan, P.S. Suchithra, S. Rijith, Amine-modified polyacrylamide-bentonite composite for the adsorption of humic acid in aqueous solutions, Colloids Surf., A, 326 (2008) 147-156.

Chapter 8 . Half antibody fragements improve biosensor sensitivity without loss of selectivity

8.1. Introduction

Antibodies, due to their selectivity, are commonly used as recognition molecules in biosensing. For use in biosensors, they are to be immobilized on the sensor surfaces. Traditionally, reactive surface functional groups are generated on the sensor using wet-chemistry methods such as silanization on silica and other oxide surfaces that are reacted with complimentary functional group(s) on antibodies for immobilization. For sensors with a gold surface, self-assembled monolayers (SAM) of thiolated molecules containing a reactive functional group as well as physisorption of proteins such as protein A and protein G are commonly used as an initial layer for antibody immobilization via the F_c region for achieving right orientation[1]. We hypothesize that the use of the intermediate layer of protein G for immobilization can lower device sensitivity as the added mass effect may be reduced.

Antibodies are made of two heavy chains and two light chains of amino acids held together by disulfide bridges between the cysteine residues [2]. Reduction of these disulfide bridges will cleave an antibody into two equal halves and each of these halves will have active thiol groups that can directly chemisorb on Au<111> sites. Immobilization of reduced antibody can help with proper orientation of the antigen-binding F_{ab} regions because the thiol groups are at the far end and away from F_{ab} region and may also improve responses on evanescent wave biosensing platforms such as Surface Plasmon Resonance.[3] In this work we hypothesize that the use of half antibody

molecules by directly immobilizing them on the sensor surface can simplify the immobilization procedure and lead to properly oriented antibody resulting in improved device sensitivity. We test this hypothesis by comparing the responses obtained for the detection of pathogenic *E.coli* O157:H7 using Protein G as an intermediate for proper orientation of antibody to those obtained by direct physisorption of whole antibody molecules, as well as the proposed reduced and cleaved antibody. An established biosensing platform, quartz crystal microbalance (QCM), was used to measure the extent of immobilization and detection and binding responses.

Enzymes such as pepsin and papain are used to digest antibody (Ab) molecules to expose their native thiol groups for chemisorption on gold surfaces.[4] Pepsin digests the F_c region of the antibody to give a divalent Ab structure whereas the papain digest gives individual antigen-binding F_{ab} fragments. The fragments produced by enzyme digestion need further preparation steps for oriented immobilization on biosensor surfaces. A schematic for commonly used methods for cleaving antibodies is shown in Figure 8-1.

Chemicals commonly used for reducing antibodies are 2-mercaptoethanol (MEA) and dithiothreitol (DTT) [5]. DTT is a stronger reductant than MEA. Both, MEA and DTT, contain thiol groups that compete with the reduced antibodies for gold sites on the sensor surface. Therefore, the reducing agent should be removed prior to immobilization on the gold surface and adds an additional step to the protocol.

The use of MEA as a reducing agent for biosensing application has been investigated.[6, 7] Since MEA contains a thiol group, the unreacted MEA is removed from the cleaved antibody fragments using gel columns. Inefficiency of the separation

step can lead to MEA present in the reduced antibody solution that will compete for gold sites and also continue reduction of the disulfide group in the F_{ab} region of the antibody molecule. Some of the Ab fragments are lost during the separation step which might also explain why the first study did not find any improvement in sensitivity. In the second study gold nanoparticles were used to increase the surface area for immobilization of half Ab fragments which led to enhanced sensitivity and faster response rates.

An alternate to the sulfur containing reducing agents, which require a separation step, is a trialkylphosphine such as tris(2-carboxyethyl)phosphine (TCEP) that can be used for reduction of disulfides.[8] To the authors' knowledge, the use of TCEP for cleaving antibody for use as recognition molecules on a biosensor platform has not been investigated. A schematic of the reaction between the TCEP and the disulfide bonds in the antibody is shown in Figure 8-1. TCEP can be used for all molecules containing disulfides.

TCEP is a more stable and a stronger reducing agent than DTT. Since, TCEP is devoid of sulfur-containing groups, it does not compete with the reduced antibody for Au<111> sites and therefore a separation step is unnecessary making it a convenient reagent for gold-coated biosensors[9, 10].

8.2. Experimental Section

8.2.1. Reagents and equipments

All solutions were prepared using deionized(18MΩ) water. Bond-Breaker® TCEP solution was purchased from Thermo Scientific. Goat antibody against *Escherichia coli*

O157:H7 as well as the heat-killed positive *Escherichia coli* O157:H7 along with rabbit anti-goat IgG antibody were purchased from Kirkegaard and Perry Laboratories, Inc. Bovine Serum Albumin (BSA), Phosphate-buffered saline (PBS), sinapinic acid and acetonitrile were purchased from Sigma-Aldrich.

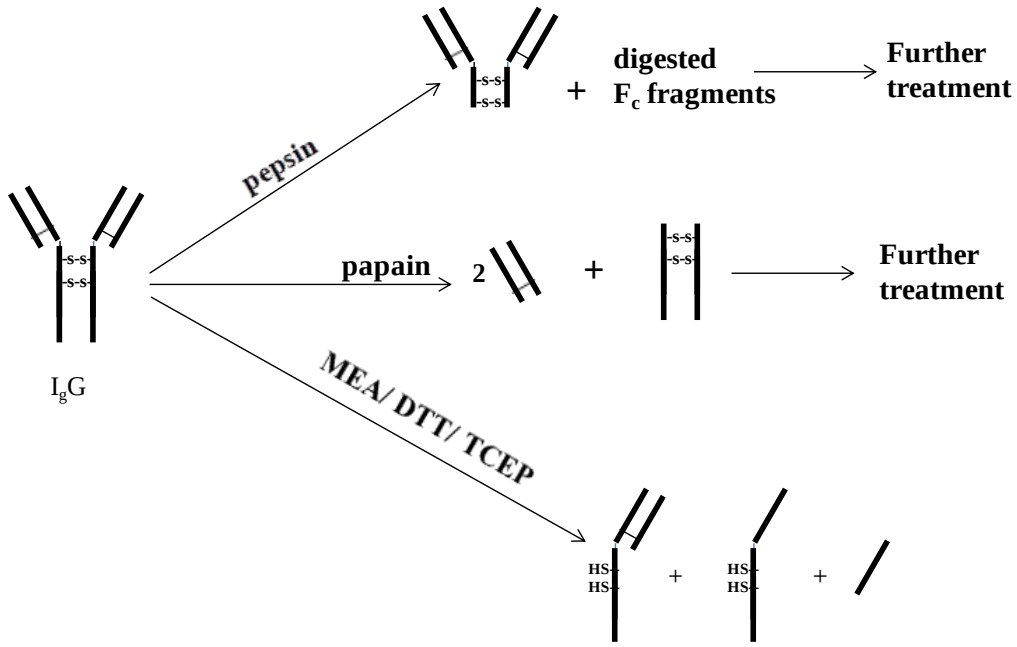

Figure 8-1 Schematic of the typical reactions used to cleave antibodies. Enzymes such as pepsin and papain cleave the antibodies around the disulfide bridges and these fragments can then be reacted for immobilization. MEA, DTT and TCEP reduce the disulfide bridges in the antibody molecules both in the F_c and F_{ab} regions.

Detection experiments were performed using a 5 MHz AT-cut quartz crystal and a teflon flowcell (Stanford Research Systems). The resonance frequency was measured using an impedance analyzer (HP 4192A) which was managed by a PC using a custom designed LabView® program.

8.2.2. Reduction of antibodies

TCEP solutions for antibody reduction were prepared in 10 mM PBS at 5 mM concentration. 10 µL of TCEP was added to 1mL of 10 µg/mL antibody in PBS. This solution was mixed well and the reduction reaction was carried out at room temperature for 60 min before injecting into the flow loop.

Different mole ratios of TCEP:Ab were run for two different lengths of time and the cleaved products were tested using SDS-PAGE. The reaction mixture of mole ratio of 100:1 TCEP:Ab for 1 hour was to give the desired results and was used for this study. Further optimization of this step was not done.

8.2.3. MALDI mass spectrometry

MALDI mass spectrometry (MALDI-MS) analysis was carried out using a linear detector on a Bruker Daltonics autoflex III equipped with smartbeam. Spectra obtained were externally calibrated using bovine serum albumin. For MALDI experiments rabbit anti-goat antibody was used as a substitute for the anti-*E.coli* O157:H7. Protein samples at 1 mg/mL in DI water were typically deposited (1 µL) on a dried film of 1 µL of

aqueous solution of sinapinic acid containing 50% acetonitrile using a stainless steel stage. Each spectrum was obtained under identical conditions.

8.2.4. QCM measurements

The quartz crystal was cleaned by exposing the gold surface to piranha solution (3:1 concentrated sulfuric acid to hydrogen peroxide) for 30 seconds followed by rinsing with copious amounts of DI water. The crystal was then exposed to oxygen plasma for 2 minutes which ensured a clean gold surface. The crystal was then rinsed with copious amounts of DI water and dried in nitrogen stream before installation in the flowcell. The reagent reservoirs were connected to the flowcell via a 5-port manifold and a syringe pump downstream from the flowcell pumped at a constant flowrate of 5 µL/min.

Once the crystal resonance frequency reached a stable value, 1mL of reagent was injected into the flowcell via the 5-port manifold to contact the crystal surface. The flow loop was flushed thoroughly with PBS before introduction of the second reagent to the crystal. As the reagents become immobilized on the crystal surface a decrease in resonance frequency was observed and recorded.

8.3. Results and Discussion

8.3.1. MALDI-MS

In Figure 8-2 we compare the antibody that was treated with TCEP for reducing the disulfide bridges with the control untreated antibody. The spectrum for native Ab exhibits the peaks for the monovalent (a), divalent (b) and trivalent (c) antibody molecular ions. The molecular weight of the antibody monomer is ~143.6 kDa. The intensity of the monovalent and the divalent molecular ions is almost identical for the native Ab sample. On the other hand, the spectrum for TCEP-reduced Ab exhibited almost double intensity for the divalent molecular ion peak (b). The peak widths for the divalent, trivalent and quatravalent ions should be ½, $^{1}/_{3}$, and ¼ of the peak width for the monovalent molecular ion.[11] This can sometimes be difficult to see for polyclonal antibodies but is visible in Figure 8-2. We expect TCEP to cleave the disulfides holding the two halves of the antibody molecules. A monovalent molecular ion of half the antibody molecule will coincide with the divalent ion of the whole antibody molecule and for the spectrum of TCEP-reduced Ab, the intensity of the peak at ~71.8 kDa increased which can be attributed to the presence of half antibody molecules. The TCEP-reduced Ab spectrum also exhibited increased intensity for the peak at ~35.9 kDa (e) which can correspond to quatravalent ion of the whole antibody or divalent ion for half antibody molecules. When compared to the native Ab spectrum which does not exhibit a peak at ~35.9 kDa, the inference that the increase in intensity of peak (e) was due to the presence of the half antibody fragments can be made.

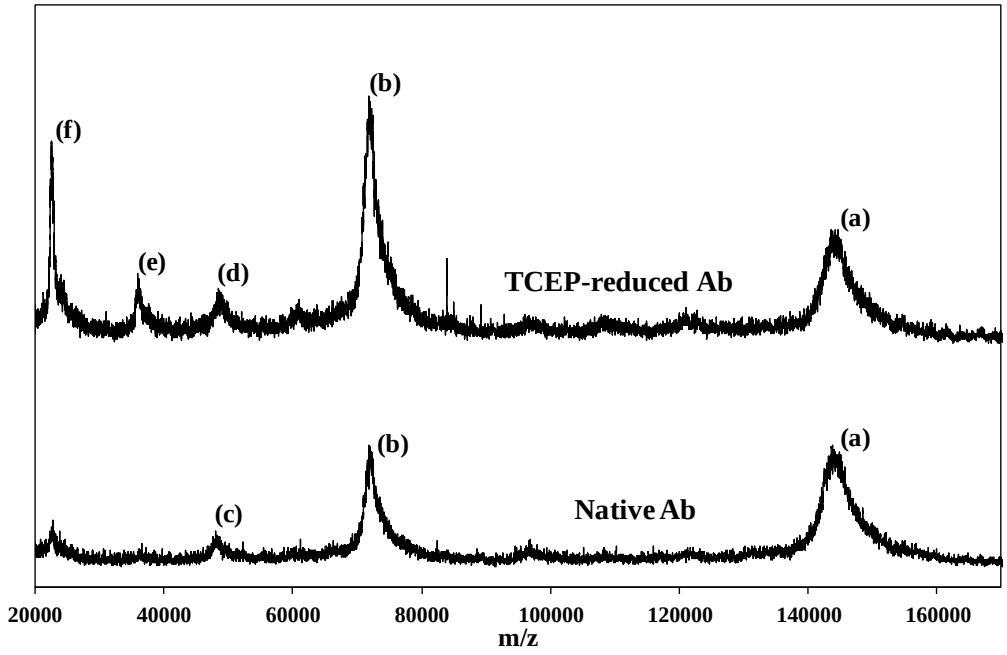

Figure 8-2 MALDI-MS of native and TCEP-reduced Ab molecules. The native Ab exhibits 3 peaks at ~143.6 kDa (a), ~71.8 kDa (b) and ~47.9 kDa (c) which correspond to the monovalent, divalent and trivalent molecular ions of whole antibody molecules, respectively. The upper spectrum of TCEP-reduced Ab exhibits the peaks (a) and (b) in addition to three other peaks ~48.5 kDa (d), ~36 kDa (e) and ~22.6 kDa (f). Peak (e) can correspond to a quatravalent ion of the whole antibody or a divalent ion of half antibody molecules. The presence of the peak (e) along with the almost double intensity of peak (b) corresponding to the divalent whole antibody or monovalent half antibody molecules for TCEP reduced Ab leads to the conclusion that TCEP-reduction cleaves the antibody molecules into halves. Presence of peaks (d) and (f) suggests that TCEP also reduces the disulfides holding the heavy and light chains together.

Since TCEP does not selectively target disulfide bridges, we expected the disulfide bridge holding the light and heavy chains in the F_{ab} regions to also get reduced. As compared to the native Ab spectrum, we see increased intensity of peaks positioned at

~48.5 kDa (d) and ~22.6 kDa (f) in the TCEP-reduced Ab spectrum. The heavy chains and light chains have molecular weights of ~50 kDa and ~25 kDa respectively.[12] The increased intensities of peaks (d) and (f) in the TCEP-reduced Ab spectrum suggested that some of the disulfide bridges between the heavy and light chains were also reduced and were observed via MALDI-MS. One hour reaction of 100:1 mole ratio of TCEP:antibody reduced the disulfides in the F_c region more than the F_{ab} region and gave us half antibody fragments that can be immobilized on gold surfaces and used for biosensing.

8.3.2. TCEP-reduced antibodies as recognition molecules

A clean QCM crystal was installed in the flowcell with PBS as the circulating buffer. The crystal resonance frequency was measured and recorded as it came to a stable value which took ~7 minutes. The reduced antibody solution was introduced to the flow loop for immobilization on the clean gold surface. As the antibody fragments chemisorbed on the gold surface the mass of the oscillating crystal increased and the resonance frequency decreased in value. As shown in Figure 8- 2, immobilization of 10 µg/mL TCEP-reduced antibody lead to a resonance frequency decrease of 13 ± 3 Hz (n=5). Following this immobilization, the flowcell was flushed thoroughly with PBS to remove any loosely-bound antibody fragments and to prepare the flow loop for the next reagent. The PBS flush was followed by the introduction of one mL of 10^7/mL *E.coli* O157:H7 antigen in the flow loop. As the antigen bound to the chemisorbed antibody the resonance frequency decreased further by 41 ± 4 Hz (n=5) as shown in Figure 3.

Following the binding of the pathogenic cells to the sensor-bound antibody fragments, one mL of anti-*E.coli* O157:H7, at 10 µg/mL, was introduced to the flow loop which bound to the sensor-bound target cells and induced a further resonance frequency decrease of 30 ± 3 Hz (n=5). The secondary antibody step confirms that the antibody fragments formed by TCEP-reduction retain the activity in the target-sensing F_{ab} region. As a negative control, one mL of whole antibody was sent right after immobilization of the TCEP-reduced fragments without an antigen binding step in between. No sensor response was observed for the control experiement.

After showing that the TCEP-reduced antibody fragments retain their antigen binding property the next steps are to examine if the proposed method enhances biosensor sensitivity and if the antibody fragments retain selectivity.

8.3.3. TCEP-reduced antibodies improve sensitivity

Establishing that TCEP-reduced antibody can be used for biosensing lead us to examine how the performance of the cleaved antibody compares to some commonly used protocols for antibody immobilization. For this study, we chose two methods; (1) direct physisorption of whole antibody on the gold crystal surface and (2) the method of chemisorption of protein G followed by the whole antibody. In the latter method, F_c region of the antibody binds to the surface-bound protein G and correctly orients the antigen binding F_{ab} region. For antigen, we chose *E.coli* O157:H7, a common food-borne pathogen in pure samples as well as samples mixed with wild strain of *E.coli* JM 101.

Various antigen concentrations, 10^5-10^6-10^7/mL were used to compare the observed binding responses using the three immobilization methods. A summary of the resonance frequency response curves on the 5 MHz QCM crystal to 10^7/mL concentration of *E.coli* O157:H7 is shown in Figure 8- 4. For the same target concentration the response for directly physisorbed whole antibody molecules as the sensing layer was 17 ± 2 Hz (n=3) and was lower than that observed with protein G as an intermediate layer, 29 ± 3Hz (n=4). TCEP-reduced antibody fragments immobilized on gold manifested the largest frequency decrease of 39 ± 5 Hz (n=5) for the same antibody concentrations. Given that the noise level was comparable, the antibody fragments were approximately twice as sensitive as just the native antibody.

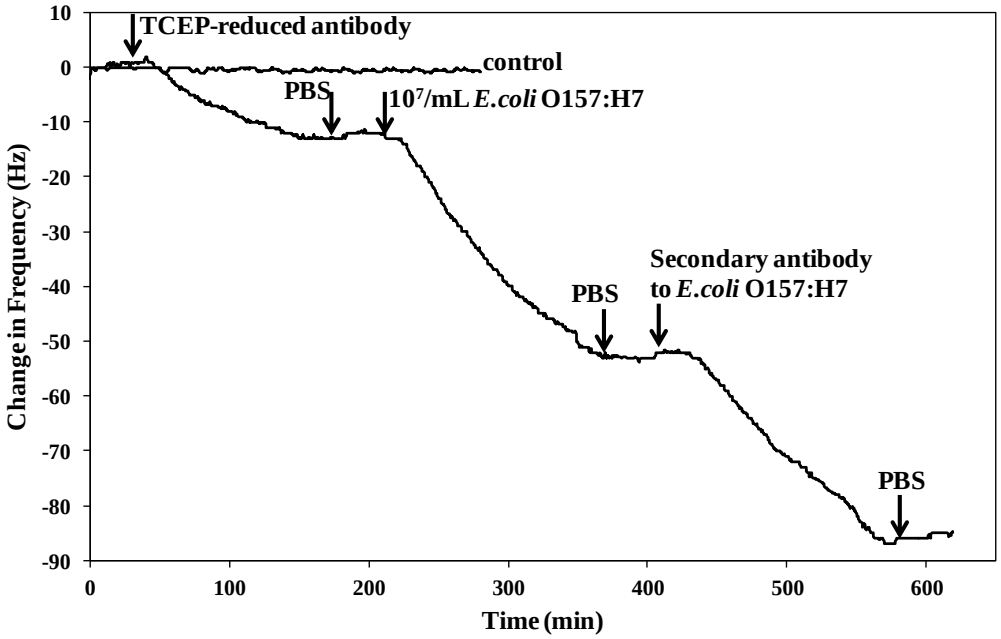

Figure 8-3 TCEP-reduced Ab work well for biosensing. Change in frequency vs time plot of a typical experiment is shown with time points for introduction each reagent to the QCM crystal. 10µg/mL of TCEP-reduced Ab led to a response of 13 Hz. 10^7/mL of *E.coli* O157:H7, when introduced to the sensor after a PBS rinse, bound to the TCEP-reduced Ab immobilized on the QCM and gave a shift of 40 Hz. A confirmation step of antigen binding using whole antibodies subsequently gave a frequency shift of 30 Hz.

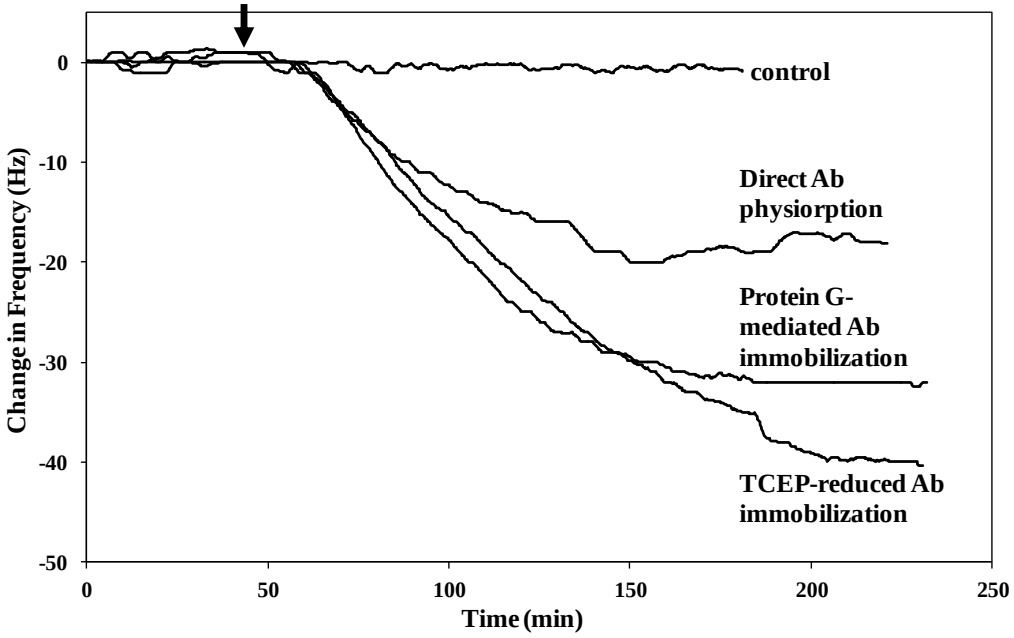

Figure 8-4 Summary of the observed response for 10^7/mL *E.coli* O157:H7 concentrations obtained for all three methods. The control experiment did not cause any change in the frequency. When direct physisorption of antibody is used for immilization the response for the specific target cells was 17 ± 2 Hz as compared to 29 ± 3 Hz when protein G was used to mediate the oriented immobilization of antibodies and 39 ± 5 Hz when TCEP-reduced Ab were used for sensing.

We believe that direct physisorption of antibody on gold leads to random orientation of antibodies. This random orientation causes a steric hindrance of the target binding F_{ab} region, thereby limiting the number of binding interactions with the antigen resulting in a smaller sensor response. Use of protein G as an intermediate layer leads to oriented immobilization of antibody molecules but the extent of immobilization is dependent on the amount of protein G bound to and its orientation on the gold surface. Since only a fraction of the initial concentration of protein G introduced to the sensor surface binds, we believe that the total amount of oriented antibody immobilized on the sensor surface is lower. TCEP-reduced antibody, on the other hand, contain thiol groups that lead to oriented chemisorption of the half antibody fragments on the sensor surface that caused a larger shift in resonance frequency for binding to the same initial concentration of the target cells.

The above trend observed in sensor responses held true for all concentrations of the target cells investigated. A summary of the changes in frequency observed for the three concentrations for all the three methods of antibody immobilization on the sensor surface is shown in Figure 8- 5. A linear regression fit for the data in Figure 8- 4 lead to y = 3E-06x + 8.17 (R^2 = 0.95), y = 3E-06x + 5 (R^2 = 0.97) and y = 1E-06x + 2.56 (R^2 = 0.90), respectively for TCEP-reduced antibodies, Protein G mediated antibody immobilization and direct physisorption of whole antibodies. The slope for TCEP-reduced antibodies and Protein G mediated immobilization of antibody is comparable and is higher than that for direct antibody physiorption method. We can therefore conclude

that TCEP-reduction of antibody does not interfere with the antigen binding property of the halved antibody fragments.

8.3.4. Selectivity of TCEP-reduced antibodies

The ability of antibody molecules to bind only to the specific targets has led to their wide-spread use for biosensing. To ensure that the proposed method of generating two half antibody fragments via TCEP-reduction is useful, it is important to show that their specificity is not compromised. We examine specificity by introducing spiked samples of *E.coli* O157:H7 with *E.coli* JM 101. To examine selectivity we used three ratios of the pathogenic target cells to non-pathogenic cells; 1:0, 1:1 and 1:10, where the concentration of the target cells was kept the same at 10^7 cells/mL. Figure 8- 6A compares the sensor response observed for the three ratios of target to non-target cells when TCEP-reduced antibody fragments were used. For the pure sample of target *E.coli* cells, the observed frequency decrease was 38 ± 2 Hz (n=5). As the concentration of non-target increased going to the ratios of 1:1 and 1:10 the frequency response decreased. For 1:1, the observed response was 25 ± 1 Hz (n=5) which was higher than that observed for 1:10 ratio of target to non-target cells, 20 ± 1 Hz (n=5).

We compare the sensor responses observed for TCEP-reduced antibody fragments against those observed for protein G mediated immobilized antibody. A summary chart for this comparison is shown in Figure 8- 6B. For Protein G mediated antibody immobilization the response to the ratio; 1:1, for target to non-target cells was ~30% less compared to the pure sample with only target cells (1:0). The response was ~44% less in the presence of ten times higher concentration of non-target cells (1:10). For

the TCEP-reduced antibody the response was ~35% lower for 1:1 and ~48% lower when this ratio was 1:10, when compared to the pure sample response. The decrease in sensor response magnitude can be attributed to the interfering presence of non-target cells that limit the binding interactions between the antigenic sites and the immobilized antibody. We can, thus, conclude that the TCEP-reduction does not compromise the selectivity of antibody. It should be noted that the compromise in selectivity might be a function of the affinity of the antibody to its specific target. A poorly binding antibody might exhibit a larger loss in selectivity.

The TCEP-reduced antibody, thus far, has been shown to generate a larger sensor response for the same concentration of antigen as compared protein G mediated antibody immobilization without loss of selectivity in the presence of non-target cells. The next step should be to study the kinetics of antibody immobilization via the three methods to show the usefulness of the proposed method. In the following section we also study the kinetics for the selectivity experiments in which the TCEP-reduced antibody fragments were used.

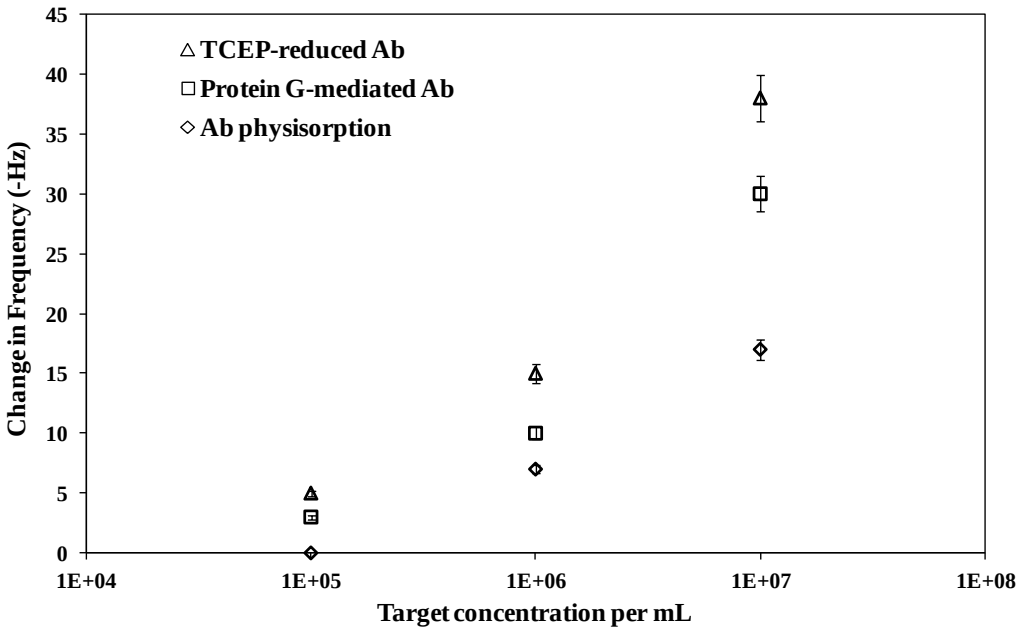

Figure 8-5 Summary of responses to three different concentrations, 10^5-10^6-10^7/mL of target *E.coli* O157:H7. This comparison helps establish that TCEP-reduction of antibodies helps improve sensitivity of the biosensing platform. A linear regression for the three methods of immobilization with R^2 = 0.95, 0.97 and 0.90 for TCEP-reduced antibodies, Protein g mediated antibody binding and direct antibody physisorption respectively.

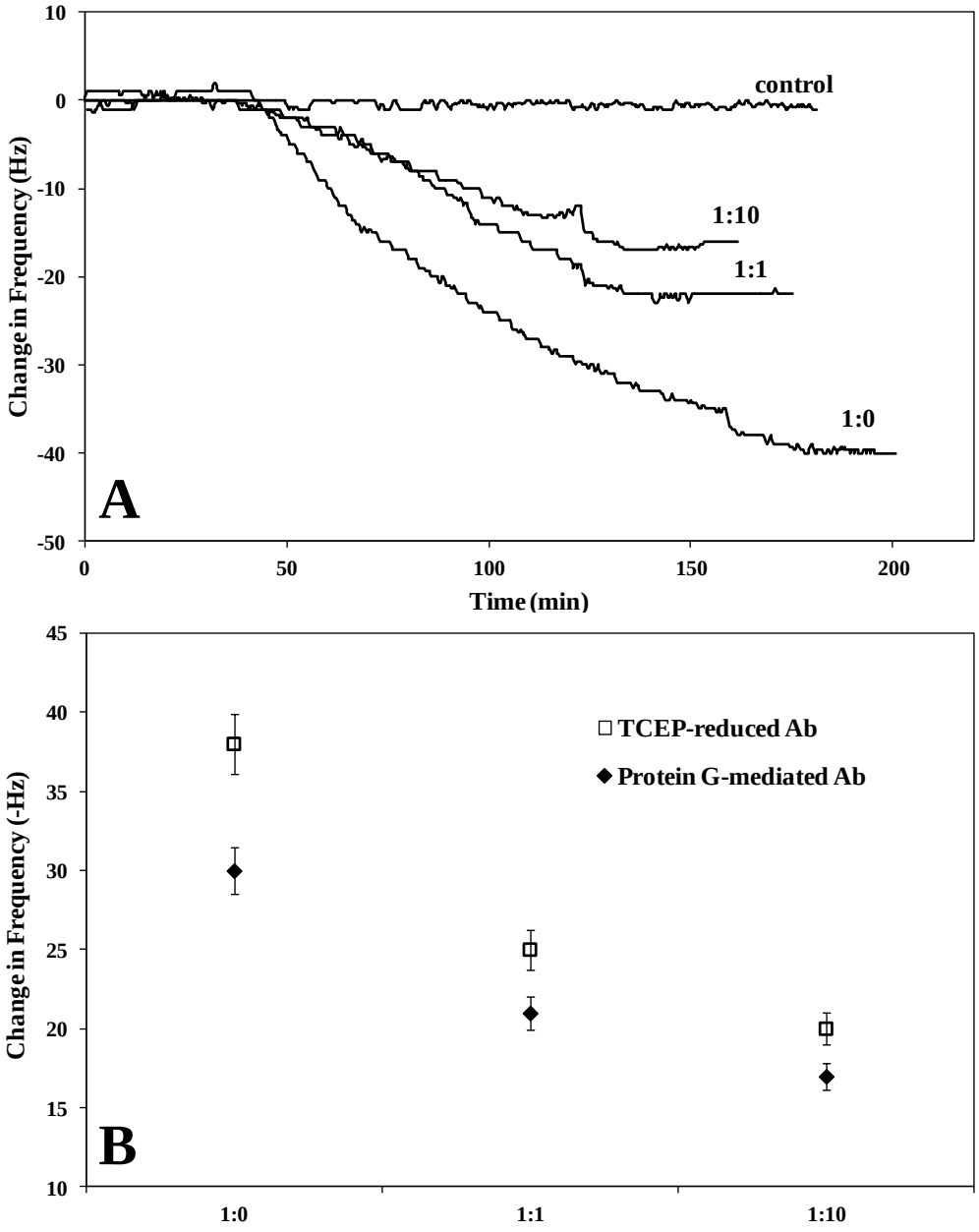

Figure 8-6 Selectivity of TCEP-reduced antibodies. Panel A. QCM responses to detection of target *E.coli* O157:H7 mixed with non-target *E.coli* JM101 at ratios of 1:0, 1:1 and 1:10 with the concentration target *E.coli* kept the same at 10^7cells/mL is shown. Panel B. A summary of responses observed using Protein G mediated oriented immobilization TCEP-reduced immobilization methods for testing selectivity is shown. For protein G mediated immobilization there was 30% and 44% reduction in observed response for 1:1 and 1:10, respectively as compared to 1:0 which was comparable for TCEP-reduced antibody 35% and 48% reduction, respectively.

8.3.5. Impact of immobilization method on kinetics

The observed rate constant of antigen binding has been shown to follow Langmuir kinetics. [7, 13] Antibody binding to the sensor by the three methods employed in this study can also be similarly modeled. Since the bulk concentration of the antibody introduced to the flow loop and that of *E.coli* O157:H7 is known initially, the rate analysis was limited to initial time period. The observed rate constants were determined by analyzing the experimental data as per the following relationship,

$$ln\left(\frac{(-\Delta f_\infty)-(-\Delta f)}{(-\Delta f_\infty)}\right) = -k_{obs}t \qquad (1)$$

where ($-\Delta f$) and ($-\Delta f_\infty$) are the changes in frequency at time t and at steady state respectively.

For the antibody directly physisorbing on sensor surface, fitting the experimental data gave an observed rate constant of 0.0094 min^{-1} (R^2 = 0.9) while the rate constants obtained similarly for protein G mediated immobilization and TCEP-reduced antibody immobilization were 0.0135 min^{-1} (R^2 = 0.9) and 0.0174 min^{-1} (R^2 = 0.96) respectively.

The native thiol groups on TCEP-reduced antibody fragments directly and strongly bind to gold surfaces unlike physisorption of whole antibody. For the other antibody immobilization method, the amount and rate of immobilization strongly

depends on the amount of protein G present on the sensor surface. We find the kinetics of TCEP-reduced antibody to be faster than the other methods investigated in this study.

Similar analysis of the sensor response for the pure sample of target *E.coli* O157:H7 binding to the sensor-bound TCEP-reduced antibody fragments gave a value of 0.0164 min^{-1} (R^2 = 0.99). In the presence of non-target cells (1:1 and 1:10) the observed rate constants were 0.0174 min^{-1} (R^2 = 0.97) and 0.0166 min^{-1} (R^2 = 0.92), respectively. In the presence of competing non-target cells only the magnitude of sensor response decreased whereas the kinetics of binding were comparable.

8.4. Conclusion

TCEP can be used for reducing the disulfide bridges holding the heavy chains of the antibodies together. The thiol groups on the half antibody fragments thus obtained; cause direct, oriented immobilization on gold surfaces. This method of antibody immobilization was shown to give approximately twice the response, for the same concentration of antigen, when compared to the conventional protein G mediated immobilization method. The property of these fragments to bind to target antigens is retained without loss of selectivity.

8.5. References

[1] B. Akerström, L. Björck, A physicochemical study of protein G, a molecule with unique immunoglobulin G-binding properties, Journal of Biological Chemistry, 261(1986) 10240-7.

[2] W.E. Paul, Fundamental immunology, Illustrated 6th ed.: Wolters Kluwer/Lippincott Williams & Wilkins; 2008.

[3] N. Backmann, C. Zahnd, F. Huber, A. Bietsch, A. Plückthun, H.-P. Lang, et al., A label-free immunosensor array using single-chain antibody fragments, Proceedings of the National Academy of Sciences of the United States of America, 102(2005) 14587-92.

[4] G.T. Hermanson, Bioconjugate Techniques: Academic Press; 1996.

[5] P.C. Jocelyn, Chemical reduction of disulfides, in: O.W.G. William B. Jakoby (Ed.) Methods in Enzymology, Academic Press1987, pp. 246-56.

[6] A.A. Karyakin, G.V. Presnova, M.Y. Rubtsova, A.M. Egorov, Oriented Immobilization of Antibodies onto the Gold Surfaces via Their Native Thiol Groups, Analytical Chemistry, 72(2000) 3805-11.

[7] H. Wang, J. Wu, J. Li, Y. Ding, G. Shen, R. Yu, Nanogold particle-enhanced oriented adsorption of antibody fragments for immunosensing platforms, Biosensors and Bioelectronics, 20(2005) 2210-7.

[8] U.T. Rüegg, J. Rudinger, [10] Reductive cleavage of cystine disulfides with tributylphosphine, in: C.H.W. Hirs, N.T. Serge (Eds.), Methods in Enzymology, Academic Press1977, pp. 111-6.

[9] J.C. Han, G.Y. Han, A Procedure for Quantitative Determination of Tris(2-Carboxyethyl)phosphine, an Odorless Reducing Agent More Stable and Effective Than Dithiothreitol, Analytical Biochemistry, 220(1994) 5-10.

[10] E. Burmeister Getz, M. Xiao, T. Chakrabarty, R. Cooke, P.R. Selvin, A Comparison between the Sulfhydryl Reductants Tris(2-carboxyethyl)phosphine and Dithiothreitol for Use in Protein Biochemistry, Analytical Biochemistry, 273(1999) 73-80.

[11] A.J. Alexander, D.E. Hughes, Monitoring of IgG Antibody Thermal Stability by Micellar Electrokinetic Capillary Chromatography and Matrix-Assisted Laser Desorption/Ionization Mass Spectrometry, Analytical Chemistry, 67(1995) 3626-32.

[12] E. Harlow, D. Lane, Antibodies: A Laboratory Manual, 1st ed., Cold Spring Harbor, New York: Cold Spring Harbor Laboratory Press; 1988.

[13] H. Ebato, C.A. Gentry, J.N. Herron, W. Mueller, Y. Okahata, H. Ringsdorf, et al., Investigation of Specific Binding of Antifluorescyl Antibody and Fab to Fluorescein Lipids in Langmuir-Blodgett Deposited Films Using Quartz Crystal Microbalance Methodology, Analytical Chemistry, 66(1994) 1683-9.

Chapter 9 . Sensitive and selective detection of mycoplasma in cell culture samples using cantilever sensors

This chapter presents a collaborative study on the detection of mycoplsmas using PEMC sensors. Detailed discussion of this work is presented in Appendix C. Cell-culture of human skin cells was done by me for use in the simulated cell-culture matrix. The detection experiments were performed by myself and a fellow graduate student; Sen Xu. My contributions to this chapter, in addition to writing a part (30%) of it, are shown in Figures 9.3B, 9.4, 9.5A, 9.6A and 9.7.

We reported a new biosensor-based method that is more sensitive and rapid than the current approach for detecting mycoplasma in cell culture samples. Piezoelectric-excited millimeter-sized cantilever (PEMC) sensors respond to mass change via resonant frequency change. They are sensitive at femtogram level, and can be used directly in liquid for label-free detection. Common cell culture contaminant, *Acholeplasma laidlawii* was detected in both buffer and cell culture medium. Two different sources (positive control from a commercial kit and ATCC 23206) were analyzed using antibody-immobilized PEMC sensor. Resonant frequency decrease caused by binding of *A. laidlawii* was monitored in real-time using an impedance analyzer. Positive detection was confirmed by a second antibody binding. The limit of detection (LOD) was lower than 10^3 CFU/mL in cell culture medium using PEMC sensor while parallel ELISA assays showed LOD as 10^7 CFU/mL. This study shows PEMC sensor can be used for sensitive and rapid mycoplasma detection in cell culture samples.

Chapter 10 . Rapid and sensitive immunodetection of *Listeria monocytogenes* in milk using a novel piezoelectric cantilever sensor

10.1. Introduction

In the United States, each year, food-borne pathogens have been estimated to cause over 76 million illnesses leading to hundreds of thousands of hospitalizations and thousands of deaths [1, 2]. *Listeria monocytogenes* (LM) is a food-borne pathogen found in milk, milk products, eggs, poultry and meat [3, 4]. Outbreaks of listeriolysis caused by LM in milk and milk products have caused great concern in the dairy industries due to high mortality rate [5, 6]. Pasteurized milk has a high risk ranking as an infection vector. LM can grow at 4 °C in the refrigerator and increase almost 10-fold in 7 days; also LM grows more rapidly in pasteurized milk than in raw milk.[7] A recent outbreak of listeriosis caused by infected ricotta cheese had at the time of preparing this manuscript affected 14 persons in 11 states with 3 reported deaths.[8] Pregnant women and immune-compromised persons such as infants and elderly are most susceptible. A low infectious dose (<1000 cells) and LM's ability to grow in refrigerators at 4°C make this an especially dangerous pathogen. [7, 9]

The slow growth rate of *Listeria monocytogenes* is a challenge for detection by the conventional culture and plating methods as the time to results (TTR) can take up to 7 days.[7, 9] The culture-based methods also consist of multiple steps and require trained personnel. Polymerase chain reaction (PCR) based detection methods have been developed to reduce TTR [10] but they still require the enrichment step for low concentration samples. Use of separation techniques such as immunomagnetic beads

[11-13] and innovative nucleic acid amplification methods [14] have reduced the TTR to 24 h while the best detection sensitivity reported to date is 10-10^2 CFU/mL. [4, 10, 15]

The long time to results is the motivator for developing a sensitive, selective and rapid biosensor. Antibody-based detection of LM has yielded detection limits ~10^4 cells/mL, but requires multiple steps, high concentrations of labeled reagents and long TTR. [13] Quartz crystal microbalance (QCM) has been investigated with buffer samples with reported sensitivities of ~10^7 CFU/mL. [16, 17] On the other hand, optical sensors using a fluorophore-labeled antibody sandwich assay showed a better detection limit (~10^5 CFU/mL) in buffer and in frankfurter samples [18]. The sandwich assay when used with an aptamer-antibody combination improved further to ~10^3 CFU/mL in meats, but required an 18 hour enrichment step. [19].

In this study, we examine the use of a novel, asymmetrically anchored piezoelectric-excited millimeter sized cantilever (aPEMC) sensor for label-free detection of LM in buffer and milk at ~100 CFU/mL using a secondary and tertiary antibody binding steps, similar to a ELISA sandwich assay, for improving sensitivity and reducing false negatives. To the authors' knowledge, this is the first report of antibody-based biosensors that demonstrate detection of LM in food matrix at a concentration below the known infectious dose, with an assay time of ~30 minutes.

10.2. Materials and Methods

Protein G was purchased from Thermo Scientific (Pierce), Rickford, IL. Polyclonal goat anti-*L. monocytogenes*, heat-killed *L. monocytogenes* positive, polyclonal

anti-*E.coli* O157:H7 and heat-killed *E.coli* O157:H7 were from Kirkegaard & Perry Laboratories, Inc. 6-mercapto-1-hexanol and phosphate-buffered saline (PBS; 10mM, pH 7.4) were from Sigma-Aldrich (St. Louis, MO). Whole milk was obtained locally. Quartz crystal microbalance (QCM; 5 MHz, AT cut) and flow cell were purchased from Stanford Research Systems. Protein G (10 µg/mL), antibody (10 µg/mL) and the positives were prepared from the stock solutions in PBS and stored at -20 °C.

Novel aPEMC sensors reported earlier [20] were fabricated from 5x1x0.127 mm^3 lead-zirconate-titanate (PZT) strip (Piezo Systems, Woburn, MA). Anchoring was done by ensuring embedding both sides of PZT to the same depth in epoxy. Additional epoxy was applied to one side of PZT for fabricating anchor asymmetry. The other side of the sensor remained at the original free length (L). The asymmetric dimension (α) for the sensors used in this study varied from 20% to 35% of the free length, L. A polyurethane coating was applied to sensor for experiments in liquids. A 100 nm thick gold layer was sputtered at the distal 1 mm^2 area of the cantilever.

The flow apparatus used for experiments has been described previously.[21] In a typical experiment, a sensor was vertically installed in a custom flow cell and the flow rate was set at 0.6 mL/min facilitated by a peristaltic pump. The installed sensor was connected to an impedance analyzer (Agilent, 4294A) which was interfaced to a computer running a custom LabVIEW® program for measuring and recording the resonance frequency. Batch protein G physisorption at room temperature was used for oriented immobilization of antibody on the sensor.[4] The sensor was rinsed with PBS prior to installation in the flow cell. For the detection in buffer, the installed sensor was allowed to reach a stable value with PBS as the running buffer before the introduction of

the sample spiked with LM. The flow loop was flushed with PBS between reagent changes to clear the lines of any residuals. For detection in milk, the sensor was initially stabilized in PBS, and then 1 mL whole milk was introduced into the flow loop and the flow was set in recirculation. Since the total volume of flow loop was ~4 mL, injection of 1 mL milk gave ~25% milk content in PBS. LM samples were also prepared in milk:PBS (1:3) to ensure the background was the same as that in the flow loop just prior to introduction. For detection confirmation, the same goat polyclonal antibody was used. The secondary antibody would bind to the LM target bound to the antibody immobilized on the sensor surface. To further reduce false negatives and to improve sensitivity, a tertiary binding step using anti-goat I_gG was introduced.

10.3. Results and Discussion

10.3.1. Sensitivity of aPEMC sensors

The second flexural resonance mode of aPEMC sensors, located at 60-85 kHz in liquid, was used in detection experiments. The peak shape factor (Q) of this mode ranged from 20 – 35 under liquid immersion. Typical frequency spectra is shown in Figure 10-1A. When submerged in a liquid medium, the liquid adjacent to the sensors acts as added mass and causes the resonance frequency to decrease. The increase in density of the medium from air to PBS caused a frequency decrease of ~15 kHz as shown in Figure 10-1A. Although this frequency change due to density change is related to sensor sensitivity, molecular chemisorption more closely simulates the condition of antigen binding.

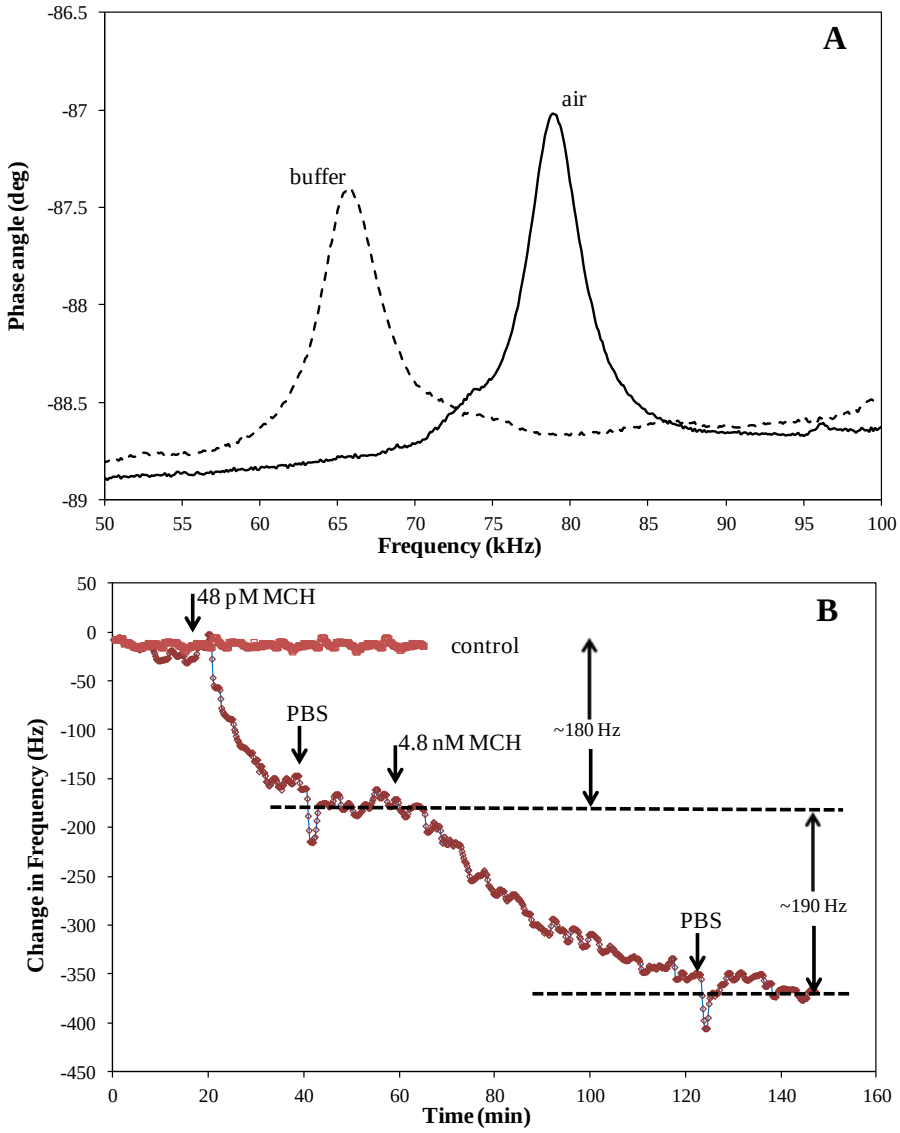

Figure 10-1 Panel A. Typical spectra of the AAPEMC sensors in air and in buffer. The resonance frequency decreases by ~15 kHz due to change in the density of the surrounding medium. **Panel B.** A typical chemisorption response to 6-mercaptohexanol (MCH) on gold coated AAPEMC sensors is shown to characterize sensor sensitivity. A resonance frequency decrease of ~180 Hz is observed for one mL of 48 pM solution of MCH followed by one mL of 4.8 nM solution which further decreased the resonance frequency by ~190 Hz. The device sensitivity can be calculated to be ~36 fg/Hz.

A six-carbon thiolated molecule, 6-mercapto-1-hexanol (MCH) was used to determine the sensitivity of the aPEMC sensors. A gold-coated aPEMC sensor was installed in the flow cell and allowed to reach a stable frequency in PBS (0.6 mL/min). One mL 48 pM MCH in PBS was introduced into the flow loop. The chemisorption of MCH on gold <111> sites on the sensor increased the sensor mass and induced a resonance frequency decrease of ~180 ± 7 Hz (n=3) and is shown in Figure 10- 1B. After the frequency shift reached equilibrium, 1mL of 4.8 nM MCH was introduced and a further decrease of ~190 ± 12 Hz (n=3) was obtained. Total mass of MCH present in 1mL, 48 pM solution is ~6.4 pg. We expect only a fraction of this is expected to chemisorb on the gold surface. A conservative assumption that all 6.4 pg chemisorbed on the sensor that induced ~180 Hz of response yields a sensitivity value of ~28 Hz/pg. From six experiments using three different sensors, the sensitivity ranged from 20 - 40 fg/Hz. Since the mass of a single pathogen is ~ 2 pg, we theoretically expect aPEMC sensors can be used to detect the presence of a single pathogen in the target matrix. Detection of LM at low concentration should thus be possible using aPEMC sensors and is the focus of our experiments.

10.3.2. Detection of LM in PBS

After establishing sensitivity, the aPEMC sensors were immobilized with protein G followed by anti-LM for detection experiments. For protein G physisorption, the sensors were incubated in protein G solution (10µg/mL) at room temperature for 1 hour. The sensor was then rinsed with PBS and installed in the flow cell with PBS as the

running buffer at a constant flow rate (0.6 mL/min) and the resonance frequency was allowed to reach a stable baseline. Subsequently, 1mL of anti-LM (10 µg/mL) was introduced into the flow loop in recirculation mode for accommodating maximum binding. A typical sensor run is shown in Figure 10- 2A. The sensor resonance frequency decreased in response to antibody binding by 204 ± 17 Hz (n = 7). A thorough PBS rinse was employed in between different reagents to remove the earlier reagent from the flow loop before introducing the next one. A shift of 40 ± 4 Hz (n = 7) was obtained subsequent to introduction of LM at 10^3/mL.

Further addition of LM at 10^4/mL decreased the frequency further by 111 ± 10 Hz (n = 7). The sensor response to target cells was achieved within 35 minutes of introduction into the flow loop. The detection time scale is far more favorable when compared to sensitive detection techniques such as culture and plating (~7days) and PCR (8-24 hrs).

In order to confirm that the observed response was due to LM, goat anti-LM was injected in to the flow loop. The rationale for this step is that if the sensor exhibits a further decrease in resonance frequency, it would be due to the secondary antibody binding to LM cells that are already attached to the antibodies immobilized on the sensor. The schematic of this sandwich-type approach, somewhat similar to the ELISA format, is illustrated in Figure 10- 3A-B. ELISA assays use labeled reagents whereas aPEMC detection experiments are performed with label-free reagents.

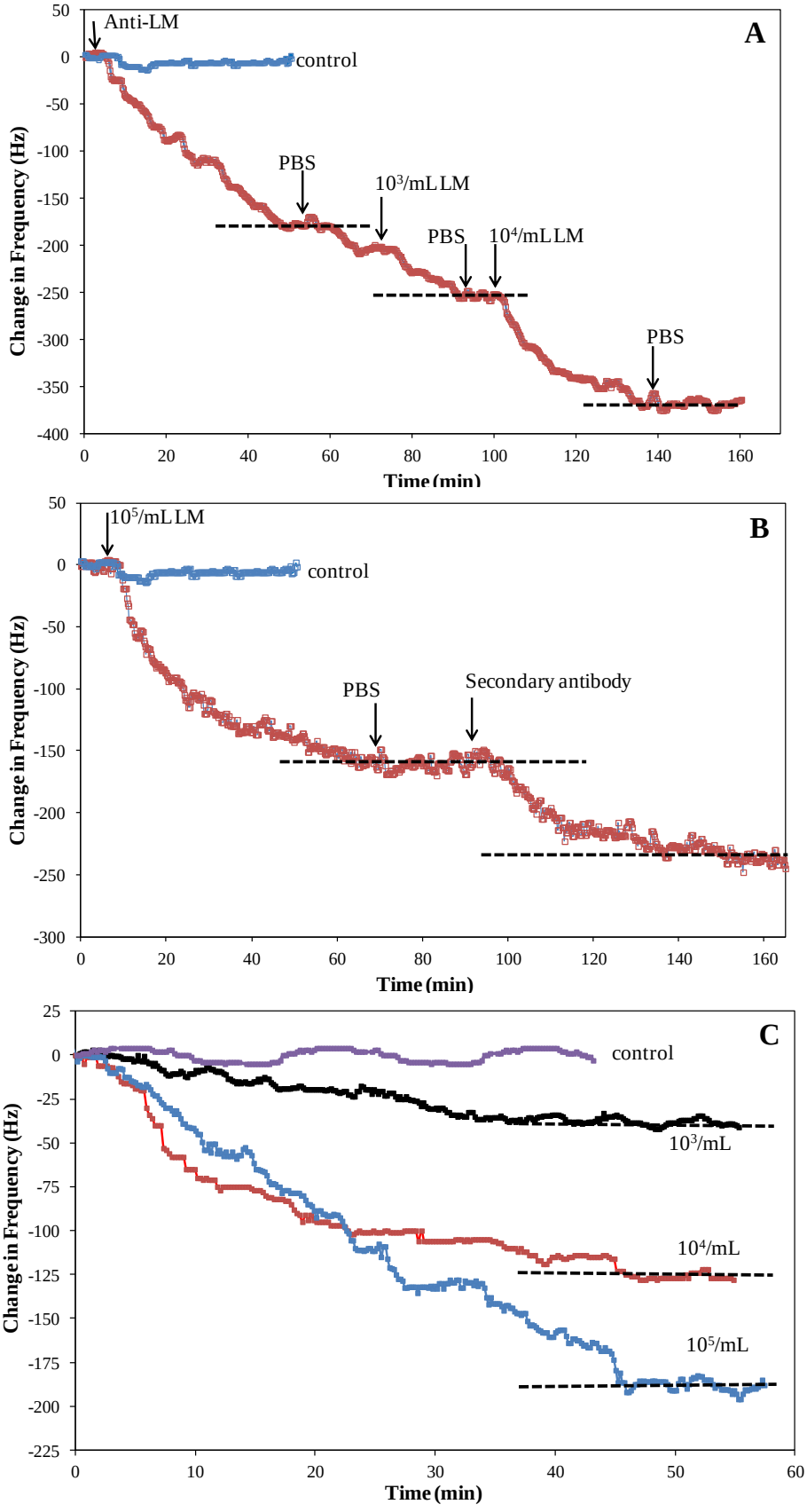
A
Anti-LM
control
PBS
10³/mL LM
PBS
10⁴/mL LM
PBS
Change in Frequency (Hz)
Time (min)
B
10⁵/mL LM
control
PBS
Secondary antibody
Change in Frequency (Hz)
Time (min)
C
control
10³/mL
10⁴/mL
10⁵/mL
Change in Frequency (Hz)
Time (min)

Figure 10-2 Panel A shows a typical experiment showing the response of AAPEMC sensor to anti-LM (1mL, 10µg/mL) and target *Listeria* monocytogenes.The sensor resonance frequency decreased by 204 Hz in response to antibody binding. Further decrease of 43 Hz and 109 Hz were due to injection of 10^3/mL and 10^4/mL LM. **Panel B** shows the reponse of a sensor that has undergone the same surface chemistry preparation. After antibody immobilization (1mL, 10µg/mL), the sensor gave a further shift of 165 Hz for introduction of 10^5/mL LM into the flow loop. A second antibody binding to LM was done to confirm the initial response. Introduction of the secondary anti-LM (1mL, 10µg/mL) into the flow loop induced a resonance freuquency change of ~76 Hz. **Panel C** gives a summary of the frequency responses exhibited by AAPEMC sensors. These responses were obtained when a freshly antibody immobilized sensor was exposed to one mL of the different concentration of LM in PBS.

The frequency response for one such experiment is shown in Figure 10- 2B. Introduction of 10^5/mL of LM to the antibody-immobilized sensor caused the frequency to decrease by 180 ± 16 Hz (n = 7) which was followed by a further decrease of 83 ± 13 Hz (n=7) when the secondary antibody was injected into the flow loop. The secondary antibody step provided confirmation of detection of LM and is expected to reduce the false negative results significantly.

For the three increasing concentrations of *Listeria monocytogenes*, larger frequency decreases were obtained (Figure 10- 2C). Introduction of higher concentration lead to a higher number of LM to bind to the sensor that induced a larger frequency shift. The frequency responses exhibited by aPEMC sensors were 40 ± 4 Hz (n=7), 111 ± 10 Hz (n=7) and 181 ± 15 Hz (n=5) for 10^3/mL, 10^4/mL and 10^5/mL respectively.

In the literature, biosensor-based detection of *Listeria monocytogenes* using antibodies has not been extensively investigated. The publications on detecting LM using antibodies with quartz crystal microbalance (QCM, 10 MHz) reported detection limit of 10^7/mL in a batch experiments. [16, 17] QCM sensors have been used for immunosensing of pathogens with detection limits as low as ~ 10^2 - 10^3 /mL. [22, 23] The LM detection limit for LM by aPEMC (10^3/mL) is comparable to the reported value using optical biosensors[18], which is four orders of magnitude improvement over what has been demonstrated for LM in the QCM literature. One of the factors that govern the device sensitivity is the binding affinity of the antibody to the target antigen. The avidity of commercially available antibodies against *Listeria monocytogenes* has not been reported and their avidity appears to be low based on the detection sensitivities observed in literature. We hypothesize that the antibody with poor avidity is a limiting factor in achieving a lower limit of detection for LM in QCM experiments. One way to test this hypothesis is to compare the response of LM binding to anti-LM with the response generated by *E.coli* O157:H7 (EC) binding to anti-EC. The latter antibody is known to have high avidity for its target.[22, 24, 25]

10.3.3. Comparison of *Listeria monocytogenes* and *E.coli* O157:H7 responses

The aPEMC detection limit for LM was shown as 10^3 / mL even though the sensors are sensitive enough for detection of a single LM cell. To test if the poor antibody avidity was the limiting step, detection experiments were performed using a QCM (5 MHz) setup identical to the one used for the aPEMC sensors but at a constant flow rate of

5 µL/min, as the QCM flow cell cannot tolerate high flow rates. The gold electrode of the QCM was incubated in protein G solution (10 µg/mL) and rinsed with PBS prior to installation into the flow cell. The detection experiments were run in an identical manner as the aPEMC experiments. Introduction of anti-LM, post frequency stabilization, led to a resonance frequency decrease of 29 ± 3 Hz (n=3) but no change in resonance frequency was observed upon exposure to various concentration of LM as high as 10^7 /mL, as shown in Figure 10- 4A. Higher concentrations were not used since 10^7 /mL was shown to be the detection limit on the QCM.[17]

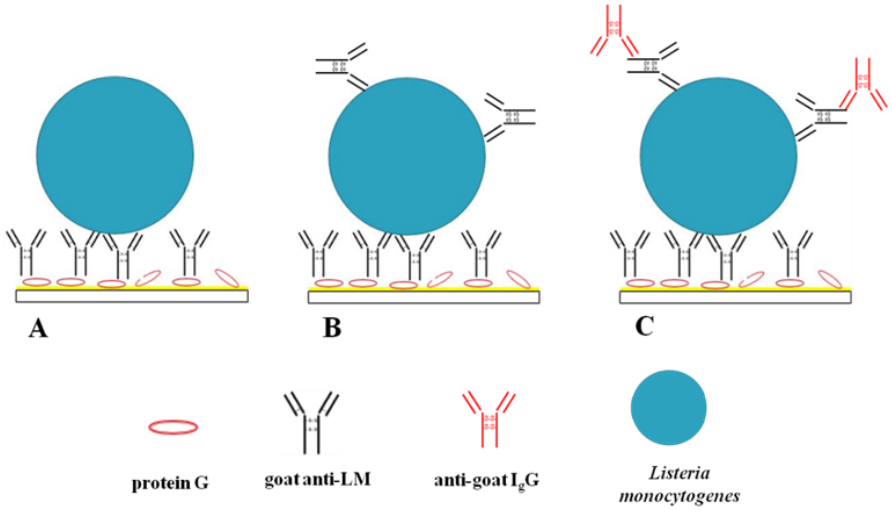

Figure 10-3 Schematic representation of the secondary and tertiary antibody binding. Panel A shows a gold coated sensor surface with protein G chemisorbed on it. Target pathogen cell is bound to the goat anti-LM that is bound to the protein G on sensor surface. Panel B shows the secondary goat anti-LM binding result. Panel C illustrates the third binding step. The anti-goat I_gG bound to the secondary antibody molecules, and amplified the sensor response in addition to providing a confirmation of detection response.

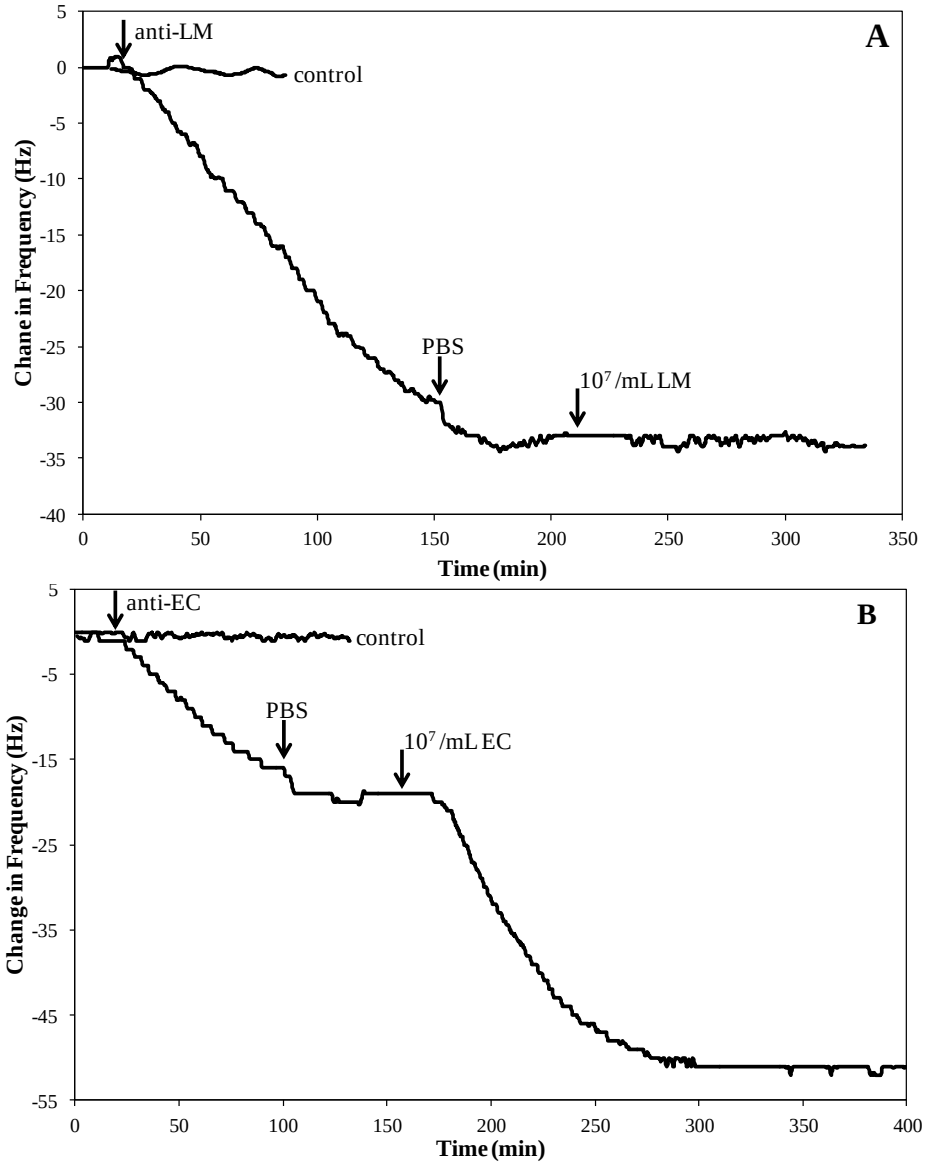

Figure 10-4 Anti-LM is shown to have lower avidity than anti-EC. **Panel A** shows a typical detection experiment for *Listeria monocytogenes* on a QCM running at 5 µL/min flow rate. After immobilization of the anti-LM on a protein G prepared gold surface, introduction of the LM cells failed to induce a resonance frequency decrease. **Panel B** shows an experiment run in identical conditions for *E.coli* O157:H7. Introduction of EC cells, at the same concentration as LM, after antibody immobilization caused a decrease in resonance frequency due to the EC cells binding to the sensor. Lack of an observable response for the *LM* shows that the anti-LM did not bind LM. Comparing the responses in Panels A and B we infer that the anti-LM has a lower affinity for its target than the anti-EC.

The performance of anti-LM was compared with anti-EC in QCM experiments of the respective targets. The vendor supplied anti-EC has demonstrated detection at 1-10 cell/mL. [24, 26, 27] A typical detection experiment for EC on the QCM is shown in Figure 10- 4B. Upon exposure to anti-EC the protein G immobilized crystal exhibited a frequency decrease of 17 ± 5 Hz (n=3) and a further decrease of 30 ± 2 Hz (n=3) was observed when 10^7 /mL of EC were introduced into the flow loop in recirculation.

For the same concentration of target cells the QCM showed a frequency decrease for EC but not for LM. We interpret this lack of response as anti-LM having poor avidity for its target as compared to anti-EC for EC. The poor avidity results in poorer or no binding and consequently antibody-based detection of LM at low concentrations require highly sensitive sensor platforms such as aPEMC sensors used in the current study. This, in part, explains the dearth of immunosensor literature for detection of LM and the poor sensitivities reported in those studies.

10.3.4. Detection in milk

Earlier designs of PEMC sensors have been shown to be highly sensitive for detection in complex matrixes. [24, 28] To examine if the current design of aPEMC sensors is equally sensitive in complex matrixes, we examined it for detection of LM in milk. After immobilizing the antibody on the sensor, 1mL of milk was introduced into the flow loop (4 mL volume) and the flow was put in recirculation mode so that the concentration of the running buffer was effectively 25% milk in PBS. Milk has a higher density because of the dissolved sugars, proteins and fats present in it. This increase in

density caused the sensor resonance frequency to decrease by 175 ± 30 Hz (n = 10). (Figure 10- 5A) The flow loop, subsequently, was rinsed with PBS so as to return the running buffer to PBS. The sensor frequency recovered in response to this density change of the sensor medium to within 10 Hz of the initial value. Several repeat experiments gave the same response and nearly full recovery of resonance frequency was obtained when the running buffer was returned to PBS. This control experiment establishes that the sensors show no significant non-specific adsorption of the fats, proteins and carbohydrates present in the milk.

Typical detection response obtained for LM in milk-PBS medium is shown in Figure 10- 5B. Introduction of 10^5 /mL LM, prepared in 25% milk-PBS, to antibody immobilized sensors induced a frequency decrease of 100 ± 18 Hz (n = 6). To confirm that the response observed was due to LM cells bound to the sensor, a secondary antibody binding step was performed (Figure 10- 3A-B). The sensor frequency exhibited a further decrease of 106 ± 22 Hz (n = 6) for the secondary antibody binding.

Detection of *Listeria* in food matrix is of greater significance because the proteins and fats present in these matrixes can non-specifically bind to the sensor surface and also interfere with the interaction between the immobilized antibody and the LM cells. Figure 10- 6 shows the comparison between aPEMC responses obtained in PBS and in milk. The comparison results show that there is a 45% decrease in sensor response for 10^5/mL samples. This loss of signal increased to 55% at 10^4/mL and 70% at 10^3/mL of LM cells. In spite of the significant loss of response signal, we can obtain significant response consistently for 10^3 *Listeria monocytogenes* per mL of milk in about 45 minutes.

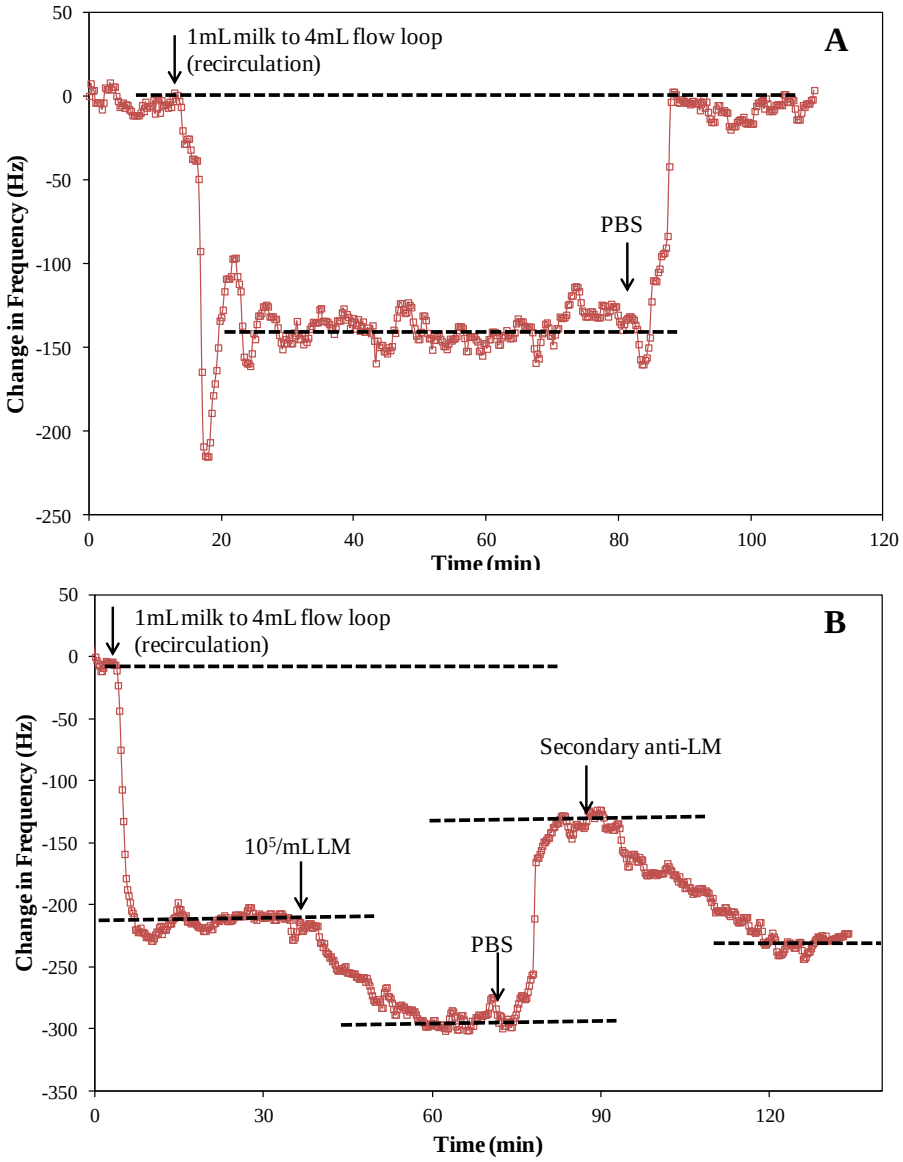

Figure 10-5 Panel A. 1 mL milk was introduced to total 4 mL of flow loop in recirculation. Higher density of milk caused a resonance frequency decrease of 198 Hz and it recovered within 10 Hz of the initial value upon returning back to PBS as the running buffer. This suggests that no significant non-specific adsorption occurred on the sensor surface from milk. (carbohydrates, proteins and fat particles) **Panel B** shows a typical detection of *Listeria monocytogenes* in milk. One mL of 10^5/mL of LM caused the sensor resonance frequency to decrease by 104 Hz. A PBS rinse of the flow loop led to a recovery in the frequency which was followed by a 106 Hz decrease in the sensor frequency in response to the secondary antibody binding (1mL, 10 µg/mL) that confirmed the detection of LM.

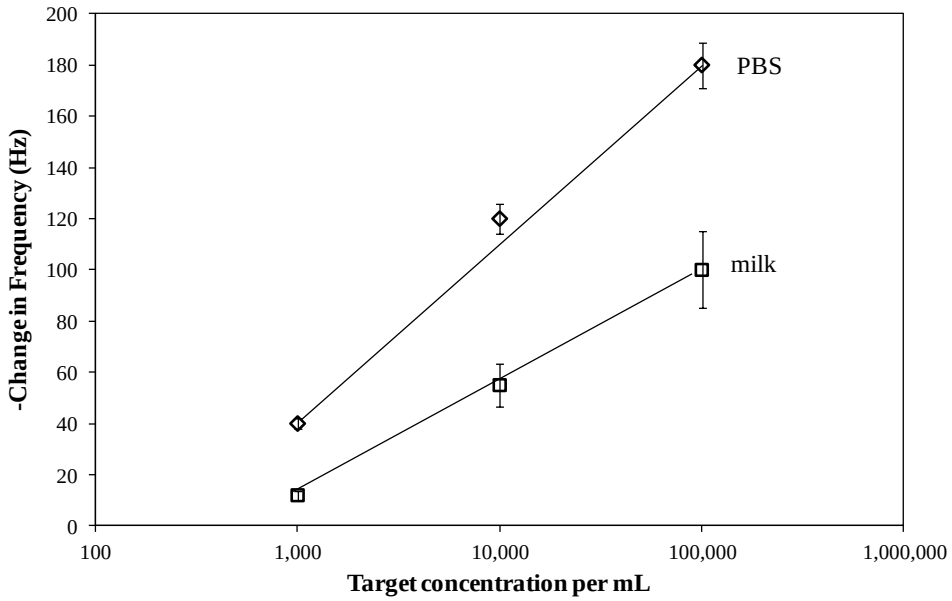

Figure 10-6 Comparison of sensor response for various concentrations of target *Listeria monocytogenes* in PBS and 25% milk-PBS. The responses in milk were 70%, 55% and 45% lower respectively than in PBS.

10.3.5. Enhancement of detection sensitivity by tertiary binding

The sandwich assay format employed led to confirmation of detection and reduction of false negatives. This secondary binding step also leads to mass addition on the sensor and thus an increase in sensor response. This approach of secondary antibody binding was extended further to a tertiary binding step as shown in Figure 10- 3A-C, as a means of amplifying sensor signal. Such an approach enabled detection of LM at a much lower concentration of 10^2 /mL in milk matrix directly. A typical detection experiment at this concentration in milk is shown in Figure 10- 7. After the sensor frequency had stabilized in the detection medium of 25% milk in PBS, addition of 10^2 /mL of LM did not induce a statistically measurable change in resonance frequency. The frequency recovered upon PBS rinse and then a decrease in the frequency of 37 ± 6 Hz (n = 4) was observed upon introduction of goat anti-LM as the secondary binding step. To confirm that this change in frequency was indeed due to the secondary antibody binding to target cells on the sensor, a tertiary binding step of anti-goat I_gG (10µg/mL, 1mL) was done. Tertiary binding induced a frequency decrease of 62 ± 9 Hz (n = 4), thereby confirming and amplifying the sensor response.The three binding steps approach pushed the detection limit for LM to 10^2 /mL in milk. Several repeated experiments with the tertiary binding step have consistently shown that LM can be detected at concentrations lower than the infectious dose within 60 minutes.

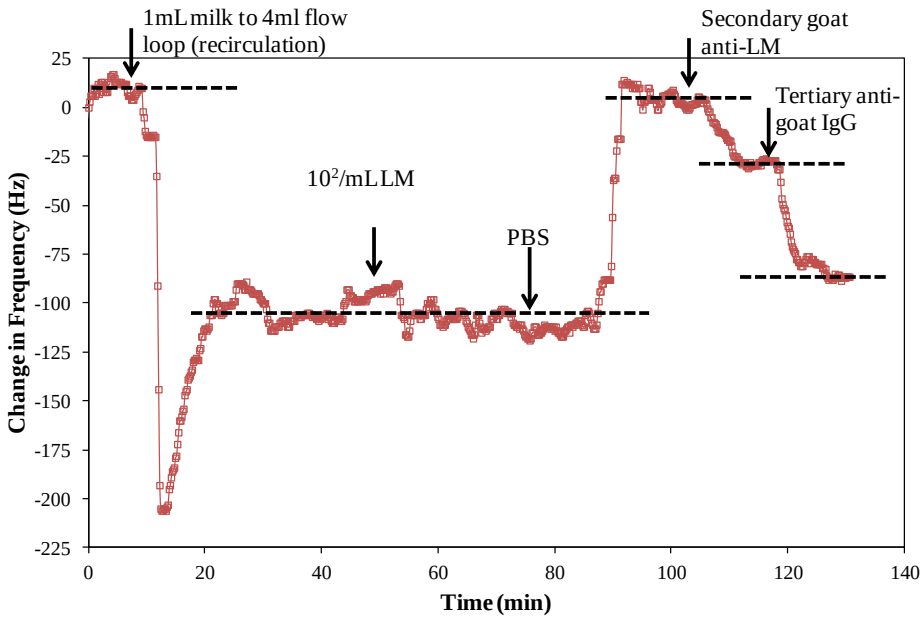

Figure 10-7 Enhancement of sensor sensitivity is exhibited by amplifying mass addition. The relatively poor affinity of anti-LM for its target limited detection to 10^3/mL. Here, the response to 10^2/mL was too small to be measured but a secondary goat anti-LM binding step (after a PBS rinse) caused the resonance frequency to decrease by ~37 Hz as it bound to the LM cells bound to the sensor surface. This was further confirmed by a third binding reaction of anti-goat I_gG that bound to the secondary goat anti-LM and exhibited ~62 Hz frequency decrease.

10.4. Conclusion

The asymmetrically anchored cantilever sensors with measured sensitivity of ~36 fg/Hz are theoretically capable of detecting the presence of a single *Listeria monocytogenes* in a sample if high-avidity antibody is available. The commercially available antibody for *Listeria monocytogenes* limited detection at 10^3 /mL in PBS and milk in a single binding assay. Secondary antibody binding step confirmed the observed sensor response. Such an approach also reduces false negatives while enhancing sensor

response. A tertiary antibody step enabled signal amplification and detection limit improved to 10^2 /mL in the two matrixes tested. Such a low concentration is at the infectious dose and can be potentially used for testing food safety.

10.5. References

[1] P.S. Mead, L. Slutsker, V. Dietz, L.F. McCaig, J.S.Bresee, C. Shapiro, et al., **Food-Related Illness and Death in the United States**, Emerg Infect Dis, 5(1999) 607-25.

[2] WHO, Food safety and foodborne illnesses., Fact sheet no. 237, 2007.

[3] H. Zhou, Z. Gao, G. Luo, L. Han, S. Sun, H. Wang, Determination of Listeria Monocytogenes in Milk Samples by Signal Amplification Quartz Crystal Microbalance Sensor, Anal Lett, 43(2010) 312-22.

[4] G. Amagliani, G. Brandi, E. Omiccioli, A. Casiere, I.J. Bruce, M. Magnani, Direct detection of Listeria monocytogenes from milk by magnetic based DNA isolation and PCR, Food Microbiol, 21(2004) 597-603.

[5] M.W. Griffiths, Listeria monocytogenes: Its importance in the dairy industry, J Sci Food Agric, 47(1989) 133-58.

[6] C.W. Donnelly, Detection and Isolation of *Listeria monocytogenes* from Food Samples: Implications of Sublethal Injury, J AOAC Int, 85(2002) 495-500

[7] M.P. Doyle, L.R. Beuchat, Food Microbiology: Fundamentals and Frontiers, 3rd ed., ASM Press2007.

[8] CDC, Multistate Outbreak of Listeriosis Linked to Imported Marte Brand Frescolina Ricotta Salata Cheese, Center for Disease Control and Prevention2012.

[9] A.D. Hitchins, K. Jinneman, Detection and Enumeration of *Listeria monocytogenes* in Foods, Bacteriological Analytical Manual 8th ed., AOAC International1998.

[10] A. Germini, A. Masola, P. Carnevali, R. Marchelli, Simultaneous detection of Escherichia coli O175:H7, Salmonella spp., and Listeria monocytogenes by multiplex PCR, Food Control, 20(2009) 733-8.

[11] E.T. Ryser, E.H. Marth, Listeria, Listeriosis and Food Safety, Food Science and Technology, 3rd ed., CRC Press2007.

[12] J. Vytřasová, I. Zachová, L. Červenka, J. Štěpánková, M. Pejchalová, Non-Specific Reactions during Immunomagnetic Separation of Listeria, Food Technol Biotechnol, 43(2005) 397-401.

[13] H.-S. Kim, I.-H. Cho, S.-M. Seo, J.-W. Jeon, S.-H. Paek, In situ immuno-magnetic concentration-based biosensor systems for the rapid detection of Listeria monocytogenes, Mater Sci Eng, C, 32(2012) 160-6.

[14] T. Murakami, J. Sumaoka, M. Komiyama, Sensitive isothermal detection of nucleic-acid sequence by primer generation–rolling circle amplification, Nucleic Acids Res, 37(2009) e19.

[15] G. Amagliani, C. Giammarini, E. Omiccioli, G. Brandi, M. Magnani, Detection of Listeria monocytogenes using a commercial PCR kit and different DNA extraction methods, Food Control, 18(2007) 1137-42.

[16] M. Minunni, M. Mascini, R.M. Carter, M.B. Jacobs, G.J. Lubrano, G.G. Guilbault, A quartz crystal microbalance displacement assay for Listeria monocytogenes, Anal Chim Acta, 325(1996) 169-74.

[17] R.D. Vaughan, C.K. O'Sullivan, G.G. Guilbault, Development of a quartz crystal microbalance (QCM) immunosensor for the detection of *Listeria monocytogenes* Enzyme Microb Technol, 29(2001) 635-8.

[18] V. Nanduri, G. Kim, M.T. Morgan, D. Ess, B.K. Hahm, A. Kothapalli, et al., Antibody immobilization on waveguides using a flow-through system shows improved Listeria monocytogenes detection in an automated fiber optic biosensor: RAPTOR (TM), Sensors, 6(2006) 808-22.

[19] S.H. Ohk, O.K. Koo, T. Sen, C.M. Yamamoto, A.K. Bhunia, Antibody–aptamer functionalized fibre-optic biosensor for specific detection of Listeria monocytogenes from food, J Appl Microbiol, 109(2010) 808-17.

[20] H. Sharma, R.S. Lakshmanan, B.N. Johnson, R. Mutharasan, Piezoelectric cantilever sensors with asymmetric anchor exhibit picogram sensitivity in liquids, Sens Actuators, B, 153(2011) 64-70.

[21] G.A. Campbell, R. Mutharasan, Detection of Bacillus anthracis spores and a model protein using PEMC sensors in a flow cell at 1 mL/min, Biosens Bioelectron, 22(2006) 78-85.

[22] O. Lazcka, F.J.D. Campo, F.X. Munoz, Pathogen detection: A perspective of traditional methods and biosensors, Biosens Bioelectron, 22(2007) 1205-17.

[23] P.D. Skottrup, M. Nicolaisen, A.F. Justesen, Towards on-site pathogen detection using antibody-based sensors, Biosens Bioelectron, 24(2008) 339-48.

[24] D. Maraldo, R. Mutharasan, 10-minute assay for detecting *Escherichia coli* O157 : H7 in ground beef samples using piezoelectric-excited millimeter-size cantilever sensors, J Food Prot, 70(2007) 1670-7.

[25] B. Ilic, D. Czaplewski, M. Zalalutdinov, H.G. Craighead, P. Neuzil, C. Campagnolo, et al., Single cell detection with micromechanical oscillators, J Vac Sci Technol, B, 19(2001) 2825-8.

[26] G.A. Campbell, R. Mutharasan, A method of measuring Escherichia coli O157 : H7 at 1 cell/mL in 1 liter sample using antibody functionalized piezoelectric-excited millimeter-sized cantilever sensor, Environ Sci Technol, 41(2007) 1668-74.

[27] G.A. Campbell, J. Uknalis, S.-I. Tu, R. Mutharasan, Detection of *Escherichia coli* O157:H7 in ground beef samples using piezoelectric excited millimeter-sized cantilever (PEMC) sensors, Biosens Bioelectron, 22(2007) 1296-302.

[28] D. Maraldo, R. Mutharasan, Preparation-free method for detecting Escherichia coli O157 : H7 in the presence of spinach, spring lettuce mix, and ground beef particulates, J Food Prot, 70(2007) 2651-5.

Chapter 11 . *hly*A gene-based sensitive detection of *Listeria monocytogenes* using a novel cantilever sensor

11.1. Introduction

Consumption of foods contaminated with *Listeria monocytogenes* (LM) causes listeriosis in humans and animals. *Listeria monocytogenes* is found in a variety of foods such as milk, milk products, eggs, poultry and meat[1, 2]. The FDA maintains a zero tolerance policy for LM [3] since it has a low infectious dose (<1000 cells)[4] and 30% mortality rate[5, 6]. The pathogen can survive and grow in the refrigerator at 4°C and can increase almost 10-folds in 7 days[7]. A recent outbreak of listeriosis due to infected ricotta cheese had, at the time of preparing this manuscript, affected 14 persons in 11 states with 3 deaths.[8] Pregnant women and immunocompromised persons such as new-borns and elderly people are most susceptible to listeriolysis.

The slow growth rate of *Listeria monocytogenes* is a challenge for detection of *Listeria monocytogenes* (LM) by the conventional culture and plating methods as the time to results (TTR) takes up to 7 days to yield results.[4, 7] The culture-based methods also consist of multiple steps and require trained personnel. Lack of high avidity antibodies has limited the use of antibody-based detection of LM and as a result a greater importance has been placed on nucleic acid-based methods. In this regard, polymerase chain reaction (PCR) based methods have been reported for reducing TTR[9] but they still require the enrichment step for low concentration samples. More importantly, the detection sensitivity deteriorates in proteinous backgrounds[10]. Use of separation techniques such as immunomagnetic beads[11-13] and innovative nucleic acid

amplification methods[14] have reduced the TTR to ~24 hrs while the best detection sensitivity reported to date is pre-enrichment concentrations of 10-10^2 CFU/mL.[1, 9, 15]

For gene-based detection, genes such as *prf*A[9, 16], a transcriptional activator of the virulence factor, phospholipases and internalins[17] and *hly*A[1, 18, 19], the gene that codes for the listeriolysinO toxin (LLO), have been used. The *hly*A gene (Gene Accession No. X 12157) is 1717 base pairs (bp) long and only a single copy of this gene is present in the genome of pathogenic LM. Since this gene codes for the toxin of the pathogen, it is used in identifying LM in the presence of other *Listeria* strains. Even for the culture and plating method of detection, the last confirmation step for identifying the presence of LM involves plating LM on blood agar which shows the LLO activity derived from *hly*A gene.

In this study, we propose the use of asymmetrically-anchored piezoelectric-excited millimeter-sized cantilever (aPEMC) sensors for detection of LM via the *hly*A gene sequence. We designed a detection sequence using the *hly*A gene and measured hybridization on aPEMC sensors for a range of target strand concentrations. Confirmation of hybridization on the senor surface was achieved in multiple ways: 1) the use of a dye that intercalates only in double stranded DNA (ds-DNA) fluoresces as a consequence, 2) a secondary ss-DNA strand that would hybridize to the target strand downstream from the probe hybridization region and 3) hybridization of gold nanoparticle (Au-NP) tagged secondary ss-DNA strand that would confirm and amplify the sensor response. We then extracted genomic DNA (gDNA) from LM and exposed it against the hlyA probe immobilized on the aPEMC sensor in the presence of competing non-target gDNA strands from *E.coli* JM101 (EC) to show that aPEMC sensors can

detect the presence of gDNA equivalent to 7×10^3 cells/mL of LM, less than the reported infectious dose, in the presence of non-target gDNA strands within 90 minutes.

11.2. Materials and methods

11.2.1. aPEMC Sensor Fabrication

Novel aPEMC sensors reported earlier[20] were fabricated from 5x1x0.127 mm^3 lead-zirconate-titanate (PZT) strips (Piezo Systems, Woburn, MA) by embedding both sides of the PZT strip to the same depth in epoxy. Additional epoxy was applied to one side of PZT for fabricating anchor asymmetry as shown in Figure S-1 (see supplementary materials). The other side of the sensor remained at the original free length (L). The asymmetric dimension (α) for the sensors used in this study varied from 0.2 to 0.35 times the free length, L. The free length, L, of the sensors used varied from 2.6 mm to 2.8 mm. A polyurethane coating was applied to sensor for experiments in liquids. A 100 nm thick gold layer was sputtered at the distal 1 mm^2 area of the cantilever for immobilization of ss-DNA probe.

11.2.2. DNA Probe and target selection

The sequences of all the ss-DNA strands used in this study along with their modifications are given in Table 1. The 18-mer ss-DNA probe sequence (strand P) was designed using Primer 3[21]. A synthetic target (strand Q; 54-mer long) complementary

to the probe sequence (strand P) was designed based on *hly*A gene. On the target strand (Q), downstream from the probe hybridization region, a 15-mer secondary region was used to design a secondary target (strand R). Strand S was derived by adding a 9-mer thymine tail to the 3' end of strand R. All ss-DNA strands were obtained from Integrated DNA Technologies (IDT, Coralville, IA). The melting and hybridization temperature and Na^+ concentration were determined using OligoAnalyzer 3.1[22].

11.2.3. Reagents

Ethylenediaminetetraacetic acid (EDTA), tris-hydrochloride (Tris-HCl) and 1-mercapto-6-hexanol (MCH) were purchased from Sigma Aldrich. Sodium chloride (NaCl), tris(2-carboxyethyl) phosphine (TCEP; 500 mM) and sodium dodecyl sulfate (SDS) were purchased from Fisher Scientific. Lyophilized DNA strands obtained from IDT were re-suspended in Tris-EDTA (TE) buffer (10mM Tris, 1mM EDTA, pH 8, 1M NaCl) and stored at -20 °C until their use for experiments. Ethanol (200 proof) was obtained from Decon Laboratories. Quant-iT™ PicoGreen® ds-DNA dye was purchased from Molecular Probes, Inc and gold nanoparticles (15nm, 2.3 nM) were purchased from BB International (Cardiff, U.K.). *Listeria monocytogenes* positives were purchased from Kirkegaard & Perry Laboratories, Inc.

Table 11-1 Summary of DNA strands

strand name	**strand sequence (5'→ 3')**	**modification**	**molecular weight (kDa)**
probe; **P**	**5'-*CTC CGC CTG CAA GTC CTA-3'***	thiol-C_6-5'	5.7
target; **Q**	**5'**-ATC **CGC GTG TTT CTT TTC** GAT TGG CGT CT***T AGG ACT TGC AGG CGG AG***A TGC TGG-**3'**	none	16.7
secondary target; **R**	**5'-GAA AAG AAA CAC GCG-3'**	none	4.7
secondary target for Au-NP; **S**	**5'-GAA AAG AAA CAC GCG** TTT TTT TTT-**3'**	3'-thiol	5.2

11.2.4. Genomic DNA (gDNA) extraction protocol

Genomic DNA (gDNA) extraction protocol was adapted from reference.[23] For LM, 1×10^9 cells and for EC, 5×10^7 cells were used for genomic DNA extraction. Bacterial cells were centrifuged at 10,000g for 15 min. The supernatant was discarded and the cell pellet was re-suspended in 200 µL TE buffer. 100 µL of SDS (10% in de-ionized water) was added to the cell suspension. The cells were incubated at 100 °C for 15 minutes and then immediately chilled at 2-4 °C for 10 min. Chloroform (600 µL) was added to the suspension and gently mixed by inverting over a period of 1 min. The suspension was centrifuged at 10,000g for 2 min to separate the aqueous from the organic phase. The aqueous supernatant (~250 µL) was pipetted into a separate aliquot without disturbing the aqueous-organic interface and NaCl solution (1M; 50 µL) was added to it to prevent precipitation of SDS. Cold ethanol (800 µL, 200 proof, -20 °C) was added to the aliquot and mixed well. The aliquot was placed in the freezer at -20 °C for 12 hrs for DNA precipitation. The aliquot was then centrifuged for 30 min at 10,000g and the supernatant was discarded. The pellet was washed with cold ethanol (300 µL) and the ethanol was allowed to evaporate at room temperature for 5 min. The resulting DNA pellet was then re-suspended in 1 mL TE buffer and stored at -20 °C until its use. The gDNA was sheared by squeezing through a 30-gauge ½ inch hypodermic needle 25 times. This method sheared the gDNA randomly to strands about 100-300 base pairs (bp) in length.[24] Just prior to a hybridization experiment, gDNA sample was melted at 100 °C for 10 min followed by chilling at 2-4 °C for 10 min. For gDNA hybridization experiments the stock solution of gDNA extract was serially diluted to the concentrations used.

11.2.5. Gold nanoparticle tagging of strand S

Stock solution (200 µL; 2.3 nM; ~10^8/mL) of gold nanoparticles (Au-NP) was incubated with 300 µL of 5 µM secondary target (strand S) and 1 µL of 500 mM TCEP at room temperature for 1 hr. The reaction solution was centrifuged at 10,000g for 30 min to separate the Au-NP from the reaction mixture. The pelleted Au-NP were resuspended in 300 µL of TE buffer and the centrifugation steps were repeated twice to remove the unbound ss-DNA and TCEP from the Au-NP suspension. After the final centrifugation step the Au-NP pellet was re-suspended in 1mL TE buffer for direct injection into the flow loop.

11.2.6. aPEMC sensor experiments

The flow apparatus used for experiments has been described previously.[25] The installed sensor was connected to an impedance analyzer (Agilent, 4294A) which was interfaced to a computer running a custom LabVIEW® program for measuring and recording the resonance frequency. In a typical experiment, a sensor was vertically installed in a custom flow cell and resonance frequency was allowed to reach a stable value under a constant flow of TE buffer (0.6 mL/min) while the temperature was controlled at 35 ± 0.2 °C. All hybridization experiments were performed at these conditions.

The DNA probe (strand P; 50 pM; 1mL) was reduced using 10 µL, 50 µM TCEP for 1 hour at room temperature and was introduced to the flow loop for immobilization on the gold-coated sensor. The total flow loop volume was 4 mL so the probe concentration was effectively reduced to 25% of sample concentration. Probe

immobilization caused the resonance frequency to decrease in value and reach a new stable value as the immobilization reached a steady state. The flow loop was thoroughly rinsed with TE buffer between additions of different reagents. Unoccupied Au <111> sites were back-filled by introducing MCH (10 μM; 1mL) to the flow loop.

Synthetic target strands (strand Q) were introduced to the flow loop to obtain hybridization responses at increasing concentrations. One LM cell has approximately 3 fg of gDNA. For detection experiments, gDNA equivalent to various cell concentrations were introduced to the flow loop after the MCH step.

11.3. Results and Discussion

11.3.1. aPEMC sensor characteristics and probe immobilization sensitivity

Approximately ~20 sensors were fabricated and characterized. Those that exhibited a pronounced second flexural resonance mode (n=9), located in the region of 60-85 kHz in liquid, were selected for detection experiments. Typical frequency spectra of aPEMC sensors are shown in Figure S-2 (see supplementary materials). The peak shape factor (Q) of this mode ranged from 20 – 35 under liquid immersion. In a liquid medium, the liquid film adjacent to the sensors acted as added mass resulting in decreased resonance frequency. The increase in density of the medium from air to TE buffer caused a frequency decrease of ~15 kHz; see Figure S-2. Although this frequency change due to density change is related to sensor sensitivity, molecular chemisorption is a better measure of device sensitivity for DNA detection.

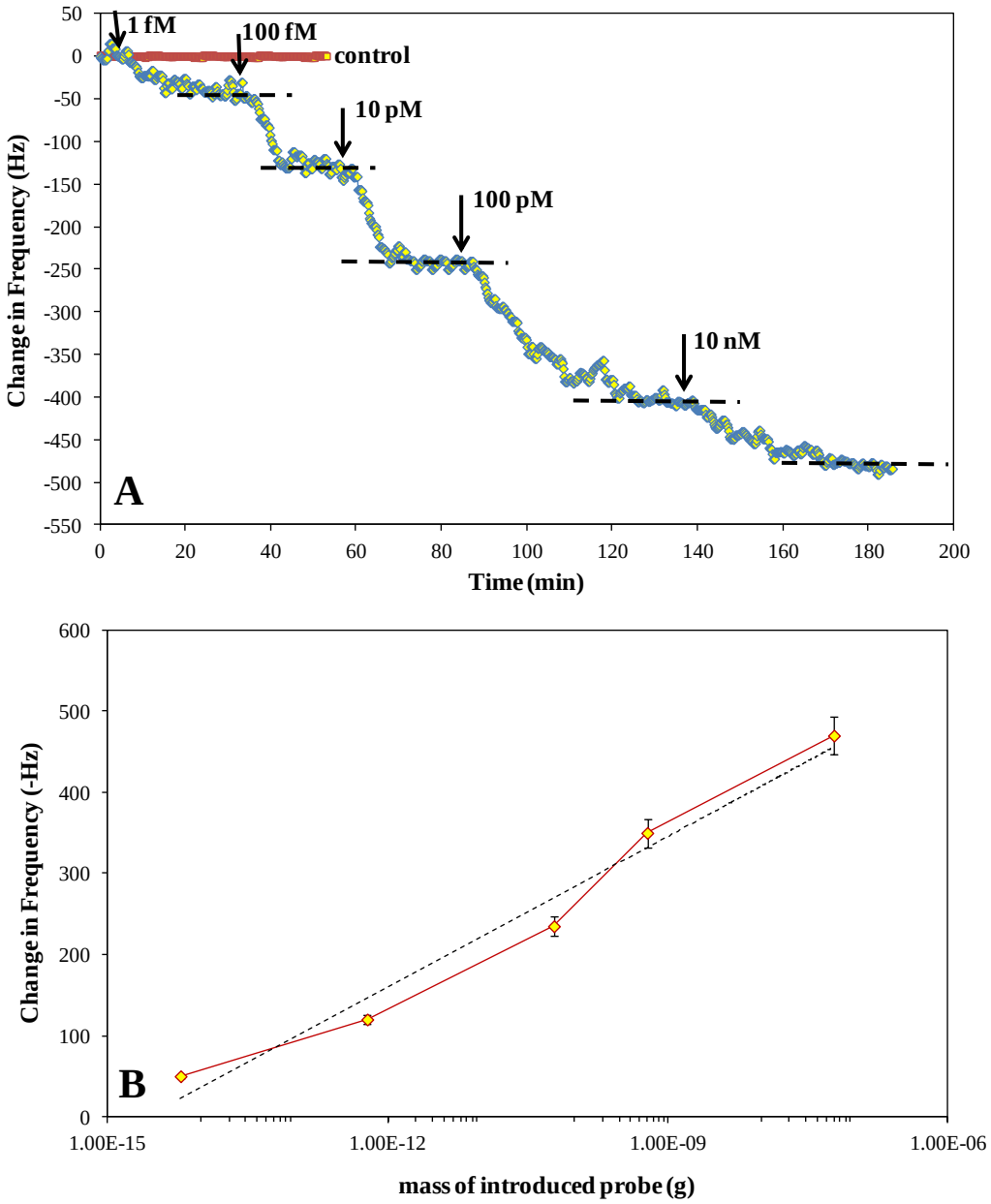

Figure 11-1 Panel A. Immobilization of sequentially increasing concentration of the designed probe (strand P) was used to characterize aPEMC sensor sensitivity. Resonance frequency shifts of ~50 Hz, ~120 Hz, ~235 Hz, ~380 Hz and ~470 Hz were observed upon introduction of 1mL of probe at 10 fM, 100 fM, 10 pM, 100 pM and 10 nM concentrations. The sensor sensitivity was calculated to be ~100-300 ag/Hz. **Panel B.** shows the log0linear relation between the frequency response and the probe strand (P) mass introduced.

Immobilization of the probe (strand P) at increasing concentrations was used to obtain aPEMC sensor sensitivity. Gold-coated aPEMC sensors were allowed to reach stable frequency value under TE buffer flow followed by the introduction of 1mL, TCEP-reduced probe at 1 fM concentration. Chemisorption of strand P on the sensor surface induced a frequency decrease of 50 ± 7 Hz (n=3) as shown in Figure 1A. This was followed by 1mL additions of the reduced probe at increasing concentrations of 100 fM, 10pM, 100 pM and 10 nM till the sensor surface was saturated as the available biding gold sites, in 1 mm^2 area, were filled. Corresponding to each of these concentrations the frequency decreased in value by 120 ± 11 Hz (n=7), 235 ± 19 Hz (n=7), 380 ± 24 Hz (n=7) and 470 ± 31 Hz (n=7), respectively. The sensors exhibited a log-linear frequency change response to the sequential mass additions as shown in Figure 1B. The various mass additions correspond to the mass of probe strands present in 1mL of the different concentrations introduced into the flow loop.

Total mass of the probe present in 1mL of 10 fM solution is ~ 6 fg and we expect only a fraction of this mass to chemisorb on the sensor surface. A conservative estimate of all 6 fg chemisorbing on the sensor surface inducing a resonance frequency decrease of 50 ± 7 Hz gives us an estimate of aPEMC sensor sensitivity to the be in the range of ~ 100-300 ag/Hz. For all hybridization experiments, probe concentration of 50 pM was used in order to ensure that the sensor surface was not very densely packed, a condition at which target hybridization can become inhibited.[26]

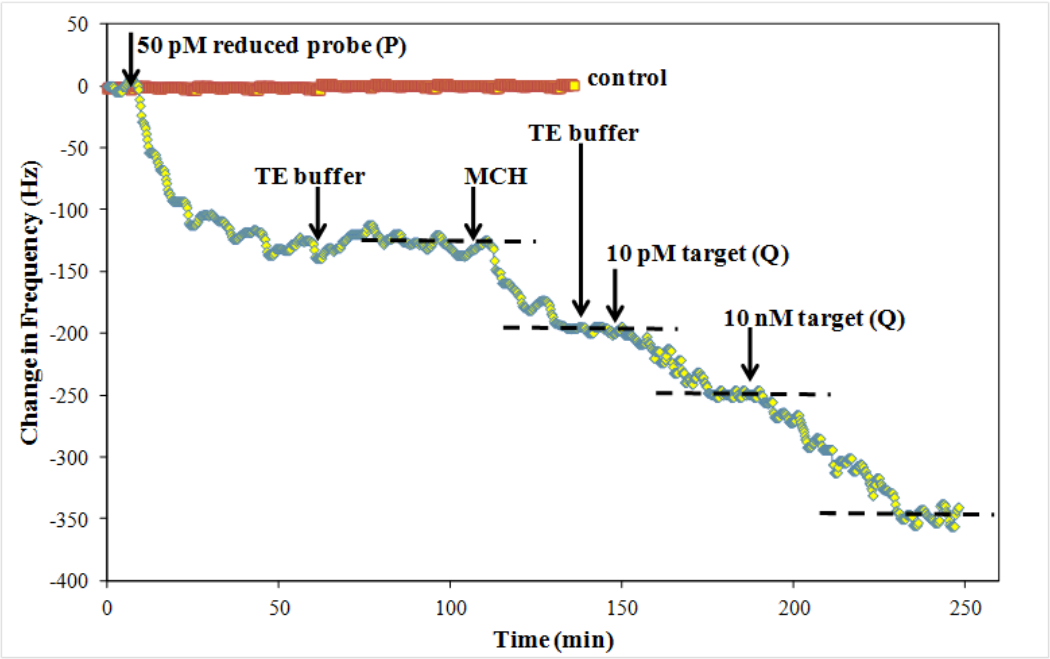

Figure 11-2 A typical experiment showing immobilization of probe (P) at 50 pM followed by MCH immobilization (10 µM) to orient the probe strands. Increasing concentration of target (Q) strands at 10 pM and 10 nM induced increasing hybridization responses.

11.3.2. Hybridization of target (strand Q) and confirmation

The high sensitivity values obtained from the concentration dependant response of aPEMC sensors to increasing probe concentrations should enable *hly*A gene-based detection of LM at low concentrations. MCH was used to back-fill the unfilled Au <111> sites after 50 pM probe immobilization to ensure probe strand orientation.[27] Concentration dependant decrease in the resonance frequency was observed upon introduction of the 54-mer target (strand Q) as shown in Figure 2. Frequency decreases of

55 ± 10 Hz (n=5) and 104 ± 17 Hz (n=5) were obtained for introductions of 1 mL of target strand concentrations at 10 pM and 10 nM respectively.

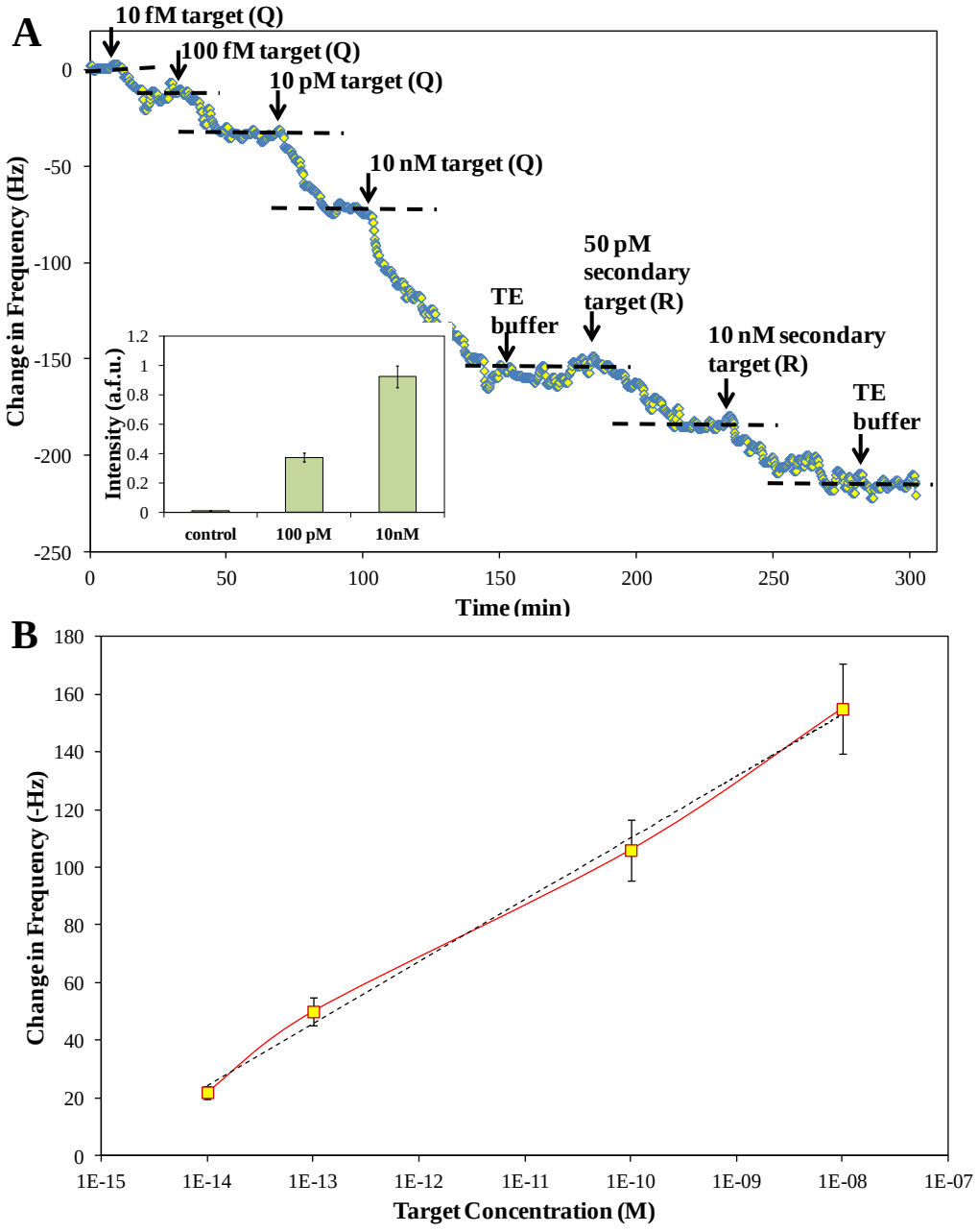

Figure 11-3 Panel A. Concentration dependent decreases in resonance frequency were observed for sequential additions of increasing concentrations of the target strands (Q) at 10 fM, 100 fM, 100 pM and 10 nM. The hybridization response confirmed using the secondary hybridization target (R) at different concentrations. The inset shows the comparison of relative fluorescence response observed on sensors that were exposed to target strand (Q) at 100 pM and 10 nM for hybridization to a control sensor that was not exposed to the target. **Panel B.** Concentration dependence of the target hybridization response is shown in. Frequency change and target concentration follow a log-linear relationship.

To better understand the concentration dependant target strand (Q) hybridization responses and to get a measure on the dynamic range of these experiments, increasing concentrations of strand Q, from 10 fM to 10 nM, were introduced to the flow loop after the MCH step as shown in Figure 3A. Responses at each of the target concentrations were measured in five separate experiments and the resulting resonance frequency decreases were 22 ±7 Hz, 50 ± 9 Hz, 106 ± 11 Hz, 155 ± 18 Hz for 10 fM, 100 fM, 100 pM and 10 nM respectively. There are 10 attomoles of target strands present in 1mL addition of strand Q at 10 fM concentration which induced a response of ~22 Hz. Since the hybridization response is equilibrium driven, it is reasonable to assume that a part of the 10 attomoles of target strands hybridized to strand P on the sensor. The response is encouraging for detecting low concentrations of gDNA from LM. The hybridization response of target strand (Q) followed a log-linear relationship with target concentrations over 6 orders of magnitude as shown in Figure 3B.

Confirmation of the hybridization response is imperative for establishing the application of these sensors for *hly*A gene-based detection of LM. The designed

secondary hybridization strand (strand R) was used in this study in a ELISA-like binding assay format. After the concentration dependant response was observed for 54-mer target (strand Q), as shown in Figure 3A, sequential introduction of 10 pM and 10 nM of strand R induced further resonance frequency decreases of 30 ± 10 Hz (n=5) and 40 ± 13 Hz Hz (n=5) respectively. Thorough TE buffer rinses employed in between additions of different reagents helped in removal of any poorly bound reagents to the sensor surface. These observed decreases in resonance frequency are dependent on the presence of the target strand Q hybridized to the probe on the sensor surface and thus confirm that the hybridization responses observed were indeed due to the target hybridizing to the probe strands on the sensors surface.

Another strategy employed in this study for confirmation of hybridization response is the use of Quant-iT™ PicoGreen® dye that fluoresces in the presence of ds-DNA and discriminates from ss-DNA strands. The excitation and emission wavelengths for this dye are 480 nm and 520 nm respectively. aPEMC sensors that were exposed to 100 pM and 10 nM target (strand Q) concentration and 10 nM of strand R and the hybridization response was allowed to reach equilibrium gave increasing fluorescence signals when allowed to react with the stain under identical conditions as the control sensor that was not exposed to the target. Comparison of fluorescence response is shown in inset of Figure 3A. The fluorescence results show concentration dependence and when compared to the control sensor give confirmation that the probe and target strands are hybridized on the sensor surface.

11.3.3. Au-NP amplification

Target hybridization at low concentration (10fM; 10 attomoles) gave small magnitudes of frequency decrease (~22Hz) upon hybridization. An approach to confirm and amplify low sensor response is to add further mass to the sensor. Gold nanoparticles (Au-NP) tagged secondary strands that hybridize to the non-hybridized part of the target (strand Q) would add mass to the sensor only if the target strands were present. The thiolated secondary target (strand S) with 15 nm diameter Au-NP (1mL, ~10^8/mL) was introduced to the flow loop after strand Q hybridization step. A typical experiment that demonstrates Au-NP amplification of hybridization response is shown in Figure B. After exhibiting hybridization responses of -19 Hz and -54 Hz for 1mL introduction of 10 fM and 100 fM strand Q, introduction of strand S-tagged Au-NP induced a much larger resonance frequency decrease of 250 ± 30 Hz (n=3). The frequency decrease is possible only if the target strand Q had hybridized to the probe on the sensor surface and the hybridization of Au-NP induced a large response thereby providing confirmation and amplification of the sensor response. Au-NP without any DNA strand, when introduced after the target response failed to induce any frequency change (< 10 Hz). Successful low concentration target hybridization and amplification responses were encouraging for low cell concentration equivalent gDNA detection.

11.3.4. gDNA hybridization and selectivity

Genomic DNA was prepared as described in Materials and Methods section. Absorbance spectra run on the extracted gDNA gave $A_{260/280}$ values of 1.9 which

suggests the presence of ~25% bacterial proteins with the extracted DNA.[28] All gDNA hybridization experiments were thus carried out in the presence of proteinous background. PCR of protein contaminated gDNA is known to be troublesome and leads to unreliable results.[10]

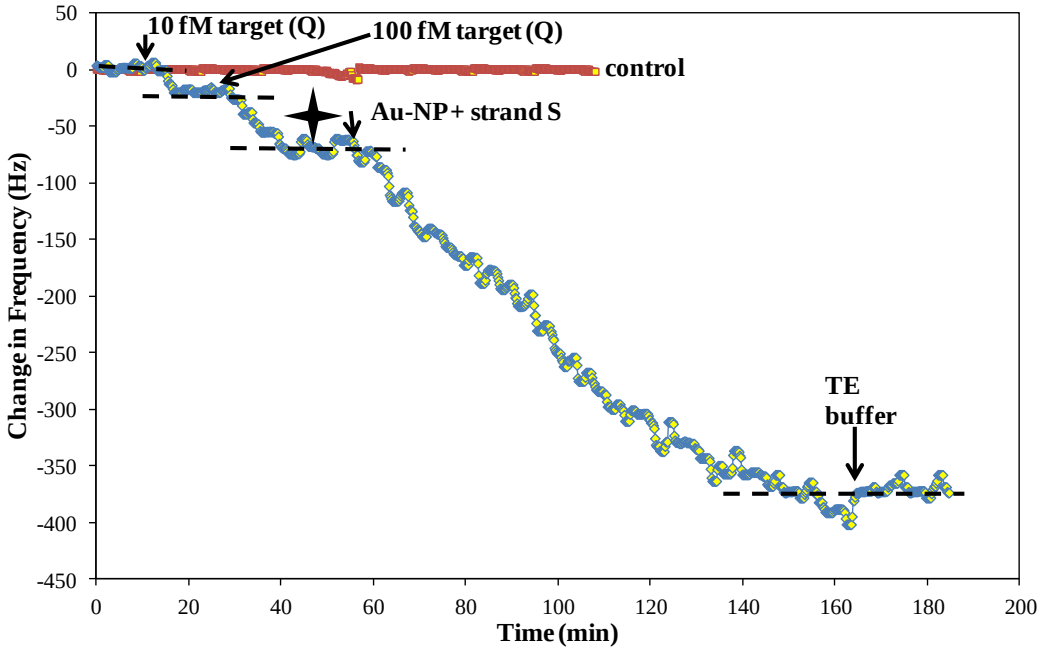

Figure 11-4 The small hybridization responses; ~22 Hz and ~50 Hz, obtained for low concentration of target (Q); 10 fM and 100 fM, respectively, were amplified by the introducing Au-NP tagged with secondary target strand (S). The frequency decreased by ~250 Hz due to the mass of the Au-NP.

The absorbance value gave us a concentration of ~2.32 µg of gDNA extracted from 1×10^9 cells of LM. At ~3.3 fg/cell of genomic DNA in LM theoretically 3.3 µg of gDNA should be extracted from the 1×10^9 cells. We thus were able to extract DNA from ~70% of the cells. The LM gDNA extract stock solution is at ~2.32 µg/mL. This solution was serially diluted by one order of magnitude to get to the concentration used in the hybridization experiments.

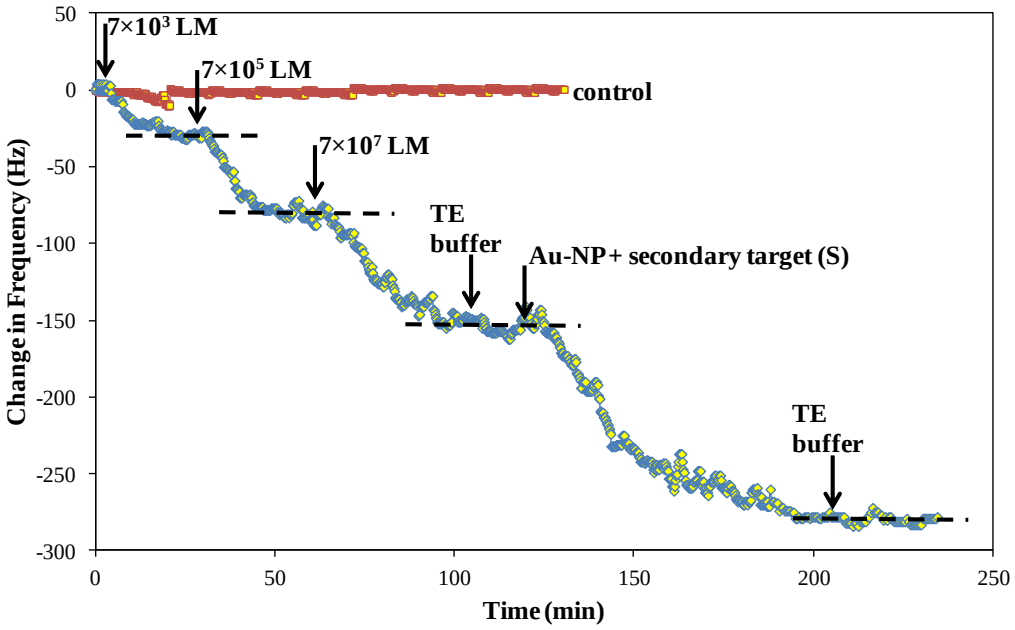

Figure 11-5 Hybridization of genomic DNA (gDNA) from LM was tested at increasing concentration in the presence of proteinous background. Introducing gDNA equivalent to the cell concentrations of 7×10^3, 7×10^5 and 7×10^7 (23 pg, 2.32 ng and 232 ng of gDNA, respectively) gave concentration dependent decreases in resonance frequency; ~34 Hz, ~85 Hz and ~167 Hz , respectively. gDNA hybridization was confirmed using Au-NP tagged with secondary target strand (S).

A typical hybridization response for *hly*A gene in the extracted gDNA is shown in Figure 5. aPEMC sensors prepared with immobilized probe (strand P) and backfilled MCH were exposed to sequentially increasing concentration of gDNA showed a concentration dependent response. Introduction of gDNA equivalent of 7×10^3/mL LM cells induced a resonance frequency decrease of 31 ± 9 Hz (n=5). Further addition of gDNA equivalents of 7×10^5 and 7×10^7 LM cells caused resonance frequency decreases of 83 ± 13 Hz (n=5) and 160 ± 17 Hz (n=5) respectively. Hybridization responses reached steady state in ~40 min after each gDNA introduction into the flow loop. The hybridization responses were confirmed and amplified by 10^8/mL Au-NP tagged with strand S. The amplifying hybridization responses reached steady state in ~90 min with frequency decrease magnitudes of ~140 ± 16 Hz (n=5).

To test if the response amplification protocol could improve detection at an even lower concentration, gDNA equivalent of 7×10^2 cells of LM (~2.3 pg) was introduced to the flow loop after the probe and MCH immobilization steps were done. A typical aPEMC sensor response shown in Figure 6 shows that introduction of gDNA of 7×10^2 cells induced a net frequency decrease of 17 ± 4 Hz (n=3). Further hybridization of Au-NP tagged strand S caused a further net decrease of 100 ± 13 Hz and amplified the small hybridization response. The Au-NP amplification strategy, thus, enables *hly*A gene-based detection of LM in proteinous background in less than an hour at detection limits comparable to PCR.

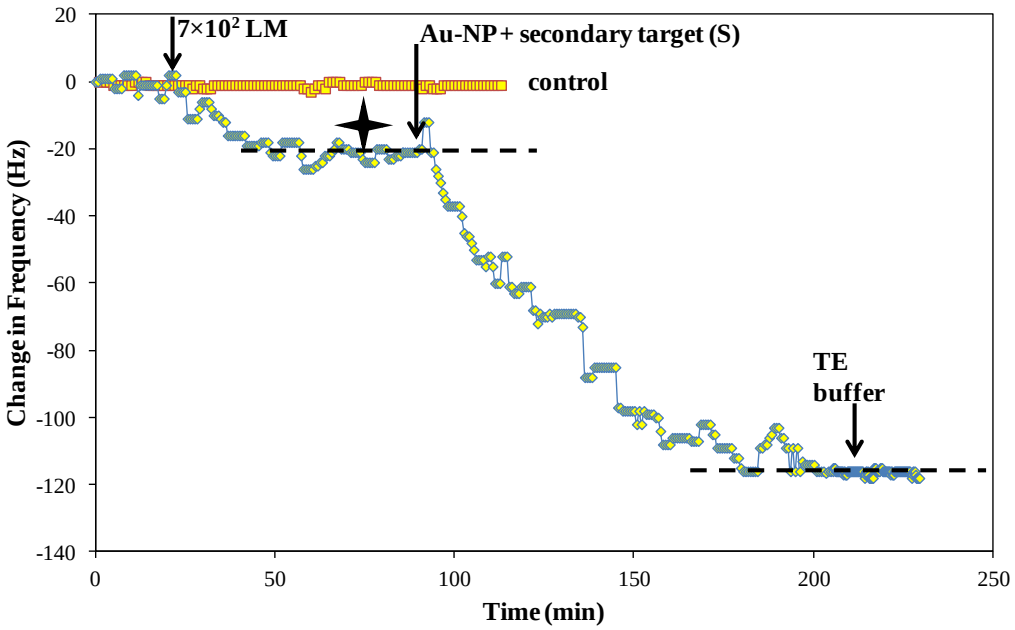

Figure 11-6 The detection limit for gDNA in proteinous background was established to be 7×10^2 cells equivalent of gDNA; 2.3 pg. Introduction of 2.3 pg of LM gDNA induced a resonance frequency decrease of ~16 Hz which was amplified by a further decrease of ~97 Hz upon introduction of 1 mL of 10^8/mL Au-NP tagged with strand S.

Selectivity of the aPEMC sensors was investigated by performing the hybridization experiments in the presence of not only the LM cells' proteinous gDNA but also proteinous non-target gDNA of *E.coli* JM101 (EC) that underwent the same shearing and melting steps as LM. From the absorbance values, we extracted ~160 ng of gDNA from EC cells. In these experiments we introduced sheared and melted gDNA sample from 5×10^7 EC cells (~160 ng) into the flow loop after probe for *hly*A (strand P) and MCH had been immobilized. The running buffer was set in re-circulation mode. No

decrease in the resonance frequency was obtained indicating that the EC gDNA did not hybridize with strand P, as shown in Figure 7.

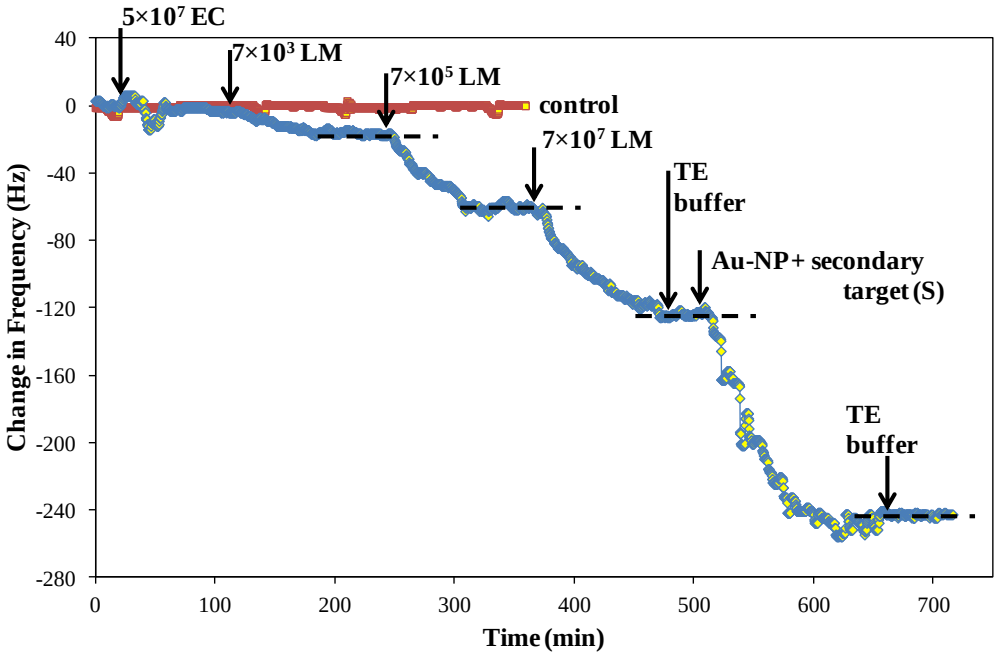

Figure 11-7 Selectivity of aPEMC sensor response was tested in the presence of ~160 ng of gDNA from 5×10^7/mL *E.coli* JM 101 (EC). In the presence of competing gDNA from EC the frequency responses observed for LM-gDNA equivalent to 7×10^3, 7×10^5 and 7×10^7 of cells were ~20 Hz, ~62 Hz and ~ 125 Hz respectively. Amplification using Au-NP tagged strand S gave a further frequency decrease of ~ 150 Hz.

Subsequently gDNA equivalent to 7×10^3, 7×10^5 and 7×10^7 cells (23 pg, 2.3 ng and 232 ng of gDNA, respectively) were introduced into the flow loop containing ~ 160 ng/mL of EC gDNA. The resonance frequency decreases for the increasing LM gDNA concentrations were 20 ± 4 Hz (n=5), 62 ± 9 Hz (n=5) and 125 ± 17 Hz (n=5) respectively and reached steady state in ~ 90 min. After the final hybridization response, the flow loop was rinsed with TE buffer and 1mL, 10^8/mL Au-NP tagged with strand S was introduced into the flow loop. Further hybridization amplified the frequency decrease by 150 ± 21 Hz (n=5). The detection limit LM gDNA in the presence of EC gDNA was 7×10^3 cells.

A summary of the sensor responses to various concentrations of LM cells (equivalent gDNA) in proteinous background with and without the presence of gDNA of EC is shown in Figure 8. The sensor response follows a log-linear relationship over the various concentrations tested in this study. There was ~21% loss of response magnitude for 7×10^7cells of LM and the loss of response increased to ~38% for 7×10^3cells. The reduced number of hybridizing interactions between the target and probe strands in the presence of competing non-target DNA strands is suggested as the reason for the observed decrease in response and the significant decrease in hybridization kinetics. The observed rate constant for hybridization of gDNA in the absence of EC-gDNA was found to be 0.21 ± 0.004 min^{-1} while that in the presence of EC-gDNA was 0.021 ± 0.002 min^{-1}. [29]

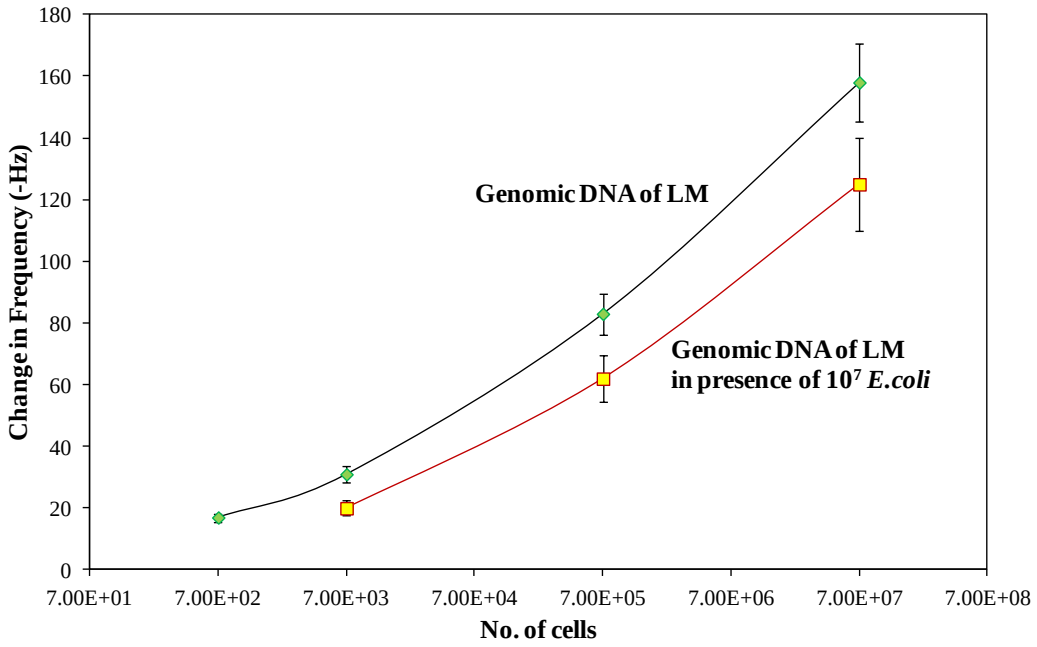

Figure 11-8 Summary of the hybridization responses observed for increasing concentrations of LM cells (gDNA equivalent) in proteinous background with and without the presence of EC gDNA is shown to follow a log-linear relationship over 5 orders of magnitude.

11.4. Conclusion

aPEMC sensors provide sensitive and selective detection of *Listeria monocytogenes* by the use of the specific virulence gene, *hly*A. Detection limit of 7×10^2 cells/mL was achieved for sensing in a proteinous background within 40 min but in the presence of 10^4 times excess competing non-target DNA and proteins the lowest detectable concentration was 7×10^3/mL within 90 min. These detection results are

significant improvements in terms of the time to results and no sample preparation steps were needed. The detection limits were comparable with the conventional detection techniques.

11.5. Supplementary materials

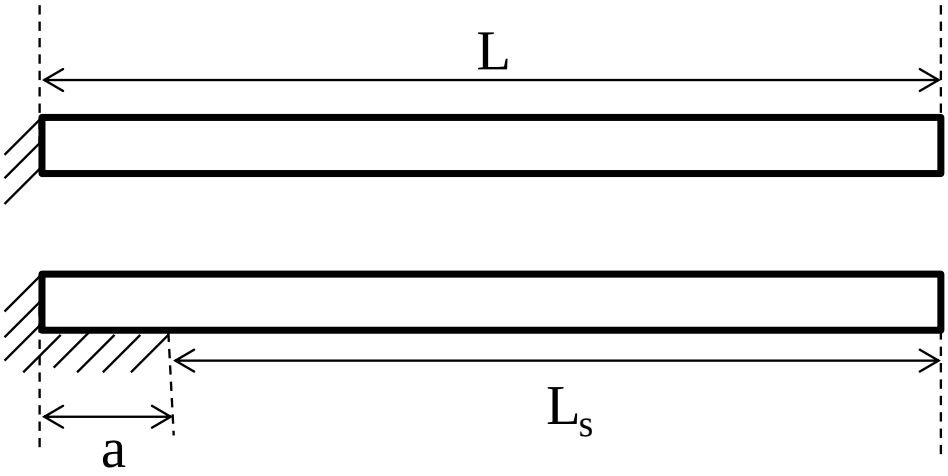

Figure S-1. Cross-section of a single layer, PZT cantilever of length 'L' is shown. The hatched surface is anchored rigidly to fix one end. Rigidly achoring small length 'a' on the underside of the PZT layer leads to an asymmetrically anchored PZT cantilever. Detailed discussion on fabrication of these sensor is presented in Ref. [20]

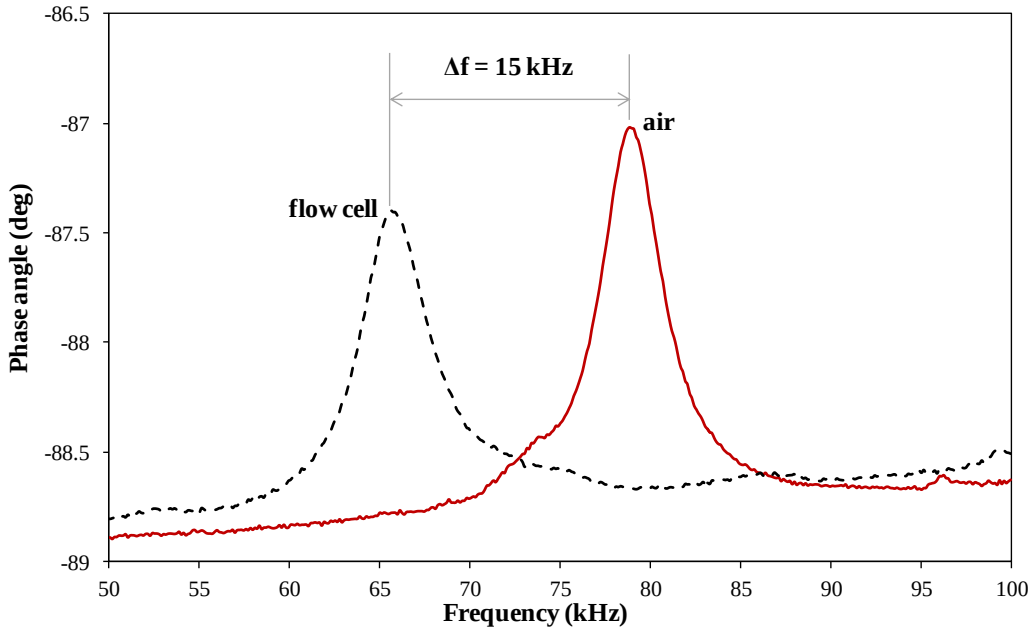

Figure S-2. Typical spectra of the AAPEMC sensors in air and in buffer. The resonance frequency decreases by ~15 kHz due to change in the density of the surrounding medium.

11.6. References

[1] G. Amagliani, G. Brandi, E. Omiccioli, A. Casiere, I.J. Bruce, M. Magnani, Direct detection of Listeria monocytogenes from milk by magnetic based DNA isolation and PCR, Food Microbiol, 21(2004) 597-603.

[2] H. Zhou, Z. Gao, G. Luo, L. Han, S. Sun, H. Wang, Determination of Listeria Monocytogenes in Milk Samples by Signal Amplification Quartz Crystal Microbalance Sensor, Anal Lett, 43(2010) 312-22.

[3] FDA, Quantitative Assessment of Relative Risk to Public Health from Foodborne Listeria monocytogenes Among Selected Categories of Ready-to-Eat Foods, 2003.

[4] A.D. Hitchins, K. Jinneman, Detection and Enumeration of *Listeria monocytogenes* in Foods, Bacteriological Analytical Manual 8th ed., AOAC International1998.

[5] C.W. Donnelly, Detection and Isolation of *Listeria monocytogenes* from Food Samples: Implications of Sublethal Injury, Journal of the Association of Official Analytical Chemists: International, 85(2002) 495-500

[6] M.W. Griffiths, Listeria monocytogenes: Its importance in the dairy industry, Journal of the Science of Food and Agriculture, 47(1989) 133-58.

[7] M.P. Doyle, L.R. Beuchat, Food Microbiology: Fundamentals and Frontiers, 3rd ed., ASM Press2007.

[8] CDC, Multistate Outbreak of Listeriosis Linked to Imported Marte Brand Frescolina Ricotta Salata Cheese, Center for Disease Control and Prevention2012.

[9] A. Germini, A. Masola, P. Carnevali, R. Marchelli, Simultaneous detection of Escherichia coli O175:H7, Salmonella spp., and Listeria monocytogenes by multiplex PCR, Food Control, 20(2009) 733-8.

[10] N.L. Rosi, C.A. Mirkin, Nanostructures in Biodiagnostics, Chemical Reviews, 105(2005) 1547-62.

[11] E.T. Ryser, E.H. Marth, Listeria, Listeriosis and Food Safety, Food Science and Technology, 3rd ed., CRC Press2007.

[12] J. Vytřasová, I. Zachová, L. Červenka, J. Štěpánková, M. Pejchalová, Non-Specific Reactions during Immunomagnetic Separation of Listeria, Food Technol Biotechnol, 43(2005) 397-401.

[13] H.-S. Kim, I.-H. Cho, S.-M. Seo, J.-W. Jeon, S.-H. Paek, In situ immuno-magnetic concentration-based biosensor systems for the rapid detection of Listeria monocytogenes, Mater Sci Eng: C, 32(2012) 160-6.

[14] T. Murakami, J. Sumaoka, M. Komiyama, Sensitive isothermal detection of nucleic-acid sequence by primer generation–rolling circle amplification, Nucleic Acids Research, 37(2009) e19.

[15] G. Amagliani, C. Giammarini, E. Omiccioli, G. Brandi, M. Magnani, Detection of Listeria monocytogenes using a commercial PCR kit and different DNA extraction methods, Food Control, 18(2007) 1137-42.

[16] K.J. Cooray, T. Nishibori, H. Xiong, T. Matsuyama, M. Fujita, M. Mitsuyama, Detection of multiple virulence-associated genes of Listeria monocytogenes by PCR in artificially contaminated milk samples, Appl Environ Microbiol, 60(1994) 3023-6.

[17] S. Kathariou, Listeria monocytogenes virulence and pathogenicity, a food safety perspective, J Food Prot, 65(2002) 1811-29.

[18] M.-J. Tang, S. Zhou, X.-Y. Zhang, J.-H. Pu, Q.-L. Ge, X.-J. Tang, et al., Rapid and Sensitive Detection of Listeria monocytogenes by Loop-Mediated Isothermal Amplification, Curr Microbiol, 63(2011) 511-6.

[19] S. Lomonaco, R. Patti, S.J. Knabel, T. Civera, Detection of virulence-associated genes and epidemic clone markers in Listeria monocytogenes isolates from PDO Gorgonzola cheese, Int J Food Microbiol, 160(2012) 76-9.

[20] H. Sharma, R.S. Lakshmanan, B.N. Johnson, R. Mutharasan, Piezoelectric cantilever sensors with asymmetric anchor exhibit picogram sensitivity in liquids, Sensors and Actuators, B: Chemical, 153(2011) 64-70.

[21] S. Rozen, H. Skaletsky, Primer 3 on the WWW for general users and for biologist programmers, in: S. Krawetz, S. Misener (Eds.), Bioinformatics Methods and Protocols: Methods in Molecular Biology, Humana Press, Totowa, NJ, 2002, pp. 365-86.

[22] IDTDNA, OligoAnalyzer 3.1, http://www.idtdna.com/analyzer/Applications/OligoAnalyzer/.

[23] K. Wilson, Preparation of Genomic DNA from Bacteria, Current Protocols in Molecular Biology, John Wiley & Sons, Inc1997.

[24] R.B. Towery, N.C. Fawcett, P. Zhang, J.A. Evans, Genomic DNA hybridizes with the same rate constant on the QCM biosensor as in homogeneous solution, Biosens Bioelectron, 16(2001) 1-8.

[25] G.A. Campbell, R. Mutharasan, Detection of Bacillus anthracis spores and a model protein using PEMC sensors in a flow cell at 1 mL/min, Biosensors and Bioelectronics, 22(2006) 78-85.

[26] A.W. Peterson, R.J. Heaton, R.M. Georgiadis, The effect of surface probe density on DNA hybridization, Nucleic acids research, 29(2001) 5163-8.

[27] M. Calleja, M. Nordstrom, M. Alvarez, J. Tamayo, L.M. Lechuga, A. Boisen, Highly sensitive polymer-based cantilever-sensors for DNA detection, Ultramicroscopy, 105(2005) 215-22.

[28] J. Sambrook, D.W. Russel, Molecular Cloning: A Laboratory Manual, Cold Spring Harbor, New York: Cold Spring Harbor Laboratory Press; 2001.

[29] K. Rijal, R. Mutharasan, PEMC-based method of measuring DNA hybridization at femtomolar concentration directly in human serum and in the presence of copious noncomplementary strands, Anal Chem, 79(2007) 7392-400.

Chapter 12 . Conclusions and future work

12.1. Summary and conclusions

The main results of the research work presented in this thesis are summarized here:

1. It was shown for the first time that self-exciting and self-sensing piezoelectric cantilevers consisting only of lead zirconate titanate (PZT) measure resonance only if they are asymmetrically anchored. Chemisorption experiments, where binding was localized to 1 mm^2 distal tip of the PZT cantilever gave improved sensitivity values of 2 pg/Hz and 414 fg/Hz for the same two resonant modes.

   We also fabricated novel cantilever designs that express torsional and lateral modes that exhibited excellent mass-change sensitivity to molecular self-assembly on gold (75 – 135 fg/Hz) which was superior to that of widely investigated bending modes.

2. The response of resonant-mode cantilever sensors depends on the binding strength of analyte mass to the sensor surface. Comparison of cantilever response to attachment of three macro-sized pieces showed that sronger adhesion causes a larger frequency decrease for the same mass.
3. Characterization of the type of oscillation exhibited by the higher-order resonance mode of the composite PEMC design as having a shear component, similar to a quartz crystal microbalance (QCM) was demonstrated. For various binding strengths and various masses, the fundamental modes decreased in resonance

frequency. For the same mass addition experiments on the high-order modes of PEMC sensors, anomalous increase in resonance frequency was observed.

4. A dry and rapid method of pulsed-plasma assisted grafting of amine surface functional groups, using ammonia gas on polyurethane surfaces is successfully demonstrated by using pulse cycle times of 1s-180s (on-off). One cycle of plasma treatment was found to generate higher amine groups as they tend to degrade upon longer exposure to the high-energy radicals. Successful amination of the polyurethane surfaces was demonstrated by Fourier transform infrared spectroscopy (FTIR). To establish the availability of the surface amine groups for reaction, 1 μm carboxylated polybeads were reacted to polyurethane-coated piezo-electric excited millimeter-sized cantilever (PEMC) sensors before and after plasma treatment. Scanning electron microscope micrographs of PEMC sensors exposed to the same concentration of beads show more than four-fold increase in the presence of beads post pulsed-plasma treatment. Application of this method for protein immobilization was established by BSA chemisorption on plasma treated PEMC sensors.
5. We showed for the first time that half antibody fragments containing the *E.coli* O157:H7 antigen binding region give a larger response with shear-mode resonating mass sensors. Tris(2-carboxyethyl)phosphine (TCEP) was used to reduce the disulfide bridges in antibodies to cleave them into two half antibody fragments, while preserving the antigen- binding region. Cleavage exposes the native thiol group in the antibody that readily chemisorb on gold surfaces with proper orientation for immobilized antibody to bind to its antigen. Comparing

responses obtained on a quartz crystal microbalance for the detection of pathogenic *E.coli* O157:H7 using TCEP-reduced antibody fragments with conventional antibody immobilization protocols showed that the proposed method enhances device sensitivity. Examining the half antibody fragments for detection of target cells in the presence of non-target *E.coli* JM 101 showed that the fragments retain their specific antigen binding capability without loss of selectivity upon reduction by TCEP.

6. We reported a new biosensor-based method that is more sensitive and rapid than the current approach for detecting mycoplasma in cell culture samples. Piezoelectric-excited millimeter-sized cantilever (PEMC) sensors respond to mass change via resonant frequency change. They are sensitive at femtogram level, and can be used directly in liquid for label-free detection. Common cell culture contaminant, *Acholeplasma laidlawii* was detected in both buffer and cell culture medium. Two different sources (positive control from a commercial kit and ATCC 23206) were analyzed using antibody-immobilized PEMC sensor. Resonant frequency decrease caused by binding of *A. laidlawii* was monitored in real-time using an impedance analyzer. Positive detection was confirmed by a second antibody binding. The limit of detection (LOD) was lower than 10^3 CFU/mL in cell culture medium using PEMC sensor while parallel ELISA assays showed LOD as 10^7 CFU/mL. This study shows PEMC sensor can be used for sensitive and rapid mycoplasma detection in cell culture samples.
7. Listeria monocytogenes (LM), an important food-borne pathogen that has a high mortality rate (~30%), was successfully detected within an hour at the

infectious dose limit of 10^3 /mL, both in buffer and milk. LM detection was demonstrated using a highly sensitive (~28 Hz/pg), novel asymmetrically anchored cantilever sensor and a commercially available antibody. Sensor responses were confirmed using a secondary antibody binding step, similar to the sandwich ELISA assays, as a means of signal amplification that also reduced the occurrence of false negatives. Detection of LM at a concentrations of 10^2/mL was achieved, by incorporating a third antibody binding step, which is an order of magnitude smaller than the infectious dose (< 1000 cells) for LM. The commercially available antibody for LM used in this work is shown to have low avidity which partially explains the relatively low sensitivity reported for LM as compared to other pathogens.

8. Piezoelectric cantilever sensors were shown to exhibit sensitive and selective detection based on a specific identifying gene from genomic extract at 10^2-10^3 cells of foodborne pathogen, Listeria monocytogenes (LM). A probe designed for the virulence hemolysin gene, hlyA, was immobilized on the gold-coated sensor and hybridization detection of a synthetic target (based on the hlyA sequence) is shown that spans over 6 orders of magnitude in concentration. Hybridization response was confirmed using two methods: 1) the use of a fluorescent indicator for the presence of double-stranded DNA (ds-DNA) and 2) hybridization response of a secondary single-strand DNA (ss-DNA) to the target much like in the ELISA sandwich format. Hybridization of the secondary ss-DNA tagged to gold nanoparticles amplified as well as confirmed the target hybridization to the hlyA probe on the sensor. Genomic

DNA from LM was extracted, sheared and melted and was exposed to the hlyA probe on the sensor in proteinous background with and without the presence of up to 10^4 times excess non-target genomic DNA extracted from E.coli JM 101 (EC), for the gene-specific detection of LM. Discernable detection limit of 7×10^2 LM cells (equivalent genomic DNA) was achieved in proteinous background. The detection limit deteriorated to 7×10^3 LM in the presence of genomic DNA from EC. Hybridization response times were within ~90 min, thus significantly improving over the conventional detection techniques in terms of detection time with comparable detection limit.

12.2. Recommended future work

Cantilever technology has been developed over the past decade for sensing applications of chemical and biological entities such as proteins, cells and nucleic acids. As the technology matures its application in different fields will be pursued. Some of the projects that can be worked upon are as follows:

1. **Cantilevers as a biomarker discovery platform**

As opposed to the use of single cantilever sensor, an array of cantilevers can be used towards this work. Arrays enable high throughput screening of large libraries in a short time. Control sensors can be incorporated in the array to better understand the results of the screening. Various protein and nucleic acid biomarkers for several diseased

states are present in bodily fluids. Several array existing array technologies can be used for this work but most of these required labeled reagents for signal amplification to detect low concentrations. Early stages of the diseased states might possible lead to small concentration presence of these biomarkers which emphasizes the need of highly sensitive devices to measure them. The high sensitivity of the aPEMC sensors and improvement in fabrication reproducibility can be advantageous towards this end.

2. Nucleic acid amplification

Isothermal rolling circle amplification technology has been developed.[1, 2] The use of this technology with the cantilever sensor platform will not only help achieve amplification of sensor response for hybridization assays but can also be used for discovery processes. The real time amplification monitoring capability can be used to understand thermodynamics of nucleic acid amplification and can be extended to monitoring the efficiency of the polymerase to correctly replicate the strand.

3. Polymers and biological film formation studies

The real time monitoring capability of cantilever sensors can be used to study the change in properties of a film on the cantilever. Most film formations change the elasticity of the oscillating body. The resonance frequency of the cantilever is a function of the device elasticity, changes to which can be monitored and studied for understanding polymer films under various conditions. It can also be used to monitor film formation processes such as blood clotting and bio-fillm formation and gain a better understanding of these processes.

12.3 References

[1] H. Takahashi, A. Matsumoto, S. Sugiyama, T. Kobori, Direct detection of green fluorescent protein messenger RNA expressed in Escherichia coli by rolling circle amplification, Analytical Biochemistry, 401(2010) 242-9.

[2] S.F. Kingsmore, D.D. Patel, Multiplexed protein profiling on antibody-based microarrays by rolling circle amplification, Current Opinion in Biotechnology, 14(2003) 74-81.

Appendix A: Piezoelectric cantilever sensors with asymmetric anchor exhibit picogram sensitivity in liquids

A.1. Introduction

Cantilever sensors have enjoyed considerable interest among researchers because of their high sensitivity and their potential for high throughput applications with label-free reagents[1-4]. Resonant-mode cantilever sensors respond to attached mass of analytes by reduction in resonant frequency. The change in resonant frequency is proportional to analyte concentration, and is measured by a variety of methods, which include integrated transducing elements within the oscillating cantilever [5-11] and external instrumentation [12-16] that measures the cantilever oscillation amplitude. In both cases, the actuation of the cantilever is provided by natural thermal fluctuations [17-19] or by actuating the base of the cantilever electromechanically [5, 6, 8, 11]. In earlier investigations, we showed that a sensor consisting of an anchored piezoelectric layer (typically, lead zirconate titanate; PZT) bonded to an anchored non-piezoelectric material (typically, glass) resulted in an effective design for both exciting and sensing resonance [20-22]. Such a design is significantly simpler than a sensor consisting of separate excitation and sensing electronics and instrumentation. The PZT layer was excited at 10^3 v/m and the resulting current was measured. The phase angle (Φ) between the excitation voltage and the resulting electric current in the piezoelectric layer exhibited sharp change in Φ at resonance due to altered electrical impedance of PZT caused by higher than normal strain at resonance. The glass layer served to constrain longitudinal deformation

of PZT, thus inducing bending mode vibration of the integrated cantilever. Such an integrated sensor has yielded successful label-free biosensing in liquid at 50 picograms using low-order (<60 kHz) resonant modes[23, 24]. In this paper, we investigate PZT cantilever sensors that are devoid of the parasitic non-piezoelectric glass layer, and report a novel approach for anchoring PZT that enables induction of measurable bending mode resonance. A PZT cantilever anchored uniformly or symmetrically and excited electrically exhibits primarily longitudinal deformation and logitudinal resonant modes.[25] Transverse or bending vibration is present weakly and are not transduced into significant electrical impedance changes because the resulting symmetric mode shapes cause no net charge in PZT. Since the bending modes have been associated with sensitive detection, we investigated methods that induce measurable impedance change at bending resonant modes of PZT cantilevers. By anchoring the PZT in epoxy *asymmetrically* (Figure A- 1), we find bending modes that are not normally measurable, became electrically measurable. Because one side of the PZT cantilever is longer than the other, differential longitudinal deformation occurs inducing transverse vibration that causes change in impedance of PZT such that the bending mode resonances become electrically measurable. We show that the low order bending modes are more sensitive than previous designs containing a non-piezoelectric layer anchored symmetrically.

A.2. Materials and Methods

A.2.1. Experimental section

Chemicals.

Phosphate buffered saline (PBS, 10 mM, pH 7.4) purchased from Sigma-Aldrich (Alletown, PA) was prepared in deionized water (18 MΩ, Milli-Q system, Millipore), and subsequently diluted to obtain 2.5 and 5.0 mM solutions. Ethanol (analytical grade) and dodecanethiol (99%) were purchased from Sigma.

PEMC sensor fabrication.

The sensor was fabricated from 5x1x0.127 mm^3 PZT strip (Piezo Systems, Woburn, MA). A schematic and photographs of the sensors is in Figure A--1. The top and bottom surfaces of the PZT layer at the anchored end were connected via soldered 30 gauge wire to excitation voltage source. The cantilever was embedded in a 6 mm glass tube with a non-conductive epoxy. Initial anchoring was obtained by ensuring that both sides of PZT were embedded to the same depth in epoxy. After the spectral properties were determined, additional epoxy was applied to one side of PZT to introduce anchor asymmetry. The other side of the sensor remained at the original free length (L). After the applied epoxy had cured, its spectral property was measured. Several sensors (n>60) were prepared with asymmetric anchor for spectral property evaluation. The asymmetric dimension (α was varied from 10% to 65% of the free length, L. For in-liquid applications, the sensors were parylene C coated following the vendor supplied protocol for providing electrical insulation. For chemisorption experiments gold was sputtered at 100 nm thickness at distal 1 mm^2 area of a PZT cantilever in a Denton DESK IV sputtering unit (Denton Vacuum LLC, Moorestown, NJ).

Experimental apparatus and methods .

The experimental setup consists of an impedance analyzer (Agilent 4294A), a peristaltic pump, a custom flow cell and several fluid reservoirs. The flow cell (hold-up volume = 120 μl) was maintained in an incubator at 30 ± 0.1 °C to ensure isothermal conditions. Prior to an experiment, the entire flow loop was rinsed with 100 % ethanol followed by copious amount of deionized (DI) water. The resonant frequency change during an experiment was monitored continuously by a custom-written LabView® program. The flow loop was operated in either a single pass mode or in a recirculation mode.

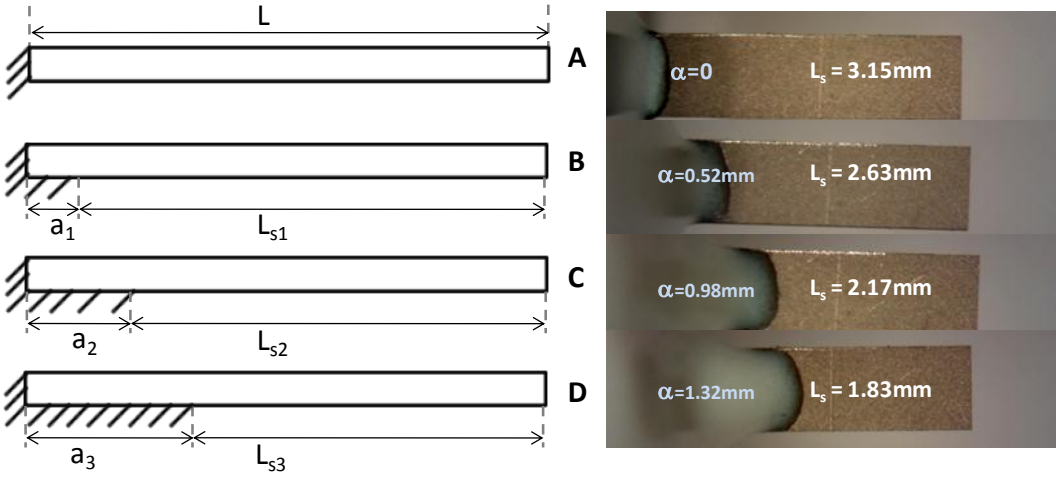

Figure A-1 Left Panel. Cross sectional view of symmetrically and asymmetrically anchored PZT cantilevers. Hatched surface is anchored rigidly. **Right Panel.** Sample of fabricated PZT cantilever sensors, view is from underside of sensor (schematic in Left Panel) with variouss asymmetries is shown. The top picture shows a symmetrically-anchored sensor while the rest have increasing asymmetry; α increases.

In a typical experiment, a sensor was vertically installed in the flow cell and the flow rate was set at 0.6 mL/min. In the density change experiments the flow loop was filled with DI water and the resonant frequency was allowed to reach steady state. Subsequently, the flow was switched to PBS and the sensor was allowed to reach a new steady state. To confirm that the sensor response was due to density change we alternated between DI water and PBS of various concentrations. In chemisorption experiments, after the gold-coated sensor stabilized at 0.6 mL/min ethanol, the flow was switched to 30 pM dodecanethiol in ethanol and the changes in resonant frequency of the first two resonant modes were monitored.

A.2.2. Finite Element Model.

The PZT cantilevers of thickness t, and of free lengths L and L_s containing asymmetry α (=L- L_s) shown in Figure A--1 were simulated using a commercial finite element modeling (FEM) software, COMSOL 3.4 (COMSOL Group, Burlington, MA). The expected deformation in PZT at 100 mV excitation is small, and thus plane stress model was invoked for cantilever deformation mechanics. We imposed zero deflection boundary condition at the anchor (denoted by hatching in Figure A--1A-D). The properties of PZT-5A used for simulation are given in supplemental materials (Table S1). Constitutive equations that represent the coupling between the electric field and mechanical deformation of the PZT layer are given by [26]:

$$T = c^E S - e'E \quad (1)$$

$$D = eS + \varepsilon^S E \quad (2)$$

where T, S, E, and D denote stress, strain, electric fields, and electric displacement (or induction), respectively. The term c^E is the elasticity tensor evaluated at a constant (zero, short and open circuit) electric field, e is the piezoelectric tensor, and ε^S is the dielectric permittivity measured at constant (zero, clamped) strain.

Resonance Frequency Calculation.

The finite element model included the coupling of electrical and mechanical effects in the PZT domain. Loss factor damping in PZT was adjusted manually until the results were close to the experimental quality factors. Such an empirical approach is consistent with previous work in this area [27]. Loss factor used in this paper was 1% in all calculations. The total number of elements in each simulation ranged from 72 to 1152; convergence was obtained with minimal mesh resolution due to the simple geometry. Simulations neglect fluid-structure interaction and were conducted in vacuum. The number of elements used was increased such that the calculated resonance frequencies and phase angles converged within < 0.01 %. Initial charge in PZT, initial stress, and external force were set to zero. Using the principle of virtual work option, resonance frequencies of the finite element model were computed. An eigenvalue solver was used for determining resonance frequencies and eigenvalues. As a check, cantilevers of uniform cross-section and isotropic properties yielded eigenfrequency values within an accuracy of few part per million when compared with the analytical model (Equation (3)).

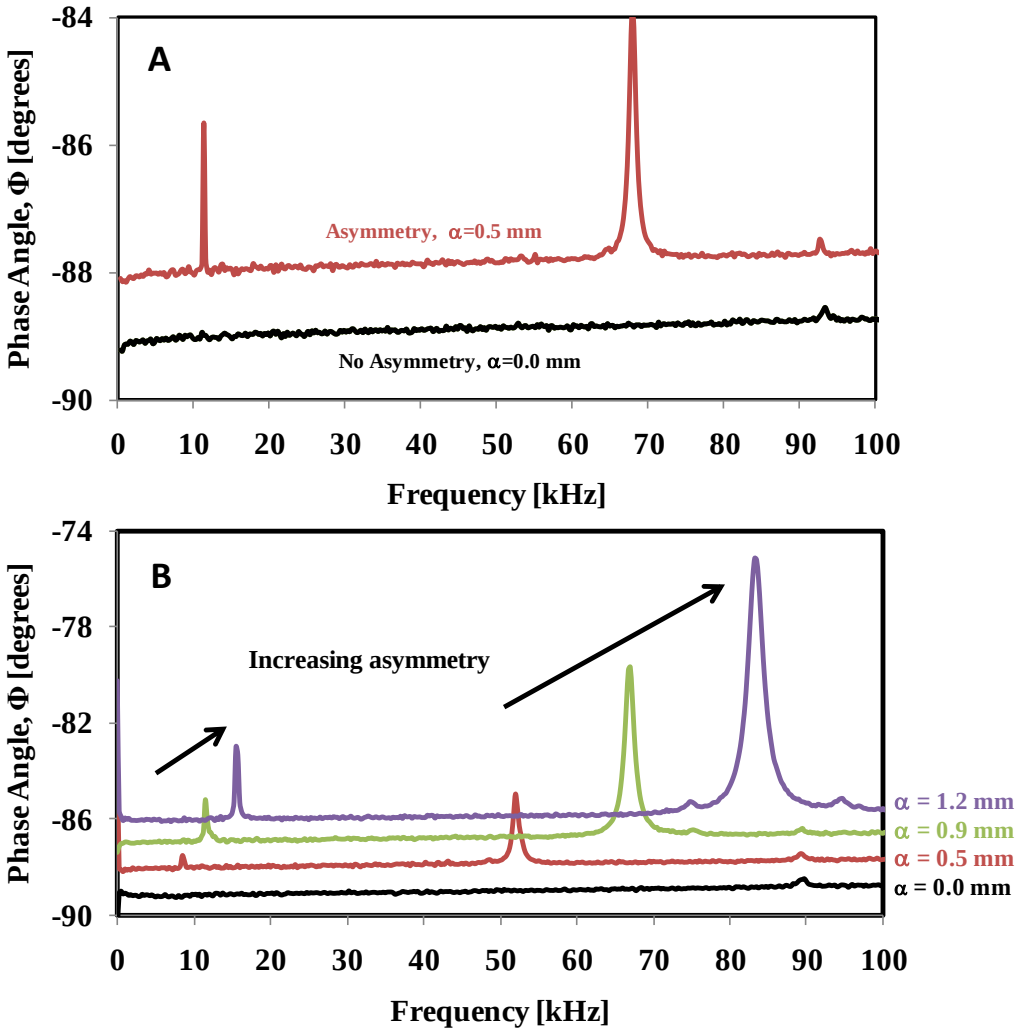

Figure A-2 Panel A. Experimental frequency response spectra showing the measurability of bending modes due to anchor asymmetry of a sensor (L = 2.5 mm; α=0.3). **Panel B.** Measured changes in the resonant frequencies as a function of extent of anchor asymmetry of sensors shown in Figure A--1B. L=3.15 mm. Plots are with 1^{o} offset for clarity.

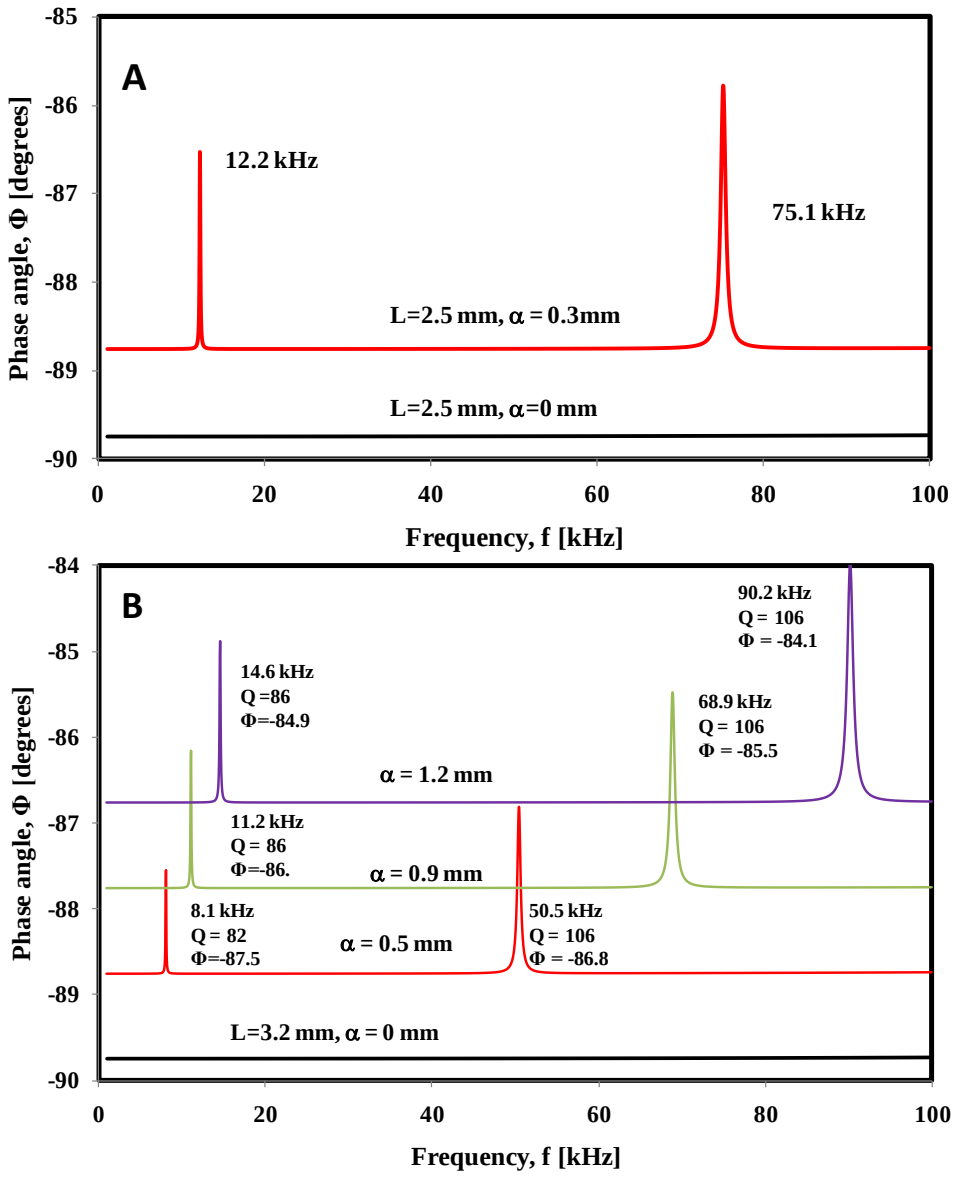

Figure A-3 Panel A. FEM solution show the effects of anchor asymmetry and phase angle behavior at resonance for sensors given in Fig 2A**. Panel B.**FEM solution for resonant modes as a function of anchor asymmetry extent. The solutions correspond to fabrication shown in Figure A--1B and experimental spectra given in Figure A--2B. Plots are presented with a 1^{o} offset for clarity.

Boundary current density obtained from the FEM calculation was integrated over the electrode area to obtain total current (I) as a function of excitation frequency. The response output variables, phase angle ($\Phi = \tan^{-1}[\mathrm{Im}(I)/\mathrm{Re}(I)]$) and impedance ($Z = V/I$) were then calculated. Average current density values (I) were obtained by normalizing I to electrode area. Since sharp changes in average current density manifest as phase-angle peaks, we report ΔI as the height of the average current density peak at resonance, which is equal to difference between average current density at resonance and baseline value.

A.3. Results and Discussion

A.3.1. Effect of asymmetric anchor on resonance measurability.

The electrically measurable resonant modes of excited PZT cantilever sensors manifest resonance by a sharp peak in phase angle (Φ) between excitation voltage (V) and resulting current (**I**) in PZT at the corresponding excitation frequency. PZT cantilevers that are anchored symmetrically (3- 1A) showed phase angle values close to -90° for the frequency range of 0-100 kHz indicating that the device acts electrically as a pure capacitor; see Figure A--2A. Since PZT is a dielectric ceramic with piezoelectric properties, at resonance the impedance change of PZT is small or nearly zero such that one measures no deviation from capacitive behavior. In the example shown in Figure A--2A, the length of the sensor was 2.5 mm, and such a device has bending modes determined by FEM eigenfrequency analysis at 9.79 and 60.75 kHz, but the modes were not observed experimentally. When the PZT (L=2.5 mm) was asymmetrically epoxy-

anchored (Figure A--1B-D) with α = 0.3 mm, two bending modes became electrically measurable at 11.3 kHz (Φ = -85.7°, Q = 37) and at 67.8 kHz (Φ = -83.9°, Q = 44), as shown in Figure A--2A. All sensors fabricated (n > 60), in the size range L = 2 to 4 mm, and with asymmetry □□= 0.2 to 1.5 mm exhibited at least two resonant modes in 0-100 kHz as measured by phase angle. Two questions emerge from the results in Figure 2. Namely, what is the effect of asymmetry, in relation to the length L on resonant frequency and its intensity as measured by Φ? Second, what geometric parameter(s) determines resonant frequency and its intensity? We recognize from previous work that cantilever length is a significant parameter. We answer both of these questions using experiments, finite element model and an approximate analytical model.

A.3.2. Effect of asymmetric anchor extent (α) on resonant frequency and its intensity.

To determine the effects of the asymmetry parameter α, we fabricated sensors with symmetric anchor first and then progressively increased asymmetry by adding epoxy to one side of the base of the PZT cantilevers in a pre-determined fashion. After the epoxy had cured, the frequency spectrum of the modified sensor was determined. This progressive approach allowed us to modify a single sensor and evaluate changes in its spectral properties in a systematic fashion. In Figure A--2B we show the spectrum of one such sensor (L =3.15 mm; Figure A--1B) and was typical of other similarly fabricated sensors (n=16). Sensors with symmetric anchor (α =0) showed no measurable resonant modes. When anchor asymmetry was introduced by reducing the length on one side from 3.15 mm to 2.63 mm (Figure A--1B), two low-order modes appeared with the first mode

at 8.54 kHz (Φ=-88.5°; Q=16) and the second mode at 52.03 kHz (Φ =-86°; Q=52). Upon increasing the extent of asymmetry further by reducing the length from 2.63 to 2.17 mm (Figure A--1C) the two resonant modes increased both in location (11.5 and 66.5 kHz) and phase angle (Φ= -87.1°, -81.8°). We found that the peak amplitudes depend on the extent of asymmetry introduced, a result confirmed by the finite element model discussed in the next section. A key conclusion we draw from examining the spectra of over 16 similarly constructed sensors is asymmetry increases both resonant frequency and the phase angle.

A.3.3. Comparison of finite element model and experiments.

A two dimensional (2D) FEM of the PZT cantilever was constructed to determine the effects of anchor asymmetry on resonance frequency and the corresponding current density in PZT at resonance. Mathematically, a symmetric anchor is one in which no constraint is specified along both top and bottom length of the cantilever, and the distal end. Zero displacement is specified at the left plane (shown as hatched boundary) in Figure A--1A. Electrical boundary condition of excitation voltage is specified on the electrodes- top and bottom surfaces. Such a boundary condition excites the sensor at the same 100 mV potential used experimentally. Eigenfrequency analysis yielded resonant frequency values and current in PZT. For a symmetrically-anchored PZT cantilever ($L=L_s$=3.2 mm) resonance occurs at 5.98, 37.25, and 103.29 kHz, but experimentally resonance was not to be present as measured by phase angle, Φ in the same frequency range (Figure A--3B).

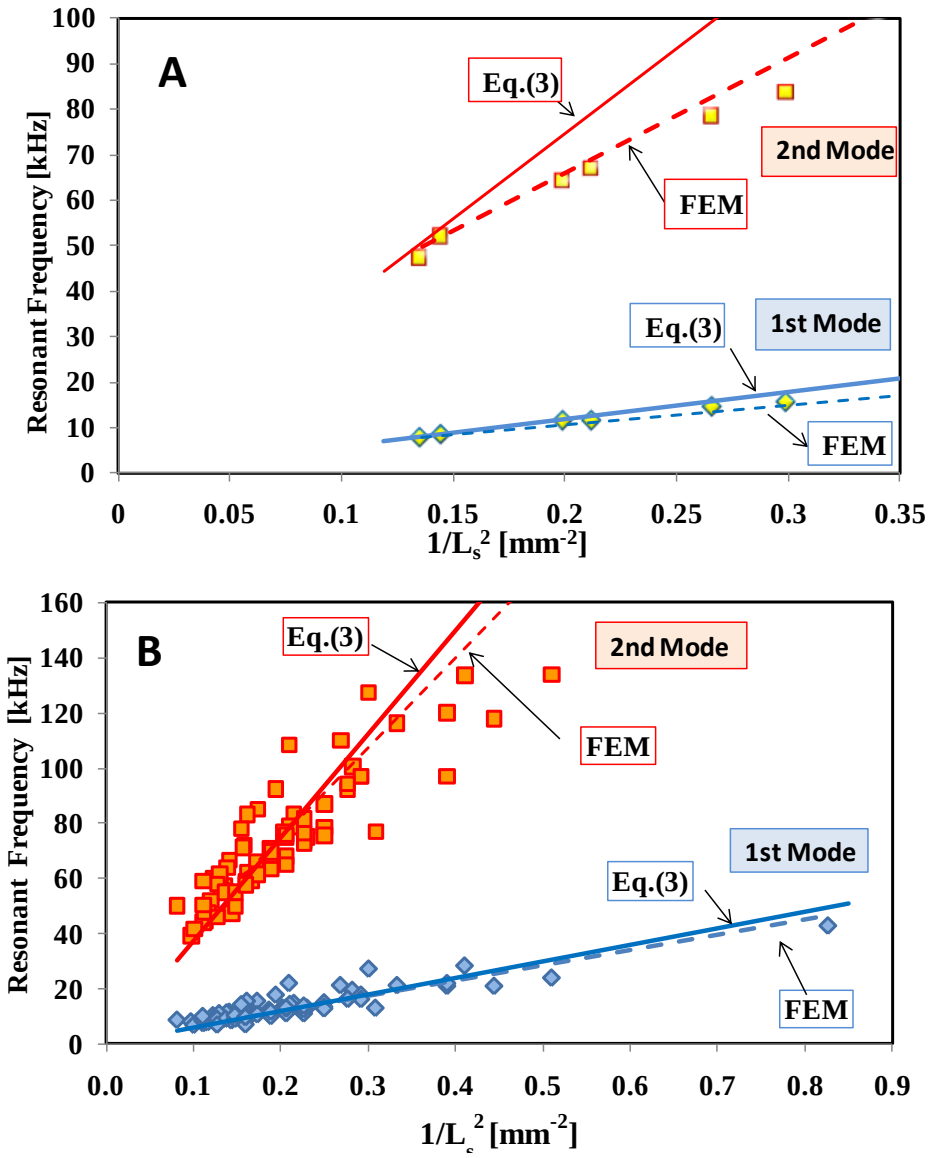

Figure A-4 Dependence of resonant modes on the shorter length (L_s) of asymmetrically anchored cantilevers. **Panel A.** Sensors of same initial length (L=3.15 mm) anchored asymmetrically to various extent; sensors shown in Fig.1B. **Panel B.** Sensors of various initial lengths asymmetrically anchored. Both first and the second mode resonant frequency strongly depend on L_s. Results are compared with FEM calculations and model in Eq.(3) with $L = L_s$.

Frequency response analysis of the finite element model enabled calculation of dynamic steady-state response as a function of the excitation frequency, and yields spatial current density profiles. For symmetrically-anchored PZT cantilevers no significant change in average current density was obtained at resonance frequencies obtained from eigenfrequency analysis. That is, there was no change in phase angle at the calculated resonance frequencies for a symmetric anchor (Figure A--3B). This result compares exactly with the experimental measurement that a perfectly symmetric anchor (α =0) leads to no electrical manifestation of resonance. To confirm the experimental observation that resonant modes become observable with anchor asymmetry, the FEM was modified with asymmetric anchor boundary condition (Figure A--1B-D). The results (Figure A--3B) show that the resonant modes become measurable by phase angle measurement. The asymmetry causes change in average current density (ΔI, equals peak value minus base value) at resonance resulting in a sharp phase angle change. In Figure A--3B the FEM frequency response spectra of cantilevers with various anchor asymmetries (L=3.2, α =0.5, 0.9, 1.2 mm) are shown. Asymmetry extent affects both the resonant frequency values and Φ strongly, but minimally affects the Q-values, and is consistent with experiments (Figure A--2). For the case α =0, average current density (I) did not vary at resonant frequency, but remained nearly constant at 2.3 and 14.4 A/m^2 for the two modes. For the case α = 0.5 mm, the first and second modes were determined by FEM frequency response analysis at 8.1 kHz (Q = 82, Φ = -87.5°) and 50.5 kHz (Q = 106, Φ = -86.8°), respectively. Further increase in asymmetry α to 0.9 or 1.2 mm led to further increases in resonant frequency and phase angle, and are consistent with experimental results. The FEM and experimental results, f, Φ, Q and ΔI for the various

asymmetries investigated are summarized in Table S2 in the supplementary materials. The FEM results correlate well the increase in current density (ΔI) at resonance with higher phase angle values. For example, the current density change (ΔI) for α = 0.5 mm was 12.2 and 127 A/m^2 for the first and second modes, respectively. For the case of α = 0.9 mm the phase angle values were higher compared to the α = 0.5 mm case, and FEM results show that the current density change was also higher for both modes, being ΔI = 19.4 and 200 A/m^2, respectively. As observed experimentally the case α = 1.2 mm led to the highest Φ and ΔI for both the modes (ΔI = 33.3 and 316 A/m^2, respectively). Since the frequency of resonant modes was dependent on the asymmetry level, we further investigate the role of α on resonant frequency values.

A.3.4. Role of asymmetry extent on frequency response of PZT cantilevers.

Resonant frequency (f_n) of an uniform cross section cantilever depends on the spring constant and effective mass, and hence on the cantilever length. That is,

$$f_n = \frac{\lambda_n^2}{2\pi}\ \frac{1}{L^2}\sqrt{\frac{EI}{wt\rho_c}} = \frac{1}{2\pi}\sqrt{\frac{k}{m_{e,n}}} \qquad (3)$$

where λ_n is the nth root of: 1 + cosh(λ_n) cos(λ_n) = 0. The parameters k and $m_{e,n}$ are the effective spring constant ($=3EI/L^3$; E is Young's modulus of PZT, I is moment of inertia $wt^3/12$) and the effective cantilever mass (= $3m_c/\lambda_n^4$, m_c is cantilever mass $\rho_c wtL$), respectively. Equation (3) suggests that the resonant frequency depends on inverse of L^2. Since asymmetric anchor was created by modifying the cantilever length, and experimentally we find increasing α increased the resonant frequency, it is reasonable to

expect the increase depends linearly with $1/L_s^2$. Such a relationship holds true and is illustrated in Figure A--4A for the two sets of sensors fabricated with L=3.15 mm, and α was modified in steps (Figure A--1B). The resonant frequency values show a near perfect linear relationship for both modes. On the same plot FEM solution corresponding to the boundary condition illustrated in Figure A--1A is also shown. The agreement between experiment and FEM suggest that the resonant frequency of asymmetrically anchored sensor can be calculated with reasonable accuracy from Equation (3) by setting the length as L_s.

A plot similar to Figure A--4A was prepared in which we included all sensors tested (n > 60). These cantilevers varied in length (L = 1.2 to 3.5 mm) and anchor asymmetry ranging from α = 0.03L to 0.69L. When L_s was greater than 1.5 mm both the first and the second modes were present in 0-100 kHz and for sensors with L_s < 1.5 mm only a single mode was found to be present in the same frequency range. As one can see in Figure A--4B, deviation from linear dependence for the second mode is seen for the sensors $1/L_s^2 > 0.3$ mm^{-2}, which represents sensors with large asymmetry values, α. We believe that this deviation is because long asymmetric anchor made of epoxy is likely to act as an "epoxy cantilever" attached to the PZT cantilever. In addition, for large α values, the sensor geometry deviates significantly from a cantilever and approaches that of a plate anchored on one side because length and width dimensions become nearly equal. The data in 3-4 show that small asymmetry (α ~0.3 mm) is sufficient to express resonant modes that are measurable, and if fundamental resonant frequency is to be increased, extent of asymmetry should be increased. It is reasonable to ask if the short length controls the eigenfrequency, what advantage is there in having additional PZT that

is anchored on only one side in epoxy. The answer is that a sensor with equal length on both sides, whether be it short or long, would constitute a symmetric anchor and the bending resonant modes are not be measurable. Although the resonant mode may be present in a highly diminished state in a sensor with perfect anchor, its impedance change at resonance is far too small for measurement. Consequently asymmetry in the anchor is paramount for measuring resonance electrically in PZT only cantilevers.

A.3.5. Sensitivity of asymmetrically-anchored PZT cantilever sensors

Sensitivity to changes in density of surrounding medium.

When a PZT cantilever is immersed in DI water the resonant frequency decreases because of increase in the density of the surrounding medium and the Q-values decrease slightly as well. For a typical sensor the Q-values for the first mode decreased from 41.6 in air to 24.6 in deionized water and those of the second mode decreased from 50.7 in air to 30.4 in deionized water. The fluid adjacent to the sensor acts as added mass and one can estimate the mass-change sensitivity using density change experiments. It is important to investigate the frequency shifts for small density changes in liquid, as that represents more closely sensing response to target analytes. We emphasize here that the purpose is not to show that the PZT cantilevers as density sensors, but we use such an experimental approach to quantify mass-change sensitivity. A change from DI water to 2.5 mM PBS is a small change in density of 0.003 g/cm^3, and hence the frequency response to such a density change can provide a measure of sensitivity. Figure A--5A shows frequency response to various density fluids.

The sensor (L= 3.1 mm, f_1= 11.7; f_2=63.1 kHz) was installed in a custom-built flow cell and allowed to reach steady state (t < 15 minutes) in DI water flow at 0.6 mL/min. DI water was replaced by admitting 10 mM PBS and the resonant frequency response of the two modes were monitored continuously. The decrease in resonant frequency occurred in a few minutes, and reached a new steady state value. Re-introduction of DI water caused the resonant frequency to return to the original value. In a similar fashion we alternately switched between DI water and 5 mM and 2.5mM PBS (Figure A--5A). Frequency shifts of 18, 8 and 2 Hz in f_1 and 63, 32 and 14 Hz in f_2 were obtained in response to density changes from DI water to the three PBS solutions. The near linear dependence of average responses (n=8) to density is plotted in Figure A--5B. The results confirm that higher frequency modes exhibit a greater response for the same imposed density change.

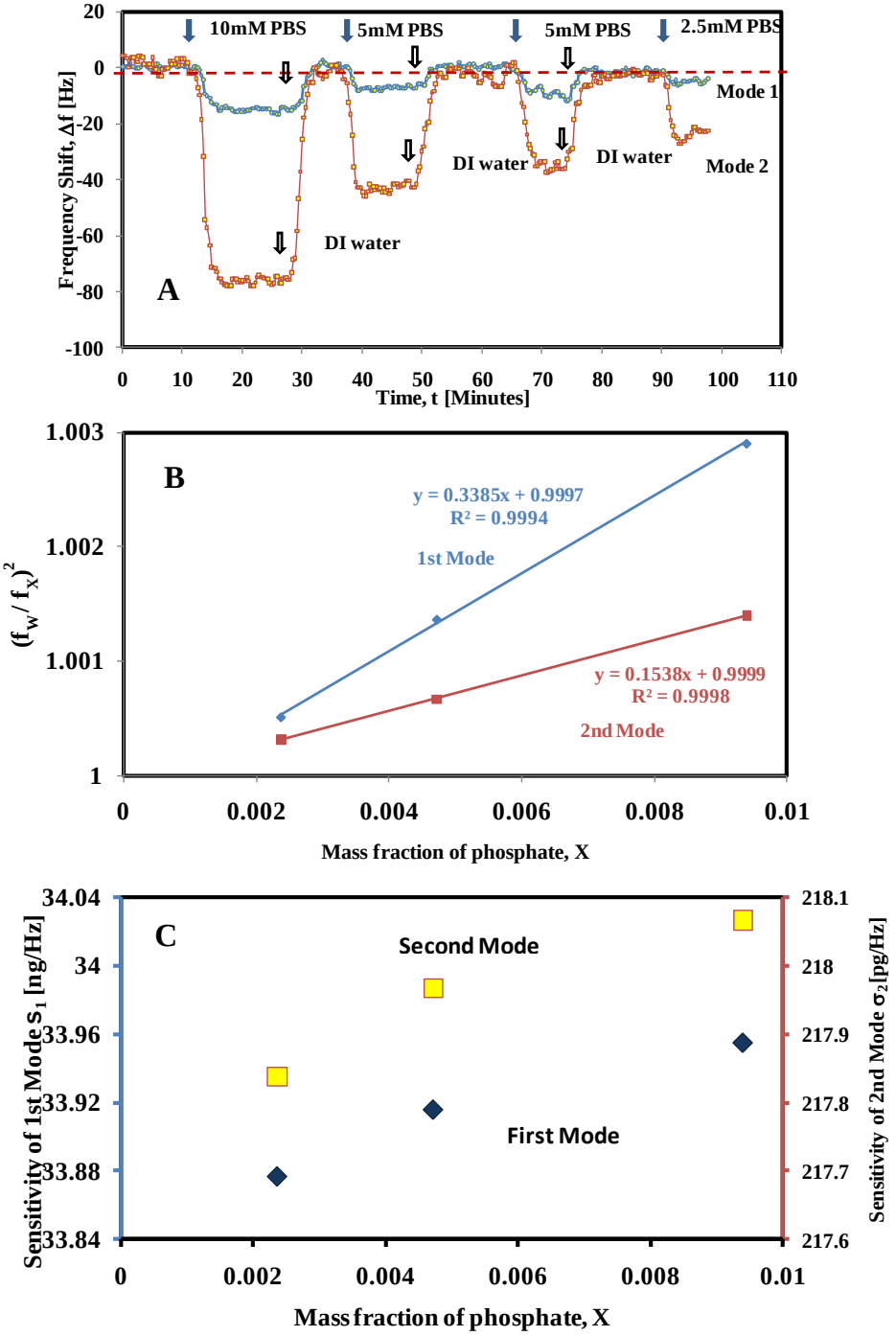

Figure A-5 Panel A. Frequency shift responses for alternate changes in liquid density from DI water to various concentrations of PBS. **Panel B.** Frequency shifts obtained for various density liquids agree with the model given in Eq. (8). **Panel** C. Sensitivity of the two modes is a function of added mass, and is plotted as a function of solute (phosphate) mass fraction. The density values corresponding to the three mass fractions are: 1.001, 1.004 and 1.008 g/cm^3.

If we consider the density change as an added mass (Δm) response, Equation (3) can be written as:

$$f_n' = \frac{1}{2\pi}\sqrt{\frac{k}{\left[\frac{3}{\lambda_n^4}(m_c+\Delta m)\right]}} = \frac{1}{2\pi}\sqrt{\frac{k}{(m_{c,n}+\Delta m_n)}} \quad (4)$$

where f_n' is the resonant frequency with the added fluid mass distributed uniformly along the entire cantilever length. Thus, the effective mass addition (Δm_n) due to density change can be written as:

$$\Delta m_n = \frac{k}{4\pi^2}\left[\frac{1}{f_n'^2} - \frac{1}{f_n^2}\right] \quad (5)$$

In the above, all parameters are known and thus the effective mass change due to density change can be calculated, and the sensor mass-change sensitivity (□□= ratio of mass change/resonant frequency change) can be computed from:

$$\sigma = \frac{\Delta m_n}{(f_n - f_n')} = \frac{k}{4\pi^2}\left[\frac{f_n + f_n'}{f_n^2 f_n'^2}\right] \quad (6)$$

For the case of shift from DI water to 2.5 mM PBS, the first mode and second mode responses were 3 and 10 Hz, and effective mass change for the two modes were 101.6 and 6.9 ng, yielding □ values of 33.9 pg/Hz and 217.8 pg/Hz. A plot of □ values of the two modes is given as a function of added equivalent mass computed using Equation (5), and is shown in Figure A--5B. The increasing trend with increasing mass fraction of solute indicates that numerically σ increases with added equivalent mass(Δm_n). That is, mass-change sensitivity decreases.

An alternate method of analyzing density change results is to use the density response relationship reported in the literature for uniform cross section cantilevers. That is [28]:

$$\frac{f_{fluid}}{f_{vac}} = \left(1 + \psi . \frac{\pi \rho w}{4 \rho_c t}\right)^{-1/2} \qquad (7)$$

where f_{fluid} and f_{vac} are resonant frequency in fluid of density (ρ) and resonant frequency in vacuum. The geometric factor ψ introduced originally by Lindholm et al [28] corrects for the geometric aspect ratio of the cantilever. The PBS density can be expressed as $\rho(X) = \rho_w (1 + \gamma X)$ where X is the mass fraction of solute phosphate, ρ_w is the density of water at 20^o C (0.998 g/mL) and γ is a dimensionless coefficient that fits experimentally determined solution density. Thus, Equation (7) can be arranged to

$$\left(\frac{f_{fluid}}{f_{vac}}\right)^2 = 1 + \gamma \frac{\psi\beta}{1+\psi\beta} X \qquad (8)$$

where $\beta = \pi\rho_w w / 4\rho_c t$ contains only physical properties and geometric parameters and $\psi = 0.613 L\sqrt{L} / \rho_c \sqrt{t}$ for the first mode [29] and for higher modes the value is determined experimentally [28]. Although ψ depends on the geometry and mode number, it is a constant for a given cantilever. Therefore, we expect a plot of $\left(f_{fluid} / f_{vac}\right)^2$ against solute mass fraction X to be a straight line as was confirmed in Figure A--5C. As can be seen in that figure the experimental correlation is linear with correlation coefficient for both modes being better than 0.999. The slope obtained for the first mode with experimental data is 0.315 and compares favorably with 0.312 and 0.351

determined from Equation (7) and ψ from [29] and [28], respectively. For the second mode we note that the experimental results follow the predicted straight line relationship, but a quantitative comparison of slope is not possible without the empirical constant that is specific to the geometry tested for the second mode.

Sensitivity measured using a binding reaction.

Density shifts provided an estimate of sensitivity of the two modes. A density change causes a uniform loading of mass all along the entire cantilever. In a sensing application, the target analyte binds to receptor immobilized on the sensor. The receptor is often immobilized at the distal tip of the cantilever. Therefore, a truer measure of sensitivity is the response associated with binding reaction to the sensor surface. In order to examine this property of the fabricated PZT cantilevers, we measured resonant frequency response to chemisorption reaction of dodecanethiol. The sulfur in dodecanethiol binds to gold <111> sites with binding energy comparable to a covalent bond[30].

A thin layer of gold (100 nm) was sputtered down at the distal end of $\approx 1\text{mm}^2$, which provided Au <111> sites[22]. This experiment was carried out in ethanol at 0.6 mL/min. Once the resonant frequency reached a steady state, the flow was changed from ethanol to 30 pM dodecanethiol in ethanol. As soon as dodecanethiol came in contact with the sensor the resonant frequency began to decrease monotonically and reached a new steady state resonant frequency in ~ 10 minutes. The resulting frequency shifts obtained were 26 Hz and 123 Hz for the first and second modes, respectively. Since the

response reached steady state in 14 minutes during which the sensor was exposed to 50.9 pg of dodecanethiol. If we assume that all entering dodecanethiol chemisorbed to Au<111> sites on the sensor (an unlikely event) one would conservatively estimate sensitivity as 2 pg/Hz for the first mode, and 414 fg/Hz for the second mode. As expected, the mass-change sensitivity for sensing application of the PZT cantilever is higher than the value calculated from density change experiments, because mass loading was localized instead of over the entire sensor.

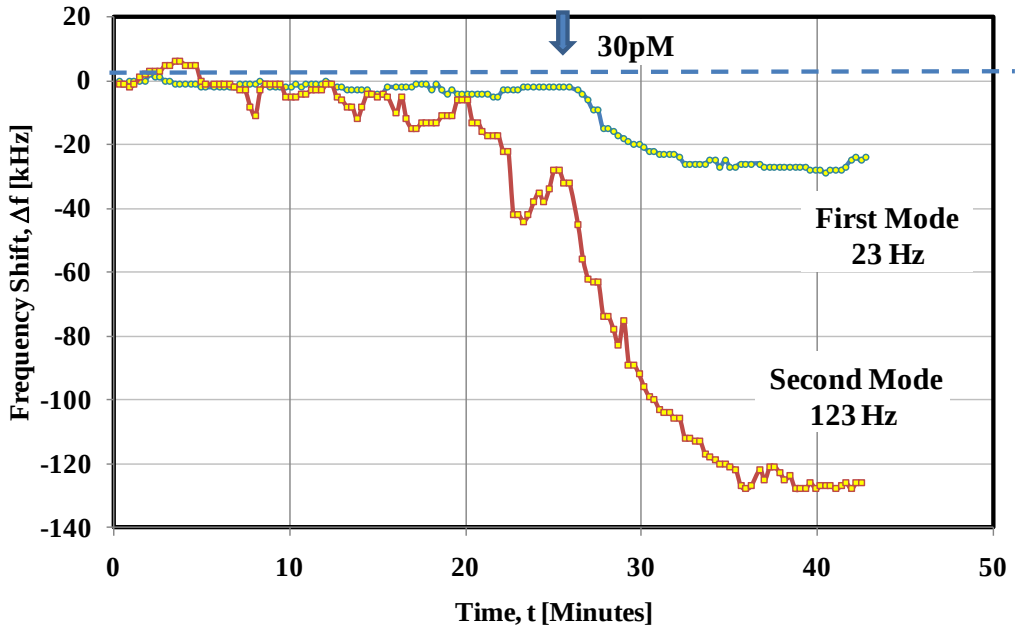

Figure A-6 Frequency response of the first and second bending modes in response to 30 pM dodecanethiol. Once the thiol comes in contact with the sensor the frequency begins to decrease and reaches a steady state. The frequency shifts obtained for the first and the second mode were 23 Hz and 123 Hz for the same chemisorbed mass.

In an earlier study with PZT composite cantilever sensors in which PZT was bonded to a stainless steel film to induce bending mode, a 1 nM hexadecane thiol induced a 116 Hz response when measured in batch mode[24]. The sensor was wider (2 mm) and length of stainless steel was 3 mm and the third resonant mode at 45.5 kHz was used for sensing. In the reported experiment, if we assume that all hexadecanethiol in the sample chemisorbed onto the sensor, the sensitivity is ~ 2.2 pg/Hz and is poorer than the sensitivity obtained for second mode in the present study. In another study of PZT/glass cantilevers that were 1 and 1.5 mm long, sensitivity was reported in the range of 16 to 70 pg/Hz in air[23]. Mass was added to the sensor operated in air, and the resonant frequency shift was measured to determine sensitivity. In the current study the second mode PZT cantilever is more sensitive (lower σ) under submerged environments than the second and third modes of composite cantilever sensors because of the absence of parasitic mass.

A.4. Summary and Conclusions

In summary, it was shown that by asymmetrically anchoring PZT, one can measure the first two resonant bending modes electrically without any external instrumentation. This approach is a significant improvement over the previous approach of bonding a non- piezoelectric material to induce measurable bending modes as it improves mass-change sensitivity due to avoidance of parasitic mass of non-piezoelectric layer. The sensitivity is ~30 ng/Hz for the first mode and ~217 pg/Hz for the second mode when mass loading occurs along the entire cantilever length. In chemisorption

experiments where binding occurred in the tip region, the same sensor showed an order of magnitude higher sensitivity of 2 pg/Hz and 414 fg/Hz for the two modes. The latter is more sensitive than similar sized composite cantilever sensors containing a non-piezoelectric layer.

A.5. Supplementary Materials

Table S1: Material properties of PZT-5A used in simulation and for fabrication of experimental sensors

Material	Density [kg/m^3]	Young's Modulus [Pa]	Poisson Ratio	Elasticity Matrix [Pa]	Coupling Matrix [C/m^2]	Relative Permittivity
PZT-5A	7750	-	-	c11 = 1.20 e11 c12 = 7.52 e10 c13 = 7.51 e10 c22 = 1.20 e11 c23 = 7.51 e10 c33 = 1.11 e11 c44 = 2.11 e10 c55 = 2.11 e10 c66 = 2.26 e10	e31 = -5.35 e32 = -5.35 e33 = 15.78 e24 = 12.29 e15 = 12.29	ε11 = 919.1 ε22 = 919.1 ε33 = 826.6

Property data used in model given in Eq.(3)

E = 66 GPa

ρ_c = 7800 kg/m^3

Table S2: Comparison of FEM calculations (vacuum) and experimental measurements (air)

		Experimental					
L_s	α	First Mode			Second Mode		
mm	mm	*f* (kHz)	*Phase* Φ	*Q-value*	*f* (kHz)	*Phase* Φ	*Q-value*
2.62	**0.52**	8.5	-88.5°	16	52.0	-85.9°	52
2.17	**0.98**	11.5	-87.2°	23	66.8	-81.8°	61
1.82	**1.32**	15.5	-85.9°	31	83.3	-78.1°	45

		Finite Element Model (FEM)							
L_s	α	First Mode				Second Mode			
mm	mm	*f* (kHz)	*Phase* Φ	*Q-value*	□I (A/m^2)	*f* (kHz)	*Phase* Φ	*Q-value*	□I (A/m^2)
2.62	**0.52**	8.06	-87.5°	86	12.2	50.45	-86.8°	106	127
2.17	**0.98**	11.15	-86.2°	86	19.4	68.85	-85.5°	106	199
1.82	**1.32**	14.6	-84.9°	86	33.3	90.15	-84.1°	106	316

A.6. References

[1] C. Ziegler, Cantilever-based biosensors, Analytical and Bioanalytical Chemistry, 379 (2004) 946-959.

[2] R. Raiteri, M. Grattarola, H.J. Butt, P. Skladal, Micromechanical cantilever-based biosensors, Sensors and Actuators B-Chemical, 79 (2001) 115-126.

[3] M. Alvarez, L.M. Lechuga, Microcantilever-based platforms as biosensing tools, Analyst, 135 (2010) 827-836.

[4] J. Fritz, Cantilever biosensors, Analyst, 133 (2008) 855-863.

[5] T. Itoh, T. Suga, Piezoelectric force sensor for scanning force microscopy, Sensors and Actuators A: Physical, 43 (1994) 305-310.

[6] T. Itoh, T. Suga, Self-excited force-sensing microcantilevers with piezoelectric thin films for dynamic scanning force microscopy, Sensors and Actuators A: Physical, 54 (1996) 477-481.

[7] Y.-C. Li, M.-H. Ho, S.-J. Hung, M.-H. Chen, M.S.-C. Lu, CMOS micromachined capacitive cantilevers for mass sensing, Journal of Micromechanics and Microengineering, 16 (2006) 2659–2665.

[8] H. Sone, H. Okano, S. Hosaka, Picogram Mass Sensor Using Piezoresistive Cantilever for Biosensor, Japanese Journal of Applied Physics, 43 (2004) 4663-4666.

[9] J. Teva, G. Abadal, F. Torres, J. Verd, F. Pérez-Murano, N. Barniol, A femtogram resolution mass sensor platform, based on SOI electrostatically driven resonant cantilever. Part I: Electromechanical model and parameter extraction, Ultramicroscopy, 106 (2006) 800-807.

[10] S.M. Yang, T.I. Yin, C. Chang, Development of a double-microcantilever for surface stress measurement in microsensors, Sensors and Actuators B: Chemical, 121 (2007) 545-551.

[11] X. Xia, Z. Zhang, X. Li, A Latin-cross-shaped integrated resonant cantilever with second torsion-mode resonance for ultra-resoluble bio-mass sensing, Journal of Micromechanics and Microengineering, 18 (2003) 3502-3507.

[12] T. Ono, X. Li, H. Miyashita, M. Esashi, Mass sensing of adsorbed molecules in sub-picogram sample with ultrathin silicon resonator, Review of Scientific Instruments, 74 (2003) 1240-1212-1244.

[13] R. Erlandsson, G.M. McClelland, C.M. Mate, S. Chiang, Atomic force microscopy using optical interferometry, Journal of Vacuum Science & Technology A: Vacuum, Surfaces, and Films, 6 (1988) 266-270.

[14] Y. Martin, C.C. Williams, H.K. Wickramasinghe, Atomic force microscope--force mapping and profiling on a sub 100-[A-ring] scale, Journal of Applied Physics, 61 (1987) 4723-4729.

[15] G. Meyer, N.M. Amer, Novel optical approach to atomic force microscopy, Applied Physics Letters, 53 (1988) 1045-1047.

[16] C.A.J. Putman, B.G.D. Grooth, N.F.V. Hulst, J. Greve, A detailed analysis of the optical beam deflection technique for use in atomic force microscopy, Journal of Applied Physics, 72 (1992) 6-12.

[17] H. Jianqiang, Z. Changchun, L. Junhua, H. Yongning, Dependence of the resonance frequency of thermally excited microcantilever resonators on temperature, Sensors and Actuators A: Physical, 101 (2002) 37-41.

[18] N.S. Lavrik, M; Datskos, P., Cantilever transducers as a platform for chemical and biological sensors, Review of Scientific Instruments, 75 (2004) 2229.

[19] N.V. Lavrik, P.G. Datskos, Femtogram mass detection using photothermally actuated nanomechanical resonators, Applied Physics Letters, 82 (2003) 2697-2700.

[20] R.S. Lakshmanan, S. Xu, R. Mutharasan, Impedance change as an alternate measure of resonant frequency shift of piezoelectric-excited millimeter-sized cantilever (PEMC) sensors, Sensors and Actuators B: Chemical, 145 (2010) 601-604.

[21] D. Maraldo, K. Rijal, G. Campbell, R. Mutharasan, Method for Label-Free Detection of Femtogram Quantities of Biologics in Flowing Liquid Samples, Analytical Chemistry, 79 (2007) 2762-2770.

[22] K. Rijal, R. Mutharasan, Method for measuring the self-assembly of alkanethiols on gold at femtomolar concentrations, Langmuir, 23 (2007) 6856-6863.

[23] G.A. Campbell, R. Mutharasan, PEMC sensor's mass change sensitivity is 20 pg/Hz under liquid immersion, Biosensors and Bioelectronics, 22 (2006) 35-41.

[24] G.A. Campbell, R. Mutharasan, Monitoring of the self-assembled monolayer of 1-hexadecanethiol on a gold surface at nanomolar concentration using a piezo-excited millimeter-sized cantilever sensor, Langmuir, 21 (2005) 11568-11573.

[25] C. Castille, I. Dufour, C. Lucat, Longitudinal vibration mode of piezoelectric thick-film cantilever-based sensors in liquid media, Applied Physics Letters, 96 (2010) 154102-154103.

[26] J. Yang, An Introduction to the theory of piezoelectricity, Springer, New York, 2005.

[27] J. Vázquez, P. Sanz, J.L. Sánchez-Rojas, Behaviour of forbidden modes in the impedance characterization and modeling of piezoelectric microcantilevers, Sensors and Actuators A: Physical, 136 (2007) 417-425.

[28] U.S. Lindholm, D.D. Kana, W.H. Chu, H.N. Abramson, Elastic vibration characteristics of cantilever plates in water, Journal of Ship Research, 9 (1965) 11-22.

[29] J. Zhang, C. Dai, X. Su, S.J. O'Shea, Determination of liquid density with a low frequency mechanical sensor based on quartz tuning fork, Sensors and Actuators B: Chemical, 84 (2002) 123-128.

[30] J.C. Love, L.A. Estroff, J.K. Kriebel, R.G. Nuzzo, G.M. Whitesides, Self-assembled monolayers of thiolates on metals as a form of nanotechnology, Chemical Reviews, 105 (2005) 1103-1169.

Appendix B: Torsional and Lateral Resonant Modes of Cantilevers as Biosensors: Alternatives to Bending Modes

B.1. Introduction

Although cantilever sensors have been investigated for biochemical sensing using the resonant frequency change of bending modes [1-3], cantilevers also exhibit other types of resonant modes which include torsional[4-7], lateral[8-10], and longitudinal[11, 12] modes, whose sensitivity to molecular binding has not yet been examined to date. In particular, in-plane lateral modes have been suggested to have superior sensitivity[8, 13] and possess desirable liquid-phase sensing properties[11, 12], but they have not been investigated for surface molecular binding. Although sensitive measurement of volatile organic compounds based on absorption into a polymer coating was demonstrated using the lateral mode [9], surface-based molecular sensing is more important than absorption or volume-based approaches in biosensing applications. In this study, we show for the first time lateral and torsional modes can be used for measuring surface molecular self-assembly in liquid and that their sensitivity compares with that of torsional and bending modes. Both torsional and lateral modes also enable continuous measurement of self-assembly rate.

One main reason why bending modes have been the choice of most research investigations in biosensing is due to ease of deflection-based measurement by traditional optical transduction principles [14]. However, deflection of torsional and lateral modes is far lower, limiting their measurement optically. Thus, measuring non-bending modes, especially in-plane modes, has required either non-uniform cantilever geometry which

enhances local deflection[6] or non-optical transduction principles[15]. Electrically-active piezoelectric materials, such as lead zirconate titanate (PZT), offer attractive properties as their electrical impedance can be coupled with all resonance modes [8, 16, 17]. However, we show here using experiment and theory that impedance-coupling of lateral and torsional modes in PZT cantilevers is not inherent in traditional cantilever design, but can be achieved via asymmetric anchoring. This approach of novel anchor design can be extended to microcantilever designs, thus creating a potentially new class of cantilever-based biosensors.

B.2. Materials and Methods

B.2.1. Reagents.

Phosphate buffered saline (PBS, 10 mM, pH 7.4) was purchased from Sigma-Aldrich (Alletown, PA). Deionized water (18 MΩ, Milli-Q system, Millipore) and used for buffer preparation and rinsing protocols. Thiol 6-mercapto-1-hexanol (MCH) was obtained from Fluka (Milwaukee, WI). Concentrated sulfuric acid and 30% hydrogen peroxide were purchased from Fisher Scientific.

B.2.2. Fabrication.

All sensors (n=20) were fabricated from lead zirconate titanate (PZT-5A, Piezo Systems, Woburn, MA) as described previously [18]. For in-liquid applications, sensors were

electrically-insulated by a polyurethane spin-coat and subsequent chemical vapor-deposited parylene-c layer. Details in coating procedure have been reported previously[18]. For chemisorption experiments, 100 nm of gold (Au) was sputtered over 0.5 mm^2 area on both sides of the PZT cantilever tip (Desktop DESK IV, Denton Vacuum, Moorestown, NJ).

B.2.3 Apparatus and Methods.

The experimental setup consists of an impedance analyzer (Agilent HP4294A), a peristaltic pump, a custom microfluidic flow cell, and fluid reservoirs. For details the reader is referred to previous reports[18]. Prior to an experiment, the entire flow loop was cleaned by rinsing with ethanol and copious amount of deionized (DI) water. In a typical experiment, a sensor was installed in the flow cell and the resonant frequency was allowed to reach steady state at a flow rate of 500 μL/min with recirculating flow. After the resonant frequency reached a constant value, 1 mL of MCH solution (50 pM – 100 nM) was introduced to the loop without interrupting the flow by opening the valve to the feed reservoir containing MCH. The resonant frequency was monitored continuously as the MCH solution was continuously recirculated.

B.2.4 Anchor Design.

The traditional cantilever sensor design has a uniform rectangular geometry (dimensions L-w-t) as shown schematically in Figure B-1.A. The new anchor designs

examined here modify the anchor on either the top or side of the cantilever thus creating two different lengths on opposite sides, one being equal to the original length (L) and one shortened by the extended anchor (L_s). Figures 4-1.B and D show such designs where the anchor was extended on the top and side of the anchor, respectively. In such designs, the magnitude of anchor asymmetry, characterized by the ratio $\alpha = 1\text{-}L_{s,L}/L$, was varied from 0 – 0.4 in the present study. The anchor was also modified by varying the length of the anchored region on the top face in the width dimension as shown in Figure B-1.C. In such designs, magnitude of torsional anchor asymmetry, characterized by the angle $\theta_T = \arctan[(L\text{-}L_{s,T})/w]$, was varied from 0 – 45° in the present study. Cantilever design shown in Figure B-1.C has an asymmetric anchored domain that induces a torsional angle on the top surface which we term as torsional anchor asymmetry. Cantilever design shown in Figure B-1.D has an extended anchored domain on the lateral side that induces a length-based asymmetry ratio which we term as lateral anchor asymmetry. It should be noted that for both designs, $\theta_T = \alpha = 0$ corresponds to an ideal, or parallel, anchor found in a conventionally anchored cantilever biosensor (see Figure B-1.A).

B.2.5 Finite Element Model.

Conventionally-anchored and asymmetrically-anchored PZT cantilevers of thickness (t = 127 μm), width (w = 1 mm) , and of free lengths (L = 4 mm; $L_{s,L} = L_{s,T} = 4$ – 2.5 mm) were modeled using commercially available finite element modeling (FEM) software (COMSOL 3.5a, COMSOL Group, Burlington, MA). The expected deformation in PZT at 100 mV excitation is small, and thus, plane-stress assumption was invoked in

model development. Zero-deflection boundary condition was imposed on the anchored regions (denoted by hatching and grey-shaded regions in Figure B-1). Electromechanical properties of PZT-5A used for simulation have been reported previously[17]. For PZT cantilever simulations, an electromechanical model enabled coupling of electrical and mechanical effects exhibited by piezoelectric materials. Material damping was modeled by a loss factor ($\eta = 0.01$) in all frequency response calculations and is fully described in a previous report [17]. The following mechanical properties of silicon microcantilevers were used: density = 2,330 kg/m^3, Young's modulus = 131 GPa, Poisson ratio = 0.27. The total number of tetrahedral elements in each simulation ranged from 389 – 3,752 and 1,986 – 8,482 for PZT and silicon models, respectively. Quadratic basis functions were used for constructing elemental displacement fields. Resonant frequencies and mode shapes were obtained as minimizing eigenstates of the cantilever strain-energy functional (Π) accomplished by invoking the stationarity of Π (i.e. $\delta\Pi=0$)[19]. For the conventional cantilever model, the results from FEM were validated against Euler-Bernoulli Beam Theory which showed resonant frequencies agreed within < 2.4 % for all modes. The number of elements was increased until the calculated resonance frequencies and phase angles converged within < 1 % and < 0.03% of values obtained using the preceding mesh for PZT cantilever and silicon microcantilever models, respectively. Frequency response was carried out using course mesh (~ 300 – 500 elements) at 10 Hz resolution. Current and charge densities on electrode surfaces were integrated over the electrode area to obtain total current (I) or charge (Q) as a function of excitation frequency. The experimentally measured electrical response output variable, phase angle $\varphi = \arctan[-\mathrm{Im}(I)/\mathrm{Re}(I)]$, was then calculated.

B.3. Results and Discussion

B.3.1 Conventionally anchored PZT cantilevers exhibit absence of impedance-coupling

Cantilever sensors with ideal symmetric anchor (Figure B-1.A) did not express any significant electrically-observable resonant modes in the 0 – 80 kHz range (Figures 2.A and 3.A, $\theta_T = \alpha = 0$). However, FEM eigenfrequency analysis gave four resonant modes over this frequency range (Table 1). This suggests the resonant modes that were present did not couple with impedance changes in PZT. In other words, these modes were not electrically-observable. Likewise, as shown in Figure B-2.B, FEM frequency response analysis of symmetrically anchored PZT sensors did not exhibit measureable-resonance, consistent with experimental measurement. The condition for impedance-coupled resonant modes can be derived by inspection of the following relationship for change in impedance ($Z = \Delta V/I$):

$$\frac{dZ}{df} = d\left(\frac{\Delta V}{I}\right) = \Delta V d(I^{-1}) = \Delta V d\left(\frac{dt}{dQ}\right) = \Delta V dt[d(dQ^{-1})] \qquad (1)$$

where f is the frequency, ΔV is the applied voltage, $I=dQ/dt$ is the current, t is the time, Q is the charge, and d is the linear differential operator. Thus, as per Equation (1), for a resonant mode to be impedance-coupled dZ/df must differ from its off-resonance value. As reflected in Equation (1), given ΔV dt is constant with respect to frequency change, impedance-coupling can occur only if dQ differs at resonance from its off-resonance value. As shown in Table 1, change in accumulated net charge at resonance relative to

off-resonance values (Δ(dQ/df)) did not occur to any significant extent. In all calculations, distance of 5 kHz was used as off-resonance value based on average resonant mode Q-values. We note selection of a different basis would not change conclusions regarding impedance-coupling, but only the numerical values of Δ(dQ/df).

B.3.2 Torsional anchor asymmetry causes impedance-coupling

Length asymmetry (Figure B-1.B) was previously shown by our group to give rise to measureable bending modes that were mass sensitive to molecular binding [18, 20, 21]. Since both torsional and lateral modes have been recently suggested to be useful in sensing [6, 7, 9, 22], we designed various new cantilevers (see Section 2.4) with asymmetric anchor that induce expression of torsional and lateral modes in lieu of bending modes via designs shown in Figures 4-1.C and D, respectively. We first examined both experimentally and using FEM simulation the effects of successive changes in θ_T. Interestingly, as shown in Figure B-2.A, modifying the ideal anchor from $\theta_T = 0$ to $\theta_T = 23°$ enabled four new resonant modes to be measured in the 0 – 80 kHz range which were essentially absent at $\theta_T = 0$.

Table B-1 Summary of FEM calculations in terms of anchor asymmetry effects on charge accumulation mechanism of impedance-coupling and mode shapes. Unmodified cantilever lengths (L) of torsional and lateral anchor asymmetry sensors were 3.2 and 3.7 mm, respectively.

Asymmetry	Resonant frequency,f [kHz]	Mode	ΔdQ/df [pC/kHz]
$\theta_T = 0$	6.4	Bending	<0.01
	35.6	Torsional	<0.01
	39.0	Bending	<0.01
	41.5	Lateral	<0.01
$\theta_T = 45°$	9.5	Bending	8.9
	42.8	Torsional	3.3
	56.4	Torsional-Lateral	1.7
	61.8	Torsional	12.6
$\alpha = 0$	4.7	Bending	<0.1
	29.3	Bending	<0.1
	30.8	Torsional	<0.1
	31.7	Lateral	<0.1
$\alpha = 0.39$	10.1	Bending	<0.1
	38.4	Torsional	<0.1
	61.7	Lateral	47.1
	62.6	Bending-Torsional	3.9

As shown in Figure B-2.A, successively increasing θ_T caused successive increase in: (1) magnitude of impedance-coupling, (2) magnitude of resonant frequencies, and (3) separation of adjacent resonant modes. For the case of the highest magnitude of asymmetry examined ($\theta_T = 45°$), four resonant modes were present at 13.9, 37.2, 55.6, and 66.6 kHz with Q-values of 35, 42, 43, and 39, respectively. In Figure B-2.B, we show the FEM results for the same θ_T values (0, 23°, 29°,45°) which agree well with

experimental results. For example, modifying the ideal anchor with $\theta_T = 23°$ caused four resonant modes to manifest that were absent at $\theta_T = 0$. Likewise, as θ_T was increased, so did magnitude of impedance-coupling, resonant frequencies, and separation of adjacent modes. For the largest magnitude of asymmetry investigated ($\theta_T = 45°$), four modes at 9.5, 42.8, 56.4, and 61.8 kHz were present. List of resonant modes is summarized in Table 1, and a detailed discussion on mode shapes follows this section. Inspection of net charge accumulation at resonance for all modes (Table 1), confirms that the torsional anchor induces significant charge accumulation not found at $\theta_T = 0$, causing impedance-coupling as per Equation (1). Not only did FEM simulation agree well with experimental measurements qualitatively, but also quantitatively based on resonant frequency and phase angle values which were within 13.3 % and 12.7 %, respectively. Such agreement suggests that experimentally observed changes were indeed caused by anchor asymmetry.

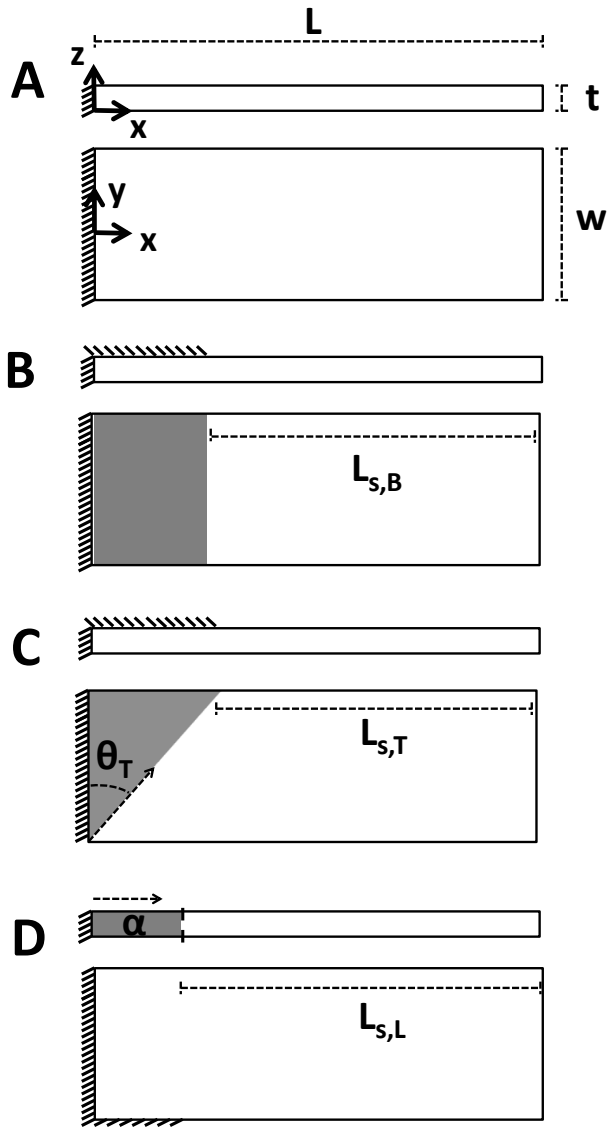

Figure B-1 Schematic of asymmetric anchor designs. Four anchor designs (A, B, C, and D) are illustrated. In each case a side- and top-view are shown. (A) Conventional anchor showing length (L), width (w), and thickness (t) dimensions with no anchor asymmetry. (B) Previously investigated bending asymmetry design exhibits difference in cantilever length in which one side is L and the other is $L_{s,B}$ [18]. (C) Torsional asymmetry design showing asymmetry in length and width creates an anchored torsional angle (θ_T). (D) Lateral asymmetry design showing asymmetry in side length creates a short length ($L_{s,L}$).

B.3.3 Lateral anchor asymmetry causes impedance-coupling

Given torsional anchor asymmetry exhibited electrically-observable modes, it was of interest if similar results could be achieved using lateral anchor asymmetry (α). As shown in Figure B-3.A, introduction of lateral anchor asymmetry (α = 0.11) caused expression of one resonant mode at 42.4 kHz which was absent at α = 0. As α was successively increased (0 – 0.39) both magnitude of impedance-coupling and resonant frequency increased. For the largest magnitude of asymmetry examined (α=0.39), a dominant mode at 65.2 kHz was present with Q = 39, in addition to three weakly expressed modes at 13.8, 41.6, and 51.2 kHz. FEM results, shown in Figure B-3.B, closely reflect the experimental results. For example, modifying the ideal anchor with lateral asymmetry (α = 0.11) caused a single resonant mode to manifest at 34.2 kHz with minimal coupling. Likewise, as α was increased (α = 0 - 0.39) so was magnitude of impedance-coupling and resonant frequency. For the largest value of α examined, a single resonant mode was highly expressed at 61.7 kHz (Table 1). Although three additional modes were found over the 0 – 70 kHz range (Table 1), only the mode at 61.7 kHz gave high Δ(dQ/df) = 47.1 pC/kHz which is consistent with the presence of only a single dominant mode observed experimentally at 65.2 kHz.

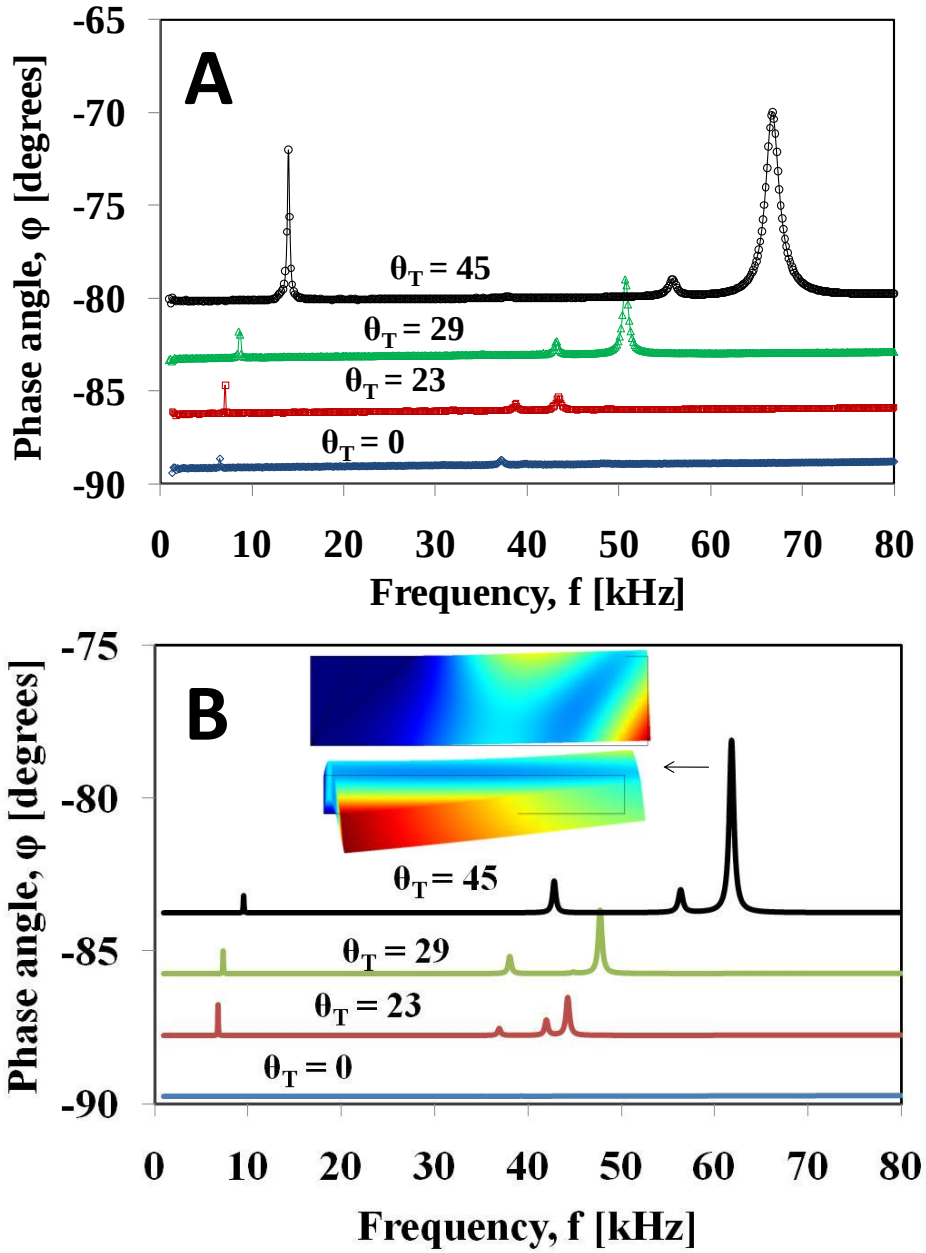

Figure B-2 (A) Experimental spectra of cantilever (L = 3.2 mm) fabricated with torsional anchor asymmetry (θ_T = 0°, 23°, 29°, 45°), and (B) FEM simulation of the fabricated sensor.

B.3.4 Type of dominant resonant mode differs depending on anchor asymmetry

Interestingly, not only did increasing the magnitude of anchor asymmetry in both torsional and lateral anchor designs cause increase in impedance-coupling and resonant frequency values, but it also caused different characteristic spectra. Specifically, not only did number of modes actuated differ, but so did magnitude of impedance-coupling. As shown in Table 1, torsional asymmetry coupled a greater number of modes to impedance change, but lateral asymmetry led to stronger impedance-coupling of modes as indicated by higher $\Delta(dQ/df)$ values. This suggests that the nature of the resonant modes that became actuated were inherently different and depended on the type of asymmetry used. To further elucidate these notable differences, we examined the resulting mode shapes in each design, descriptions of which are included in Table 1. Figures 4-2.B and 4-3.B contain insets showing both the top- and front-views of the mode shape expressed in the dominant mode of each design. For the case of torsional asymmetry, the dominant resonant mode consisted of out-of-plane torsional motion. Analysis of the other smaller phase angle modes revealed they also had torsional character, which in the third mode, was present in combination with lateral motion. For the case of lateral asymmetry, the dominant resonant mode exhibited only in-plane lateral character. Analysis of mode shapes suggests that although both anchor asymmetries enabled resonance-coupling to impedance changes, different types of modes are coupled. Such modes have not yet been investigated for measuring surface molecular binding in the literature which is important in their use as biosensors.

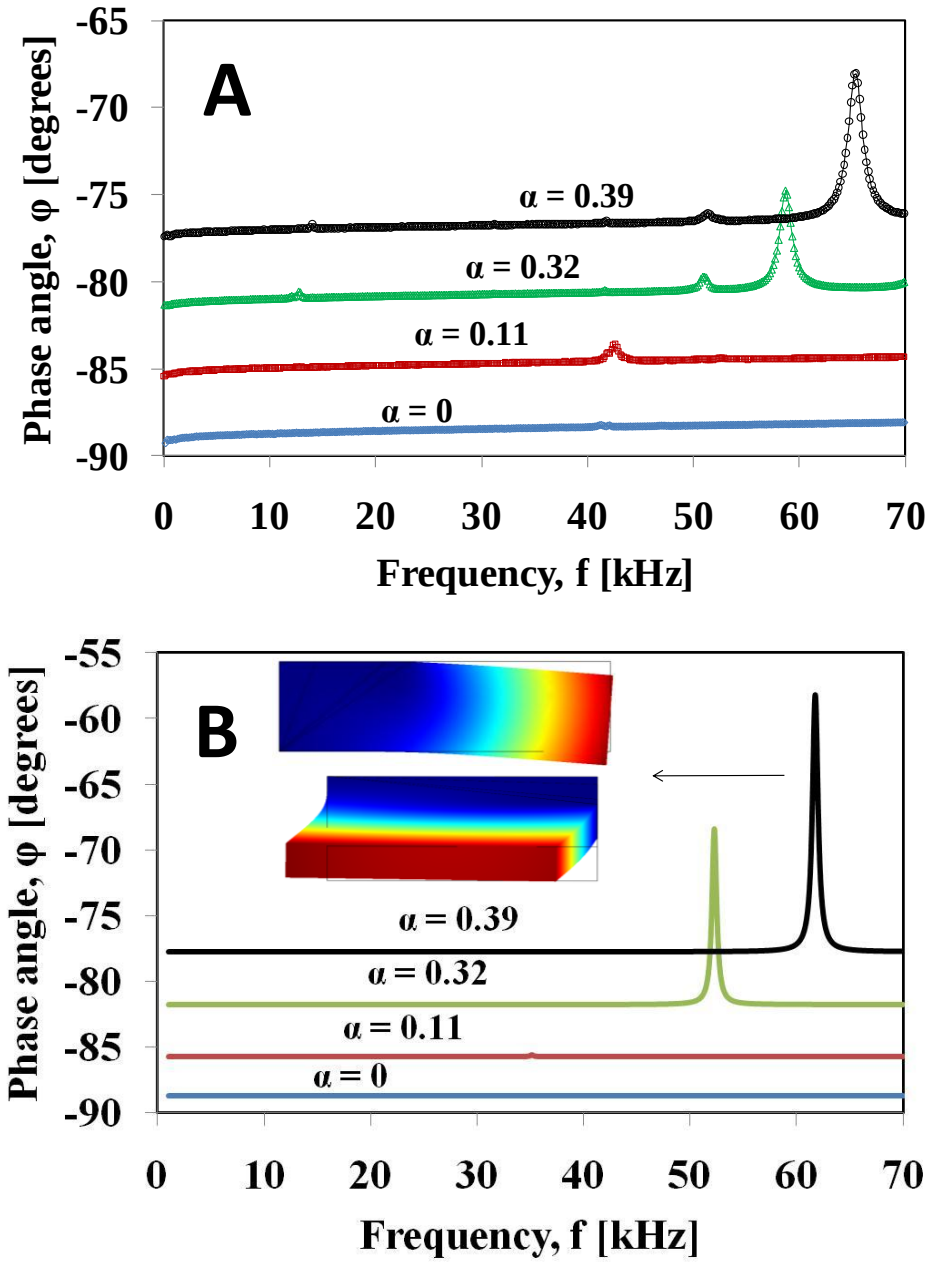

Figure B-3 (A) Experimental spectra of cantilever (L = 3.7 mm) fabricated with lateral anchor asymmetry (α = 0, 0.11, 0.32, 0.39) and (B) FEM simulation of the fabricated sensor.

Prior to examining their liquid phase sensing characteristics, we first examined if anchor asymmetry can also impart new and improved characteristics to microcantilvers, as they are extensively used in sensing[14, 23]. We selected to examine only lateral asymmetry (see Figure S.1.A inset) given the ease of fabricating such asymmetry by traditional microfabrication techniques and since it may already arise inherently in micro- and nanocantilevers to a small extent due to unavoidable fabrication imperfections. Thus, FEM models of silicon microcantilevers ($L \cdot w \cdot t = 100 \cdot 10 \cdot 1\ \mu m^3$) were constructed to examine effects of lateral anchor asymmetry on microcantilever properties. We found even though the microcantilevers differed in terms of material, size, and method of introducing the anchor asymmetry, the effects of lateral anchor asymmetry were similar to those we observed in PZT millimeter-sized cantilevers. Detailed analyses of results are given in Supplementary Materials. We note that lateral anchor asymmetry caused changes in conventional mode shapes (Figure S.2). Data also suggested that lateral asymmetry can be used to increase sensitivity of microcantilever sensors by 97% due to combined effects of increase in resonant frequency and deflection characteristics (Figures S.1 and S.3, respectively). We also note that the ability to tune local deflection profiles (Figure S.3) has high potential for affecting new applied techniques, such as determination of node locations in non-uniform cantilevers [24]and bianalyte sensing on a single cantilever[25]. Based on such interesting effects, we examined the aspect of sensitivity further in the PZT millimeter-cantilever sensors.

B.3.5 Torsional and lateral modes are sensitive to molecular binding

It was of interest to determine if the torsional and lateral modes are sensitive to mass-change caused by surface binding of molecules. The dominant mode expressed was investigated in both designs for sensing. Sensors with highest magnitude of anchor asymmetry examined were used.

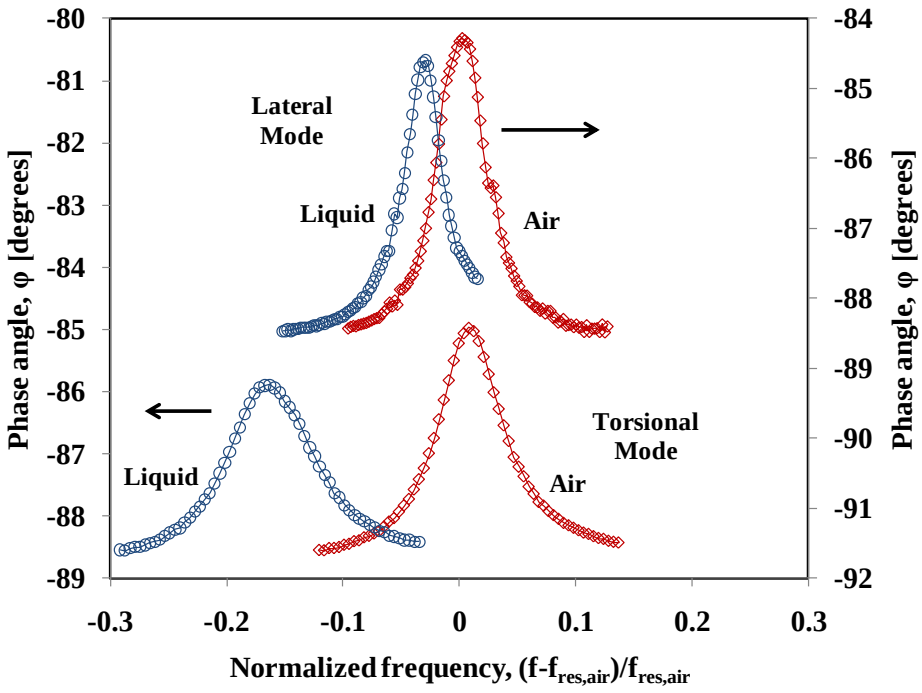

Figure B-4 Comparison of frequency response spectra of torsional ($\Delta f_{air\text{-}liquid}$ = 4.1 kHz, Q_{air}= 23.3 $\Delta Q_{air\text{-}liquid}$= 9.5, Re_c = 5,270) and lateral sensors ($\Delta f_{air\text{-}liquid}$ = 1.5 kHz, Q_{air}= 37.4, $\Delta Q_{air\text{-}liquid}$= 6.4, Re_c = 190) in air and liquid.

The experimentally measured frequency spectra of both sensor designs in air and liquid are shown in Figure B-4. Interestingly, the torsional mode exhibited larger shift in frequency and Q-value upon immersion in liquid ($\Delta f_{air\text{-}liquid}$ = 4.1 kHz, Q_{air}= 23.3, $\Delta Q_{air\text{-}liquid}$= 9.5) than did the lateral mode ($\Delta f_{air\text{-}liquid}$ = 1.5 kHz, Q_{air}= 37.4, $\Delta Q_{air\text{-}liquid}$= 6.4), suggesting that the fluid-structure interaction differs depending on the resonant mode shape. One explanation of these effects could be due to the greater amount of fluid which is displaced by the out-of-plane torsional mode as it vibrates, and thus greater added-mass effect, relative to the amount of fluid displaced by the in-plane lateral mode. However, interestingly examination of the associated cantilever Reynolds number ($Re_c = \rho f L_{char}^2/4\mu$, where the characteristic length (L_{char}) is the cantilever width for the torsional mode and the thickness for the lateral mode, reveals the torsional mode is less damped in liquid than the lateral mode due to quadratic dependency of the L_{char} term (Re_c = 5,270 and 190, respectively, based on resonant frequency in liquid of 19.0 and 42.8 kHz, respectively). After examining the air-liquid sensor properties, the electrically-insulated cantilever sensors with 1 mm^2 gold sensing area for facilitating thiol chemisorption were installed in a flow cell, thus positioning the sensor directly in a flowing stream of buffer. After resonant frequency reached a steady-state in flowing buffer, one mL of dilute MCH (50 pM) prepared in the same buffer was introduced to the flow loop in recirculation mode. As shown in Figure B-5.A, resonant frequency of both modes decreased exponentially over a 35 minute period due to mass increase caused by MCH binding to sensor gold surface. Ultimately, in both cases, the resonant frequency reached a new steady state due to binding equilibrium resulting in a net decrease in the resonant frequency of 89 and 49 Hz for torsional and lateral modes, respectively. Switching the

flow back to pure buffer caused no further change in the resonant frequency indicating that the shift was entirely due to added-mass and not due to fluid effects. Given one mL of 50 pM MCH contains 50 fmol or 6.7 pg, the mass-change sensitivity can be estimated at 75 and 135 fg/Hz, respectively, based on the measured net frequency shifts and the assumption that all mass introduced binds. We note that complete binding is unlikely; however, it provides a conservative estimate of each mode's mass-change sensitivity. Concentration-dependent binding response of each mode was then measured (see Figure B-5.B) which showed that torsional modes were also slightly more sensitive than lateral modes at higher analyte binding concentration. Most importantly, previous studies carried out on bending modes showed mass-change sensitivity of ~ 400 fg/Hz [18]. Thus, this study suggests that torsional and lateral modes are excellent complements or even alternatives to bending modes. Torsional modes appear to be slightly more sensitive than lateral modes.

B.3.6 Effect of different types of resonance vibration on assembly rates

Given the differences in sensitivity between the two resonant modes, it was of interest to examine if the binding rates differed due to the two different vibration characteristics. This is important since molecular self-assembly measured on resonant-mode cantilever sensors does not involve molecular binding to a static surface, as it commonly occurs in many other sensor platforms (e.g. microarray , ELISA), but on a vibrating surface. Surface binding has been suggested to affect the thermodynamics of molecular adsorption [26-28].

Mass transfer limitations of the sensor were first examined to determine if the sensor response rate was limited by mass transfer or corresponded to the rate of surface molecular binding phenomena. Given the external flow field conditions (Q=500 µL min^{-1}, D_{inlet} = 1.14 mm, ρ = 1,008 kg/m^3, µ = 9E-04 Pa s, L = 1 mm), the associated Reynolds number ($Re_L = \rho vL/\mu$) was ~ 2.3. Assuming MCH has a molecular diffusivity of 1E-06 cm^2s^{-1}, the ratio of momentum to mass diffusivity, the Schmidt number ($Sc = \mu/[\rho D]$), was 8,930. Thus, approximating the physical situation as laminar flow across a flat plate (L = 1 mm) the dimensionless mass flux to the sensor, the Sherwood number ($Sh_m = k_mL/D = 0.664Re_L^{1/2}Sc^{1/3}$) [29], was 2,260, indicating convective mass transfer effects are reasonably rapid. In the current study, mass transport-limits are determined post-kinetic analysis by comparing measured binding rates with expected rates based on the film mass transfer coefficient (k_m = 2.3E-04 m s^{-1}) calculated from Sh.

We analyzed sensor measured binding rate using the second-order reversible Langmuir adsorption model:

$$\frac{\Delta f}{\Delta f_\infty} = [1 - \exp(-(k_a c + k_d)t)] \qquad (2)$$

where $k_ac+k_d = k_{obs}$ is the observable rate constant[30]. As shown in Figure B-5.A, the rate constants for self-assembly on the torsional and lateral mode were same within experimental error (k_{obs} = 0.061and 0.065 min^{-1}, respectively). Analysis of the initial binding rate over the first five minutes, gave slightly higher values of k_{init} = 0.069 and 0.072 min^{-1}, respectively. Assuming mass transfer was limiting binding, the associated rate would be k_m/L ~ 13 min^{-1}. However, since $k_{init} \sim k_{obs} << k_m/L$, the measured rates are indeed limited by the binding reaction and not mass transfer.

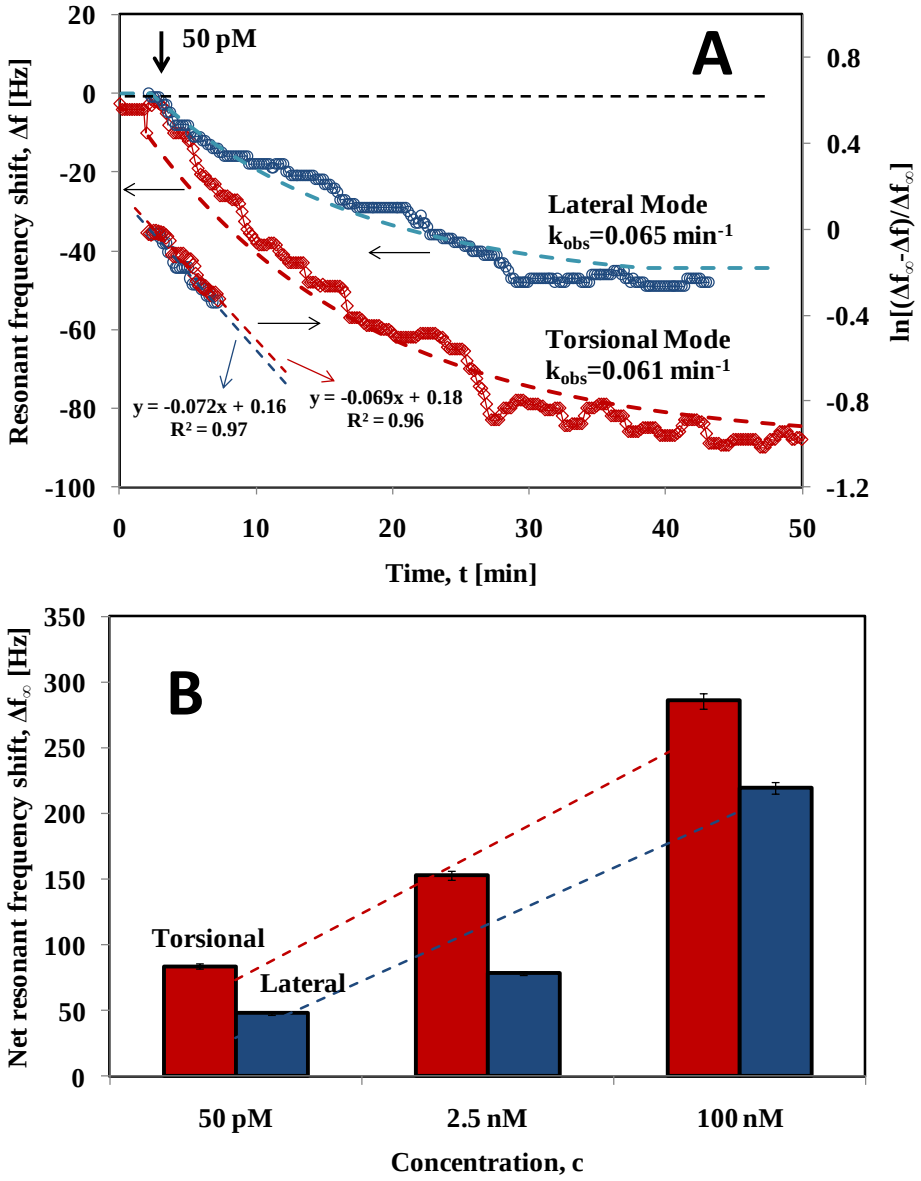

Figure B-5 (A) Demonstration of sensitivity to molecular binding of MCH on gold-coated asymmetric torsional and lateral anchor cantilever sensors by one mL injection of 50 pM MCH. (B) Concentration-dependent binding responses for both modes.

Therefore, the cantilever-measured binding response is indeed directly associated with rate of SAM assembly. The reaction kinetics and mass transfer analyses indicate that regardless of the type of resonant mode used, the rate of the self-assembly is not affected.

B.4 Conclusion

The current study showed torsional and lateral modes can be highly sensitive to molecular binding under fully submerged conditions, a characteristic essential for biosensing. It also expanded fundamental insight into relationship between anchor asymmetry and charge accumulation mechanisms in piezoelectric cantilevers. The technique of anchor asymmetry expands options for making new cantilever sensors by incorporating newly constrained areas at the base, as alternatives and complements to modification of cantilever size and geometry. It was also shown that the fundamental rate parameters extracted from self-assembled monolayer formation are unaffected by the use of different resonant modes used to obtain them. Sensitivity to molecular assembly in liquid suggests torsional and lateral modes have promise in future analytical biosensing applications.

B.5 Supplementary Materials

These supplementary materials describe extension of asymmetry in cantilever anchor design to microcantilevers as discussed in Section 3.3 of the main text.

S.1 Extension of anchor design to microcantilevers

Figure S.1.A shows the effect of asymmetry in the anchor design on the resonant frequencies of the first four modes. As the level of asymmetry increased (α = 0 - 0.25), the resonant frequency of all modes also successively increased, although not all to the same degree. For α=0.25, the resonant frequencies increased by 54%, 43%, 22%, and 39%, respectively. This difference is due to the fact that the four resonant modes do not have the same mode shapes. For example, the first (n=1), second (n=2), and fourth modes (n=4) are transverse modes, while the third mode (n=3) is a torsional mode. Given the metric for determining cantilever sensitivity ($\sigma_{n,bulk}$) suggests realizable sensitivity is proportional to the ratio of cantilever mass (m_c) and resonant frequency (f_n), given by [1]:

$$\sigma_{n,bulk} = \frac{\Delta m}{\Delta f_n} \propto \frac{m_c}{f_n} \qquad \text{(S.1)}$$

where Δf_n is the resonant frequency shift caused by an added-mass (Δm). Thus, as per Equation (S.1), the sensitivity of each mode likewise successively increased with inclusion of lateral anchor asymmetry as summarized in Figure S.1.B. The analysis shows that sensitivity of microcantilevers can be enhanced by as much as 54% based only on the resonant frequency increase that arises from non-uniform anchoring. Thus, this suggests inclusion of lateral asymmetry could be a useful method for further improving sensitivity in smaller cantilevers based on corresponding resonant frequency increase.

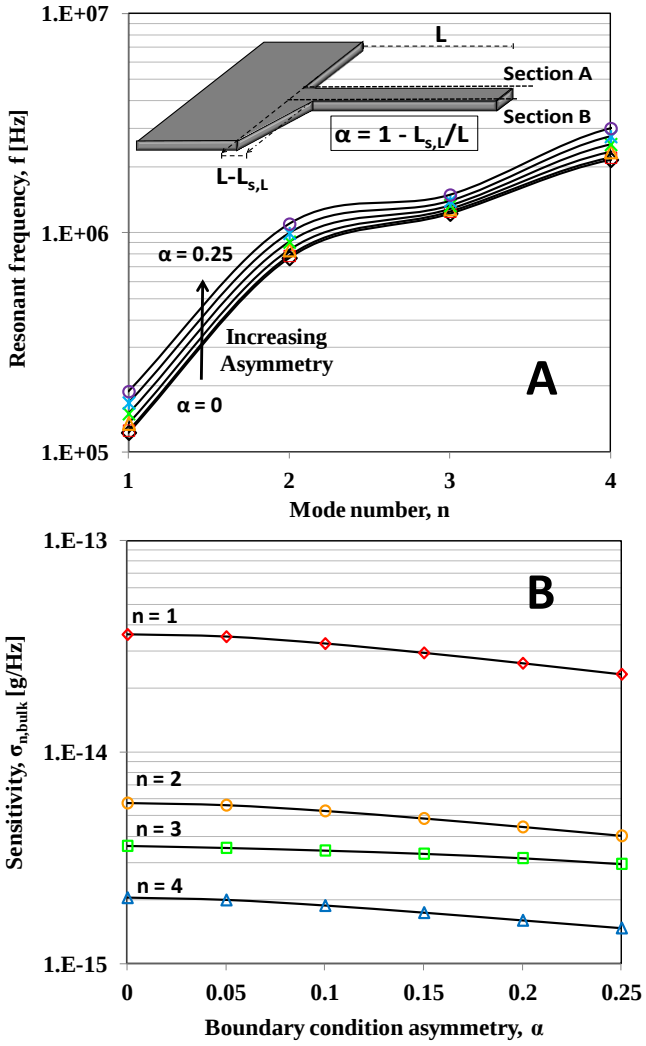

Figure S.1. (A) Effect of asymmetry on resonant frequency of the first four modes in a silicon microcantilever for successively increasing asymmetry parameter α=0, 0.05, 0.1, 0.15, 0.2, 0.25. (B) Effect of asymmetry on cantilever sensitivity for the first four resonant modes showing sensitivity increase caused by asymmetry.

As shown in PZT cantilevers, not only did lateral asymmetry increase resonant frequency, but it also caused changes in mode shape. Figure S.2 shows top-view comparing the modes shapes that arise in the conventional cantilever design versus those

in a cantilever modified with small level of lateral anchor asymmetry (α = 0.05) for the first four modes. Results shows the non-uniform anchor eliminates the x=0 symmetry plane in the conventional mode shapes and causes concentration of the deflection towards the edges. We note that such is an important effect since in addition to sensitivity increase based on frequency and mass as per

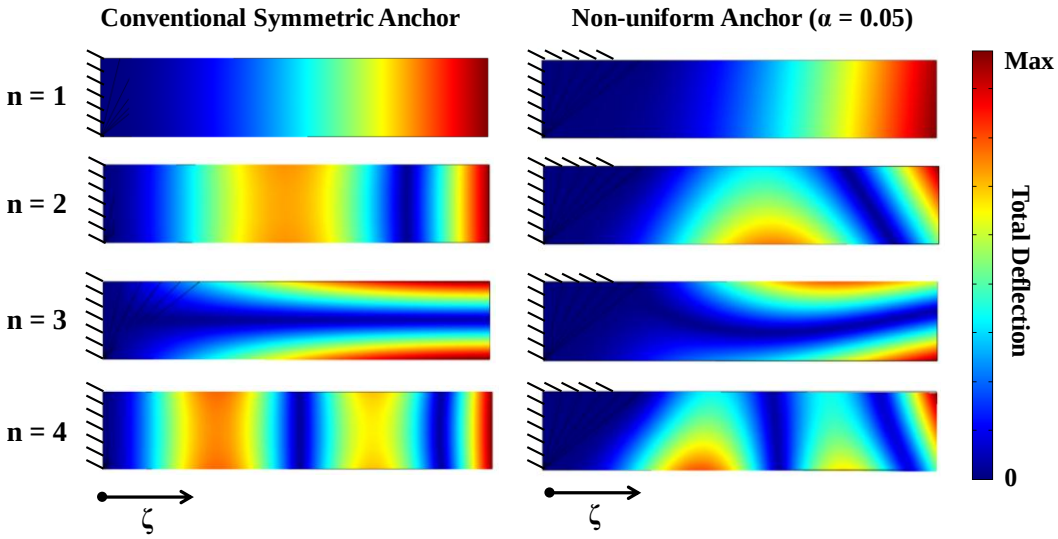

Figure S.2. Effect of non-uniform anchor on mode shape (top-view) shown for the case of 5% asymmetry in the constrained boundary (α=0.05). Hatching denotes a constrained surface over which zero-deflection boundary conditions are applied.

Equation (S.1), sensitivity can also be interpreted from a localized perspective by the following relation [2]:

$$\sigma_{n,local} \propto {w_n}^2(x) \frac{f_n}{m_{n,eff}} \qquad \text{(S.2)}$$

where $w_n(x)$ is the length-dependent normalized transverse deflection of the n^{th} mode, and $m_{n,eff}$ is the effective mass = $\rho_c Lwt/4$. Such is an important observation since Equation (S.2) suggests the modified deflection profiles may correlate with increased sensitivity if they enhance deflection relative to the conventional design. In Figure S.3, the effects of the non-uniform anchor design on the local transverse deflection profiles are given in terms of the normalized transverse deflection (w) in the fundamental mode along the sections A and B depicted in Figure S.1.A. All deflection profiles are normalized to the tip-deflection of the uniformly anchored microcantilever (the conventional case). We use the notation Δw_ζ to denote the percent change in deflection caused by anchor asymmetry at the dimensionless length position $\zeta = x/L$. As shown in Figure S.3.A, the tip-deflection increased by 13% at α=0.25 along section A. The increased tip-deflection can be explained by the requirement of the conservation of strain energy. Examination of the deflection profiles at $\zeta = 0.4$ accounts for the required reduction in energy that must accompany the increase in strain energy at the tip. As shown in Figure S.2.B, similar characteristics are observed on the opposite side of the microcantilever (section B) which is the side that contains the extended anchor domain. However, tip-deflection increased by 8% instead of 13%.

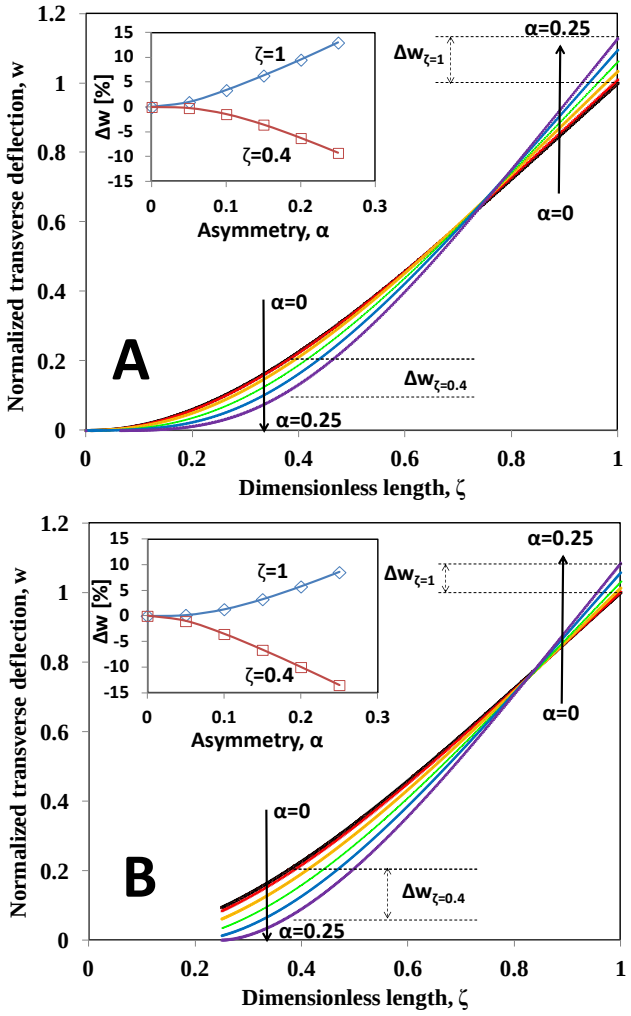

Figure S.3. Effect of asymmetry on the transverse deflection profiles relative to conventional cantilever deflection. (A) Deflection profile corresponding to the unmodified side of the cantilever designated as section A in Figure S.1.A. (B) Deflection profile corresponding to the modified side of the cantilever designated as section B in Figure S.1.A.

Thus, as per Equations (S.1) and (S.2), FEM simulations suggest that lateral asymmetry can be used to increase sensitivity by 97% based on combination of increase in resonant frequency and deflection. We also note that the ability to tune local

deflection profiles has high potential for affecting new applied techniques, such as determination of node locations in non-uniform cantilevers [3] and bianalyte sensing on a single cantilever [2].

B.6 References

[1] C. Ziegler, Cantilever-based biosensors, Analytical and Bioanalytical Chemistry, 379(2004) 946-59.

[2] N.V. Lavrik, M.J. Sepaniak, P.G. Datskos, Cantilever transducers as a platform for chemical and biological sensors, Rev Sci Instrum, 75(2004) 2229-53.

[3] B.N. Johnson, R. Mutharasan, Biosensing using dynamic-mode cantilever sensors: A review, Biosensors and Bioelectronics, 32(2012) 1-18.

[4] X.Y. Xia, X.X. Li, Resonance-mode effect on microcantilever mass-sensing performance in air, Rev Sci Instrum, 79(2008).

[5] H. Xie, J. Vitard, S. Haliyo, S. Regnier, Enhanced sensitivity of mass detection using the first torsional mode of microcantilevers, Measurement Science & Technology, 19(2008).

[6] X.Y. Xia, Z.X. Zhang, X.X. Li, A Latin-cross-shaped integrated resonant cantilever with second torsion-mode resonance for ultra-resoluble bio-mass sensing, Journal of Micromechanics and Microengineering, 18(2008).

[7] D.Z. Jin, X.X. Li, H.H. Bao, Z.X. Zhang, Y.L. Wang, H.T. Yu, et al., Integrated cantilever sensors with a torsional resonance mode for ultraresoluble on-the-spot bio/chemical detection, Applied Physics Letters, 90(2007).

[8] W. Pang, L. Yan, H. Zhang, H.Y. Yu, E.S. Kim, W.C. Tang, Femtogram mass sensing platform based on lateral extensional mode piezoelectric resonator, Applied Physics Letters, 88(2006).

[9] L.A. Beardslee, K.S. Demirci, Y. Luzinova, B. Mizaikoff, S.M. Heinrich, F. Josse, et al., Liquid-Phase Chemical Sensing Using Lateral Mode Resonant Cantilevers, Analytical Chemistry, 82(2010) 7542-9.

[10] J.E. Sader, C.P. Green, In-plane deformation of cantilever plates with applications to lateral force microscopy, Rev Sci Instrum, 75(2004) 878-83.

[11] C. Castille, I. Dufour, C. Lucat, Longitudinal vibration mode of piezoelectric thick-film cantilever-based sensors in liquid media, Applied Physics Letters, 96(2010).

[12] C. Castille, I. Dufour, M. Maglione, H. Debéda, C. Pellet, C. Lucat, Sensor Application Using Longitudinal Mode of Screen-Printed PZT Cantilever, Procedia Chemistry, 1(2009) 971-4.

[13] L.B. Sharos, A. Raman, S. Crittenden, R. Reifenberger, Enhanced mass sensing using torsional and lateral resonances in microcantilevers, Applied Physics Letters, 84(2004) 4638-40.

[14] B.N. Johnson, R. Mutharasan, Biosensing Applications using Dynamic-mode Cantilever Sensors: A Review, Biosensors & Bioelectronics, (2011) Accpted for publication 10-27-2011.

[15] L.A. Beardslee, A.M. Addous, S. Heinrich, F. Josse, I. Dufour, O. Brand, Thermal Excitation and Piezoresistive Detection of Cantilever In-Plane Resonance Modes for Sensing Applications, Journal of Microelectromechanical Systems, 19(2010) 1015-7.

[16] S.N. Mahmoodi, N. Jalili, Coupled Flexural-Torsional Nonlinear Vibrations of Piezoelectrically Actuated Microcantilevers With Application to Friction Force Microscopy, Journal of Vibration and Acoustics-Transactions of the Asme, 130(2008).

[17] B.N. Johnson, R. Mutharasan, The origin of low-order and high-order impedance-coupled resonant modes in piezoelectric-excited millimeter-sized cantilever (PEMC) sensors: Experiments and finite element models, Sensors and Actuators B: Chemical, 155(2011) 868-77.

[18] H. Sharma, R.S. Lakshmanan, B.N. Johnson, R. Mutharasan, Piezoelectric cantilever sensors with asymmetric anchor exhibit picogram sensitivity in liquids, Sensors and Actuators B-Chemical, 153(2011) 64-70.

[19] K.-J. Bathe, Finite Element Procedures in Engineering Analysis, Englewood Cliffs, NJ: Prentice-Hall, Inc.; 1982.

[20] P. Sanz, J. Hernando, J. Vazquez, J.L. Sanchez-Rojas, Laser vibrometry and impedance characterization of piezoelectric microcantilevers, Journal of Micromechanics and Microengineering, 17(2007) 931-7.

[21] B.N. Johnson, R. Mutharasan, Expression of picogram sensitive bending modes in piezoelectric cantilever sensors with nonuniform electric fields generated by asymmetric electrodes, Rev Sci Instrum, 81(2010).

[22] J. Teva, G. Abadal, F. Torres, J. Verd, F. Perez-Murano, N. Barniol, A femtogram resolution mass sensor platform based on SOI electrostatically driven resonant cantilever. Part II: Sensor calibration and glycerine evaporation rate measurement, Ultramicroscopy, 106(2006) 808-14.

[23] K.M. Hansen, T. Thundat, Microcantilever biosensors, Methods, 37(2005) 57-64.
[24] B.N. Johnson, R. Mutharasan, A novel experimental technique for determining node location in resonant mode cantilevers, Journal of Micromechanics and Microengineering, 21(2011).

[25] H.T. Yu, X.X. Li, Bianalyte mass detection with a single resonant microcantilever, Applied Physics Letters, 94(2009).

[26] P. Yeh, Y. Le, J. Kizhakkedathu, M. Chiao, An investigation of vibration-induced protein desorption mechanism using a micromachined membrane and PZT plate, Biomedical Microdevices, 10(2008) 701-8.

[27] P.-Y.J. Yeh, J.N. Kizhakkedathu, J.D. Madden, M. Chiao, Electric field and vibration-assisted nanomolecule desorption and anti-biofouling for biosensor applications, Colloids and Surfaces B: Biointerfaces, 59(2007) 67-73.

[28] S. Cular, D.W. Branch, V.R. Bhethanabotla, G.D. Meyer, H.G. Craighead, Removal of Nonspecifically Bound Proteins on Microarrays Using Surface Acoustic Waves, Sensors Journal, IEEE, 8(2008) 314-20.

[29] C.O. Bennett, J.E. Myers, Momentum, Heat, and Mass Transfer, 2nd ed.: McGraw-Hill, Inc; 1962.

[30] D.S. Karpovich, G.J. Blanchard, Direct Measurement of the Adsorption Kinetics of Alkanethiolate Self-Assembled Monolayers on a Microcrystalline Gold Surface, Langmuir, 10(1994) 3315-22.

Appendix C: Sensitive and selective detection of mycoplasma in cell culture samples using cantilever sensors

C.1. Introduction

Mycoplasmas are the smallest free-living bacteria with a size of 300-800 nm. They lack a rigid cell wall and thus are resistant to common antibiotics that target cell wall synthesis. They have been found either attached to cell membrane or internalized within mammalian cells, causing compromised cell metabolic function. Among the over 100 species that have been discovered, about 20 species cause majority of cell culture contamination in both research laboratories and industrial processes [1]. About 15-35% of continuous human and animal cell lines in current use are infected with mycoplasmas [2]. Earlier surveys showed as high as 65-80% incidence of mycoplasma infection of cell culture [3]. The six species, *Mycoplasma orale, M. hyorhinis, M. arginini*, *M. fermentans*, *M. hominis* and *Acholeplasma laidlawii*, represent the majority of contaminating isolates [4, 5]. The contamination causes alternations in growth rates, morphology and cell viability. Both reduced antibody yield in hybridoma culture and total culture degradation have been reported. Therefore, routine assay of cell culture for possible contamination is an absolute requirement to ensure quality of biological products. The current industry standard for mycoplasma testing is specified in the Food and Drug Administration guideline [6].

Current method for detecting mycoplasma is by microbiological colony assay. Although this method is quite sensitive (1 – 10 CFU/mL), it requires a long incubation time (3 – 28 d) and experienced personnel for analysis [7]. Polymerase chain reaction

(PCR) is also sensitive (1 – 10 CFU/mL) for purified mycoplasma DNA, but its sensitivity deteriorates significantly to 10^3 CFU/ml in cell culture samples [1, 8-10]. Enzyme-linked immunosorbent assay (ELISA) is also used for routine mycoplasmas detection, but its sensitivity is low (10^4 – 10^7 CFU/mL, and depends on the species) [11]. Both PCR and ELISA rely on culturing as a first step for increasing mycoplasma concentration and such a step often requires several days, particularly for low concentration samples. PCR method has shortened the time to results greatly (1 – 2 d), but has been reported to give false positive/negative results for low counts ($<10^3$ CFU/mL) and is not readily implemented at production sites [12]. ELISA method is less expensive, but requires a laboratory and an instrumentation arrangement. Because of its low sensitivity, a long incubation step is necessary. Therefore, there is a great need for a rapid, sensitive, selective and inexpensive method for monitoring mycoplasma contamination in cell culture reactors.

Biosensors for cell culture systems have drawn a great deal of attention due to their rapid response, low cost and high sensitivity [13-17]. Among the biosensors that have been investigated, cantilever biosensors have been of special interest for the detection of biological analytes because of their ultra-high sensitivity and label-free detection [18, 19]. Details on cantilever sensor physics and operating principles are available in [20]. For cantilever biosensors that operate in resonant (dynamic) mode, binding of target analyte to functionalized cantilever surface causes resonant frequency decrease and is given by [21] :

$$\Delta m = \frac{k}{4\pi^2}\left(\frac{1}{f_m^2} - \frac{1}{f_0^2}\right) \tag{1}$$

where k is the effective spring constant, f_0 and f_m are the resonant frequency values pre- and post-analyte binding. We have reported on piezoelectric-excited millimeter-sized cantilever (PEMC) sensors that showed high mass-change sensitivity for the detection of a variety of pathogens and toxins. The analytes included *Escherichia coli* O157:H7 [22], *Bacillus anthracis* [23], staphylococcus enterotoxin B (SEB) [24] and *Cryptosporidium parvum* [25]. PEMC sensor is immune to damping effects in liquid and has been successfully used in sample flow arrangements. Mass-change sensitivity at levels of femtogram (fg, 10^{-15} g) was reported under sample flow conditions [26]. Such sensitivity is attractive for mycoplasma detection as mass of each is about one femtogram. In this study, we used antibody immobilized PEMC sensors for detecting the mycoplasma, *A. laidlawii*, as it is one of the more common contaminant in cell culture systems. To the best of our knowledge, in spite of a very active biosensor research over the past decade, no publication on detecting mycoplasmas has appeared in the literature. Detection experiments were conducted with readily available positive control samples from a commercial mycoplasma ELISA detection kit as well as with specially grown and calibrated *A. laidlawii* samples. Selectivity of sensor response was also evaluated in cell culture medium (5% serum) samples containing mammalian and bacterial cells.

C.2. Materials and Methods

C.2.1. Experimental approach

Although a good number of antibodies for medically important pathogenic mycoplasmas are available, only a limited few are available for cell culture mycoplasma contaminants. An ELISA kit designed specifically for cell culture contaminants that

recognizes the four species, *M. orale*, *M. hyorhinis*, *M. arginini* and *A. laidlawii*, is available. The kit contains a coating polyclonal antibody (*c*pAb) and a biotinylated polyclonal antibody (*b*pAb) against each of the four species, and a positive control containing a mixture of the four species at undisclosed concentrations. In this work, we used both antibodies for detecting *A. laidlawii* in separate experiments. Since the sensor does not require a labeled antibody, we used either the *c*pAb or *b*pAb for confirming sensor response in a sandwich format. It should be mentioned that experiments were conducted with immobilized *c*pAb as well as immobilized *b*pAb.

The positive control in the commercial kit was used initially for developing data on detection feasibility and sensitivity. The manufacturer would not provide the composition of the positive control and thus we report the concentration as a volume of the positive control used. In order to obtain quantitative information on sensor limit of detection, we grew *A. laidlawii* cells, and prepared a standard inactivated stock sample so that the same biological sample can be used for sensor response comparison studies. To ensure integrity of *A. laidlawii* sample, periodic ELISA assays using the commercial kit were carried out, and the results showed no variation over a 14 d period. Thimerosal inactivated cells were used in all PEMC experiments. For evaluating sensor performance, simultaneous measurements were carried out using the ELISA kit with both live and inactivated mycoplasma samples.

C.2.2. Reagents

Cysteamine, glutaraldehyde solution, streptavidin and phosphate buffered saline (PBS, 10 mM, pH 7.4) and other common chemicals were purchased from Sigma-Aldrich (St. Louis, MO). Deionized (DI) water was obtained locally (18 MΩ, Milli-Q system, Millipore). Calibrated *A. Laidlawii* (ATCC 23206, American Type Culture Collection, Manassas, VA) samples were prepared as described here. Mycoplasma positive control, biotinylated polyclonal antibody and coating polyclonal antibody were used from a commercial kit from Roche (#11296744001, Roche Diagnostics GmbH, Penzberg, Germany). Antibody and antigen solutions were prepared in PBS (with 0.05% sodium azide) and stored at 4°C for use. Human epidermoid squamous carcinoma cells (A431) were obtained from another research laboratory at Drexel University and cultured in Dulbecco's Modified Eagle's Medium (DMEM, Mediatech, Inc, Manassas, VA) supplemented with 5% fetal bovine serum and was grown at 37°C in 5% CO_2. *E. coli* JM 101 cells were grown in nutrient broth, killed in 1% Clorox®, centrifuged and resuspended in PBS. Concentration was determined using a hemocytometer after staining with methylene blue.

C.2.3. Fabrication of PEMC sensor and flow cell design

A PEMC sensor consists of two layers: a PZT layer (lead zirconate titanate, Piezo Systems, Woburn, MA) and a quartz layer (SPI, West Chester, PA), bonded by a non-conductive adhesive. Details of fabrication are available in a previous publication [26]. Two PEMC designs were used. One is a flush design with a 2.7 × 1.0 × 0.127 mm ($l \times w \times t$) PZT bonded to 2.0 × 1.0 × 0.160 mm quartz. The second is an overhang design in

which a 4.5 × 1.0 × 0.127 mm PZT bonded a 4.0 × 1.0 × 0.160 mm glass. In both designs, the PZT end was anchored at one end. In the flush design, the glass layer was attached at the free-end with zero protrusion; in the overhang design, the glass layer protruded from the free-end by 1.0 mm. Wires (30 gauge) were soldered to electrodes of PZT layer and epoxy fixed in 6 mm glass tubing. The sensor was polyurethane (Wasser, Auburn, WA) spin-coated for providing electrical insulation. The two designs were shown to have similar mass-change sensitivity [26, 27].

C.2.4. PEMC sensor surface functionalization and experimental procedures

Prior to immobilization, 2.0 mm^2 (flush design) or 1.8 mm^2 (overhang design) of the PEMC sensor tip surface was freshly sputter-coated with 100 nm gold in a Desk IV sputtering system (Denton Vacuum, Moorestown, NJ). Two immobilization methods illustrated in Figure C- 1 were used in the experiments. In the first method (Figure C- 1A), the sensor was incubated in 2 mM cysteamine in PBS overnight at room temperature, and then immersed in 2.5% glutaraldehyde solution for 1 h followed by 1 h incubation in 100 µg/mL anti-*A. laidlawii*. The sensor was rinsed with DI water, and installed in a custom-made flow cell apparatus. In the second method (Figure C- 1B), sensor was incubated in 100 µg/mL streptavidin solution for 2 h, followed by 1 h in 100 µg/mL *b*pAb prior to installation in the flow cell. The detection experiments were done at sample flow rate of 0.5 mL/min in an incubator maintained at 28 ± 0.1°C.

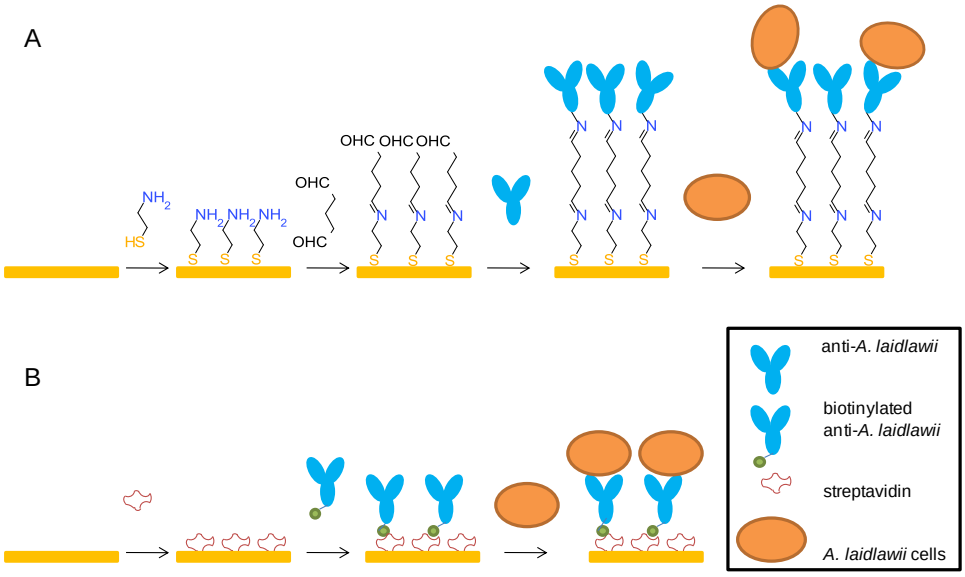

Figure C-1 Illustration of antibody immobilization and immunoassays with PEMC sensor. (A) Surface functionalization using cysteamine/glutaraldehyde chemistry on gold surface. (B) Gold surface directly modified with streptavidin, and then biotinylated antibody was attached to the sensor surface via streptavidin/biotin binding.

C.2.5. Sensor calibration

Mass-change sensitivity of PEMC sensor were determined by depositing known mass of paraffin wax on the sensor surface and measuring the resulting change in resonant frequency after solvent evaporation [23]. All measurements were made at 28 ±

0.1°C. Sensor surface was deposited with known wax mass using a stock paraffin wax in hexane solution prepared at concentrations ranging from 0.3 pg/μL to 100 ng/ μL [23].

C.2.6. A. laidlawii propagation and enumeration

Frozen glycerol stock of *A. laidlawii* was inoculated into 25 mL tryptic soy broth (Northeast Laboratory Services, Winslow, ME) in a sterile flask and incubated at 37°C in a 7% CO_2 atmosphere for 24 h. Cultures were either used immediately or stored at 4°C for several days until needed. Serial dilutions at 1:10 of the culture were made to 10^{-5} in mycoplasma phosphate buffer (28 mM monobasic sodium phosphate, 72 mM dibasic sodium phosphate in Milli-Q water, pH 7.1 ± 0.3). Aliquots of 100 μL of the three highest dilutions were spread-plated onto 100 mm BBL tryptic soy agar plates (Becton, Dickinson & Co., Franklin Lakes, NJ) in triplicate. The plates were loosely plastic wrapped and incubated at 37°C in 7% CO_2 for 4 – 5 d until colonies were distinctly observable. The plates were then counted and the concentration of the source culture calculated by averaging colony counts accounting for the dilutions used.

C.2.7. Inactivation of A. laidlawii cultures with thimerosal

Cultures were treated by adding 10% aqueous (w/v) thimerosal solution to a final concentration of 0.0001% and then incubated at 37°C with shaking for 24 h. Killing of the culture was confirmed by spread-plating 100 μL of the undiluted and treated culture

in triplicate. Plates were incubated at 37°C in 7% CO_2 for 4 – 5 d and visually examined. The treated culture was stored at 4°C until use (<14 d).

C.2.8. ELISA detection of A. laidlawii

ELISA detection of *A. laidlawii* was performed using the antibodies from Roche mycoplasma detection kit. Kit reagents were prepared according to the manufacturer instructions. Serial dilutions of viable and thimerosal-treated cells were prepared as described and then tested according to the vendor supplied protocol. The completed 96-well test plate was quantitated at 405 nm using a Wallac Victor 3 1420 Multi-label Counter (Perkin Elmer, Waltham, MA).

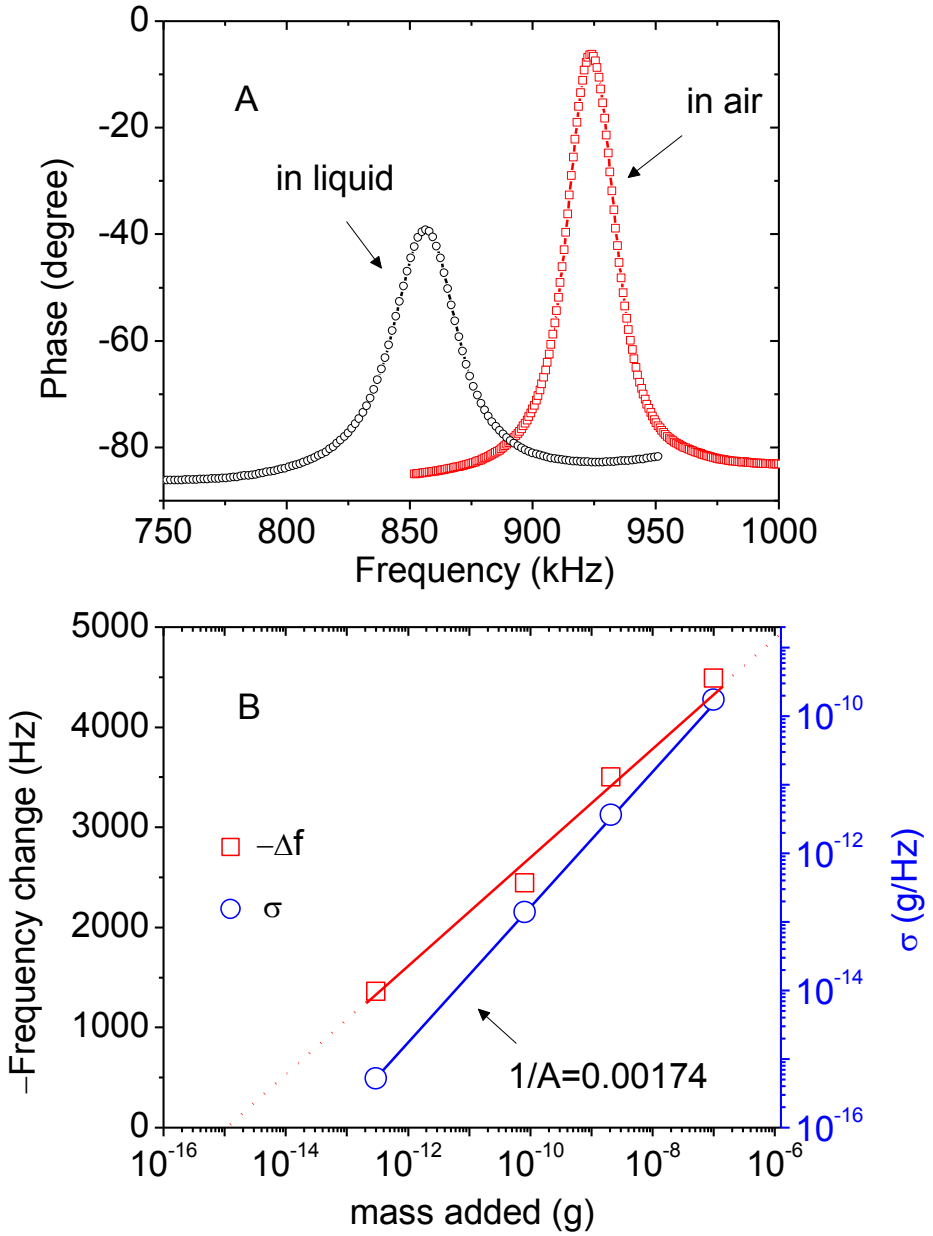

Figure C-2 Typical sensor spectra and sensitivity calibration curve. (A) Typical sensor spectra in air (□) and in DI water (○), respectively. (B) Sensitivity calibration using diluted paraffin wax solutions. Sensor response (-Δ*f*) is plotted as a function of log (mass added) (□), and log (*σ*) is plotted as a function of log (mass added) (○), respectively. PEMC sensor response to mass addition is log-linear, and is similar to previous results.

C.3. Results and discussion

C.3.1. PEMC sensor spectra and sensitivity calibration

The PEMC sensors used in this study have a resonant frequency near ~900 kHz. A number of fabricated sensors (n=23) gave similar resonant frequency values within ± 30 kHz of 900 kHz, and were used in all detection experiments. As shown in Figure C-2A, the resonant frequency decreases from 924.75 kHz in air to 856.50 kHz in DI water (Δf = 68.25 kHz) due to density increase of fluid surrounding the sensor. Although Q-factor (ratio of resonant frequency to the frequency width at half peak height) decreased from 40.3 to 29.5, it was sufficiently high for detecting resonant frequency within ± 20 Hz in stagnant or flowing liquid samples.

Mass-addition (Δm) and resonant frequency change ($-\Delta f$) of a PEMC sensor is given by the following semi-log relationship [24]:

$$\left(-\Delta f\right) = A\log\left(\Delta m\right) + B \tag{1}$$

where A and B are constants and depend on sensor geometry. In principle, the parameter B should be ~0, but in practice we find it to have a non-zero intercept. Sensitivity, defined as mass that causes unit resonant frequency change can be determined from Eq. (1) as:

$$\sigma = \frac{\partial\left(\Delta m\right)}{\partial\left(-\Delta f\right)} = \frac{\Delta m}{A} \tag{2}$$

where σ is the sensitivity of PEMC sensor at mass-addition (Δm). Since A is a constant, σ depends linearly on the magnitude of Δm. The smaller the value of Δm is, the more sensitive the sensor is for a given sensor parameter A. Lower σ value indicates a higher

mass-change sensitivity. Parameter σ is the mass of analyte that causes a unit resonant frequency decrease.

A typical sensitivity calibration result of flush design sensor is shown in Figure 2B, where resonant frequency response (-Δf) and log (σ) are plotted as function of log (mass added). The log-linear relationship between added mass and frequency response (R^2=0.99) confirms the validity of Eq. (1). The parameters are A = 573.9 Hz and B = 8442.2 Hz, with $(-\Delta f)$ in Hz and Δm in g. Sensitivity calculated using Eq. (2) is σ = 5.23 × 10^{-16} g/Hz, 1.40 × 10^{-13} g/Hz, 3.62 × 10^{-12} g/Hz and 1.75 × 10^{-10} g/Hz corresponding to the cumulative mass loading of 0.3 pg, 80.3 pg, 2.08 ng and 102 ng, respectively. One notes in Figure C- 2B that as added mass increased, the sensitivity becomes numerically larger, indicating a decrease in mass-change sensitivity. This is an intrinsic characteristic of PEMC sensor response and is quantitatively given by Eq. (1).

At the lowest added mass (300 fg) in the calibration experiments, the sensitivity was 5.23 × 10^{-16} g/Hz. If the noise level is ~20 Hz and we require a signal to noise ratio to be greater than 3, then a 60 Hz response would be caused by the attachment of ~30 mycoplasma cells.

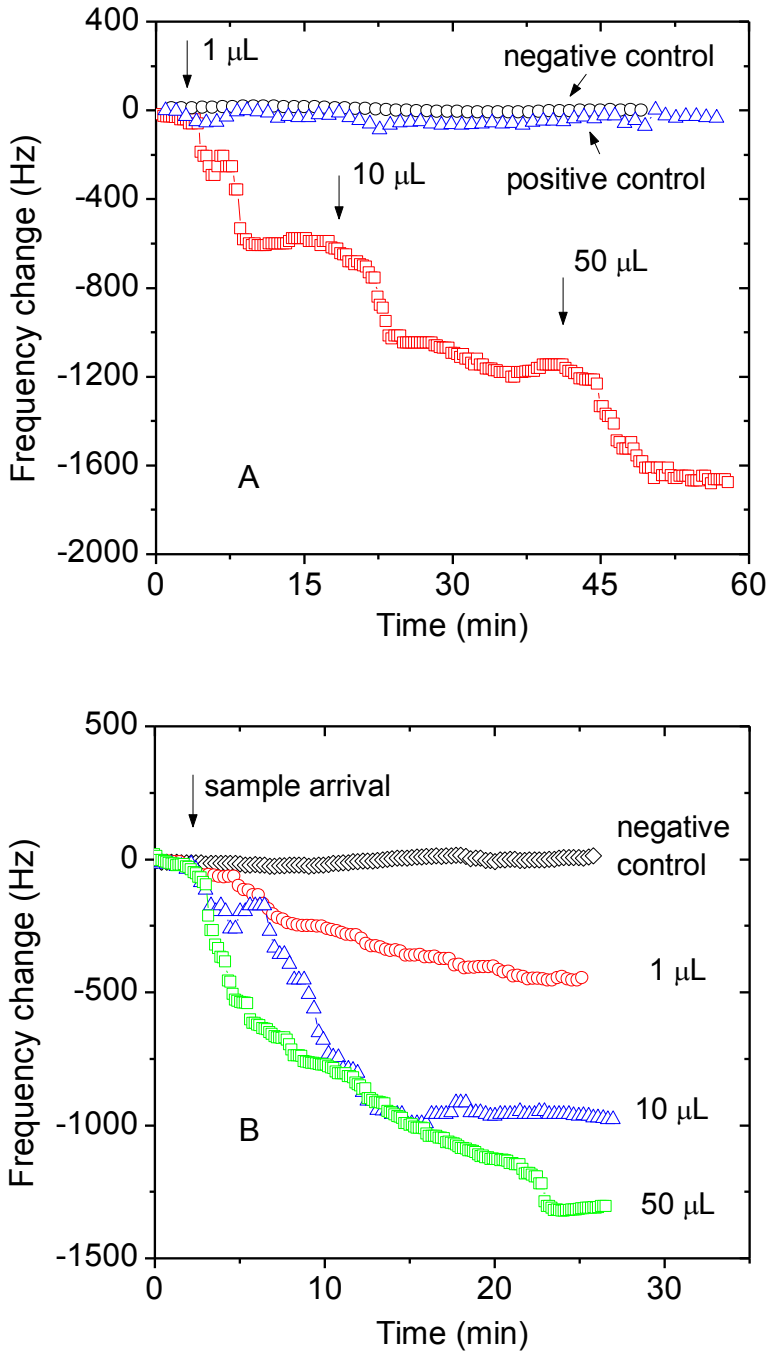

Figure C-3 Detection of positive control in PBS. (A) Response to sequential addition of mycoplasma positive control from Roche kit. PEMC sensor was exposed to 1 μL, 10 μL and 50 μL positive controls. Sequential decreases of 528 Hz, 606 Hz and 525 Hz were obtained. (B) Response to injections of 1 μL, 10 μL and 50 μL positive control using fresh sensors in each experiment. The responses were 446 Hz, 997 Hz and 1,304 Hz, respectively. The injected samples were diluted by 1:4 in flow loop.

Average mass of a mycoplasma cell is ~1 fg. In liquid, resonant frequency change of PEMC sensor is directly attributable to mass change because the Reynolds number (Re) of PEMC at ~900 kHz is ~10^6 [28]. That is, the sensor responses are due to inertial effects, and not due to viscous forces. In an earlier study we showed mass-change sensitivity in liquid decreased by 3 to 5 times compared to in air using two calibration methods; namely a wax deposition method and bovine serum albumin (BSA) binding assay [26]. The difference in sensitivity is due to the difference in surface geometries; for example, wax forms a uniform film, while bound BSA on the surface is non-uniform. Nevertheless, having a means to relate mass-change response in air gives us a reasonable framework for interpreting resonant frequency changes in liquids.

C.3.2 Detection of mycoplasma positive control and calibrated samples in PBS

Sensor responses to sequentially increasing concentration of *A. laidlawii* in PBS were first obtained (Figure C- 3A). We used the mycoplasma positive control directly from Roche mycoplasma detection kit prepared in PBS. Since the positive control contains four species, the sample analyzed contained the competing species and the antibody recognizes only *A. laidlawii*. The sensor was functionalized with *c*pAb via cysteamine-glutaraldehyde method in batch prior to the detection experiments. The sensor was installed in flow cell and resonant frequency was allowed to reach steady state with PBS as running buffer. Volumes of mycoplasma positive control sequentially introduced were 1 μL, 10 μL and 50 μL. At least 10 min steady state time was observed prior to the addition of a higher dose. The resonant frequency decreases resulting from

mycoplasma positive control injections were 528 Hz, 606 Hz and 525 Hz, respectively. The main responses for various doses were observed within the first 10 min after sample was injected.

Prior to conducting the detection experiments, responses to both positive and negative controls were obtained with the same sensor. Buffer control, which consisted of exposing unfunctionalized the sensor to running buffer produced no response. In a separate set of experiments, unfunctionalized sensor was exposed to positive control (100 μL) and yielded a very small response of -50 ± 15 Hz, which is slightly higher than the noise level. In a negative control experiment, the sensor was immobilized with anti-*A. laidlawii*, and the introduction of *A. laidlawii*-free PBS gave a small response of -37 ± 4 Hz. Comparing the detection responses with the three controls, we conclude the decrease of sensor resonant frequency as due to the binding of *A. laidlawii* cells to the sensor surface.

Besides the sequential addition of various positive control sample volumes, experiments of single volume injection to freshly prepared sensor were also carried out and a set of typical responses is shown in Figure C- 3B. For separate injection of 1 μL, 10 μL and 50 μL, the responses were 446 Hz, 997 Hz and 1,304 Hz, respectively. The correlation of sensor (n=10 for sensors used) response to mycoplasma positive control in PBS (n=3 to 5 at each separate volume) is shown in Figure C- 4. Since the exact *A. laidlawii* cell numbers in the positive control is not known, we plot the sensor response as a function of volume (μL) added. One notes the sensor response exhibits lower sensitivity beyond 35 μL, which may indicate sensor saturation. That is, the available antibody sites on the surface are not sufficient for detection of a large number of cells. As seen in the

inset, the response was plotted as a log function of volume added, which yielded $-\Delta f = 758.79 \log C + 174.78$ ($R^2 = 0.96$). The mycoplasma detection kit manual indicates a detection limit of *A. laidlawii* as $10^4 – 10^5$ CFU/mL. It is estimated that in ELISA the positive control contains two to three orders higher concentrations of *A. laidlawii* cells than detection limit value. Based on this approximation, we estimate the cells number in 1 µL sample as $\sim 10^3 – 10^5$. As seen in Figure C- 3, the response to 1 µL sample was easily measurable. Since the sensor was not limited by sample volume, we expect detection sensitivity to be far better than $10^3 – 10^5$ *A. laidlawii* cells.

C.3.3. Detection of calibrated A. laidlawii in PBS and cell culture medium

After accumulating good detection responses using positive control from the commercial kit, detection experiments with calibrated *A. laidlawii* cell samples were carried out. Spiked samples tested were in the concentration range of $10^3 – 10^7$ CFU/mL since the ELISA data showed detection limit as 10^7 CFU/mL.

In Figure C- 5, sensor responses to samples containing 1,100 and 88,000 *A. laidlawii* cells are shown. Introduction of the calibrated samples caused decrease in resonant frequency due to *A. laidlawii* binding. Injection of 1,100 cells caused a decrease of 895 Hz, as shown in Figure C- 5A. Since the volume of flow loop was ~4 mL, the effective concentration was diluted to 275 CFU/mL.

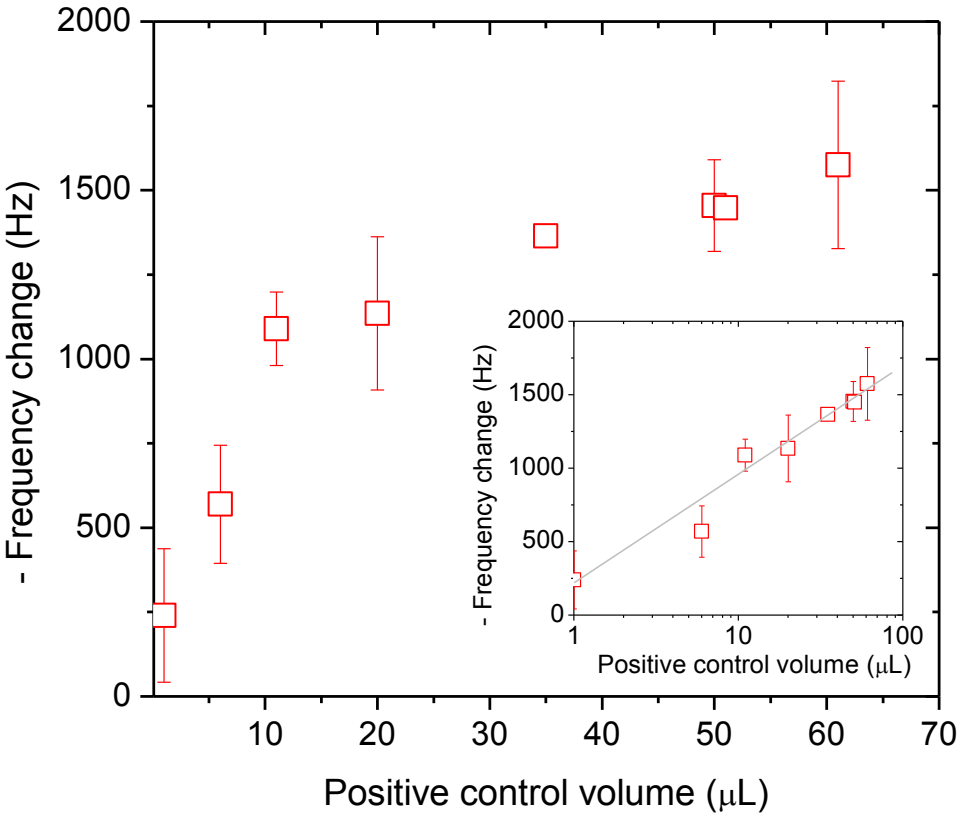

Figure C-4 Resonant frequency change as a function of positive control volume injected. Inset shows resonant frequency response of as a log function of volume injected. PEMC sensors exhibit log-linear relationship for mycoplasma positive control detection.

In order to confirm that the response was due to *A. laidlawii* binding, 500 µL of the *c*pAb was introduced into the flow loop after a PBS rinse. The logic here is that the polyclonal antibody will bind to the *A. laidlawii* cells that were already bound to the first

antibody immobilized on the sensor surface [29, 30]. Response to the antibody was strong and showed a decrease of 256 Hz, confirming the first sensor response was due to *A. laidlawii* binding. It is interesting to point out that the second antibody binding is akin to a sandwich assay in ELISA. Unlike in ELISA, both the first and second antibody contributes to detection signal and the second antibody provides for higher stringency. In a similar experiment shown in Figure C-5B, PEMC sensor was exposed to 88,000 calibrated *A. laidlawii* cells (effective concentration 22,000 CFU/mL) in the same fashion. The injection of *A. laidlawii* cells caused 1,512 Hz resonant frequency decrease. A further 336 Hz decrease was observed with the introduction of 500 μL *c*pAb. These two examples show the detection of *A. laidlawii* in PBS at as low a concentration as ~10^3 CFU/mL is feasible using PEMC sensors.

Since mycoplasma species are common contaminants in mammalian cell cultures, direct and rapid detection in cell culture containing serum without any pre-treatment is useful for evaluating practical performance of PEMC sensors. A detection experiment using PEMC sensor in cell culture medium is shown in Figure C-6B. Sensor was functionalized with *b*pAb and stabilized in PBS. Cell culture medium containing serum (DMEM with 5% fetal calf serum, FCS) and A431 cells (5×10^6 CFU/mL; human skin cells) was introduced into flow loop in a one-through fashion so as to displace the flow loop with the new medium. A decrease of 330 Hz in frequency was observed due to higher density of the cell culture medium and was verified in a separate experiment (see Figure C- 6A). After sensor stabilized in the cell culture medium, 1 mL killed *E. coli* JM101 (10^7 CFU/mL) cells were introduced into the flow loop in recirculation mode. Although one sees an increase in noise level in resonant frequency, no significant decrease in resonant

frequency occurred. After steady state was reached, the circulating fluid was DMEM-serum-A431 (1.2×10^6 CFU/mL) and *E. coli* JM101 (2.5×10^6 CFU/mL), which simulated a strongly contaminated cell culture medium environment. The absence of resonant frequency responses indicate that neither A431 nor *E. coli* JM101 attached to the sensor surface. In this background, *A. laidlawii* detection experiments were conducted. At 40 min, 1 mL 1,000 CFU/mL *A. laidlawii* (effective concentration 250 CFU/mL in flow loop) prepared in cell culture medium (DMEM with 5% FCS) was introduced into the flow loop. Note that the circulating fluid and the *A. laidlawii* sample were of the same composition except for the mycoplasma cells, and thus no density difference was introduced. Resonant frequency decrease of 692 Hz was observed shortly after sample introduction. At 62 min, 1 mL of 100,000 CFU/mL *A. laidlawii* was further injected in and an additional decrease of 428 Hz was observed. PBS flush caused a recovery of 215 Hz and was slightly less than the initial density-induced decrease of 330 Hz, which may suggest an incomplete PBS rinse. After stabilization in PBS, 500 µL freshly prepared *c*pAb from was introduced and a significant resonant frequency decrease of 575 Hz was observed. The second antibody binding response confirmed that the initial sensor response was indeed due to *A. laidawii* attachment. A similar experiment where the sensor was not exposed to *A. laidawii* sample did not result in a resonant frequency response.

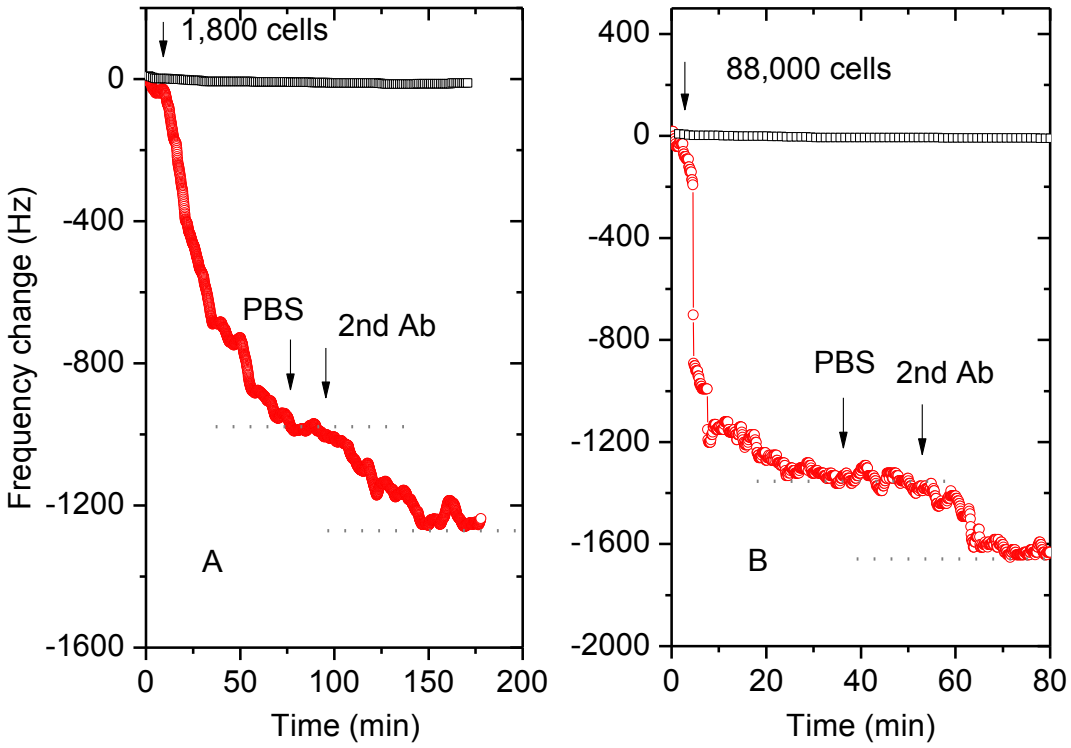

Figure C-5 Detection of *A. laidlawii* in PBS and confirmation by a second antibody binding response. (A) The PEMC sensor was exposed to 1,100 cells *A. laidlawii* (effective concentration 275 CFU/mL) for 50 min, then stabilized in PBS for 30 min before injection of 500 µL polyclonal antibody from Roche kit. The initial attachment of *A. laidlawii* gave a frequency decrease of 895 Hz, and the second antibody caused a further decrease of 256 Hz. (B) The frequency response for injection of 88,000 cells (effective concentration 22,000 CFU/mL) was 1,512 Hz. After rinsing with PBS, a further 336 Hz decrease was obtained for 500 µL second antibody binding reaction.

C.3.4. Quantification of sensor response

It is useful to examine if the response of PEMC sensor to various concentrations of *A. laidlawii* can be quantified. Sensor responses to various concentrations of calibrated *A. laidlawii* samples in PBS (n = 3 or 4) and DMEM (n = 3) are given in Figure C- 7. First order analysis indicates that the sensor response ($-\Delta f$) correlated well with *A. laidlawii* concentration (C_{Al}) with the relationship given in Eq. (1). This relationship has been tested true in other detection experiments for a pathogen and a 30 kD toxin [24, 31]. For the case of *A. laidlawii* detection in PBS, the correlation was excellent ($-\Delta f = 310.14 \log (C_{Al}) - 77.212$, $R^2 = 0.98$). For experiments conducted in DMEM, sensor response was also proportional to *A. laidlawii* concentration. Comparing the results in PBS and DMEM, one notes the response in DMEM was consistently ~50% lower than in PBS, which suggests that the sensor is ~50% less sensitive in complex serum/mammalian cells/*E. coli* background than in PBS. The decrease in response magnitude in complex medium has been observed for detection of SEB and a cancer biomarker using PEMC sensor [24, 32]. Similar sensitivity decreases in complex matrix (serum or plasma) have also been reported in other biosensor systems [33-36]. We attribute reduced sensor response to reduced access to binding sites, as well as possible loss of available antibody sites.

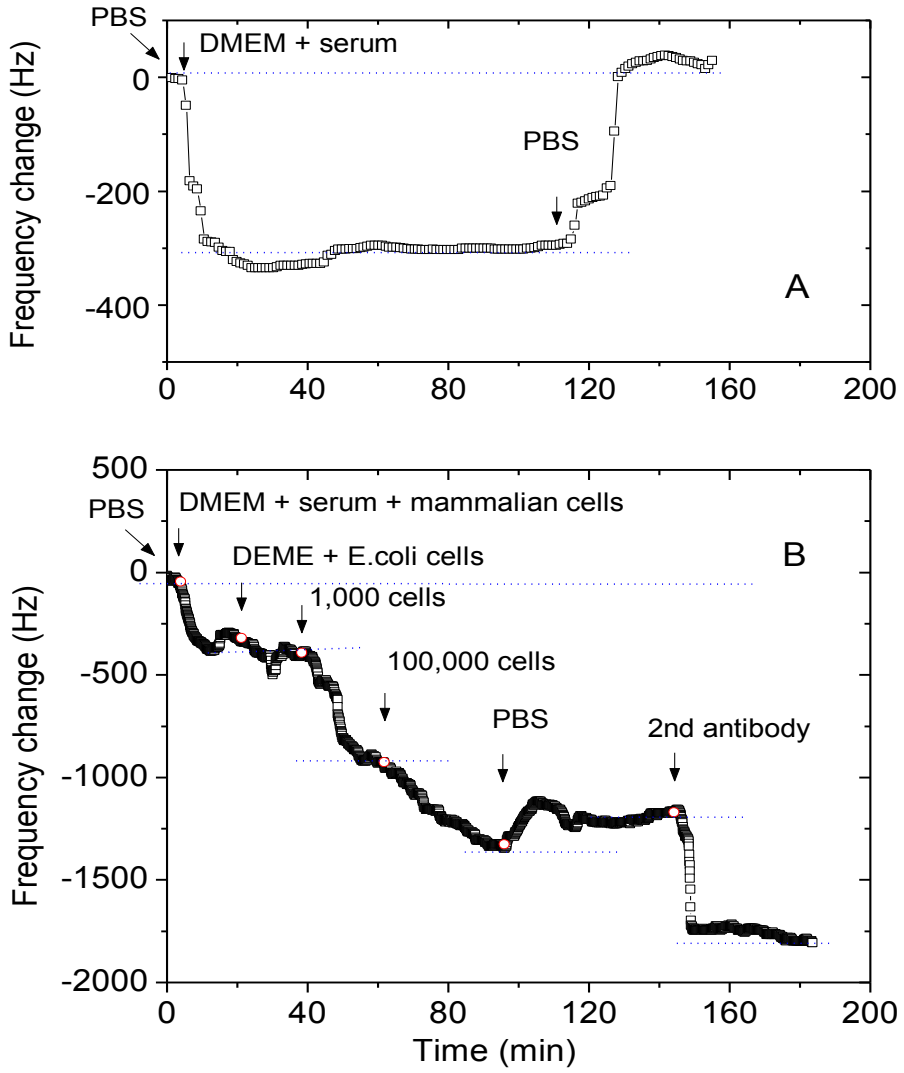

Figure C-6 (A) PEMC responds to density when DMEM was introduced to replace the running buffer PBS; resonant frequency decreased by 315 Hz due to density. Upon replacing DMEM with PBS, the resonant frequency fully recovered back to the original value. (B) Detection experiment in DMEM containing serum (5% FCS), mammalian cells (5×10^6 cells A431 cells) and *E. coli* JM 101 cells (10^7 cells) as background. The PEMC sensor was functionalized with antibody prior to experiment. 692 Hz decrease was observed for 1,000 *A. laidlawii* cells, and a further 428 Hz decrease was seen for 100,000 cells. Second antibody binding gave a further decrease of 575 Hz.

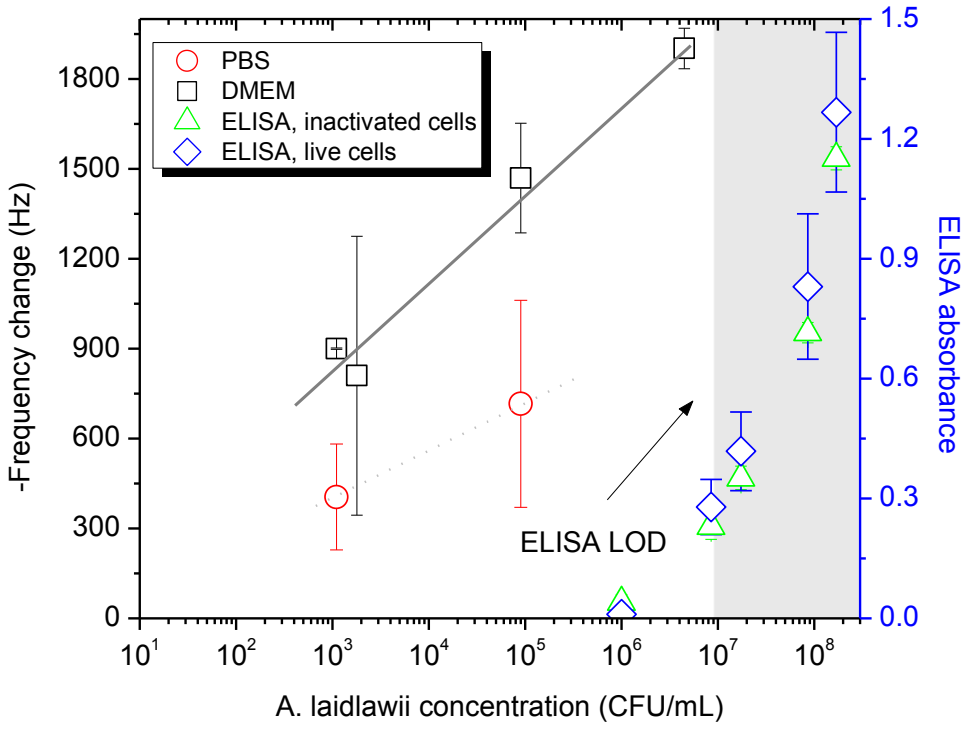

Figure C-7 Comparison of PEMC and ELISA results. For PEMC sensor, resonant frequency response is plotted as a log function of *A. laidlawii* concentration with a detection limit of 10^3 CFU/mL in the dynamic range of 10^3 – 10^7 CFU/mL. Measurements in PBS (□) consistently gave higher response in comparison to cell culture medium (○). Detection limit by ELISA assay was 10^7 CFU/mL for both live cells (◊) and inactivated cells (Δ).

C.3.5. Comparison of PEMC sensor with ELISA

ELISA assays of thimerosal-inactivated and live *A. laidlawii* cells were within ~10 - 15 %. The inactivated cells gave a slightly lower absorbance value compared to live cells. Since binding in ELISA assay was only marginally compromised by using inactivated cells, we can compare PEMC sensor responses with the ELISA results conducted with both live and inactivated cells, and the latter is included in Figure C- 7. As can be seen in Figure C- 7, detection limit of the freshly grown or thimerosal-treated *A. laidlawii* was ~10^7 CFU/mL. On the other hand, the LOD of the PEMC sensor was lower than 10^3 CFU/mL, which is four orders of magnitude lower than ELISA LOD. The results suggest PEMC sensors can significantly improve our ability to monitor contamination in cell culture systems. If one uses sample preparation steps such as centrifugation and resuspension in a buffer, a further improvement in LOD can potentially be achieved using PEMC sensors.

The FDA recommended positive control inoculation is 10 – 100 CFU/mL for testing cell culture samples. Although experiments at such a low concentration have not been carried out with PEMC sensors, it would be prudent to include a short incubation step to permit growth of contaminating mycoplasma cells prior to detection, as this will ensure detection of live cells. Because LOD is lower than 10^3 CFU/mL, the required incubation step would be shorter than that is required for plate-counting microbiological method or PCR approach. In a future report we will examine the applicability of the PEMC sensors at ultralow concentrations of 1 – 100 CFU/mL by using a second and probably a third antibody to amplify the sensor response.

C.4. Conclusion

In this study, we showed successful detection of *A. laidlawii* at 10^3 CFU/mL in both PBS and cell culture medium. Anti-*A. laidlawii* immobilized PEMC sensor showed positive responses for both positive control from the Roche mycoplasma detection kit and self-grown *A. laidlawii* cells. Detection of calibrated *A. laidlawii* samples showed positive response in the dynamic range of 10^3 – 10^7 CFU/mL in buffer medium. The PEMC sensor showed about four orders higher sensitivity compared with ELISA method conducted in parallel using the same *A. laidlawii* stock and the same antibody reagents. Furthermore, the time required for positive detection using PEMC sensor was less than 1 h, which is attractive for timely determination of mycoplasma contamination.

C.5. References

[1] G. Rawadi, O. Dussurget, Advances in PCR-based detection of mycoplasmas contaminating cell cultures, PCR Methods Appl, 4(1995) 199-208.

[2] H.G. Drexler, C.C. Uphoff, Mycoplasma contamination of cell cultures: Incidence, sources, effects, detection, elimination, prevention, Cytotechnology, 39(2002) 75-90.

[3] S. Rottem, M.F. Barile, Beware of mycoplasmas, Trends in Biotechnology, 11(1993) 143-51.

[4] G.J. McGarrity, Detection of mycoplasma infection of cell cultures, in: K. Maramorosch (Ed.) Advances in cell cultures, Academic Press, Inc., New York, 1982, pp. 99-131.

[5] C.C. Uphoff, H.G. Drexler, Comparative PCR analysis for detection of mycoplasma infections in continuous cell lines, In Vitro Cell Dev Biol, 38(2002) 79-85.

[6] FDA, Points to consider in the characterization of cell lines used to produce biological products, 1993.

[7] G.K. Masover, F.A. Becker, Methodology for detection of mycoplasmas in cell cultures used to produce human pharmaceuticals, in: W. Olsen (Ed.) Automated microbial identification and quantitation, Interpharm Press, Grove, IL, 1996, pp. 149-77.

[8] J.A. Eldering, C. Felten, C.A. Veilleux, B.J. Potts, Development of a PCR method for mycoplasma testing of Chinese hamster ovary cell cultures used in the manufacture of recombinant therapeutic proteins, Biologicals, 32(2004) 183-93.

[9] J. Tang, M. Hu, S. Lee, R. Roblin, A polymerase chain reaction based method for detecting *Mycoplasma*/*Acholeplasma* contaminants in cell culture, Journal of Microbiological Methods, 39(2000) 121-6.

[10] M. Wirth, E. Berthold, M. Grashoff, H. Pfutzner, U. Schubert, H. Hauser, Detection of mycoplasma contaminations by the polymerase chain reaction, Cytotechnology, 16(1994) 67-77.

[11] C.M. Garner, L.M. Hubbold, P.R. Chakraborti, Mycoplasma detection in cell cultures: a comparison of four methods, British Journal of Biomedical Science, 57(2000) 295-301.

[12] J. Timenetsky, L.M. Santos, M. Buzinhani, E. Mettifogo, Detection of multiple mycoplasma infection in cell cultures by PCR, Brazilian Journal of Medical and Biological Research, 39(2006) 907-14.

[13] D.E. Woolley, L.C. Tetlow, D.J. Adlam, D. Gearey, R.D. Eden, Electrochemical monitoring of cell behaviour in vitro: A new technology, Biotechnology and Bioengineering, 77(2002) 725-33.

[14] T.H. Park, M.L. Shuler, Integration of cell culture and microfabrication technology, Biotechnology Progress, 19(2003) 243-53.

[15] J.L. Jordan, E.J. Fernandez, QCM-D sensitivity to protein adsorption reversibility, Biotechnology and Bioengineering, 101(2008) 837-42.

[16] C.E. Campbell, M.M. Laane, E. Haugarvoll, I. Giaever, Monitoring viral-induced cell death using electric cell-substrate impedance sensing, Biosens Bioelectron, 23(2007) 536-42.

[17] S. Kintzios, I. Marinopoulou, G. Moschopoulou, O. Manganab, K. Nomikou, K. Endo, et al., Development of a novel, multi-analyte biosensor system for assaying cell division: Identification of cell proliferation/death precursor events, Biosens Bioelectron, 21(2006) 1365-73.

[18] P.S. Waggoner, H.G. Craighead, Micro- and nanomechanical sensors for environmental, chemical, and biological detection, Lab Chip, 7(2007) 1238-55.

[19] S. Singamaneni, M.C. LeMieux, H.P. Lang, C. Gerber, Y. Lam, S. Zauscher, et al., Bimaterial microcantilevers as a hybrid sensing platform, Advanced Materials, 20(2008) 653-80.

[20] C. Ziegler, Cantilever-based biosensors, Analytical and Bioanalytical Chemistry, 379(2004) 946-59.

[21] T. Thundat, R.J. Warmack, G.Y. Chen, D.P. Allison, Thermal and ambient-induced deflections of scanning force microscope cantilevers, Applied Physics Letters, 64(1994) 2894-6.

[22] G.A. Campbell, J. Uknalis, S.I. Tu, R. Mutharasan, Detect of *Escherichia coli* O157 : H7 in ground beef samples using piezoelectric excited millimeter-sized cantilever (PEMC) sensors, Biosens Bioelectron, 22(2007) 1296-302.

[23] G.A. Campbell, R. Mutharasan, Method of measuring *Bacillus anthracis* spores in the presence of copious amounts of *Bacillus thuringiensis* and *Bacillus cereus*, Analytical Chemistry, 79(2007) 1145-52.

[24] D. Maraldo, R. Mutharasan, Detection and confirmation of staphylococcal enterotoxin B in apple juice and milk using piezoelectric-excited millimeter-sized cantilever sensors at 2.5 fg/mL, Analytical Chemistry, 79(2007) 7636-43.

[25] G.A. Campbell, R. Mutharasan, Near real-time detection of *Cryptosporidium parvum* oocyst by IgM-functionalized piezoelectric-excited millimeter-sized cantilever biosensor, Biosens Bioelectron, 23(2008) 1039-45.

[26] D. Maraldo, K. Rijal, G. Campbell, R. Mutharasan, Method for label-free detection of femtogram quantities of biologics in flowing liquid samples, Analytical Chemistry, 79(2007) 2762-70.

[27] K. Rijal, R. Mutharasan, Method for measuring the self-assembly of alkanethiols on gold at femtomolar concentrations, Langmuir, 23(2007) 6856-63.

[28] J.E. Sader, Frequency response of cantilever beams immersed in viscous fluids with applications to the atomic force microscope, Journal of Applied Physics, 84(1998) 64-76.

[29] R. De Palma, G. Reekmans, W. Laureyn, G. Borghs, G. Maes, The optimization of magnetosandwich assays for the sensitive and specific detection of proteins in serum, Analytical Chemistry, 79(2007) 7540-8.

[30] Y. Teramura, H. Iwata, Label-free immunosensing for α-fetoprotein in human plasma using surface plasmon resonance, Analytical Biochemistry, 365(2007) 201-7.

[31] G.A. Campbell, R. Mutharasan, Piezoelectric-excited millimeter-sized cantilever (PEMC) sensors detect *Bacillus anthracis* at 300 spores/mL, Biosens Bioelectron, 21(2006) 1684-92.

[32] D. Maraldo, F.U. Garcia, R. Mutharasan, Method for quantification of a prostate cancer biomarker in urine without sample preparation, Analytical Chemistry, 79(2007) 7683-90.

[33] K. Oshima, H. Nakajima, S. Takahashi, Y. Kera, M. Shimomura, S. Miyauchi, Quartz crystal microbalance assay for determination of plasma vitellogenin, Sens Actuators B Chem, 105(2005) 473-8.

[34] K.S. Hwang, H.K. Jeon, S.M. Lee, S.K. Kim, T.S. Kim, Quantification of disease marker in undiluted serum using an actuating layer-embedded microcantilever, Journal of Applied Physics, 105(2009).

[35] C. Cao, J.P. Kim, B.W. Kim, H. Chae, H.C. Yoon, S.S. Yang, et al., A strategy for sensitivity and specificity enhancements in prostate specific antigen-α_1-antichymotrypsin detection based on surface plasmon resonance, Biosens Bioelectron, 21(2006) 2106-13.

[36] X. Cui, F. Yang, Y. Sha, X. Yang, Real-time immunoassay of ferritin using surface plasmon resonance biosensor, Talanta, 60(2003) 53-61.

Vita

Harsh P. Sharma was born in Ahmedabad, India on May 25, 1985. He attended Nirma Institute of Technology, Gujarat University to get his Bachelors in Chemical Engineering. While getting his Bachelors degree, he was given the 'Best Student' award for 2005 for his curricular work and leadership qualities. He graduated with distinction in 2006 and came to Drexel University to pursue his Ph. D. the same year. At Drexel University he worked as a teaching assistant first and later as a research assistant under the supervision of Dr. Raj Mutharasan. His research at Drexel University was funded by the United States Department of Agriculture and has led to several peer-reviewed publications and he has co-filed for a patent. He has also presented at several national and international conferences and is a member of the American Institute of Chemical Engineers and the American Chemical Society.